The Thesis Committee for Angela K. Luciano
Certifies that this is the approved version of the following Thesis:

Leveraging Class I Wells as an Analog for Class VI in the Gulf Coast

APPROVED BY
SUPERVISING COMMITTEE:

Susan D. Hovorka, Co-Supervisor

Alex Bump, Co-Supervisor

Hailun Ni, Reader

Leveraging Class I Wells as an Analog for Class VI in the Gulf Coast

by

Angela Kim Luciano

Thesis

Presented to the Faculty of the Graduate School of

The University of Texas at Austin

in Partial Fulfillment

of the Requirements

for the Degree of

Master of Science in Energy and Earth Resources

The University of Texas at Austin

August, 2023

Dedication

I want to thank my mom and Esther for their steadfast support and willingness to believe in the best of me. Additionally, I am thankful to my family and friends, who have always been there to lend a listening ear whenever I needed it, as well as my research team with the Gulf Coast Carbon Center, for their valuable insights and advise throughout the past year.

Special thanks to my besties in the Energy and Earth Resources Program and the BEG – Katherine, Edna, Yushan, Hazal, and Shadya – who went through this entire experience with me for the past two years. Without them, this experience wouldn't have been as fun and memorable as it was.

Acknowledgements

This material is based in part upon work supported by the Department of Energy under Award Number DE-FE 0031830 and by the Gulf Coast Carbon Center Industrial Associates program.

Required disclaimer: “This report was prepared in part as an account of work sponsored by an agency of the United States Government. Neither the United States Government nor any agency thereof, nor any of their employees, makes any warranty, express or implied, or assumes any legal liability or responsibility for the accuracy, completeness, or usefulness of any information, apparatus, product, or process disclosed, or represents that its use would not infringe privately owned rights. Reference herein to any specific commercial product, process, or service by trade name, trademark, manufacturer, or otherwise does not necessarily constitute or imply its endorsement, recommendation, or favoring by the United States Government or any agency thereof. The views and opinions of authors expressed herein do not necessarily state or reflect those of the United States Government or any agency thereof.”

Thank you to everyone at the Texas Commission on Environmental Quality - Radioactive Materials Division as well as the Louisiana Department of Natural Resources - Injection and Mining Division who were invaluable in granting me access to all of the datasets underpinning this thesis.

Within the Texas Commission on Environmental Quality, I wish to acknowledge Alisha Stallard for her swift response and willingness to help facilitate my access to office documents. Additionally, I am deeply appreciative of Farhaud Abbaszadeh and Chelsea Brown, whose continued assistance on a weekly basis was pivotal in fulfilling my research needs. My sincere thanks also go to Bryan Smith, Ashley Forbes, Harriet Dixon, and Andrea Greenberg for their support.

Within the Louisiana Department of Natural Resources, I am grateful to Corey Shircliff and Laura Sorey for their generosity in providing me with access to essential documents and for their guidance during the early stages.

I would like to thank Daisy (Emily) Gallagher with Geostock Sandia, for her patience in answering all of my questions and enhancing my understanding of all permit-related matters. Finally, I would like to thank Ben Knape whose long history and experience with the Underground Injection Control program provided valuable insight.

Abstract

Leveraging Class I Wells as an Analog for Class VI in the Gulf Coast

Angela Luciano, M.S.E.E.R.

The University of Texas at Austin, 2023

Co-Supervisors: Susan Hovorka and Alex Bump

Class VI wells under the Underground Injection Control (UIC) program are designed for injection and long-term storage of CO_2 in deep geological formations. They are an important tool in mitigating carbon emissions and combating climate change. However, the recency of the development of the Class VI program means there is limited data available on their permitting, operation, and impact. To address this, analogous data from other wells under the UIC program can be used to provide insights on reservoir performance and best practices. In this study, dozens of permits from Class I wastewater injection wells are mined to extract information relevant to Class VI operations. This includes core tests, well logs, and falloff tests as well as injected volumes and pressure buildup over time. Permeability values available from the datasets are upscaled to analyze how well they are able to predict field-scale performance. Data from the total injected volumes, static pressure measurements, and fracture gradients are used to evaluate the injectivity as well as potential CO_2 injection rates. Utilizing core sample and well log data effectively predicts field-scale permeability, with a tendency to fall within the upper-half or higher range of potential values, especially for Miocene injection wells. Additionally,

the injection zones in this study are capable of accepting large volumes of fluid with minimal pressure buildup, have capacity to continuously accept fluid for decades even with decreased injectivity, and have shown that some wells already accept volumes at rates equivalent to 1Mton CO_2/year and can potentially accept more. These insights will help make baseline assumptions for Class VI permits and build confidence in the program.

Table of Contents

List of Tables

List of Figures

1. Introduction

1.1 Problem Statement

Carbon Capture and Storage (CCS) is an essential technology in the fight against climate change as it plays a vital role in reducing the concentration of CO_2 in the atmosphere. The primary approach involves injecting the gas under layers of rock underground for geologic storage (GS), where it can be permanently trapped. In the long run, CCS can serve as a negative emission solution that can directly extract CO_2 from any location through advanced technologies like Direct Air Capture (DAC). In the present however, its ability to divert the addition of CO_2 from current practices has strong implications for supporting and accelerating the power transition and requires rapid integration into present climate solutions, which has time sensitive demands.

Carbon dioxide makes up approximately three-quarters of all greenhouse gas emissions (Ritchie & Roser, 2020), and according to the International Energy Agency (2022), the highest share of carbon emissions comes from the power sector, emitting a record high of 14.6 gigatonnes (Gt CO_2) in 2022 out of 41.3 Gt CO_2. In addition, this sector saw the largest growth in emissions, increasing 1.8% from 2021, which was largely driven by the demand for heating and cooling in extreme weather. This trend in increasing emissions for energy generation persists because of electricity that - despite the massive expansion and growth of renewable energy - still relies on cheap, accessible, and reliable power that predominantly comes from fossil fuels. The industry sector emerges as the second highest contributor, accounting for 9.2 Gt CO_2. Unlike the power sector however, heavy industry - which includes cement, steel, and chemical processing plants - lack viable, low-carbon alternatives and face significant hurdles in decarbonization (Global CCS Institute, 2021; IEA, 2022).

This opens opportunities to support the power transition by allowing these sectors to offset their emissions immediately through integrating CCS with existing infrastructures that generate significant emissions such as fossil-fuel powered powerplants and chemical processing facilities (IEA, 2020). On one hand, it allows continued access to flexible and dispatchable low-carbon electricity while implementing more permanent shifts towards equally reliable and secure alternative energies. On the other hand, it allows a pathway for hard-to-abate industries to reach net-zero which would otherwise have limited solutions to reduce emissions. Otherwise, meeting climate goals would be virtually impossible as the impact of retrofitting these facilities with CCS capabilities is as significant to emission reduction as the hypothetical scenario of prematurely shutting down many critical infrastructures that support today's society (IEA, 2020). Incorporating CCS technologies can also contribute to decarbonizing hydrogen production, which is an energy carrier with a wide range of potential applications. This is highly beneficial not only because it is a promising source of clean energy for various sectors such as transportation and power, but also because it can help reduce the costs associated with CCS (IEA, 2020).

The current status across the globe, however, falls short of previous expectations. For example, in the Net Zero by 2050 scenario outlined by the IEA (2021), 1.67 Gt CO_2 is expected to be captured in 2030 and 7.6 Gt CO_2 in 2050. Comparatively, the global amount captured in 2020 was 40 megatonnes (Mt CO_2), representing an expected increase in captured CO_2 that is over 40 times the recorded amount within the decade. Two years later in 2022, the amount captured increased by only 5 Mt CO_2, totaling 45 Mt CO_2 captured between 35 commercial facilities (IEA, 2022).

Many other roadmaps and models exist for paths to decarbonization, but they all share the same sentiment in regards to CCS. Massive deployment and scale up is needed within a relatively short amount of time as it is a critical transitory tool. A significant portion of the captured carbon dioxide is expected to originate from industry and power generation i.e. large stationary sources, in order to divert emissions from current practices.

Policy support plays a crucial role in achieving these goals as the technology itself is almost entirely driven by it, limited by its lack of revenue or other substantive financial benefits. As outlined by GCCSI (2021), three main pillars exist to support CCS: (1) Research and Development, (2) Market Development, and (3) Infrastructure. These pillars describe early demonstration of CCS, assistance for business growth and cost reduction, and support for regulatory measures related to permitting and siting critical infrastructure such as pipelines and wells. In the United States, notable examples of policy driven initiatives include the Bipartisan Infrastructure Law of 2021 and the Inflation Reduction Act of 2022, which have provided incentives to encourage the implementation GS projects.

The Bipartisan Infrastructure Law allocates billions towards research on carbon capture technologies, front end engineering and design projects, and large-scale capture projects over the course of five years. It also provides funding towards the construction of pipelines, direct air capture hubs, storage validation and testing projects, and the permitting of carbon dioxide injection wells. Specifically, it allocates $5 million per year between 2022 and 2026 for carbon dioxide injection well permitting and $50 million for states to establish CCS programs (Johnson et al., 2021; Department of Energy, 2022).

The Inflation Reduction Act on the other hand updated the 45Q tax credit by increasing the value of storage by providing up to $85 per metric ton of carbon dioxide stored for sequestration and up to $60 per metric ton for enhanced oil recovery or industrial use. The updates also allowed for direct payments for the credit and expanded the scope for qualified facilities. As a result, the capacity requirements for power plants, DAC, and other facilities were respectively reduced to 18,750 Mt, 1,000 Mt, and 12,000 Mt CO_2 per year, and qualification of the tax credit extended to include facilities that began construction before January 2033 (Inflation Reduction Act of 2022; Clean Air Task Force, 2022).

Support such as these are integral for scaling-up CCS by offering financial incentives for investors and bringing down the costs associated with the overall supply chain of these projects i.e. capture, transport, and storage. Indeed, the current climate in CCS reflects growing momentum with heightened interest and declarations of intent to invest in GS projects. However, given the recency of increased support, barriers to wide-scale deployment remain due to regulatory challenges and the lack of experience in undertaking carbon dioxide storage projects.

Regulatory frameworks need to tackle many concerns surrounding permitting, perceived risks, long-term liability, public engagement, and more, in order to mollify the concerns from various groups. However, resolving these complexities is time intensive, and the lack of a clear timeframe in the completion of these projects combined with the uncertainty in the viability of wide scale carbon dioxide storage can be a deterrent for potential investors. Furthermore, engaging with stakeholders becomes challenging due to their diverse backgrounds, and the unfamiliarity surrounding CCS poses a significant learning curve for all parties involved, further contributing to existing obstacles.

Notably, more than 85% of known CCS projects involve fossil fuel industries, professionals who possess extensive knowledge of subsurface exploration related to hydrocarbon production, but not necessarily on the EPA's underground injection control program (Chalmin, 2021). Not only is the type of operation technologically different, but the process of approval for injection operations is more extensive and restrictive.

Other stakeholders, which include investors, landowners, residents, and the general public, often lack awareness and understanding of CCS technology and are unfamiliar with subsurface sciences. These groups often have concerns related to safe storage, induced seismicity, surface land impacts, air and noise pollution, public safety, impact to farmland, and environmental justice which requires active engagement and communication from developers to reach consensus (Warner et al. 2020). Furthermore, attitudes towards CCS and agreements on acceptable risks are often influenced by political affiliations, creating additional social resistance and skepticism that is independent of the feasibility of CCS (Wilson & Keith, 2002; Pianta et al., 2021).

Separate from the regulatory and social barriers, technical challenges also hinder the scale-up of CCS as uncertainties persist regarding the cost, storage capacity, risk management, and injection rates (Pianta et al., 2021). Cost predictions exhibit high variability, but similar to other examples of emerging technologies, they are expected to drop with time and experience. What is certain is that many of the key drivers are site specific, fluctuating based on the distance to the source, purity of CO_2, existing infrastructure, monitoring requirements, pre-existing geologic characterizations, accessibility, total storage capacity, and injectivity (GCCSI, 2021).

While all factors are important, it is particularly crucial to predict and maximize injection rates not only because of its impact on cost (which can reduce the number of wells for a site) but also because of the urgency and time constraints associated with current climate goals. Unfortunately, a significant challenge arises from the lack of available data related to GS operations.

However, there is precedents for large scale injection operations from other underground waste disposal practices which laid the foundation for regulations and procedures for carbon dioxide storage. Oversight of all injection operations in the United States falls under the Underground Injection Control (UIC) program, which is regulated by the Environmental Protection Agency (EPA). Although regulations addressing the buoyancy, mobility, and expanded pressure plumes, etc. for carbon dioxide are unique to itself, in many respects, carbon dioxide storage is more of an extension of pre-existing technologies rather than an entirely new one.

Analogous industries for injection operations include, but are not limited to: CO_2 injection for enhanced oil recovery (EOR), produced water injection, natural gas storage, and wastewater disposal. In general, most of these injection programs require similar details which broadly include geologic characterizations, description of the underground source of drinking water, and operational reports which contain historical data on injection rates. Examples of studies assessing the viability of wide scale storage from analogous datasets are exemplified by Vikara & Guinan (2019), Ni et al. (2021), and ongoing research from the Gulf Coast Carbon Center.

Recognizing that GS is not a completely brand-new technology and leveraging the experience and data from analogous technologies will be highly beneficial for increasing confidence in CCS. For this thesis, permit applications under the Class I program near the Gulf Coast of Mexico in Texas and Louisiana are analyzed to extract information applicable to carbon dioxide injection operations and permitting.

1.2 SCOPE

This study is a first step approach to the exploration of Class I - hazardous and non-hazardous wastewater - permit applications, which also contain varying amounts of data beyond those gathered for this study. Particularly of interest in this study are characteristics that describe how efficiently the rocks receive the fluids being injected i.e. the injectivity. It focuses on information available across all wells in order to be able to find a common denominator and make broad assumptions across different geographical regions. This includes data from core samples, brine analysis, well logs, fall off tests, and historical injection volumes and pressure. Aside from the injectivity, there are many other lessons from the Class I program regarding the risks and mitigation strategies or the monitoring practices associated with injecting large quantities of waste that can be studied; however, they will not be discussed much in this study.

The objective of this thesis is to build confidence in large-scale carbon dioxide storage by analyzing the precedents of long-term fluid injection through Class I wells, utilizing existing data to predict injectivity, and highlighting the value of information available in Class I permits to streamline CCS projects.

1.3 THESIS LAYOUT

There are 5 more chapters in this paper. Chapter 2 details the literature review necessary to understand the history and basis for analyzing Class I wells within the UIC program. This chapter also delves into past studies utilizing analogous industries as a proxy for Class VI CO_2 storage for injectivity analysis. Chapter 3 discusses the process for data acquisition, interpretation, and methodologies. Chapter 4 presents the data and elaborates on specific observations made from various sites, providing a deeper understanding of injection limitations and behaviors. In Chapter 5, the results from this thesis and policy implications from UIC regulatory precedents are discussed. Finally, Chapter 6 summarizes the findings and draws conclusions from the study.

2. Literature Review

2.1 Underground Injection Control

The UIC program was created to ensure protection of the Underground Source of Drinking Water (USDW) and consists of six classes of injection wells (40 CFR §144.6):

1. Class I: Hazardous and Non-hazardous Industrial and Municipal Wastewater Wells
2. Class II: Oil or Natural Gas related Injection Wells
3. Class III: Mineral Extraction and Dissolution Injection Wells
4. Class IV: Shallow Hazardous and Radioactive Injection Wells (banned)
5. Class V: Non-Hazardous Fluids and Uncategorized Wells
6. Class VI: Geologic Sequestration of CO_2 Wells

Although the UIC program and its environmental protections are regulated by the EPA, primary enforcement authority (primacy) can be granted to states, territories, or tribes to assume responsibility over the permitting process. These entities can apply for primacy at their own initiative and must uphold the rules set out by the Safe Drinking Water Act. To demonstrate eligibility, they must showcase their jurisdiction over underground injection practices as well as their ability to prevent any potential harm to the USDW. Additionally, under Section 1422, states must show that they have the necessary civil and criminal penalty and administrative enforcement authority (Safe Drinking Water Act, 1974). Applicants can either apply for primacy over Classes I-V, just Class VI, or for all of the classes, resulting in a patchwork of authority as shown in Figure 2.1.

Most states have primacy over Classes I-V, some have primacy over Class II wells alone, but only North Dakota and Wyoming have primacy over Class VI wells as of now. Rapid implementation of CCS faces a significant hurdle since the approval of every other pending Class VI permit will fall under the jurisdiction of the EPA. This becomes problematic due to the high volume of permits requiring approval from a limited staff, compounded by the increasing rate of permit applications. For reference, the number of pending permits as of August, 2023 is almost three times the amount recorded in March, 2023, jumping from 42 to 112 pending permits over the span of five months (EPA, 2023).

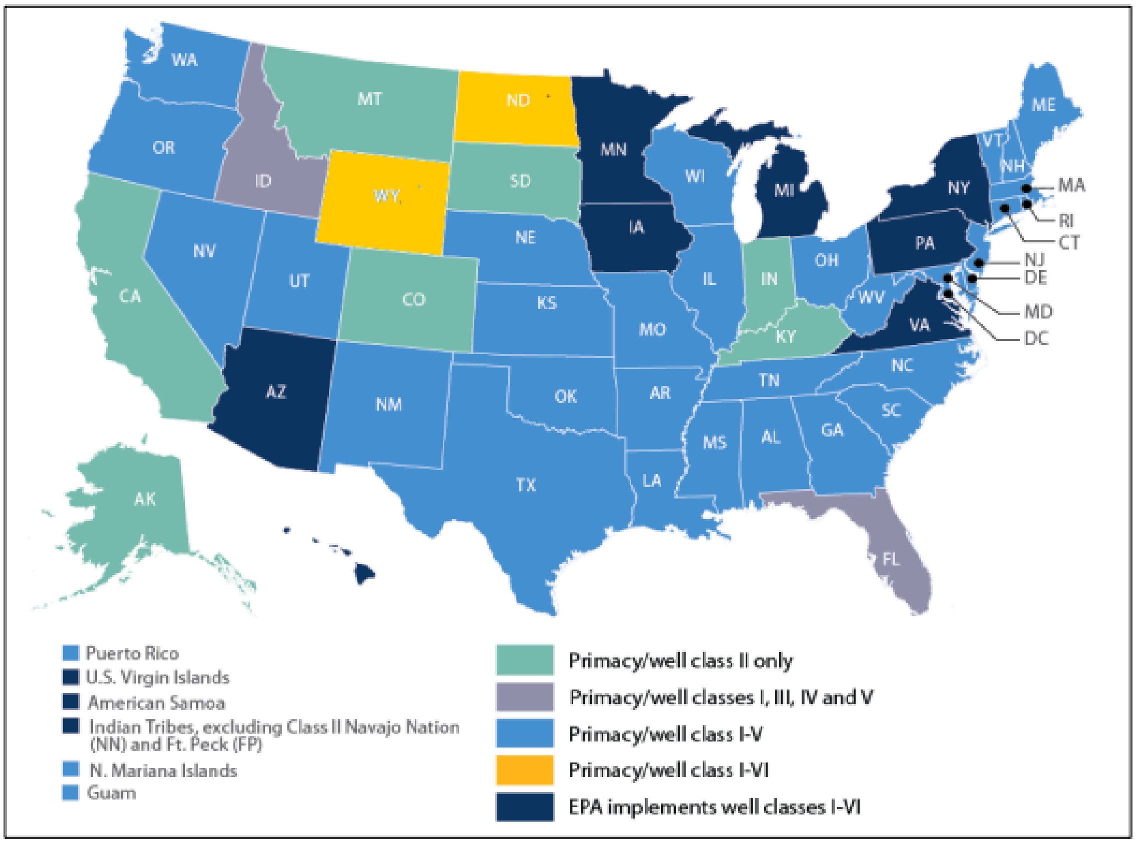

Figure 2.1. UIC Primacy Map (EPA, 2023)

A majority of these applications are from California and Louisiana, and the EPA has stated the intent to grant Class VI primacy to the latter, relieving the agency of certain responsibilities that can now be delegated to the state (EPA, 2023). Other applicants in order of the number of pending permits are: Illinois, Alabama, Texas, Indiana, Arkansas, and Ohio. Of these states, only Texas has shown progress in applying for primacy and is in the pre-application stage alongside Arizona and West Virginia (EPA, 2023).

Allocating responsibility to the states is a crucial step in streamlining the permitting process, particularly because of the vital role public engagement and open communication plays in enhancing efficiency and acceptance, which is most effective when driven by local communities. This not only disperses administrative burdens to local communities but also allows more control and flexibility in permitting, monitoring, and regulating CO_2 injections. For states like Texas and Louisiana which have suitable geology and vested interests in CCS, this allows room to take advantage of local expertise and decision-making that aligns with region-specific needs.

For operators and stakeholders wanting to invest in CCS, looking at the history and performance of local Class I wells will be useful for setting expectations regarding large-scale, long-term waste disposal in additional to better understanding the requirements needed for a successful underground injection permit. As stated in the final rule for *Federal Requirements Under the Underground Injection Control Program for Carbon Dioxide (CO_2) Geologic Sequestration (GS) Wells*, Class VI operations were largely based off existing Class I requirements (75 FR 77257, 2010; EPA, 2022). Therefore, understanding the permitting processes and operations from the extensive history spanning several decades from Class I injections helps facilitate a deeper understanding of Class VI operations.

2.1.1 Background of Class I

Deep formation waste disposal has been in practice by the oil and gas industry since the 1930s, expanding to industrial facilities and chemical processing plants by the early 1950s, with minimal oversight (Clark et al., 2005). The first and oldest of Class I wells –

DuPont's Victoria Site now operated by INVISTA S.à r.l., LLC – began operations during this time and has cumulatively injected over tens of billions of gallons of waste to date, demonstrating the ability of these geologic formations to tolerate long term, safe injection of fluid (Clark et al., 2005; Sandia Technologies, LLC, 2015).

However, in the early days of wastewater disposal, concerns were raised regarding the viability and safety of large volume injections which mirror the current sentiment towards CO_2 storage. During that time, injection wells were not closely monitored, and it was through studying the early-day well leakages that present regulations exist. A study conducted by the Government Accountability Office (GAO) highlights significant well failures that ushered in demand for stricter regulations in Table 2.1.

Table 2.1. Major Cases of Well Failures (GAO, 1987)

Year	**State**	**Company**	**Cause of Failure**	**Result**
1968	PA	Hammermill Paper Co.	Corroded Well, Effluent Migration up Abandoned Well	Leakage to surface and suspected contamination of USDW
1975	TX	Velsicol Chemical Corp.	Constructed without Tubing or Packer	Contamination of USDW
1980	LA	Tenneco Oil Co.	Constructed without Tubing or Packer	Contamination of USDW
1983	OH	Aristech Chemical Corp.	High Pressure Injection	Leakage of Injection – did not reach USDW
1975-1984	Many	7 unspecified wells	Corroded Well	Leakage to non-drinking water aquifers

After identifying the root causes of these well leakages, it was concluded that most failures were attributed to internal and external mechanical integrity failures caused by leaks in the well casing, excessive injection pressure, improperly abandoned wells in the area, leaking packer assemblies, corrosion, and injection directly through the casing (UIPC, 1986, GAO; 1987; EPA, 2001). Several other incidents unrelated to mechanical integrity failures highlight other risks associated with waste injections. For instance, at Denver's

Rocky Mountain Arsenal in the 1960s, injections with excessively high pressures were found to be linked to seismic activity, triggering faults miles away even after halting operations. The injections at the U.S. Steel Corp in Fairfield, Alabama resulted in solid-clogged formations, and the injections of acidic waste in Mulberry, Florida led to the dissolution of the rocks in the injection zone causing leakage through the confining zone (Underground Injection Practices Council, 1986; Simpson & Lester, 2009, pp. 14-22).

The demand for better environmental protections led to major changes through the implementation of policies that ensured safe waste disposal practices. Some of the enacted laws are outlined below.

- 1974 Safe Drinking Water Act (SDWA) granted EPA authority to set permitting and operating requirements for injection wells to protect the USDW (Safe Drinking Water Act, 1974)
- 1976 Resource Conservation Recovery Act (RCRA) was passed into law with the goal of establishing programs to manage waste while protecting human health and the environment (Resource Conservation and Recovery Act, 1976)
- 1980 EPA promulgated the UIC program, defining the five classes of injection wells, issues regulations, and established the USDW as drinking water sources with <10,000 mg/L TDS (EPA, 1980)
- 1984 Federal Hazardous and Solid Waste Amendments were made to the RCRA and banned hazardous waste disposal without significant demonstration of environmental protection (The Hazardous and Solid Waste Amendments, 1984)
- 1988 EPA promulgated the rules set for disposal wells and specifically for Class I hazardous injection wells, required a demonstration of 10,000 years of waste containment or chemical transformation referred to as a No-Migration Petition (53 FR 28118)

Consequently, current practices not only require continuous well integrity tests, but also require plans for constant monitoring of operations as well as analyses of seismic risk, compatibility of waste with the formation, and identification of transmissible features like faults and artificial penetrations. Despite these additional restrictions, the number of Class I wells grew significantly, starting with four wells in 1950, 30 wells by the 1960s (Smith, 1996, p.10), and 250 wells by the 1970s (Warner & Orcutt, 1973, p. 692), as cited by Clark et al. (2005). After the 1980s, noncompliant wells were decommissioned and growth slowed, but new wells still continued to be constructed. There were 533 wells by 1985 (GAO, 1987, p.13), 529 wells in 2002 (Figueiredo, 2005), 523 wells in 2010 (GWPC, 2021, p.13), and 830 wells in 2020 (EPA, 2020). It should be noted that these represent the active wells, not the total of all extant wells.

After the new safety standards were implemented, Rish et al. (1998), conducted a more extensive study using probabilistic risk assessment through a series of fault trees to identify the causes and likelihood of waste isolation loss. It was concluded that the two dominating factors for failure were the possible development of transmissive microannulus in the cement and the chance of the extraction of waste in the future, but the probability was significantly low because of the strict siting requirements, preventative care, and continued monitoring and quality check tests that allowed well failures or small leakages to be recognized and addressed before containment loss (EPA, 2001). For example, the requirements for automatic shut off systems, alarms, and presence of an on-site operator all contribute to the identification and remediation of a mechanical integrity loss.

Following the evaluations and studies of the regulations, engineering designs, and risks, the Office of Ground Water and Drinking Water concluded that properly constructed and operated wells were "safer than virtually all other waste disposal practices" such as surface storage, landfills, or incineration (EPA, 1991).

Particularly in the case of hazardous wastes (Class IH), applicants complete a No-Migration Petition in which they must prove that the waste will either remain in the permitted area for 10,000 years or become non-hazardous over that time. Depending on the state, Class IH wells may also be subject to additional restrictions e.g. more frequent mechanical integrity tests. Furthermore, as is the case with all deep injection wells, multiple layers of impermeable or low permeability rocks exist between the injection zone and the surface which act as barriers to vertical fluid flow, further ensuring safeguards against vertical migration. There has been no contamination of the USDW from Class I wells since the implementation of the UIC Program (Guinan et al., 2019, p. 2).

2.1.2 Comparing Class I and Class VI

Turning to Class I permits, especially Class IH, can have far reaching applications for Class VI which ranges from simply using them as a template to gauge ideal lengths of text and appropriate amounts of detail, to using them to gather data which describes geologic characteristics and reservoir properties that would normally cost tens of thousands of dollars to acquire. The injection zones for both wells must be isolated from the USDWs by an impermeable confining zone and are injected at depths of 1,700 ft to more than 10,000 ft (note that CO_2 is stored at depths below 800 meters, or around 2600 ft, to remain a supercritical fluid). Additionally, the formation of these zones must prove that they meet the requirements to handle large volumes of injected fluids while preventing migration into a USDW (40 CFR §146 Subpart B, 1980). Other similarities include: long-term planning for injectate (100s-1000s yrs for Class VI, >10,000 years for Class IH), targeting saline aquifers, decades long injection operations, analysis of seismic risk and more (IEAGHG, 2010; Guinan, 2019). Furthermore, similarities are noted throughout the different phases of a permit approval which can be broadly categorized into five stages: (1) Pre-permitting (2) Pre-construction (3) Pre-injection (4) Injection and (5) Post-injection (EPA, 2022).

During the first stage, applicants meet to discuss permitting intent and processes. In the next stage, information regarding the site characterization, area of review (AOR), well construction, financial responsibility, and injection plans are detailed. This step is especially critical because it requires in depth discussion of the geology to meet the standards required of minimum criteria for siting. In both UIC programs, similar language is used in need to prove that there is 'sufficient' porosity, permeability, thickness, and areal extent (40 CFR § 146.62(c)(2)(ii), 40 CFR § 146.83(a)(1)). This requires data from well logs and core plugs, but at this phase, information available from other wells or from literature review may be used but must be supplemented once drilling and well construction commences (Van Voorhees et al., 2021).

Additionally, in detailing the AOR, the affected area must be identified along with the presence of artificial penetrations, faults, and fractures that may allow vertical transmission of fluids and threaten the USDW. However, one major difference here is that the AOR for Class I is determined by the Cone of Influence – region where the increased pressure may drive fluid into the wellbore - or a fixed radius (up to 2 mi under EPA & LA or 2.5 mi for TX) decided by the agency issuing the permit, whichever is greater (30 TAC §331.42; LA Admin Code §XVII-607; 40 CFR § 146.6).

On the other hand, the AOR of Class VI is calculated by the plume extent and the pressure front which can potentially result in a larger AOR due to the mobility and buoyancy of supercritical CO_2 – the state at which CO_2 has a density closer to a liquid, but a viscosity closer to gas – because of the efficiency of CO_2 displacing the original reservoir fluid. For reference, the density of water ranges from ~994-1054 kg/m^3 while supercritical CO_2 ranges anywhere from ~500-700 kg/m^3 (see Figure 2.2).

Then, during the pre-injection phase, cores, well logs, pressure tests, and other samples are gathered for calibration and completion of the previous submission to confirm compliance with injection regulations. Once approved and operations begin, continuous updates regarding injection pressure, injection volumes, waste stream analysis, mechanical integrity tests, updates on the AOR, activity of any workovers, or any other details must be submitted (40 CFR § 146.33, 40 CFR § 146.91). One such monitoring test specific to Class VI is the possible consideration of testing the surface air or soil gas in order to detect leakage of CO_2 (40 CFR § 146.90). Finally, during post-injection, wells are plugged and abandoned to ensure the well does not become a pathway for leakage before complete site closure.

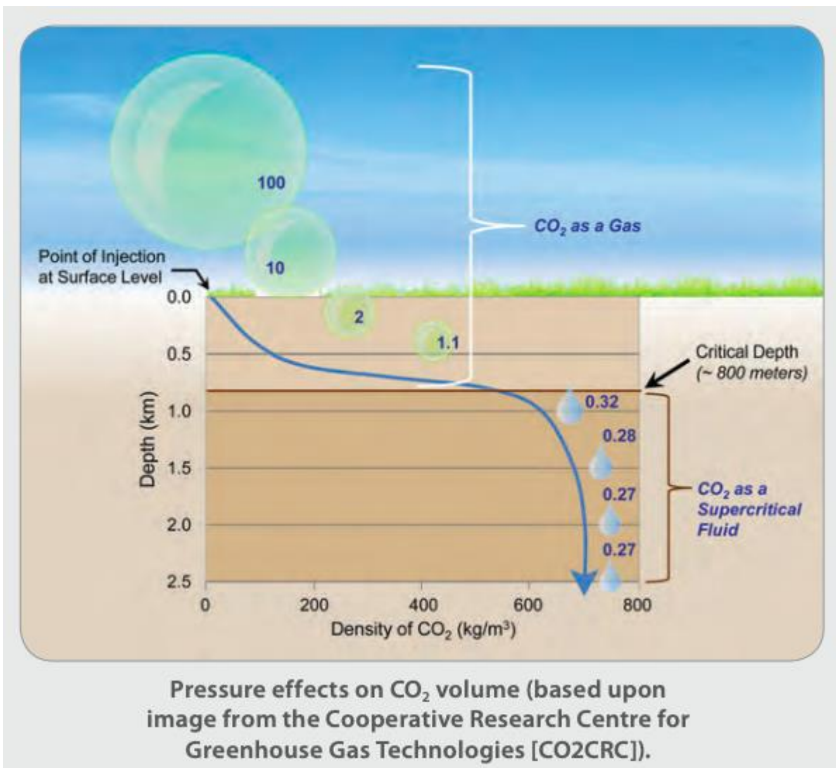

Figure 2.2. Density of CO_2 at Different Depths (NETL, 2015)

2.1.3 Background of Class VI

Class VI rules were finalized in 2010, and there are currently only two active wells, CCS1 and CCS2, which are both in operation at the Archer Daniels Midland Plant in Illinois. Illinois Basin Decatur Project's CCS1 well began its site characterization process in 2007 and started constructing the well in 2009, which was originally permitted as a Class I well. It was later converted to Class VI after the 2010 promulgation of the Class VI program and has injected ~ 925,300 tons of carbon dioxide between 2011 to 2014 (Couëslan et al., 2014; Gollakota & McDonald, 2014; Van Voorhees et al., 2021). The CCS1 well is now in the post-injection stage, monitoring the site, while the CCS2 well is actively injecting (EPA, 2023).

Though many of the insights and data gathered were applied to the Industrial Carbon Capture and Storage project for the CCS2 well, the permitting process still took approximately six years to finish with the initial filing of the permit application in 2011 finally being approved for injection in 2017 with the goal of injecting 1 Mton CO_2 per year (Van Voorhees et al., 2021; Lococo, 2021).

Looking forward, CCS is being considered for many other locations as shown in Figure 2.3 CO_2 Storage Resource Locations (NETL, 2015). CO_2 storage is being considered for depleted oil/gas fields, unmineable coal, and saline aquifers, with the latter having the highest storage potential. It should be noted however that injecting CO_2 into deep geologic rocks is not a new technology. There is history of using CO_2 for enhanced oil production under Class II (Figueiredo, 2005; Sweatman, 2009) or even for experimental purposes under Class V (Hovorka, 2004; Dougherty, 2007), which in the Frio Pilot case also incorporated Class I well construction standards.

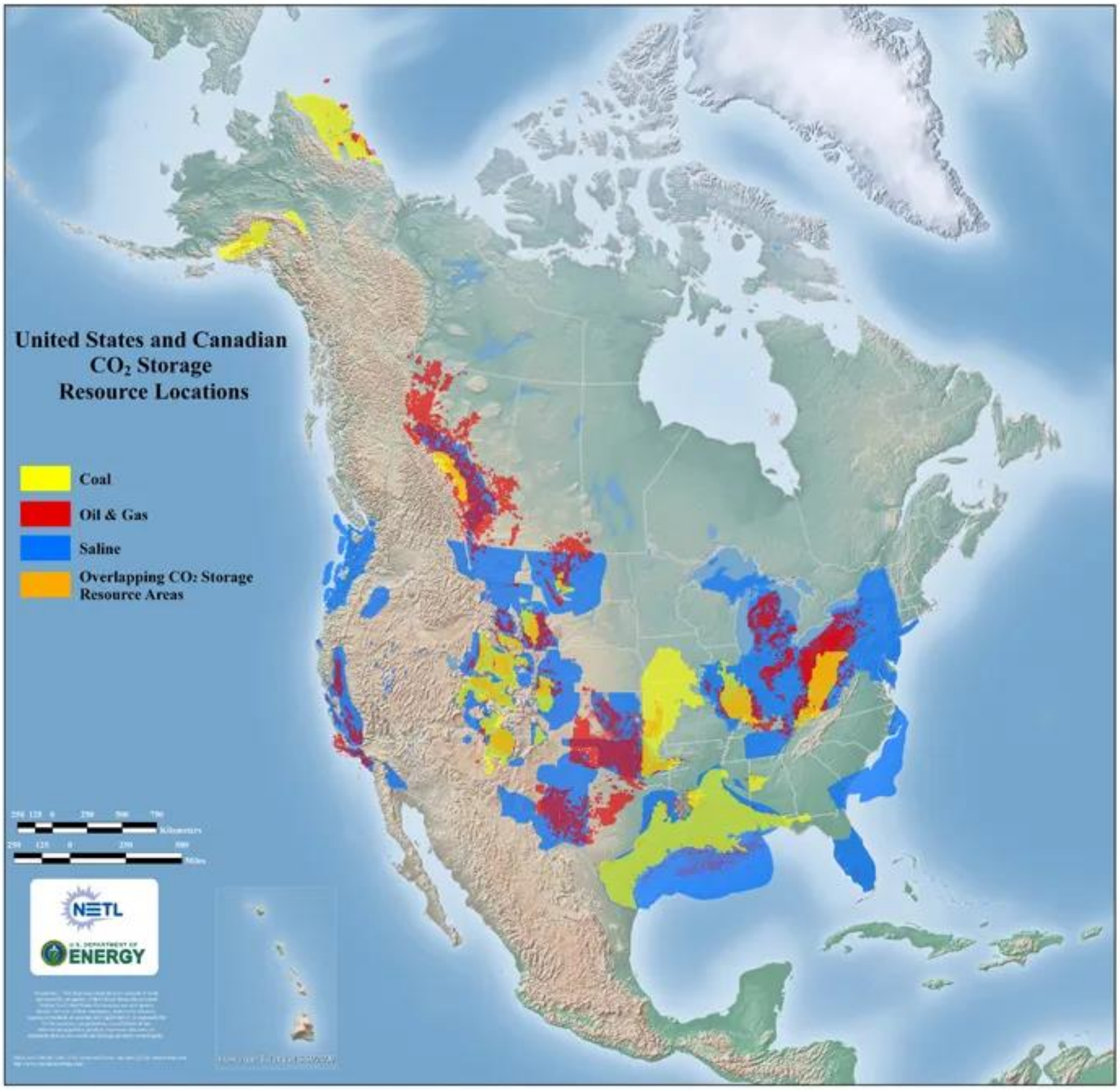

Figure 2.3 CO_2 Storage Resource Locations (NETL, 2015)

2.2 Previous Work on Analogous Technologies

2.2.1 Class I Injection Wells as an Analog

In a study from the National Energy Technology Laboratory, a series of reports analyze existing knowledge and technologies to provide high level comparisons and main takeaways of analog industries to bolster CCS. In one of those reports, *UIC Class I*

Injection Wells – Analog Studies to Geologic Storage of CO2, Guinan et al. (2019) details the similarities (and differences) and comparable characteristics between Class I and Class VI wells, all to emphasize the point that although Class VI wells are new, it is more of the same practices that have been in use for decades. Both Class I and Class VI programs are governed by the same regulatory body and have strict requirements, which is even more true for Class VI. These shared characteristics, coupled with the long history of large volumes of waste disposal under Class I and lack of significant leakage events in decades, emphasize the effectiveness of safe injections when best practices are utilized.

Some of the main similarities highlighted include: the site selection and criteria for geologic characterizations, formation type (saline aquifers), operational requirements and procedures, well designs and equipment needs, risk and hazards identification, and emergency/safety assurance protocols.

Further, Guinan et al. (2019) states that a simple approach to estimate the volume or rate of CO_2 storage for CCS purposes would be to assume the conversion of a Class I well into a Class VI well and to use the volume of that commercial Class I well. This example assumed a supercritical CO_2 density of 640 kg/m^3 (supercritical density ranges from ~500-700 kg/m^3 – see Figure 2.2) for a specific existing Class I well in Florida. Under this assumption, this well that is permitted to inject 2.4 MM gal/day is equated to injecting 2.1 Mt/yr CO_2 based on the volumetric conversions (Guinan et al., 2019, p.81). This study will use a similar approach in converting water injection volumes to an equivalent CO_2 mass using simple volumetric and density conversions.

2.2.2 Class II Salt Water Disposal Wells as an Analog

In *Evaluating Technical Feasibility of Gigaton Scale CO2 Storage,* Ni et al. (2021) uses Class II (oil and gas related wells) salt water disposal (SWD) wells in Texas and

Louisiana to answer the question of whether it is feasible to store the amount of CO_2 required to meet climate change goals. Injection volume, injection pressure, and injectivity are analyzed for these produced water injection wells. Assuming a supercritical CO_2 density of 700 kg/m^3, volume of water is converted to an equivalent mass of CO_2, and several ranges of injection rates are evaluated. Minimum rates are estimated by adding real injection volumes, medium rates are estimated assuming wells inject at their highest recorded rate, and maximum rates are estimated by assuming that the wells inject at a rate that pushes the pressure buildup to its maximum allowed value.

It was concluded that while the min and medium rates coupled with their respective number of wells fall short of the gigaton storage goal, the max rate scenario far surpasses the goal and that there was reasonable cause to believe that high-rate injections were plausible (Ni et al., 2021). Furthermore, after analyzing the disposal formations, it was found that the Frio had the highest volume injected while the Miocene had the highest injectivity as defined by the rate as a function of the pressure buildup. Likewise, this thesis will use varying hypothetical CO_2 injection rates using the data available from Class I injection wells to analyze the performance of different formations.

2.2.3 Other Analogous Industries

While there were no other examples found of the direct application of existing data from injection wells to analyze the injectivity of CO_2, there are other analogous technologies that provide insight for carbon dioxide storage and CO_2 injection. One is from natural gas storage and the other from enhanced oil recovery practices.

Natural gas storage is a technology that has existed for over 100 years in which natural gas is seasonally stored to be used during months where there is high demand. While not intending to permanently store gas, there is a strong need and emphasis to safely store gas under this technology, which has many applications for Class VI. Main points highlighted by (Vikara et al., 2019) include the study of caprock integrity and the study of single point leakages. The natural gas is stored in its gas form, to later be used, so naturally there is major concern about the buoyant gas building pressure and breaking past the caprock. There are also instances of single point leakages as a result of casing or equipment failure which may serve as an analog for Class VI. However, major differences exist in the fact that a major emphasis for natural gas storage is in maximizing the deliverability, though they also want to determine maximum injection rates. Additionally, natural gas storage operations are exempt from UIC standards, so they are largely different in that they adhere to the standards set by different regulatory bodies.

Enhanced Oil Recovery (EOR) describes techniques which aim to increase hydrocarbon production beyond that which can be achieved using conventional methods. Common practices include the injection of water, carbon dioxide, or acid gas in order to push the hydrocarbons towards production wells. Specific to CO_2 EOR, there is a clear parallel between the two practices which inject carbon dioxide into the subsurface. As summarized by Lake (2022), the petrophysical analysis and numerical simulations used for EOR are applicable as they provide insight regarding the fluid movement of CO_2 in the subsurface. This technology would be particularly useful for the sites which are considering depleted oil and gas fields for storage.

However, there are also differences between the technologies. The most prominent being that the drive for continued injection for EOR is to balance production, while for CCS, it is to mitigate carbon emissions by permanently storing the CO_2. Consequently, the plume and pressure areas for EOR projects are more compact with a much smaller Area of Review, which limits the complexity of areas to be monitored. Still, they are both regulated by the EPA under the UIC program and will have transferrable insights.

2.3 Injectivity

It is established that an ideal site selected for a carbon sequestration project would have several key characteristics: capacity, containment, and injectivity (Birkholzer, 2009; NETL, 2010; Celia et al., 2015; Krevor et al., 2023). The issue of storage capacity deals with determining the amount of volume that can be stored, containment is concerned with how securely the injected CO_2 can be stored to prevent leakage, and injectivity pertains to the ability of the formation to efficiently receive the fluid. This study focuses solely on injectivity which has two defining characteristics – permeability and rate.

While these two variables are highly correlated, it is important to recognize they do not inherently signify each other, underscoring the significance of thoroughly analyzing injectivity. In this thesis, the primary source for this quantification will be through pressure falloff test reports.

2.3.1 Pressure Transient Analysis

Pressure Transient Analysis (PTA) is the analysis of pressure change as a function of time in a controlled environment. It is a well-established practice, long used by professionals in the oil and gas industry, which enables calculation of reservoir characteristics representative of dynamic properties (EPA, 1998; Chaudry, 2004). There are many different types of PTAs such as interference tests which require a remote and receptor well, or step rate tests which are primarily used to evaluate fracture pressure (EPA, 1998) but the PTA of interest in this study are pressure falloff tests. These tests are conducted by pumping water into the well and then analyzing the pressure drop following cessation of injection. Not only are they the test used for Class I wells, but they have been historically used for monitoring purposes in CCS projects with applications to detect potential leaks, track the dry-out zone, and monitor the reservoir pressure (Abdelaal & Zeidouni, 2020; Gupta et al., 2020).

Falloff tests are similar to pressure buildup tests used in oil and gas and allows derivation of transmissibility, skin factor, records of both flowing pressure and static pressure, and notice of any boundary effects (EPA, 2002; Gupta et al., 2020). This continued monitoring of the reservoir and the pressures also provides assurance that the fluid has not migrated during its operation.

Analysis of falloff test procedures for Class I wells are summarized in *UIC Pressure Falloff Testing Guideline* (EPA, 2002). The report should include a cartesian plot, log-log plot, and a semi-log plot. The cartesian plot shows time and pressure from 48 hours prior to shut-in up to the end of the test. The log-log plot is a semi-log derivative vs. elapsed time (Δt) plot that identifies the different flow regimes from the pattern of the slope of the pressure derivative. The test is finished when the derivative plot plateaus to a horizontal slope, signifying the radial flow period as shown in the middle-time region in Figure 2.4.

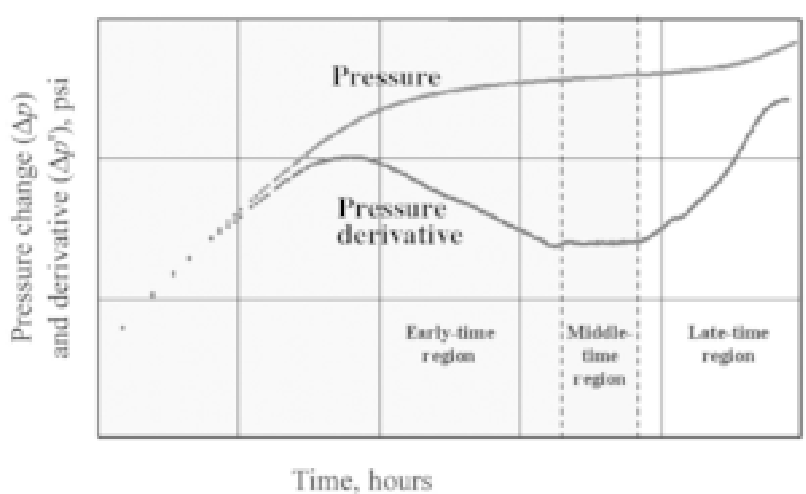

Figure 2.4 Diagnostic plot showing log-log graph of a pressure fall off test (EPA, 2002). The period of interest is the Middle-Time Region with a horizontal slope, which indicates radial flow.

Radial flow means that the pressure response has reached the end of the waste plume, has a constant change in pressure over time, and is reflecting pressure response from the reservoir as it is behaving as though it is 'infinite'. Then, the semi-log plot is used for the actual analysis of reservoir properties. There are four different semi-log plots that are used for diagnosis (Miller et al., 1950; Horner, 1951; Agarwal et al., 1970; EPA, 2002):

1. Miller Dyes Hutchinson (MDH) Plot
2. Horner Plot
3. Agarwal Equivalent Time Plot
4. Superposition Time Plot

The MDH plot is used when the pressure response has reached all of the boundaries and is a pressure vs. log (Δt) plot. The Horner plot is used when the injection rate before the shut in of the well test was constant and is a pressure vs. log $((t_p + \Delta t)/\Delta t)$ plot where t is time and t_p = (*injection volume since last pressure equalization*)/ (*rate of injection*) or the time of shut-in. The Agarwal equivalent time plot is similar to the Horner plot but it is a pressure vs. log $((t_p \cdot \Delta t)/(t_p + \Delta t))$ and is used when the injection period is very short compared to the total falloff. The superposition time plot accounts for variations in the injection rate prior to falloff. It is the most robust, but also the most rigorous, and usually requires software. The time function is $\sum_{j=1}^{n} \frac{q_i - q_{i-1}}{q_n} \log(t_i - t_{i-1})$. The most used of these is the Horner plot (EPA, 2002).

Using one of these functions, the slope of a straight line of the semi-log plot can be used to calculate variables such as the transmissibility, permeability, skin, and injectivity when combined with the pressure measurements taken during the well test.

2.4 SETTING

The structure of the Gulf Coast in the study area dips gulfward influenced by a complex interplay of sedimentary processes, sea level fluctuation, tectonic activity, and drainage basin evolution. These features materialized in regions where substantial sediment deposition occurred along an unstable, muddy continental margin. The gravitational force caused by rapid loading resulted in the development of growth faults, which progressively traversed upward through sedimentary layers as additional sediment accumulated, resulting in the down-to-coast faults seen today (Galloway et al. 2011).

This thesis is specifically focused on the Oligocene and Miocene intervals that emerged during the Cenozoic depositional episodes. They are the target zones seen in all of the Class I permits in this thesis and hold significant interest for Class VI projects. Figure 2.5 shows major stages of sediment accumulation during this period.

Within the permits themselves, operators specify the injection formations by stratigraphic unit and for Oligocene wells, this includes the Frio, Vicksburg, Anahuac, and Catahoula (which the Catahoula formation in Texas was confirmed to be the equivalent of Vicksburg and Frio (Galloway, 1977; Baker, 1978)). For Miocene wells, this includes the Oakville formation. In the context of this thesis, injection wells will mostly be divided between those that injected into the Oligocene or Miocene formations.

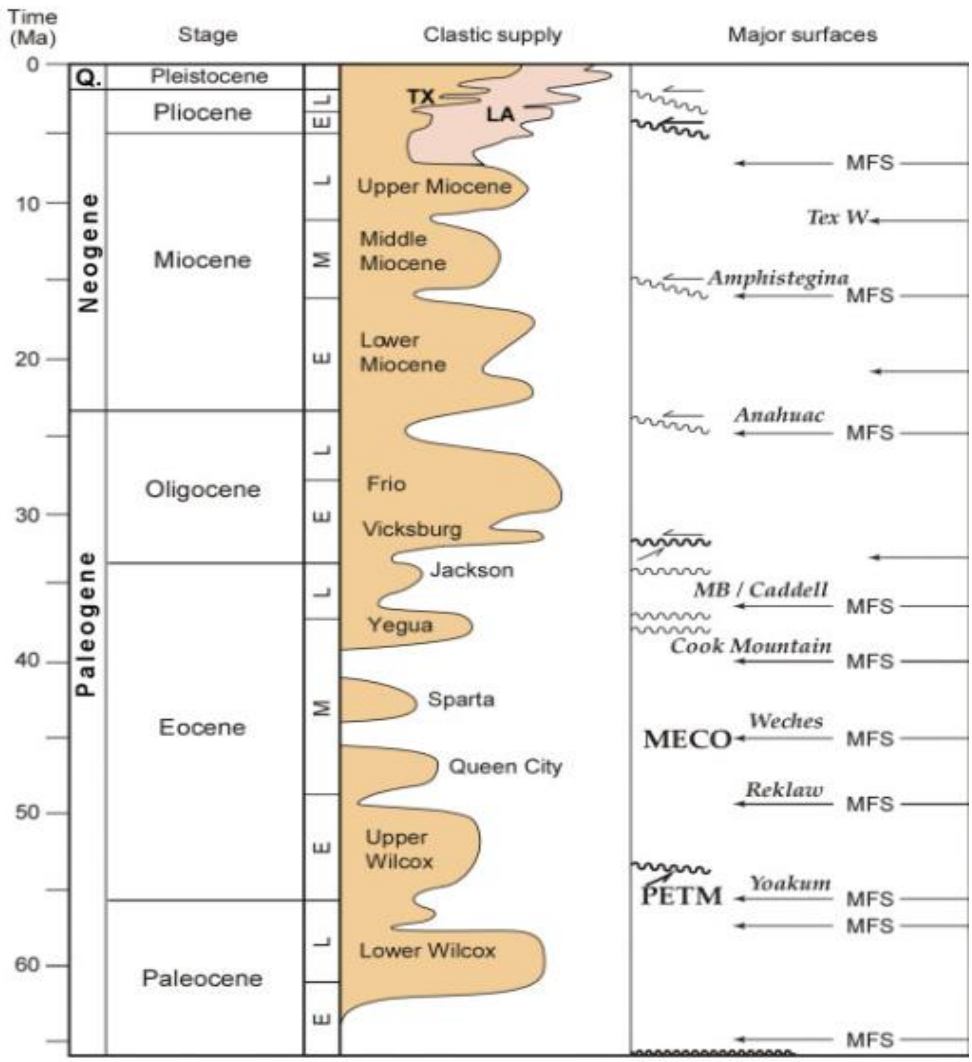

Figure 2.5 Modified from Ewing & Galloway (2019). Cenozoic depositional episodes showing major phases of sediment accumulation in the Northern Gulf of Mexico basin, Maximum Flooding Surfaces (MFS). PETM: Paleocene-Eocene Thermal Maximum. MECO: Middle Eocene Climatic Optimum. MB: Moodys Branch.

The Frio and underlying Vicksburg deposition was marked by sediment influx caused from regional uplift and volcanic activity and is one of the great progradational wedges in the Gulf Coast (Ewing & Galloway, 2019). Sea level loss, decrease in sediment supply, and the deposition of the Anahuac shale from marine transgressive flooding mark the end of the Oligocene-Frio deposition (Galloway et al., 1982).

The Miocene was deposited during fluctuating sea levels with alternating successions of sand and shale. These units are structurally thick, are marked by quartz-rich sands, has thickening intervals into salt-withdrawal basins, and the rapid deposition from deltaic sediments gave way to growth faults and salt movement out of the withdrawal basins (Galloway et al., 1991; Ewing & Galloway, 2019).

Bump et al. (2021) uses a systematic approach to translate the geologic history and knowledge of the depositional environments to determine the chance of success for different formations. Key factors include defining injection zone and confining systems determine the goodness of a reservoir for the purpose of CCS. Figure 2.6 and Figure 2.7 show the results for Oligocene and Lower Miocene reservoirs.

Beyond the geologic suitability of this area for Class VI projects, it is also located near many industrial sources of CO_2 and has a history of low risk of seismic activity, which especially make it an area of interest for CCS projects. The long history of hydrocarbon production allowed for characterization of the area which has shown that many sand bodies in the region are highly porous, capable of trapping fluids, and have highly ductile shales that are able to deform and prevent vertical transmission of fluids (Jones & Haimson, (1986) as cited in EPA, 1990). The region’s viability for CCS projects is also evident in the establishment of CCUS projects, as documented by the Clean Air Task Force (2020).

Figure 2.6 and Figure 2.7 shows a summary of locations for Oligocene and Lower Miocene reservoirs that would be well suited for CCS as defined by Bump et al. (2021), locations of all Class I wells found along the Gulf Coast (a fraction of these were analyzed for this thesis), and the Capture Capacity from CCUS projects reported by CATF (2020).

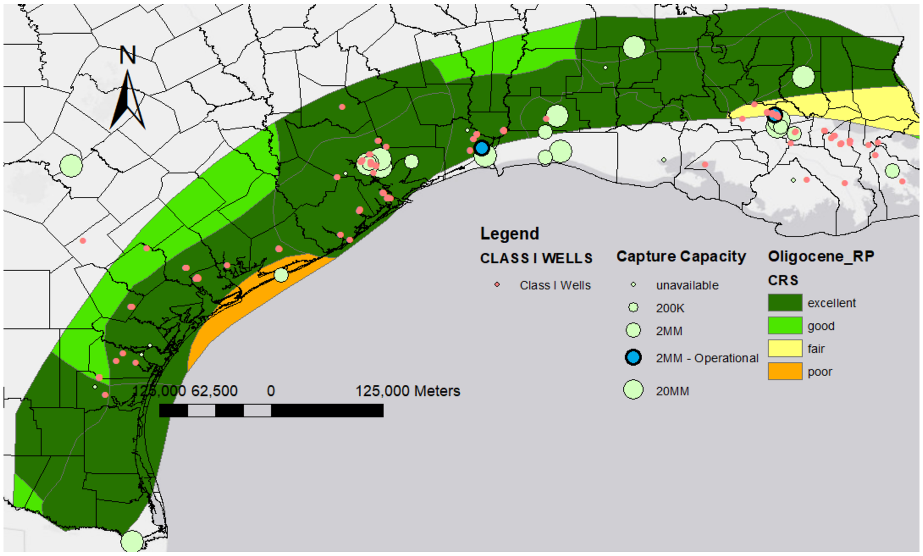

Figure 2.6 Base map shows how good the Oligocene reservoir in different regions would be according to the Common Risk Segment method in Bump et al. (2021). Overlaid are locations of Class I wells. Green bubbles show capture project sites reported in CATF (2020). The two blue bubbles with a dark ring show operational capture projects.

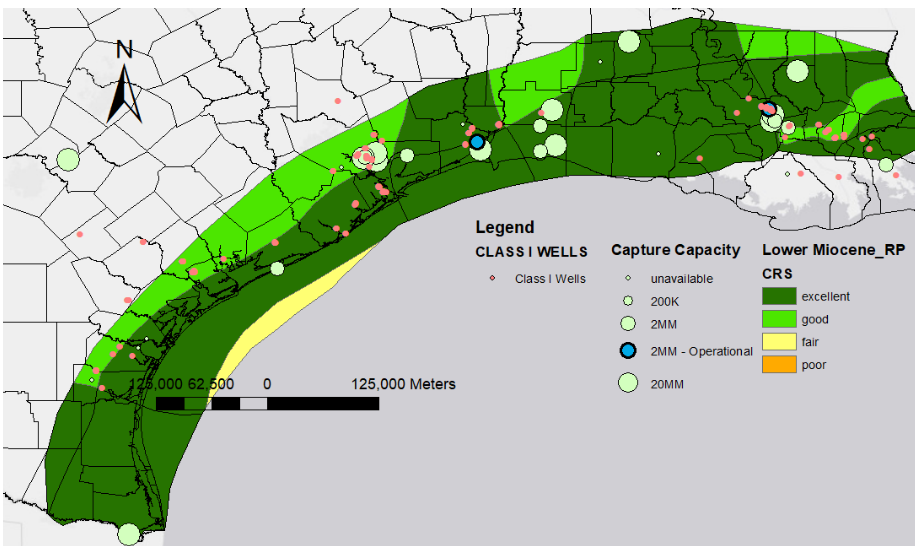

Figure 2.7 Base map shows how good the Lower Miocene reservoir in different regions would be according to the Common Risk Segment method in Bump et al. (2021). Overlaid are locations of Class I wells. Green bubbles show capture project sites reported in CATF (2020). The two blue bubbles with a dark ring show operational capture projects.

3. Methodology

The following section details the methods used in this research. The first part summarizes the process for finding data related to Class I wells with help from the Texas Commission on Environmental Quality (TCEQ) and Louisiana's Department of Natural Resources (DNR). The other sections describe the data collected and process for analysis.

3.1 Data Acquisition

Publicly available online records for Class I wells were found through TCEQ CR Query[1], TCEQ Records Online[2], SONRIS[3], and FOIA[4] (Freedom of Information Act) online under EPA Region 6. TCEQ CR Query had basic information from the permit applications which included: well latitude/longitude, target formation, injection zone depths, maximum permitted rates and volumes, type of injection fluid, current status and other administrative details. TCEQ Records Online mostly showed the record of the types of documents available with only a few downloadable reports. These documents included: correspondences, injection reports, permits, commercial well self-reporting data, inspection reports, operation reports, State Office Administrative Hearings (SOAH), Mechanical Integrity Tests (MIT), operation reports, and annual injection reports. FOIA online releases all documents that have been requested by others, but as a result, access is limited to what has been previously requested.

The available information online however, lacked the level of detail that was of interest in this study, and therefore this work required direct contact with state agencies to

---

[1] TCEQ CR Query. https://www15.tceq.texas.gov/crpub/index.cfm?fuseaction=home.welcome
[2] TCEQ Records Online: https://www.tceq.texas.gov/agency/data
[3] SONRIS: https://www.sonris.com/
[4] FOIA: https://foiaonline.gov/foiaonline/action/public/search/quickSearch

retrieve specific documents. The Injection and Mining Division with the DNR were already in the process of digitizing their records and provided access to the documents they have already digitized. These included the basic permit information (location, depth, etc.), well logs, falloff test, and well history documents, but mostly, there was a heavy concentration of the most recent operation reports. With the TCEQ, Public Information Requests were submitted to Central File Rooms (CFR) to receive documents, which can take a couple weeks for a single active permit.

Beginning with the initial permit application, additional documents are progressively incorporated over time. These encompass site descriptions, correspondences, public engagement, completion reports, site tests (core tests, log analysis, falloff tests), notice of deficiencies, final permit itself, as well as ongoing revisions that must be provided throughout the well's lifespan. These continuous updates include quarterly and annual injection reports, mechanical integrity tests, updates on new wells in the AOR, and more (40 CFR§146, TAC§331, La. Admin. Code tit. 43, § XVII). Additionally, most submissions are in paper - though some older copies (prior to the 80s) are on microfiche or floppy disks - which adds time to the process of digitizing said copies. A recent change, however, requires a flash drive version to be submitted with the permit, but this still means many of the older wells have decades worth of data sitting in rubber-banded stacks in the file rooms.

Because there was limited time to request and receive this data through CFR, for most of this study, files were viewed in person within the Radioactive Materials Division's office at TCEQ which contains the most recent version of the permits that are also currently active. This was allowed largely due to the existing relationship between TCEQ and the Bureau of Economic Geology, and around two dozen permits were viewed over a period of around six months. By only viewing the active permits however, older permits which may offer insights into wells that either had to be discontinued due to decreased injectivity or unsuitable geology may not be represented. Additionally, while CFR continuously receives operational and MIT reports, the renewed permit applications themselves do not always contain those details. A summary table may be included, but they range from reporting all values, including the injection pressures, rate, duration, etc., to only including the final calculated values necessary for comparison with their models. Similarly, while they may incorporate the original version of core test reports, they may also simply reference them as necessary to justify modeling inputs for porosity or permeability.

3.1.1 Permit Sections

To gather information that would be most applicable to geologic storage projects, the following information was collected: (1) Core tests, (2) Well logs, (3) Fall off Tests, (4) Formation Fluid Analysis, (5) Volume of fluid injected, and (6) Historical pressure rise. These were found within the geology, reservoir mechanics, and wastes and waste management sections. Full reports of falloff tests were found through a mix of online searches and through CFR.

The geology section provides descriptions of the local and regional geology, hydro-stratigraphy, depths of the USDW, regional faults, sands tops and thicknesses, surface and contour maps, well logs, mineralogical descriptions, seismic risk analysis, and sometimes, the core tests. The reservoir mechanics section details any information used for modeling purposes, which includes: formation fluid analysis, historical pressure increases, core tests (sometimes), yearly volumes injected (rarely), and results from injection fall-off tests. These test results are used to determine “the reservoir fluid pressure, fracture pressure, transmissibility, permeability, faulting or other boundaries, dual porosity, skin factor, completion anomalies, and other physical and chemical characteristics of the injection zone" (TCEQ, 2021, p.34). Finally, the waste management section contains descriptions of the type of fluid as well as the cumulative volume injected throughout the life of the well.

3.2 DATA SOURCES AND INTERPRETATION

Two important characteristics analyzed are permeability and injectivity. Permeability values are available at different resolutions i.e., core-scale, log-scale, field-scale. Values were then upscaled to see how well the field-scale permeability (from falloff tests) values can be predicted given the data from core samples and well logs.

Injectivity is analyzed by calculating the Injectivity Index from values measured during the falloff tests. This data will then be used to predict possible CO_2 injection rates.

3.2.1 Upscaling Permeability

Upscaling describes a process of substituting a fine-scale region with a single value grid cell approximated by averaging values which in this study, means using cores and well logs to approximate field-scale reservoir properties. Cores and well logs are limited to near wellbore properties with high vertical coverage while the opposite is true for well tests, which have a limited vertical coverage representative of a larger lateral space (Ma, 2019). The resolution from each dataset also widely varies from just a few centimeters (cores) to 1000s of meters (well logs) to kilometers (well tests). Particularly difficult to extrapolate and average due to formation heterogeneities and anisotropy is the permeability, which describes a rocks ability to allow fluid to flow and can only be directly measured from core plugs or be derived from well tests (Christie, 1996; Society of Petroleum Engineers, 2015; Ma, 2019).

Upscaling from a core to a well log requires porosity-permeability data from multiple core samples to find a relationship, typically log-linear (Adams, 2005). This can then be used on the well log to estimate permeability by using the log derived porosity values at suitable depths. Then, permeability can be upscaled from the log-scale to the field-scale. At this scale however, the simple log-linear relationship does not hold well since upscaled-permeability will be affected by geology and flow direction which requires identification of different geologic features and facies (Ma, 2019). However, once different zones are identified, average values can be taken to estimate permeability. There are three main methods of averaging for upscaled permeability as described by (3.1), (3.2), and (3.3).

$$Arithmetic\ Mean = \frac{x_1 + x_2 + \cdots + x_n}{n} \tag{3.1}$$

$$Geometric\ Mean = \sqrt[n]{x_1 x_2 \ldots x_3} \tag{3.2}$$

$$Harmonic\ Mean = \frac{n}{\frac{1}{x_1} + \frac{1}{x_2} + \cdots + \frac{1}{x_n}} \tag{3.3}$$

Of these, the geometric mean is best fit to estimate effective permeability with no obvious preference for a direction of flow, the arithmetic average tends to provide an overestimation of the permeability but may be suitable for lateral flow where there is horizontal bedding, and the harmonic average may underestimate the permeability but may be suitable for describing vertical flow. (Qi, 2004; Ma, 2019). To verify permeability at the field-scale however, well tests need to be used, which will be provided in the Class I permit falloff tests.

3.2.1.1 Upscaling from Dataset

Compiling the data from core test reports on porosity, permeability, and depth of the samples, histograms and depth plots were created to visualize the mean and variance of the samples as well as the vertical heterogeneity of the sand intervals where samples were taken. Additionally, log-linear cross-plots were created to relate porosity to permeability. Although cores are reported separately for each well, in this thesis, they were grouped together if cores were pulled from the same injection zone in a specific geographical region. For example, in Figure 3.1, three wells injecting in Calhoun County into the same injection zone in different sand intervals are treated as a single cluster to run a regression on log (permeability) vs. porosity.

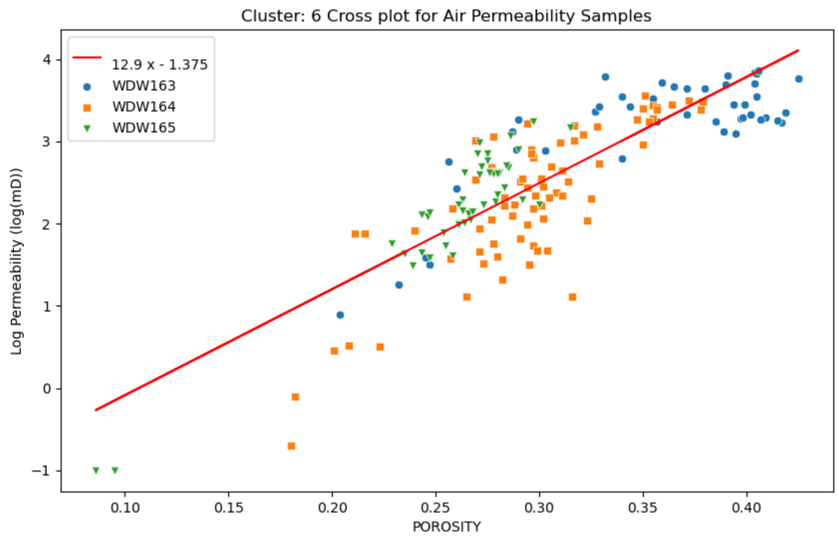

Figure 3.1 This Porosity-Permeability plot shows the logarithm of permeability (mD) on the y-axis and porosity on the x-axis. This example shows values gathered from three separate wells, and the linear regression equation is run through all three datasets.

Although some well logs were available online, majority of the well logs in this study were available on paper at the TCEQ. These wells do not have the standard identifications from API numbers as they are a different class of well than oil and gas producers. Because of this, pictures had to be taken of the logs and were sent to Well Green Tech Inc. for digitization. The resulting LAS files of the logs were loaded into Jupyter

Notebook and were analyzed using various Python packages, but predominantly include Lasio, Pandas, NumPy, SciPy, and Seaborn.

Upscaling permeability from core to well log applies the regression described above to predict permeability based on the well log porosity – typically derived from neutron/density logs. Unfortunately, those tracks were rarely included in the permit renewals; however, the resistivity logs were almost always included, so those were used to estimate porosity. To validate assumptions made in making this transformation, permits which contained the neutron/density tracks were first interpreted. Then, resistivity logs were transformed to porosity and compared to the 'real' values in order to test the model. Estimation of porosity from neutron/density requires calculation of the shale volume (C_{sh}), correction of the density and neutron logs (ϕ_D^c , ϕ_N^c), and estimation of a single porosity value (ϕ_e) as shown in (3.4) – (3.7) (Schlumberger, 1969; Asquith & Gibson, 1982; Dewan, 1983; Moradi et al., 2016).

$$C_{sh} = \frac{GR - GR_{clean}}{GR_{shale} - GR_{clean}} \tag{3.4}$$

C_{sh} = Concentration of Shale

GR = Gamma ray reading from the depth of interest

GR_{clean} = Gamma ray reading from the zone considered to be clean sand

GR_{shale} = Gamma ray reading from the zone considered to be pure shale

$$\phi_D^c = \phi_D - C_{sh}\phi_{D-sh} \tag{3.5}$$

$$\phi_N^c = \phi_N - C_{sh}\phi_{N-sh} \tag{3.6}$$

ϕ_D , ϕ_N = Porosity reading from the depth of interest

ϕ_D^c , ϕ_N^c = Shale corrected porosity

ϕ_{D-sh}, ϕ_{N-sh} = Porosity reading from the zone considered to be pure shale

$$\phi_e = \frac{\phi_D^c + \phi_N^c}{2} \tag{3.7}$$

ϕ_e = Porosity corrected for clay presence in pore space

After calculating the porosity from Neutron and Density logs, they were used as a control to test the validity of models which derives porosity from alternative well logs. Resistivity logs and Gamma Ray logs were used as a proxy to make estimations of porosity when applicable. For Resistivity transformations, estimations used the general form of Archie's equation, modified by Winsauer, as shown in (3.8) – (3.9) (Archie, 1942; Winsauer et al., 1952).

$$S_w{}^n = \left(\frac{a}{\phi^m} \times \frac{R_w}{R_t}\right) \tag{3.8}$$

S_W = Water saturation

a = Tortuosity factor (Winsauer's multiplier)

ϕ = Porosity

m = Cementation exponent

R_w = Electrical resistivity of water in Ω m (Ohm-m)

R_t = Electrical resistivity of a fluid-saturated rock

n = Saturation exponent

The injection zones only contain water, so S_W is assumed to be 1 and was simplified to (3.9) to estimate porosity (Dresser Atlas, 1975; Asquith & Krygowski, 2004).

$$\phi = \left(a \times \frac{R_w}{R_t}\right)^{1/m} \tag{3.9}$$

The only value known from the logs is R_t; however, the resistivity of the water (R_w) can be estimated from formation fluid analysis reports found in the permits, and a and m can be approximated by well-established values commonly used in well log analysis. The variables a and m represent the tortuosity – complexity of a flow path – and the cementation exponent – the cementation/compaction of the rock – and are constants found empirically. However, there are extensive studies done on the applicability of typical values used which include the combinations where a=.81 and m=2 (Schlumberger, 1969) and where a=.62 and m=2.15 (Humble formula). Table 3.1 shows other known combinations (Asquith, 2004).

Table 3.1 Archie's parameters for tortuosity and cementation exponent (Asquith, 2004)

Lithology	**a (tortuosity factor)**	**m (cementation exponent)**
Carbonate*	1.0	2.0
Consolidated Sandstone*	0.81	2.0
Unconsolidated Sandstone*	0.62	2.15
Average Sand	1.45	1.54
Shaly Sand	1.65	1.33
Calcareous Sand	1.45	1.70
Carbonate (Carothers, 1986)	0.85	2.14
Pliocene Sand, southern CA	2.45	1.08
Miocene Sand, TX-LA Gulf Coast	1.97	1.29
Clean, granular formation	1.0	$\varphi^{(2.05-\varphi)}$

** Most commonly used*

The only variable left unknown is the resistivity of water, which was estimated from the salinity of the formation fluid from the brine analysis in the permit (see Appendix F).

3.2.1.2 Formation Fluid Salinity

Formation fluid lab tests report the concentration of ions in milligrams of solute per liter of solution (MPL), which must be converted to find their contribution to NaCl equivalence, and summed to find $NaCl_{ppm}$ to calculate formation fluid resistivity. Dunlap and Hawthorne (1951), Moore et al. (1966), Desai and Moore (1969), and Schlumberger (2009) describe this methodology. First, each ion in MPL was converted to concentration in parts per million (ppm) by dividing by the specific gravity. Then, multipliers were used to find their concentration to NaCl ppm. Several solutions have been proposed, such as the Dunlap Conversion Factors; however; in this study, variable multipliers were used as shown in Figure 3.1. The online tool Ion Multiplier vs. Total Solids Concentration was used to find multipliers (Aptian Technical, 2023).

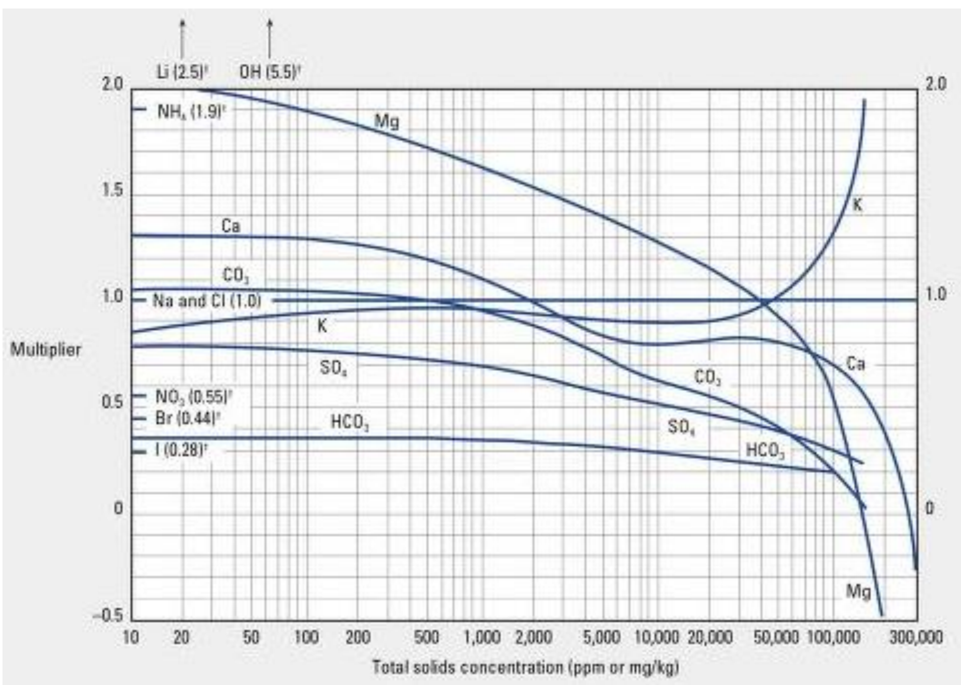

Figure 3.2 Equivalent NaCl multipliers for formation brine ions (Schlumberger, 2009)

Finally, R_w can be estimated using (3.10) which relates salt concentration to a spatial distribution given the temperature. The temperature is either included in the permit or can be estimated from the well log given the depth at which the sample was taken. Then, temperature gradients reported in the permits can be used to generate new temperatures at different depths (Arps, 1953; Bigelow, 1992; as cited in Salazar Luna, 2008).

$$R_w = \left(0.0123 + \frac{3647.5}{[NaCl_{ppm}]^{0.955}}\right)\left(\frac{81.77}{T+6.77}\right) \tag{3.10}$$

R_w= Electrical resistivity of water in Ω m (Ohm-m)

$[NaCl_{ppm}]$ = salt (NaCl) concentration of water in ppm

T= temperature in °F

Other permits reported the total dissolved solids (MPL), and no formation fluid analysis were found, so Figure 3.3 was used to interpolate a PPM value.

ENGLISH/METRIC UNITS

CONVERSION OF PERCENT SALT IN SALT WATER TO PARTS PER MILLION

Per Cent Salt	Parts per Million	Milligrams per Liter
½	5,000	5,020
1	10,000	10,050
2	20,000	20,250
3	30,000	30,700
4	40,000	41,100
5	50,000	52,000
6	60,000	62,500
7	70,000	73,000
8	80,000	84,500
9	90,000	95,000
10	100,000	107,100
11	110,000	118,500
12	120,000	130,300
13	130,000	142,000
14	140,000	154,100
15	150,000	166,500
16	160,000	178,600
17	170,000	191,000
18	180,000	203,700
19	190,000	216,500
20	200,000	229,600
21	210,000	243,000
22	220,000	256,100
23	230,000	270,000
24	240,000	279,500
25	250,000	283,300
26	260,000	311,300

The parts per million column is true parts per million by weight of the salt solution.

It is quite common for many laboratories, analyzing water samples, to report milligrams of salt per liter as parts per million. If it is known that an analysis is reported in this way, the milligram per liter column should be used in converting to percent salt rather than the parts per million column. At low concentrations the error of using the incorrect column is very small. At high concentrations the error is appreciable unless the correct column is used.

Figure 3.3 Salt in Salt Water Conversion Chart from Halliburton Red Book Cementing Data (Halliburton, 2001)

3.2.1.3 Resistivity to Porosity Transformation Model

Having found the variables needed for equation (3.9), porosity can be estimated from the resistivity log. Figure 3.4 shows an example of a well which had density, neutron, and resistivity logs. The variables for a and m were found in the permit, however when not available, a best-fit approach was taken given the three well-established variables shown in Table 3.1. The set of variables which minimized the error when plotted against the core samples was selected.

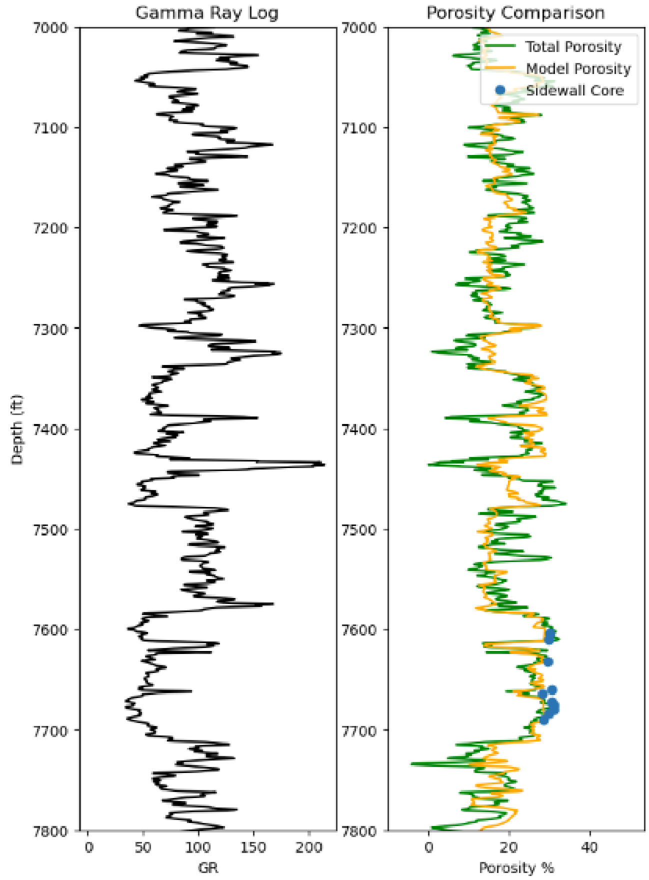

Figure 3.4 Gamma ray (left). Porosity from NPHI/DPHI are in green, porosity derived from resistivity and fluid sample are in yellow (middle). Well with resistivity log transformed to porosity cross-referenced with core samples (right).

3.2.1.4 Gamma Ray to Porosity Transformation Model

In some instances, the available well logs were run after some period of injection, so the resistivity tracks reflect the resistivity of the waste instead of the brine. For these wells, porosity was estimated by using the volumetric shale concentration as a proxy. For example, for a well in Orange County, WDW054 has Neutron and Density tracks, and porosity was estimated using (3.4) - (3.7). Assuming a linear relationship between the concentration of shale and porosity, the relationship was then applied to other wells with gamma ray logs as shown in Figure 3.5. Shale concentration (Csh) is on the x-axis and the porosity estimated from NPHI and DPHI tracks are on the y-axis.

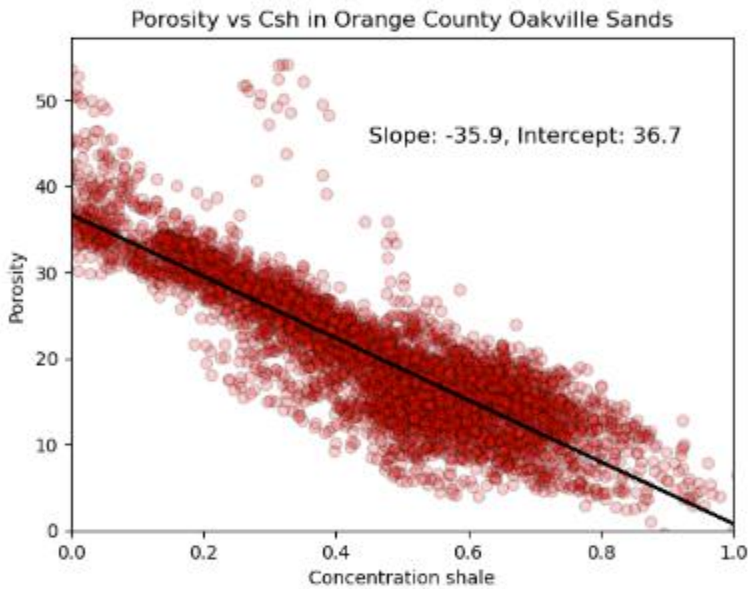

Figure 3.5 Linear relationship between Porosity and Shale Concentration is used to estimate porosity for wells which have Gamma Ray logs.

Assuming the relationship between shale content and porosity in one location is similar to another location in the general area, the linear equation was applied to WDW191. Figure 3.6 shows the porosity estimations from using the resistivity transformation and using the shale concentration conversion. The resistivity track between 6050-6330 ft shows an unexpectedly high value due to the injected waste, and the resistivity transformed porosity using Archie’s law shown in yellow fails. So, the porosity estimated from shale concentration shown in green was used.

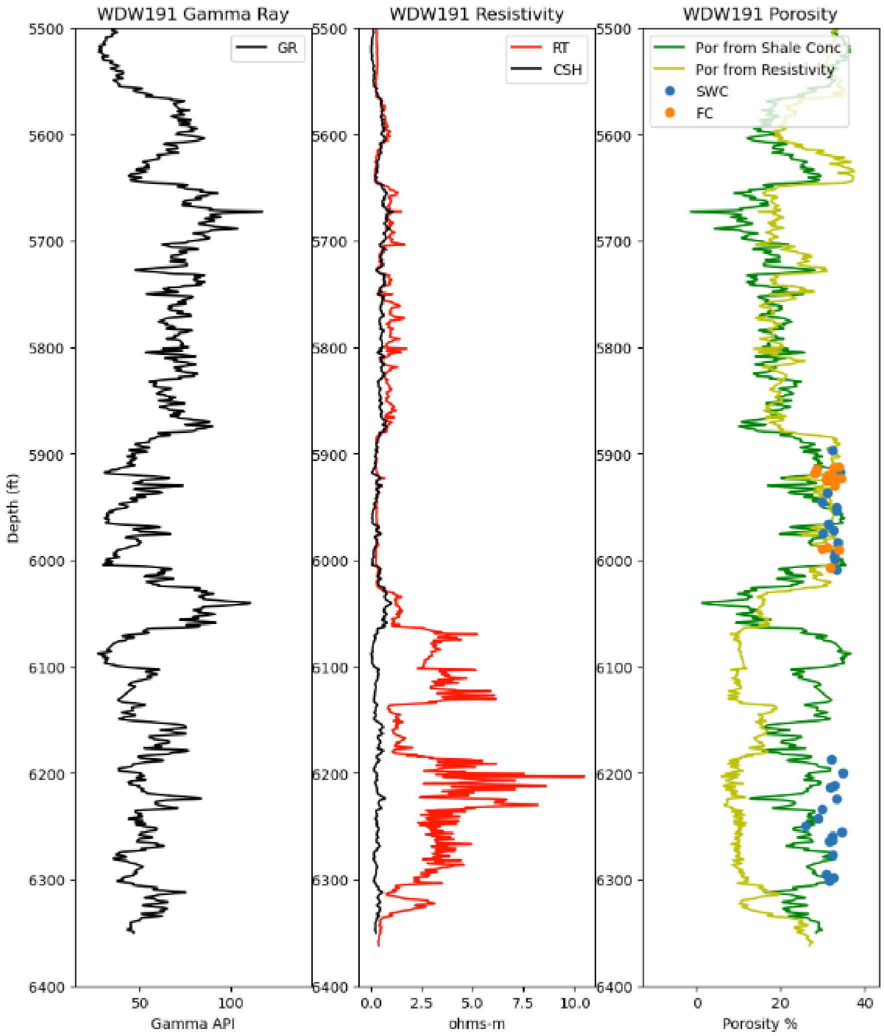

Figure 3.6 Example shows well log where the resistivity log values between 6050-6330 ft reflects the injected wastewater instead of the formation fluid. Since Archie's relationship is not applicable, the Gamma Ray log is used to estimate porosity, which is shown in green in the far-right plot.

For other logs where there seemed to be an anomaly in the resistivity without a nearby well with a shale concentration to porosity conversion, sklearn's LinearRegression was used to predict a new resistivity value based off of gamma ray logs. These areas were identified due to the lack of fit to core samples or due to abnormally high porosity values (greater than 50%).

Once porosity logs were created, the permeability was calculated on sand zones assuming a cutoff value of gamma (API) < 50. For the logs where there were no gamma logs, nearby wells were used to find the range of resistivity values which correspond to the gamma (API) < 50 condition. Then, resistivity cutoffs were used to find the sand intervals.

After porosity values for the well logs were found, the core cross-plot regression is applied to find permeability values. Then, a geometric average was taken over the interval of interest to compare to the permeability values derived from the falloff tests.

3.2.1.5 Falloff Test Analysis

Finally, permeability from falloff tests were gathered over the course of many years. First, several wells with raw data from the test were selected to confirm the validity of the reported values. Figure 3.7 shows a test for WDW148 calculating the slope of the radial flow period.

The estimated slope m from the Horner Plot is 3.7052 psi/cycle compared to the slope (m) of 3.5794 psi/cycle reported from the superposition plot. This difference can be explained by the fact that the report used a more sophisticated software that accounted for the possible variations in flow rate. Having confirmed similar analysis of the test when compared to what was reported in the report for several wells, all future falloff test reports were assumed to be accurate with no further analysis.

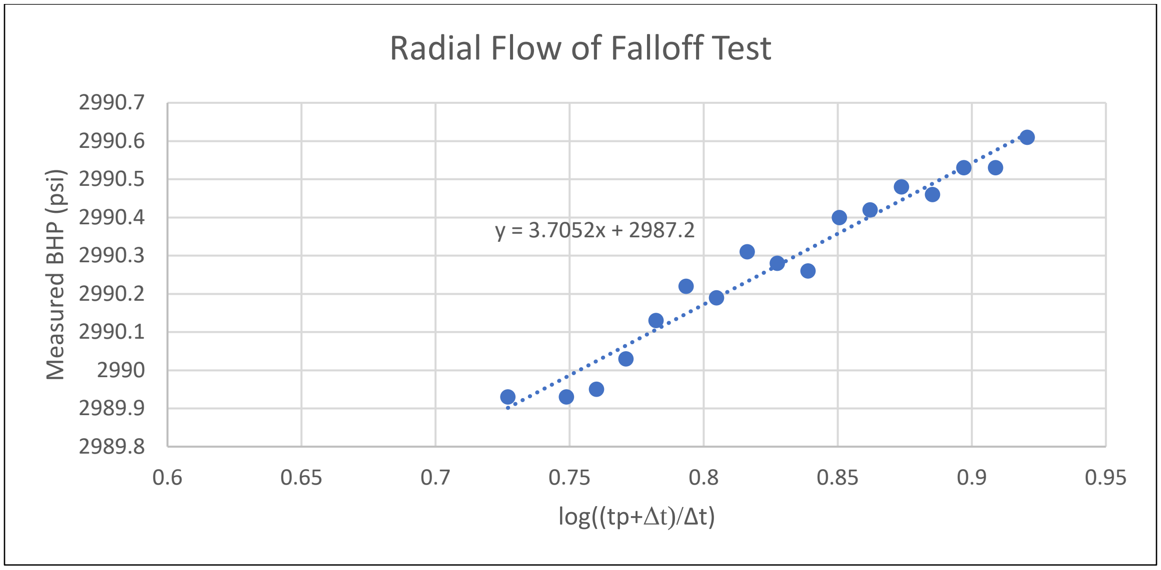

Figure 3.7 Slope (m) of the radial flow period for WDW148

Using the slope (m), and measured data points from the falloff test, transmissibility, permeability, skin, and the injectivity index are calculated. The equations used are summarized in (3.11) – (3.17) (Horner, 1951; Hasan & Kabir, 1983; Ramey, 1992, EPA, 2002) and Table 3.2 outlines the nomenclature.

Table 3.2 Nomenclature

μ	Viscosity	cp	s	skin	-
B	Formation Volume Factor	STB/bbl	ϕ	porosity	-
c_t	Total compressibility	1/psi	r_w	Well radius	ft
h	Height	ft	r_e	Drainage radius	ft
t	Transmissibility	md-ft/cp	V	Volume	bbls
k	Permeability	md	m	Slope of radial flow	psi/cycle
P_{1hr}	Pressure 1 hr after shut-in	psi	II	Injectivity Index	bbl/psi/day
P_{wf}	Flowing Bottomhole Pressure	psi	P_{BH}	Static Bottomhole Pressure	psi

$$t = \frac{162.6qB}{m} \tag{3.11}$$

$$k = \frac{t\mu}{h} \tag{3.12}$$

$$s = 1.1513\left[\frac{P_{1hr} - P_{wf(\Delta t=0)}}{m} - \log\left(\frac{k}{\phi\mu c_t r_w^2}\right) + 3.2275\right] \tag{3.13}$$

$$II = \frac{kh}{141.2B\mu(ln\frac{r_e}{r_w} + s)} \tag{3.14}$$

$$II = \left|\frac{q}{(P_{wf} - P_{BH})}\right| \tag{3.15}$$

3.2.2 Injectivity Index

The Injectivity Index (II) is described by (3.14) and (3.15) and describes the capacity of a stratigraphic interval to accept fluids. It measures fluid rate as a function of pressure buildup which is dependent on variables such as permeability, thickness of pay, size of reservoir, and formation damage.

II is most commonly calculated with (3.15) as rate and pressure data is more readily available, but (3.14) can be used in substitution if the variables are known with the assumption are that there is radial steady-state flow (Guo et al., 2008; Mishra et al. 2016; SPE, 2016; Valluri et al. 2021).

II is calculated from every falloff test gathered. Since these tests are annually performed, trends can be observed through time regarding the formations ability to accept fluid. Figure 3.8 shows an example of a well with over 20 years of falloff test data located in Calhoun County. It should be noted that although the first available test is in 1993, this well was in service since 1982, before it was required to regularly perform well tests. This is the case for many of the wells, and the first data point does not reflect the II in the first year of service.

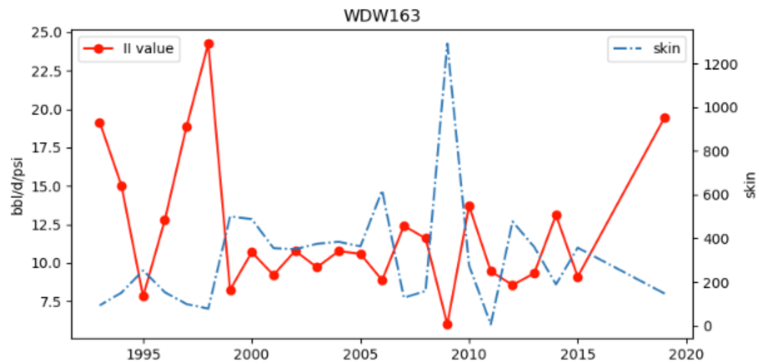

Figure 3.8 II value showing rate as a function of pressure buildup from the falloff test (red) and skin factor, which shows near wellbore damage which may hinder fluid flow and contribute to a lower II value (blue)

3.2.3 Hypothetical CO_2 Injection Rates

Approximations of possible CO_2 injection rates will use simple volumetric and density conversions from water to supercritical CO_2 assuming water is incompressible Water compressibility does technically change depending on temperature and pressure, but the impact is minimal (~1.8 % change at 2mi deep (Speight, 2020)), and it is a commonly accepted practice to neglect the formation volume factor of water i.e. B_w = 1 RB/STB. (Schlumberger, n.d.). The following conversions were used.

- 1psi = 0.00689476 MPa
- 1bbl = 0.1589872956 m3
- Bw = 1 RB/STB
- Density of supercritical CO_2 = 700 kg/m3
- 1kg = 0.001 metric ton

$$\frac{bbl}{day \cdot psi} \cdot \frac{1\ psi}{0.00689\ MPa} \cdot \frac{0.159\ m^3}{1\ bbl} \cdot \frac{700\ kg\ CO_2}{m^3} \cdot \frac{0.001\ ton\ CO_2}{1\ kg\ CO_2} \cdot \frac{365\ days}{1\ year} = \frac{ton\ CO_2}{year \cdot MPa}$$

Using this method of conversion, several cases of potential CO_2 rates are evaluated under different assumptions.

Case 1 considers a minimum rate case from the historical volume of water injected into these wells. Most permits only report a single cumulative injection value from the start of the well's service to the date of the permit renewal. Therefore, this not only represents the minimum case scenario as it reflects the actual documented values, but it also includes the days or even weeks where the well was inactive or was shut down for maintenance or other tests. Additionally, many wells inject as needed, not at maximum capacity, so the hypothetical values estimated in this scenario represents a significantly conservative value.

Case 2 aims to account for the highest rates observed during operations. However, due to incomplete data collection from the permits, the maximum rate is determined based on selecting the higher value between the two rates: (1) maximum rate from the falloff tests and (2) maximum annual injected volume, if available. Note that falloff tests only need to inject at a rate that is enough to show a pressure buildup for the well test and is not necessarily a high rate injection test.

Case 3 uses the average of the calculated II values from the falloff test and sets the flowing bottomhole pressure to 90% of the fracture pressure as is the limit according to Class VI regulations (75 FR 77257). This method rearranges the linear relationship shown in (3.15) to solve for q by analyzing the rate allowed by a maximum pressure differential for a given injectivity (Burke, 2011; Ni, 2021).

Case 4 will neglect the effect of skin (near formation damage) that reduces the injectivity. Pressure drop from the skin can be calculated from (3.16) where *m* is the semi-log plot slope and *s* is the skin (Lee, 1982, pg. 32). This will result in a much higher injectivity than the observed values since the pressure drop will be less, and using the new II value (3.17), a new rate will be calculated assuming the pressure drop observed in the falloff test had no influence from skin effects (see Table 3.2 for nomenclature).

$$\Delta P_{skin} = 0.868 \cdot m \cdot s \tag{3.16}$$

$$II = \frac{q}{(Pw_f - P_{BH} - \Delta P_{skin})} \tag{3.17}$$

$\Delta P_{skin} = pressure\ drop\ caused\ by\ near\ wellbore\ skin\ effects\ (psi)$

Case 4 accounts for the pressure drop due to skin in addition to setting the bottomhole pressure to the maximum allowed differential, combining Case 2 and 3. It is a possible maximum rate scenario representing a scenario in which there is no near wellbore damage at the maximum allowed pressure increase.

3.3 Sources of Error

Most of the data collected had to be hand typed into a database, so there may be book-keeping errors in simply typing in the wrong information.

The quality of well logs were often poor and since many permits were viewed in person, there may be errors due to poor photography, resulting in lower quality digitization. Also, estimations of porosity from the resistivity log as described in Section 3.2.1 required assumptions that may not perfectly encapsulate petrophysical properties.

The collected information often represents the best available data, not its entirety. For example, if a well in this study has only a single year's falloff test, it is because that is all that was able to be viewed, not all that is available. Others examples include:

- Data for cumulative volumes injected representing the date as of the most recent permit renewal, not the current year for which data exists.
- Average rates describing a cumulative volume over the total lifespan which includes periods where the well was not in operation for workovers, tests, etc.
- Estimations of *II* from falloff tests when pressure measurements were absent.
- Estimations of bottomhole pressure from wellhead pressure measurements. It was also noticed that while some final reports contain friction loss corrected pressure measurements, others kept the original pressure readings without incorporating the friction loss. Values were recalculated where there was a discrepancy to ensure that the II and skin values used the friction loss corrected pressures.

Filling in gaps for or working around missing data was also an ongoing issue which may result in inaccurate representation when making data comparisons across different scales.

3.3.1 Adjustments for Injectivity Index

When transmissibility values were reported in the permits without further details about the flowing and static pressures from the falloff test, II was estimated with (3.14) where $II = \frac{kh}{141.2B\mu(ln\frac{r_e}{r_w}+s)}$. Transmissibility equals kh/μ (see eq. 3.11) and B_w is assumed to be 1, which leaves the unknown variables re, rw, and s. Different ranges of $\frac{r_e}{r_w}$ and s were used in a sensitivity analysis for several to see if assumptions can be made to estimate the injectivity index. Ranges for the two unitless values were made for a well where all variables were known. The base case values extrapolated from this well were $\frac{r_e}{r_w}$ = 9221 and s = 19.3. Ranges for $\frac{r_e}{r_w}$, assuming that the drainage radius is significantly larger than the wellbore radius (re>>rw), varied from 2500 to 25000 and skin ranged from 10 to 30.

As shown in the tornado chart in Figure 3.9, the injectivity index is highly sensitive to the skin, so when values of the skin were unknown, assumptions were not made. However, the injectivity index is not very sensitive to values of $\frac{r_e}{r_w}$. As shown in the tornado chart, for wide ranges for re/rw, the difference in II is minimal (about .2 bbl/d/psi) so when applicable, a constant of 10000 was assumed. This was shown to be a conservative value when tested against multiple wells where pressure values were known.

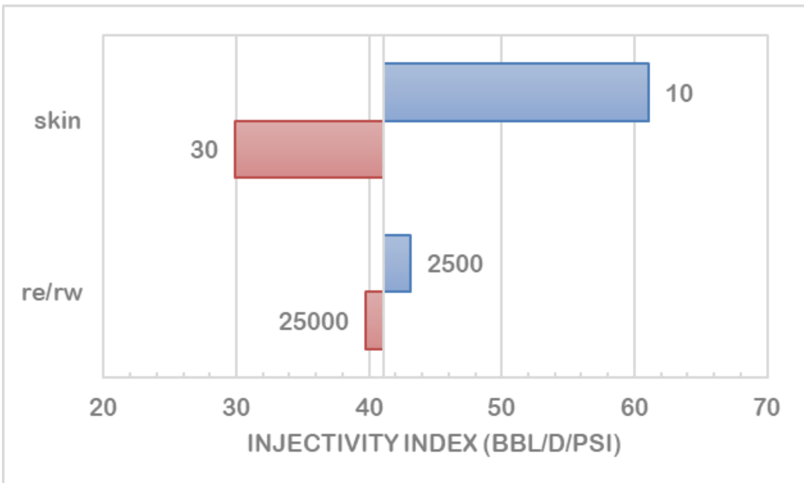

Figure 3.9 Sensitivity Analysis for II

3.3.2 Adjustments for Wellhead Pressure Measurement Adjustments

Though bottomhole measurements are much more common and are encouraged by the EPA during falloff tests, it is not a requirement, and some pressure readings report the wellhead gauge readings. To determine the bottomhole pressure, the pressure drop due to friction within the pipe must be calculated. This was determined using Hazen-Williams equation as shown in (3.18), which estimates the loss of height (head) of the liquid in a pipe (Williams & Hazen, 1905; Westaway & Loomis, 1984; LMNO Engineering, 2023).

$$h = 0.002083 \cdot L \cdot \left(\frac{100}{C}\right)^{1.85} \cdot \left(\frac{q^{1.85}}{d^{4.8655}}\right) \tag{3.18}$$

$h = head\ loss\ of\ liquid\ (ft)$

$L = length\ of\ pipe\ (ft)$

$C = friction\ factor$

$q = flow\ rate\ (gpm)$

$d = inner\ diameter\ of\ pipe\ (in)$

Various *C* values can be found in Cameron Hydraulic data book where C = 150 is typical for smooth pipes. Using the estimated head loss (*h*) and depth of the injection, the bottomhole static and flowing pressures can be calculated using the pressure reading and fluid gradient.

$$\begin{aligned} P_{wf} &= P_{wh} - P_{fric} + P_{BH} \\ &= P_{wh} - (h \cdot \rho_f) + (Depth \cdot \rho_f) \end{aligned} \tag{3.19}$$

$P_{wf} = flowing\ bottomhole\ pressure\ (psi)$

$P_{wh} = wellhead\ measured\ pressure\ (psi)$

$P_{fric} = pressure\ loss\ from\ friction\ (psi)$

$P_{BH} = static\ bottomhole\ pressure\ (psi)$

$h = head\ loss\ of\ liquid\ (ft)$

$\rho_f = fluid\ gradient\ (\frac{psi}{ft})$

3.3.3 Adjustments for Fracture Gradient

The fracture pressure in these permits is measured using Eaton's Method in (3.20) which describes the fracture gradient as a function of the overburden pressure gradient, reservoir pressure gradient, and Poisson's ratio (Eaton, 1969; Rig Worker, 2023); variables which are all reported in the permits.

$$FG = \frac{(P_{ob} - P)v}{(1 - v)} + P \tag{3.20}$$

FG = fracture gradient (psi/ft)

P_{ob} = overburden pressure gradient (psi/ft)

P = reservoir pressure gradient (psi/ft)

v = Poisson's ratio

Though the fracture gradient and pressure are usually reported in the reservoir mechanics section of the permit, when unavailable or inaccessible, this equation was used to estimate a fracture pressure when evaluating hypothetical injection rates. Overburden and Poisson's ratio was borrowed from nearby wells, and the reservoir pressure gradient was estimated from using the reported static pressure measurements at a given depth.

4. Data and Results

4.1 Summary of Collected Information

For the purpose of condensing the gathered data, wells are grouped into clusters depending on shared geographic location and injection formation as shown in Figure 4.1. An exception is Cluster 15, where wells target the formations in both the Oligocene and Miocene reservoirs. This was left as is since the wells that injected into the Oligocene-Frio formation (WDW188, WDW301, WDW302) had limited data that did not impact analysis on the injectivity. Locations will be referred to by the numbers listed in the legend of Figure 4.1 for the rest of this thesis.

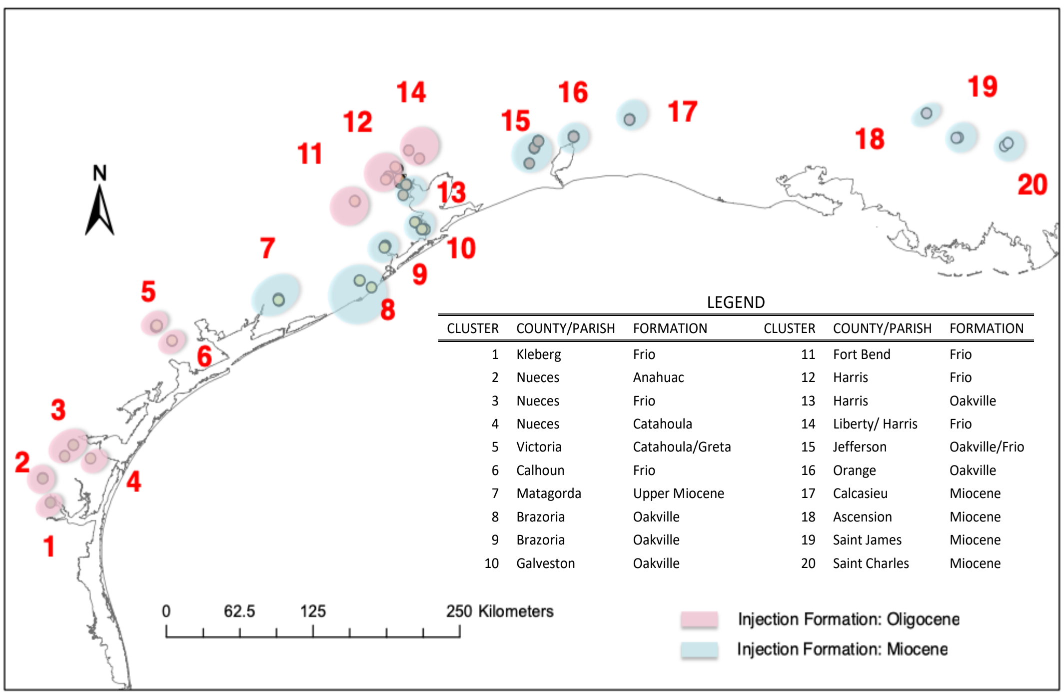

Figure 4.1 Clusters divided by location and the injection formation. The wells highlighted in pink represent injection intervals targeting Oligocene formations and wells highlighted in blue represent injection intervals targeting Miocene formations.

Appendix A contains a table with all the well locations and permit holders. Appendix B details the types of data found for each well as well as injection depths.

4.1.1 Core Porosity and Permeability

Figure 4.2 and Figure 4.3 show the ranges of porosity and permeability found from the core tests. The Seaborn boxplots were altered so the whiskers show the P10 and P90 values. Appendix C shows additional details displaying range of values, depths of samples taken, and crossplots for each well. The plots below are categorized by cluster with South Texas, Oligocene injections to the left, moving west into Louisiana and Miocene injections to the right (see Figure 4.1).

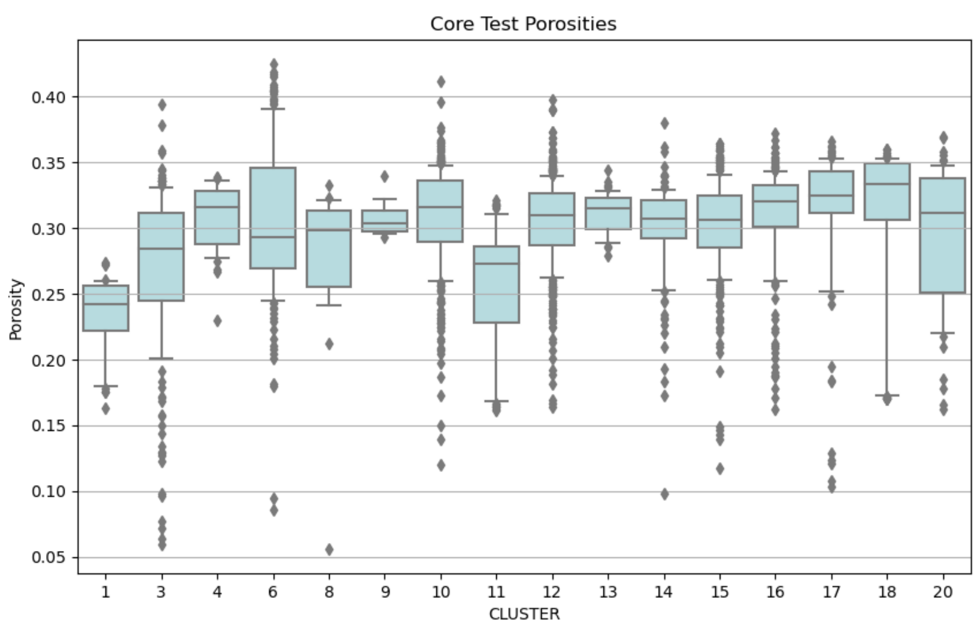

Figure 4.2 Core Porosities are split by the clusters referenced in Figure 4.1. Boxes show the P25-P75 range while the whiskers show P10-P90 range. Data outside that range is shown by individual points. From left to right, clusters are traveling from west to east of the Gulf Coast, from Oligocene to Miocene Injection Formations.

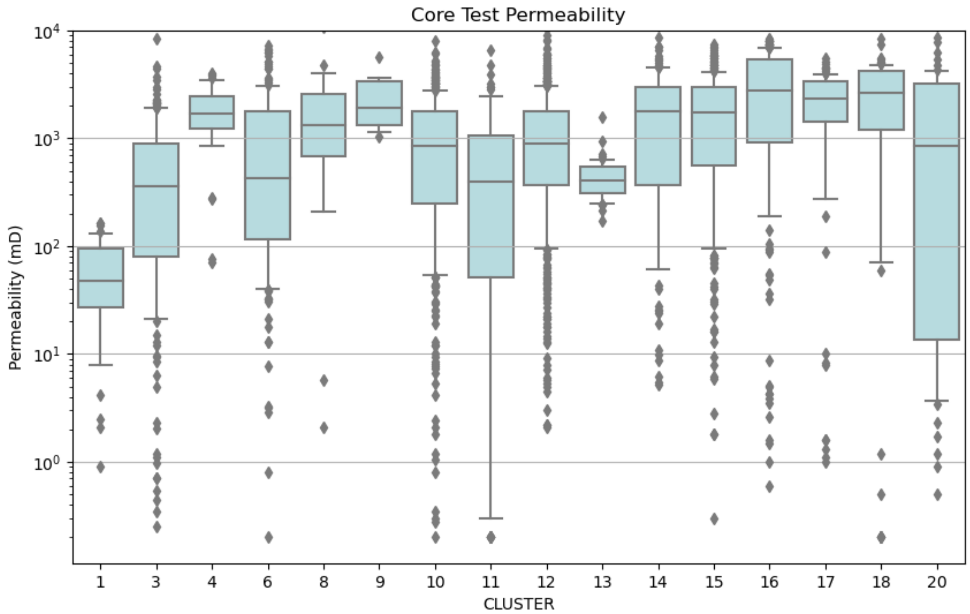

Figure 4.3 Core Permeabilities are split by the clusters referenced in Figure 4.1. Boxes show the P25-P75 range while the whiskers show P10-P90 range. Data outside that range is shown by individual points. From left to right, clusters are traveling from west to east of the Gulf Coast, from Oligocene to Miocene Injection Formations. y-axis is plotted on a log-scale.

Core samples show that there is a trend of increasing porosity and permeability as the clusters shift from South Texas to Louisiana and from Oligocene to Miocene formations.

Table 4.1 reports the values represented in Figure 4.2 and Figure 4.3, further breaking down the results between cores which tested the permeability with a liquid vs. those which tested with air. The medium used for the tests are not always included as the permits may only include the final table of the core tests. However, the liquid used for testing were usually either the formation fluid or some other brine, the air used for testing was usually Helium, but overall, it is not included.

Table 4.1 Summary of Core Test Results

CLUSTER	Count	Porosity 10%	Porosity 50%	Porosity 90%	Liquid Permeability (mD) 10%	Liquid Permeability (mD) 50%	Liquid Permeability (mD) 90%	Air Permeability (md) 10%	Air Permeability (md) 50%	Air Permeability (md) 90%
1	41	0.18	0.242	0.26				8	48	132
3	203	0.193	0.284	0.3326				13.4	340	1901.8
4	41	0.277	0.316	0.336	845	1695	3495			
6	166	0.244	0.293	0.3925				38.5	419	3105
8	12	0.2149	0.2985	0.3228	66.99	1060	3266	6.5	1530	5616
9	8	0.2951	0.304	0.3274	1120	1934	4242.3	3571	4585	7349.4
10	398	0.256	0.316	0.348	42.8	775	2750	54	950	2700
11	66	0.1675	0.273	0.313				0.2	332.5	2635
12	529	0.262	0.3097	0.34	133	786	3033.8	78.08	902	3080
13	42	0.289	0.3155	0.3307	245.6	407	653.5			
14	124	0.2523	0.307	0.329				48.45	1792	4525.9
15	293	0.2602	0.306	0.341	152.2	1430	3220	71.6	1891.5	4726
16	213	0.26	0.32	0.3438				150	2800	6940
17	94	0.2492	0.3245	0.353				214.1	2335	3995
18	86	0.1725	0.334	0.3535				0.2	2340	4785
20	53	0.2184	0.312	0.3504	829.12	1407.2	1985.28	2.52	703	4344

Additionally, some permits included core test results from the confining zone or from shaly core samples which is included in Appendix D.

Table 4.2 shows the regression equations derived from porosity and permeability. Note that the logarithm of the permeability values was used to create a linear regression, so the end product should be raised with base 10. This data was also split between liquid and air permeability. Appendix E shows porosity permeability crossplots for each cluster.

Table 4.2 Porosity Permeability Equations

Porosity vs. LOG (Permeability (mD))		
Cluster	Air Permeability	Liquid Permeability
1	17.78 ϕ - 2.586	
3	12.82 ϕ - 1.205	
4	9.272 ϕ + 0.3012	
6	12.9 ϕ - 1.375	
8	18.15 ϕ - 2.483	28.16 ϕ - 5.551
10	18.03 ϕ – 2.846	2.737 ϕ - 1.625
11	29.42 ϕ - 5.62	
12	13.95 ϕ - 1.404	9.93 ϕ - 0.1534
13	5.504 ϕ + 0.8973	
14	15.57 ϕ - 1.737	
(M) 15	23.12 ϕ - 4.229	9.031 ϕ + 0.2371
(O) 15	18.78 ϕ - 2.529	
16	16.7 ϕ - 2	
17	15.17 ϕ - 1.63	
18	23.75 ϕ - 4.638	
20	23.28 ϕ - 4.482	

(M) Miocene – Oakville Formation core samples

(O) Oligocene – Frio Formation core samples

4.1.2 Well Log Porosity and Permeability

Porosity values were estimated from available well logs in order to predict permeability. Table 4.3 summarizes the data available for each well along with the end results for the average porosity and geometric mean of permeability within the sand zones. The figures showing well log porosity estimations plotted with the core samples are in Appendix G. Only one well (WDW051) did not have core samples to match the porosity values. Figure 4.4 shows an example using WDW054 in Orange County, Texas.

WDW054 was evaluated at two different sand intervals since the falloff tests for that well injected into both intervals and made clear which tests were into which sand. The original injection was into the ‘K-Sand’ and then moved up into the ‘J2-Sand’.

Table 4.3 Summary for Log's Method of Porosity Estimation and Upscaled Permeability

CLUSTER	WELL	AVAILABLE LOGS	METHOD	POROSITY	PERMEABILITY (mD)	Sand
1	WDW248	GR, RES	RES & GR	0.28	76	
4	Other	GR, RES, NPHI, DPHI				
4	WDW070	RES	RES	0.29	564	
6	WDW163	RES	RES	0.31	615	
6	WDW165	RES	RES	0.26	101	
8	WDW051	RES	RES	0.27	408	
8	WDW435	GR, RES	RES	0.304	1112	
10	WDW080			0.34*	1514*	
10	WDW127			0.33*	1497*	
10	WDW128	GR, NPHI, DPHI	NPHI/DPHI & GR	0.309	1229	
12	WDW147	RES	RES	0.319	1117	
12	WDW169	RES	RES	0.309	847	
12	WDW157	RES	RES	0.31	983	
12	WDW397	GR, RES	RES	0.29	868	
12	WDW422	GR, RES	RES	29.9	1244	
14	WDW316	GR, RES	RES	0.29	451	
14	WDW317	GR, RES, NPHI, DPHI	NPHI/DPHI	0.26	381	
15	WDW100	RES	RES	0.321	1597	
15	WDW160	GR, NPHI, DPHI	NPHI/DPHI	0.3	1101	
16	WDW054	GR, RES, NPHI, DPHI	NPHI/DPHI	0.31	1568	(J2)
				0.316	1949	(K)
16	WDW191	GR, RES	RES & GR	0.32	2577	
16	WDW282	GR, RES	RES & GR	0.32	4393	
17	971123	GR, NPHI	NPHI	0.35	5023	
20	970802	GR, RES	RES	0.35	4106	

('Other') well is a log that was within the AOR of the permit for WDW070 which was used to confirm the parameters used for the log transformations in that area.

(*) Estimated from WDW128

The 'METHOD' column describes the process used to estimate porosity for each well where 'RES' used Archie's Law for a resistivity to porosity transformation, 'GR' used the gamma ray log to estimate porosity, and 'NPHI/DPHI' used the shale corrected neutron and density logs.

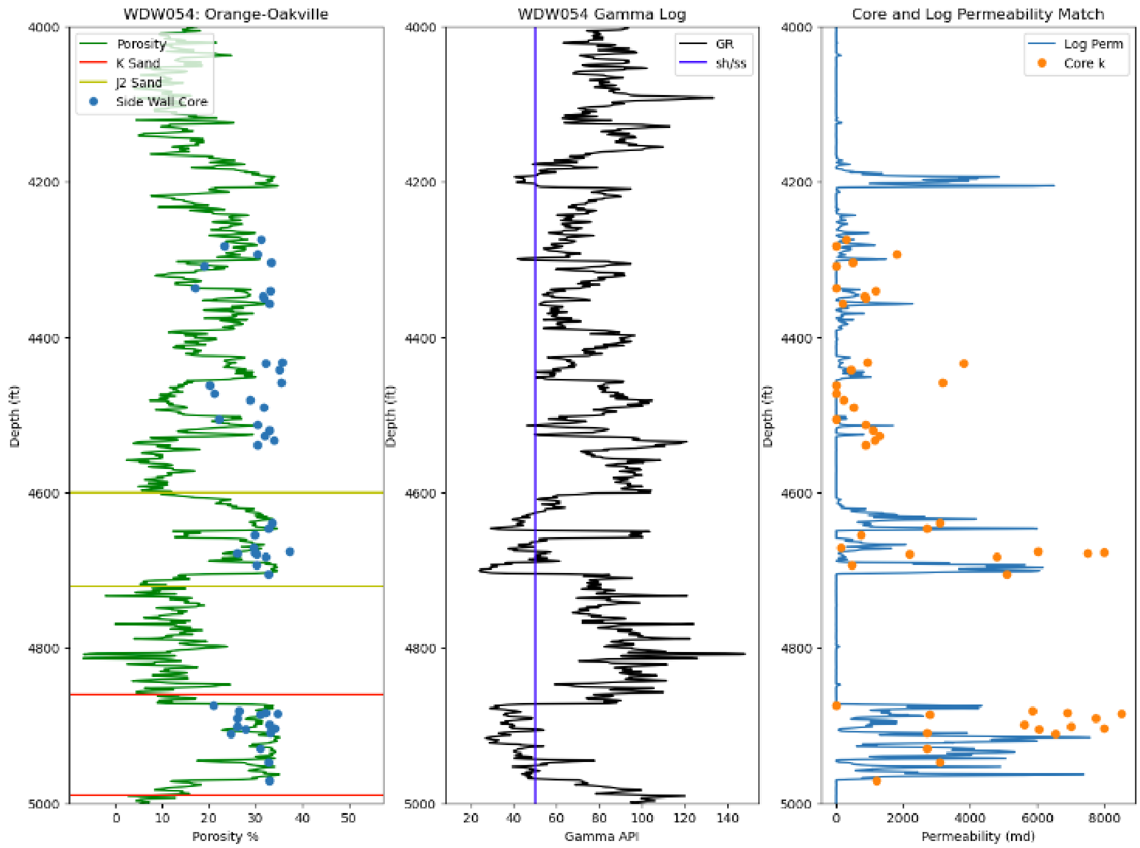

Figure 4.4 Plot on the left shows two different sand zones that were in operation. The bottom K-Sand in red was the original target for almost 26 years. Injection later moved up into the J2-Sand and operated for 2 years. K-Sand depths are from 4858-4990 ft (KB) and J2-Sand depths are from 4620 - 4750 ft (KB) (Geostock Sandia, LLC, 2018). The plot in the middle shows the Gamma Log and the cutoff line for what was considered to be the sand zone. Depths to the left of the blue line were used to estimate permeability. Plot on the right shows permeability values estimated from log upscale and from core test.

4.1.3 Falloff Test Permeability

Figure 4.5 shows the range of permeability values derived from the falloff tests and Table 4.4 shows the breakdown of the values by percentile.

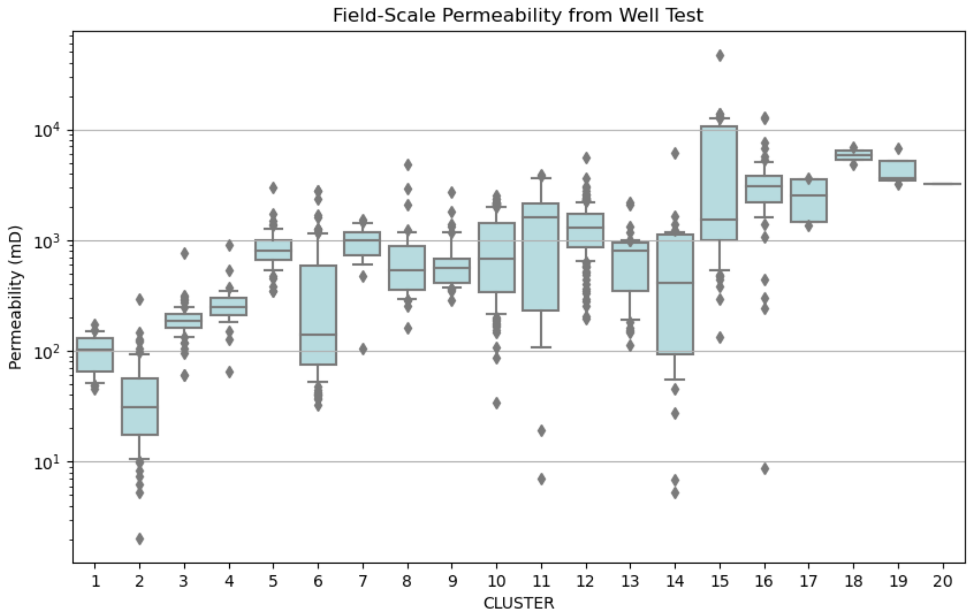

Figure 4.5 Permeability values derived from all falloff tests are split by the clusters referenced in Figure 4.1. Boxes show the P25-P75 range while the whiskers show P10-P90 range. Data outside that range is shown by individual points. From left to right, clusters are traveling from west to east of the Gulf Coast, from Oligocene to Miocene Injection Formations. y-axis is plotted on a log-scale.

Table 4.4 Field Scale Permeability Summary

FALLOFF TEST DERIVED PERMEABILITY									
CLUSTER	COUNT	10%	50%	90%	CLUSTER	COUNT	10%	50%	90%
1	32	51.76	102	150.61	11	21	107.72	1597.9	3587.72
2	69	10.55	31.24	94.10	12	174	638.55	1302.04	2239.20
3	65	134.39	184.81	248.60	13	52	184.74	796.25	1002
4	29	174.57	247.39	352.39	14	33	47.33	411.24	1211.80
5	51	529.54	810	1272	15	71	533.03	1517	12659.97
6	100	51.54	138.75	1148.45	16	56	1503.01	3037.02	5173.75
7	17	548.56	999.69	1429.27	17	4	1410.09	2501	3587.8
8	37	293.26	539	1201.4	18	2	5039.35	5896.75	6754.15
9	47	368.95	564.45	1173	19	3	3282.96	3648.85	6082.57
10	131	216.31	672.60	1990.44	20	1	3200	3200	3200

4.1.4 Falloff Test Injectivity Index

Figure 4.6 and 4.7 shows the range of injectivity index values gathered over the lifespan of each well. The units from the falloff tests are in bbl/day/psi, which is shown on the left y-axis. On the right, an equivalent CO_2 value is shown in units of ton/yr/MPa assuming a supercritical density of 700 kg/m^3. The values for Figure 4.6 are from the flowing and static bottomhole pressures during and after falloff tests. The values for Figure 4.7 are from accounting for the pressure drop due to skin and calculating a new flowing bottomhole pressure which will typically result in a lower flowing bottomhole pressure. Table 4.5 shows values shown in the figures and the more detailed values per well are included in Appendix J.

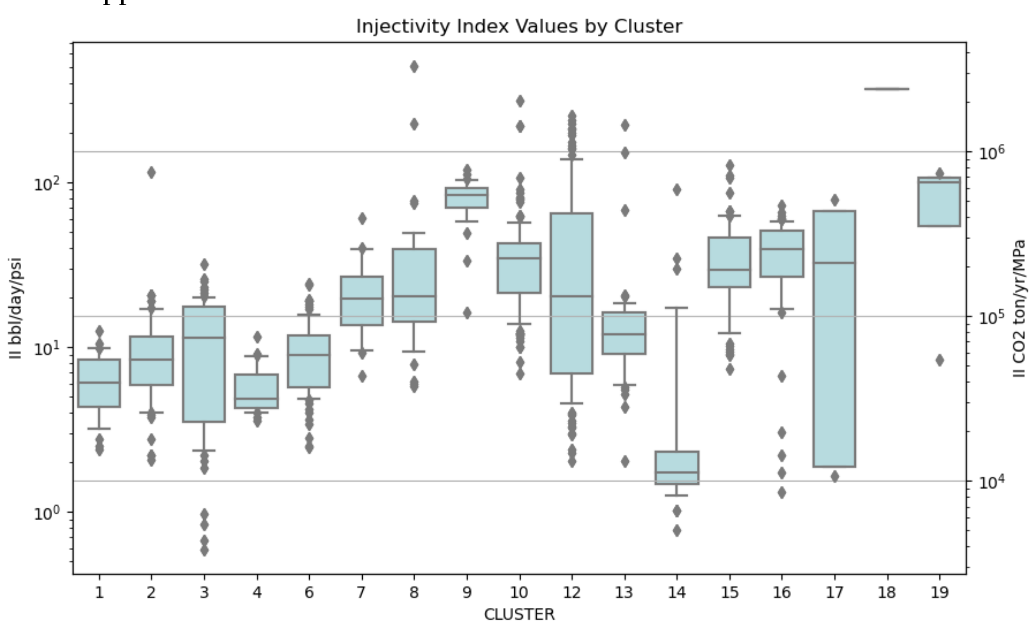

Figure 4.6 Injectivity Index is calculated from Measured Flowing and Static Bottomhole Pressures (II = q/ ($P_{\text{flowing bottomhole pressure}}$ - $P_{\text{static bottomhole pressure}}$) and are split by the clusters referenced in Figure 4.1. Boxes show the P25-P75 range while the whiskers show P10-P90 range. Data outside that range is shown by individual points. From left to right, clusters are traveling from west to east of the Gulf Coast, from Oligocene to Miocene Injection Formations. y-axis is plotted on a log-scale.

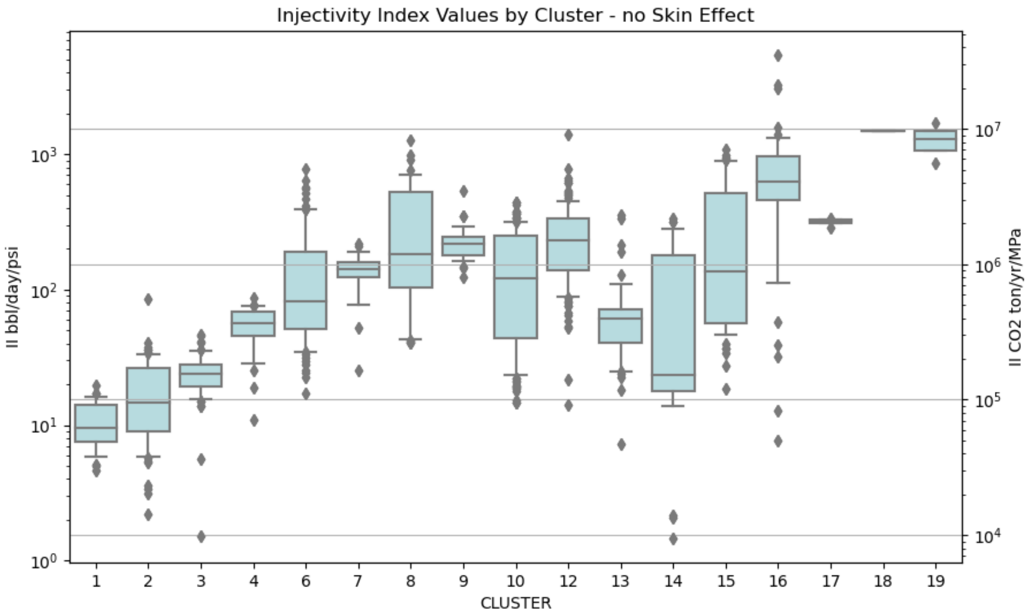

Figure 4.7 Injectivity Index is calculated by accounting for the skin effects (II = $P_{\text{flowing bottomhole pressure}} - P_{\text{static bottomhole pressure}} - P_{\text{skin}}$) and are split by the clusters referenced in Figure 4.1. Boxes show the P25-P75 range while the whiskers show P10-P90 range. Data outside that range is shown by individual points. From left to right, clusters are traveling from west to east of the Gulf Coast, from Oligocene to Miocene Injection Formations. y-axis is plotted on a log-scale.

Both Figure 4.6 and Figure 4.7, displaying injectivity index values, mirror the overall trend observed in Figures 4.2 – 4.5: An increase in porosity and permeability as the clusters move east along the Gulf Coast transitioning from Oligocene to Miocene formations. However, there are noticeable deviations in Cluster 13 and Cluster 14 (particularly in Figure 4.6). This deviation in Cluster 14 may be attributed to boundary effects, which is further discussed in Section 4.2.4.4. There is not enough data to make assumptions for Cluster 13. Still, both cases emphasize that there are limitations to injectivity and the allowed pressure increase that is not always represented by permeability.

Table 4.5 Injectivity values

Injectivity Index where: $II = \left\lvert\frac{q}{(P_{wf}-P_{BH})}\right\rvert$								Injectivity Index where: $II = \frac{q}{(Pw_f-P_{BH}-\Delta P_{skin})}$							
		II (bbl/d/psi)			**II CO_2 (Mton/yr/MPa)**					**II (bbl/d/psi)**			**II CO_2 (Mton/yr/MPa)**		
CLUSTER	**count**	**10%**	**50%**	**90%**	**10%**	**50%**	**90%**	**CLUSTER**	**count**	**10%**	**50%**	**90%**	**10%**	**50%**	**90%**
1	30	3	6	10	0.020	0.039	0.064	**1**	29	6	10	16	0.037	0.062	0.107
2	69	4	8	17	0.026	0.054	0.111	**2**	69	6	15	34	0.038	0.095	0.218
3	62	2	11	20	0.014	0.074	0.131	**3**	59	15	24	35	0.100	0.154	0.230
4	29	4	5	9	0.026	0.032	0.057	**4**	29	28	56	76	0.181	0.367	0.492
6	91	5	9	16	0.031	0.058	0.102	**6**	91	35	82	394	0.227	0.531	2.562
7	17	9	20	39	0.061	0.127	0.256	**7**	17	67	142	199	0.438	0.923	1.293
8	33	8	20	69	0.053	0.132	0.451	**8**	33	42	184	750	0.274	1.197	4.877
9	27	54	84	104	0.354	0.544	0.673	**9**	27	157	217	315	1.023	1.411	2.045
10	127	13	35	59	0.086	0.225	0.384	**10**	127	23	120	319	0.149	0.782	2.072
12	117	4	20	142	0.028	0.132	0.921	**12**	113	87	230	475	0.565	1.495	3.085
13	51	6	12	19	0.038	0.077	0.120	**13**	51	25	61	110	0.161	0.399	0.713
14	28	1	2	21	0.008	0.011	0.137	**14**	25	7	23	300	0.044	0.151	1.950
15	62	11	29	62	0.070	0.191	0.405	**15**	58	44	137	900	0.289	0.891	5.851
16	53	16	39	59	0.106	0.254	0.383	**16**	51	112	628	1309	0.727	4.080	8.504
17	4	2	32	74	0.011	0.209	0.479	**17**	4	295	321	331	1.915	2.087	2.154
18	1	364	364	364	2.365	2.365	2.365	**18**	1	1494	1494	1494	9.711	9.711	9.711
19	3	27	99	111	0.173	0.646	0.719	**19**	2	944	1284	1625	6.132	8.346	10.561

II (bbl/d/psi) are calculated directly from values found in falloff tests. II CO_2 (Mton/yr/MPa) uses conversion of:

$$\frac{bbl}{day \cdot psi} \cdot \frac{1\ psi}{0.00689\ MPa} \cdot \frac{0.159\ m^3}{1\ bbl} \cdot \frac{700\ kg\ CO_2}{m^3} \cdot \frac{0.001\ ton\ CO_2}{1\ kg\ CO_2} \cdot \frac{365\ days}{1\ year} / (10E+06) = \frac{Mton\ CO_2}{year \cdot MPa}$$

4.2 RESULTS

4.2.1 Comparing Upscaled Permeabilities

Table 4.6 Comparison of Permeability at Different Scales

ID		Porosity/Permeabilities at Different Scales						% Change During Upscale	
		Core PERM		Log PERM		FIELD		Log to Core	Field to Log
CLUSTER	WELL	POR	(md)	POR	(md)	PERM (md)	SAND	Change %	Change %
(O) 1	WDW248	0.242	48	0.28	76	102		58%	34%
(O) 4	WDW070	0.316	1695	0.29	564	247		-67%	-56%
(O) 6	WDW163	0.371	2122	0.31	615	944		-71%	53%
(O) 6	WDW165	0.269	180	0.26	101	73		-44%	-28%
(M) 8	WDW051			0.27	408	398			-2%
(M) 8	WDW435	0.311	2830	0.30	1112	753		-61%	-32%
(M) 10	WDW080			0.34	1514*	1280			-15%
(M) 10	WDW127			0.33	1497*	418			-72%
(M) 10	WDW128	0.309	552	0.33	1229	1706		123%	39%
(O) 12	WDW147	0.325	925	0.32	1117	1756		21%	57%
(O) 12	WDW169	0.262	138	0.31	847	1299		514%	53%
(O) 12	WDW157	0.31	605	0.31	983	984		62%	0%
(O) 12	WDW397	0.298	1150	0.29	868	911		-25%	-30%
(O) 12	WDW422			0.30	1243	1192			-4%
(O) 14	WDW316	0.294	408	0.29	451	124		11%	-72%
(O) 14	WDW317			0.26	381	190			-50%
(M) 15	WDW100	0.327	1720	0.32	1597	10873		-7%	581%
(M) 15	WDW160	0.292	426	0.30	1101	1196		158%	9%
(M) 16	WDW054	0.309	3706	0.31	1568	298	J2	-58%	-81%
(M) 16	WDW054	0.304	4932	0.32	1949	2050	K	-60%	5%
(M) 16	WDW191	0.32	1200	0.32	2577	2508	S	115%	-3%
(M) 16	WDW282	0.324	4472	0.32	4393	3837	T	-2%	-13%
(M) 17	971123	0.321	2195	0.35	5022	3563**		129%	-29%
(M) 20	970802	0.312	225	0.35	4105	3200***		1725%	-22%

Green highlights show wells in which upscaled permeability values overestimate the average field-scale permeability

(O), (M) Wells injected into Oligocene or Miocene

(*) There were no logs for these wells, but their injection intervals are right above the sand zone for WDW128 and are less than ½ mile away from WDW128. Assumption is that the sands here are similar to that of WDW128.

(**) No falloff test found for this well. Instead value is from other well in Calcasieu Parish, Well 971124.

(***) No falloff test found for this well. Instead value is from other well in Saint Charles Parish, Well 972060.

Observing the upscaled results in Table 4.6, more samples overestimated the permeability when compared to the historical average derived from the well tests, especially for those injecting into Miocene formations. Histograms showing the ranges of permeabilities from each dataset are included in Appendix H. Figure 4.8 shows an example from WDW054 where the geometric mean of permeability was taken for the K-Sand and J2-Sand as labeled in Figure 4.4.

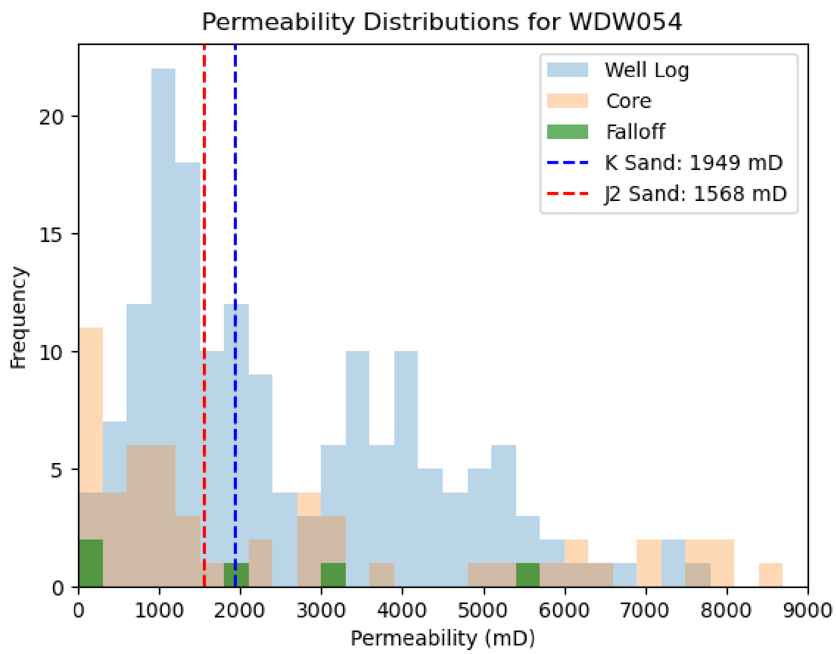

Figure 4.8 K-Sand and J2-Sand for WDW054. Permeability upscaled vs Permeability calculated from falloff tests are 1949 md vs. 2050 md for the K-Sand and 1568 md vs. 298 md for J2-Sand. In this example, the upscaled permeability predicts similar values, but in practice, the J2-Sand performed worse than expected, showing discrepancy in two injection sands which was not captured while upscaling.

Viewing the total range from all datasets is important because although there is more of a tendency for the upscaled permeabilities to overestimate the average field-scale permeability, they still fall somewhere within the whole range. This will be critical for modelers to keep in mind when setting expectations for injection performance predictions using data from core samples and well logs.

Of the wells that overestimated the field-scale permeability, they overestimated by 34% and of the wells that underestimated the field-scale permeability, they underestimated by 36%. This similarity suggests that the error in predicting the average field-scale permeability value is around 35%, in either direction, for the wells in this study.

Expanding on the logs for WDW054 in Figure 4.4, the two sands have similar porosities resulting in similar permeabilities (1568 md and 1949 md), but the permeability found from the falloff tests show that the J2-Sand has lower than predicted permeability when compared to the K-Sand (298 md vs 2050). Additionally, while over 22 million barrels (MMbbl) was injected over 26 years into the K-Sand at an average of 852 thousand barrels (Mbbl) per year, the injection rate dropped to less than 140 Mbbl/year once moving to the J2-Sand. It is assumed that the following temporary abandonment status and eventual plugging of this well is related to the comparatively reduced permeability.

In another example listed in Table 4.6, WDW163 (upper sand) and WDW165 (lower sand) both operate under the same permit in proximity to each other, injecting into separate sand intervals within the Frio formation. The permeability of WDW163 is much greater than that of WDW165 (944 md vs 73 md), and is reflected in the upscaled permeability estimates from the well logs. In this case however, both wells are active and inject about the same amount of waste per year despite the significant difference in permeabilities, with WDW165 actually injecting at a slightly higher rate at 1.63 MMbbl/yr compared to the 1.59 MMbbl/yr for WDW163.

It is observed that there can be significant discrepancies in permeability when evaluating different sand intervals within the same formation, which has varying impacts on injection activity. In one case, the lower permeability interval with an average of 73 md was sufficient for allowing significant waste injection, and in the other, the lower permeability interval with an average of 298 md led to cessation of operations. This highlights the notion that permeability alone is not enough to select ideal injection zones. Rather, looking at factors impacting injectivity as a whole need to be evaluated. This includes near wellbore effects, boundary conditions, or existence of other operations nearby, which play a critical role in constraining pressure.

The next section focuses on quantifying formations with the injectivity index using the rate and pressure increase from falloff tests.

4.2.2 Injectivity Over Time

Figure 4.9 shows an example of a falloff test taken from an individual well where the blue line represents the injectivity index of each year's falloff test and the red line represents the skin factor calculated for that year. Spearman's Rank Correlation Coefficient is printed at the bottom of the plot. This is to show the monotonic relationship between the injectivity and skin which measures the strength of the relationship between two variables even if the relationship is non-linear. For values where there were enough years of falloff tests, the correlation for the first five years of available data and the last five years of available data were also printed to see if there was any significant change in the correlation over time. Plots of each individual well are in Appendix K.

In this example, the correlation between skin and II starts as -1, indicating a strong inverse relationship where high skin causes low injectivity and vice versa. In the last years of falloff tests, this relationship changes to -0.5 meaning there is a weaker, but still inverse correlation between the two variables. This means that the effect of skin diminished over time for this well, which is also true for many of the other locations in this study. The injectivity rarely continuously drops with time. Instead, they either fluctuate throughout the entire life of the well or remain constant at some low after a period of decline in the first few years of injection.

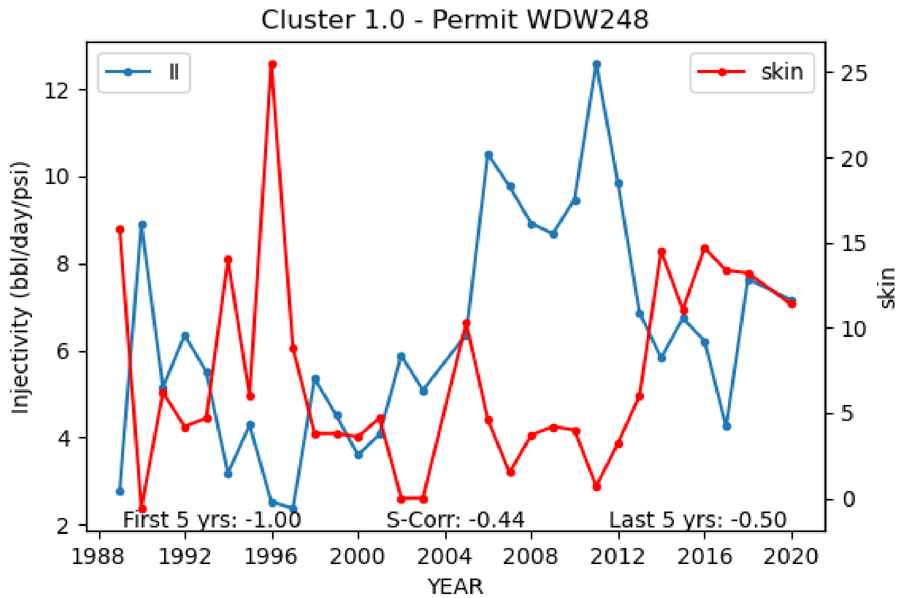

Figure 4.9 Injectivity plot shows the Injectivity Index calculated by the rate/ ($P_{\text{flowing bottomhole pressure}} - P_{\text{static bottomhole pressure}}$) for each year there was a falloff test in blue. The near wellbore damage (skin) is shown in red. The inverse relationship suggests there is a strong influence of the skin over injectivity. The texts at the bottom show Spearman's Correlation where the closer to 1, the stronger the correlation. This shows that the first five years show a strong correlation between injectivity and skin, which diminishes as the years pass.

Table 4.7 shows the correlation between skin and the injectivity index for wells with enough data to show the difference over the years. The overall correlation, correlation at the first five years of injection, and correlation at the last five years of injection is reported. More wells show a decreasing correlation between the two timeframes (smaller negative). The table also shows the P50 value for injectivity for water as well as the standard deviation.

Table 4.7 Injectivity Index and the Influence of Skin Effects

	Permit No.	Corr.	First 5 yrs	Last 5 yrs	P50 bbl/d/psi	Std Deviation
1	WDW248	-0.445	-1.0	-0.5	6	3
2	WDW210	-0.795	-0.7	-0.9	10	5
2	WDW211	-0.006	-0.7	0.1	12	23
2	WDW212	0.284	0.4	-0.9	10	4
3	WDW152	-0.409	-0.7	-0.1	18	3
3	WDW153	-0.837	-0.7	-0.5	17	6
3	WDW278	-0.878	-0.9	-0.8	5	4
4	WDW070	-0.308	-0.4	-0.9	6	2
6	WDW163	-0.738	-1.0	-0.9	11	5
6	WDW164	-0.336	-0.7	-0.2	9	5
6	WDW165	-0.660	-0.6	-0.8	8	3
6	WDW051	-0.760	-1.0	-0.9	20	12
7	WDW099	-0.802	-1.0	-0.5	31	23
7	WDW013	-0.554	-0.6	-0.2	79	22
7	WDW080	-0.874	-0.9	-0.8	36	18
8	WDW091	-0.591	-0.9	-0.4	14	4
8	WDW127	-0.185	-0.2	-0.7	41	12
9	WDW128	-0.877	-0.9	-0.9	62	68
10	WDW196	-0.203	-0.2	-0.9	20	7
10	WDW314	-0.491	-0.5	0.4	29	22
10	WDW157	-0.676	-0.7	-0.1	13	23
10	WDW169	-0.432	-0.9	-1.0	21	17
10	WDW249	-0.741	-0.1	-0.5	13	10
10	WDW083	-0.703	-0.8	-0.4	11	4
12	WDW149	0.154	0.5	-0.1	35	59
12	WDW316	0.125	-0.6	0.9	10	22
12	WDW317	0.257			4	4
13	WDW100	-0.508	-1.0	0.1	31	10
13	WDW101	-0.900			43	38
14	WDW160	-0.620	-0.9	-0.6	42	29
14	WDW358	-0.314			34	7
15	WDW054	0.600			14	16
15	WDW191	-0.522	0.0	0.7	40	16
15	WDW282	-0.679	-0.3	-0.2	45	10

Green highlights show wells where skin effects decrease with time

The wells where the skin plays a smaller influence over time are from a mix of both formations, but the wells where it seems to make a bigger impact with time predominately comes from Oligocene injection wells.

Looking at the different box plots for permeability and injectivity, they both increase as the injection formation moves from West to East of the Gulf Coast, from Oligocene to Miocene. It is evident that there is a strong correlation between permeability and II with a limitation caused by skin. To better depict this, Figure 4.10 shows all permeability-thickness and injectivity values from falloff tests. The y-axis is the hypothetical II of CO_2 value converted to ton/yr/MPa from bbl/day/psi of water. The plot shows both the II with and without skin.

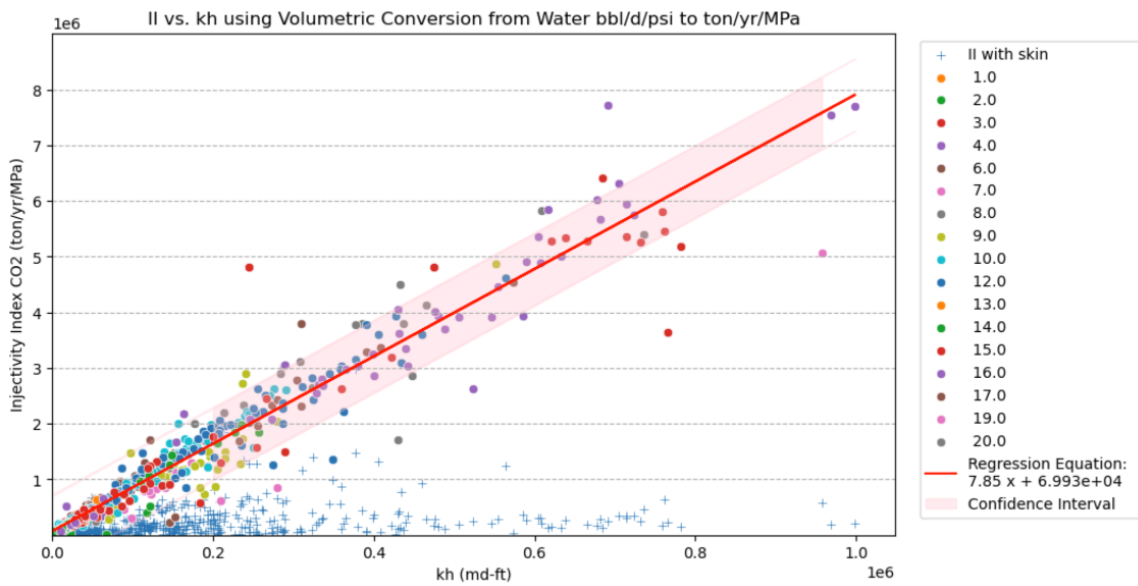

Figure 4.10 Injectivity Index (CO_2)vs. kh. The blue '+' shows the II values gathered from the measured bottomhole pressure values which include skin effects. The colored points show what the II from skin-corrected bottomhole pressure would have been.

At lower permeability-thickness values, there are points where the correlation between II and permeability seem to hold up, but after around ~30,000-40,000 md-ft, injectivity does not increase with permeability during operation. The II value at which the 'real' II plateus is around ~40,000 - 50,000 ton/yr/MPa while the original value from the water injections is around ~100 bbl/d/psi.

However, when considering the flowing bottomhole pressure accounting for skin effects, injectivity continues to increase with permeability and is color coded by cluster in the plot. There is a strong linear relationship between permeability thickness and II, where most of the values fall between the 95% confidence interval of the equation $II_{CO2}(\frac{ton}{yr \cdot MPa}) = 7.84996 * kh_{md \cdot ft} + 69926.76$ assuming a 700kg/m^3 CO_2 density. (The equation for predicting water injectivity from the original data was $II_{water}(\frac{bbl}{day \cdot psi}) = 0.001331 * kh_{md \cdot ft} + 11.8607$).

This suggests that in practice, higher permeability-thickness does not necessarily equate a higher injectivity after a certain point due to pressure limitations and that remdiating for skin effects will be critical for better injection performance. Appendix L shows detailed graphs for each region.

4.2.3 Prediction of CO_2 Injection Rates

Figure 4.11 below shows a range of possible CO_2 injection rates, which was calculated by transforming water to an equivalent CO_2 injection rates using simple volumetric and density conversions. Case 1 considers the minimum rate scenario from using the cumulative volume injected for water over time. Case 2 evaluates the maximum rate reached for each well either during the falloff test or from the annual injected volume report, whichever is greater. Case 3 uses the average injectivity index from the falloff tests to predict a maximum rate in the scenario where the flowing bottomhole pressure is 90% of the fracture pressure. Case 4 uses the average value from the skin corrected injectivity index, also at a maximum allowed pressure differential. Appendix M details these values.

Most wells have an estimate for Case 1 since the cumulative injection data is readily available, the other cases have more missing data. The final results are reported in Mton/yr (million tons per year).

In Case 1, the highest rate of fluid injection converted to CO_2 for any of the wells is 0.95 Mton/yr. However, this is a significantly conservative value since it includes any downtime for workovers and other periods when the well is not used. Case 2, which evaluates the maximum rates seen during operation, shows WDW013, WDW359, and WDW128 to have injected at converted rates greater than 1 Mton/yr. Cases 3 and 4 push more wells above the 1Mton/yr threshold. The only exceptions are injection wells which operated in South Texas, Nueces County. The significant limitation on the injectivity can most likely be attributed to the source rock in South Texas which tends to contain more volcanic grains which makes for a poorer quality rock.

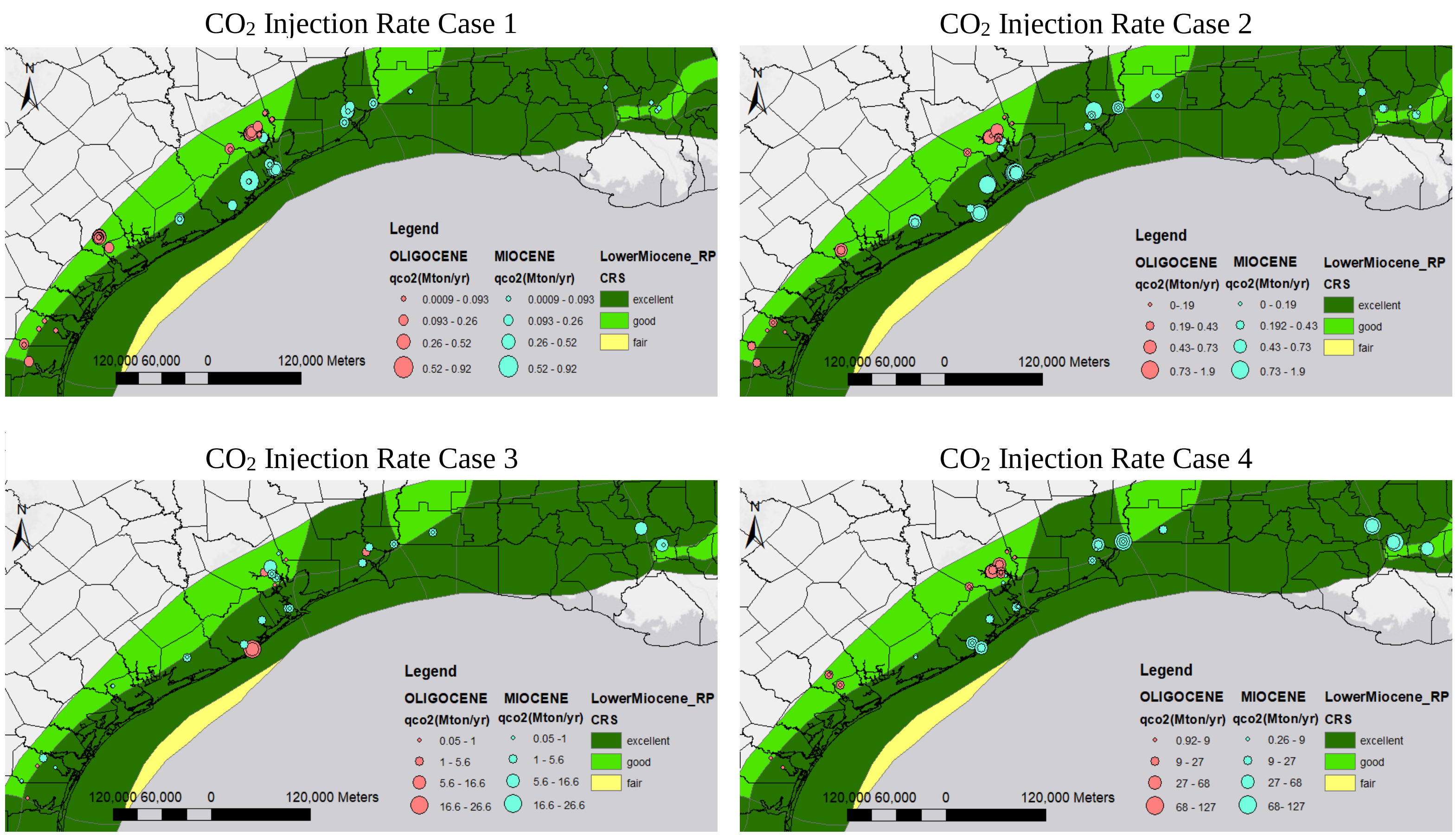

Figure 4.11 Equivalent CO_2 rates. Base Map from Bump et al. (2021) translates the geologic history and knowledge of the Lower Miocene to determine the chance of success in different areas. Case 1 represents the cumulative volume divided by the years of service. Case 2 shows the maximum rate seen during operations. Case 3 pushes the average Injectivity Index (II) to a max pressure. Case 4 pushes the average II without skin to a max pressure.

4.2.4 Specific Site Analysis

For most of these wells, annual static pressure measurements show little notable change year after year and have no issues in continuing injection activities. By examining these datasets alongside annual injected volumes (when accessible), observations can be made about the reservoir's pressure response to injection. Specific sites with good data coverage are selected for analysis to see if there are any discernable pressure interactions. It is assumed that hydrologic communication between wells or between sand intervals will be shown through similar pressure responses.

The first case will briefly discuss how most of these injections well behave, which can be summarized as having long history of regular injections, stable pressure, and little to no major noticeable issues. The next case shows a site which managed many wells throughout time, some which had to be discontinued to due injection issues. The next two discuss sites which had issues with injectivity. Section 4.3.6 looks at some Frio injection wells in Houston, TX as the area has higher well density than any other location. Finally, some Oligocene injection wells are highlighted for some quick comments.

4.2.4.1 Typical Operations

Two facilities, which were selected to show examples from both Oligocene and Miocene injection zones, are discussed: (1) BASF Corporation in Freeport, Texas injecting into the Miocene formation and (2) INEOS Nitriles USA in Port Lavaca, Texas injection into the Frio formation. The injection intervals for BASF well WDW051 is between 5886-6186 ft below ground level (bgl), and for WDW099, it is 6845-7367 ft bgl (WDW408 and WDW409 are active wells, but have limited data) (Terra Dynamics, INC, 2003).

The injection intervals for INEOS well WDW163 is 5352-5692 ft bgl, for WDW164 is 7413-7983 ft bgl, and for WDW165 is 6578-7478 ft bgl (Strata Technologies, LLC, 2020). Figure 4.12 shows the historical annual pressure and volumes recorded in the permits for these facilities. These figures were chosen to demonstrate general observations for most of the wells studied.

There is consistent injection for many years with minimal pressure increase between multiple wells which are managed by a single operator/facility. Most facilities operate 1-3 wells, and in this example, all wells inject into their own sand interval within the same formation, allowing the operator to have flexibility into which well/sand interval they allocate their waste. While operations are constrained by a maximum allowable pressure, permits also impose restrictions on the total permitted injection volumes, both for individual wells and the entire facility.

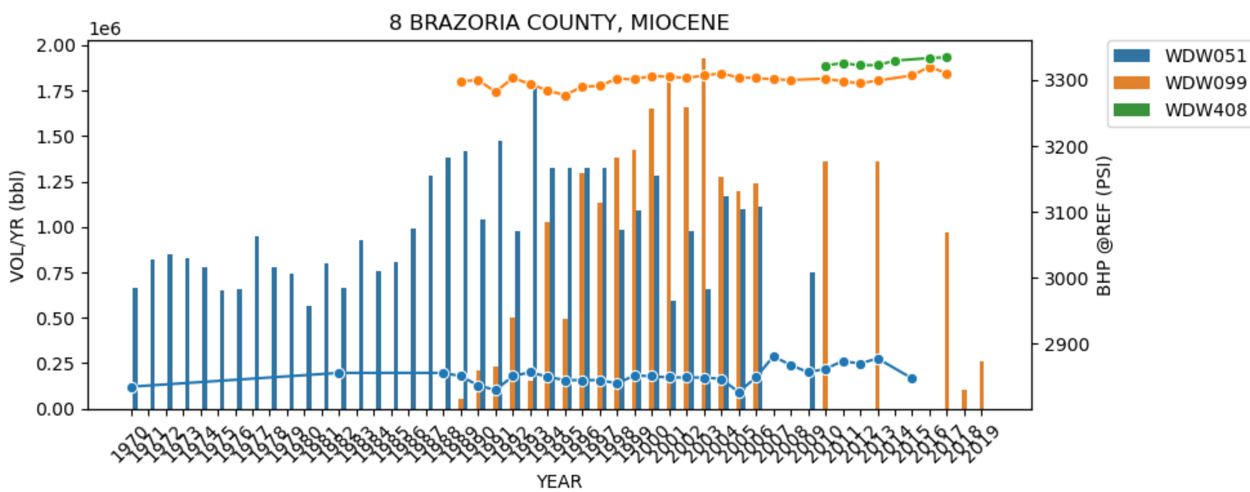

Figure 4.12 BASF wells into Miocene sands. Volume (bar chart) and measured static bottomhole pressures (line plot) are shown to visualize the pressure change caused by injection. The maximum pressure buildup ever recorded between the two wells is 54 psi from WDW051, representing a less than 2% increase.

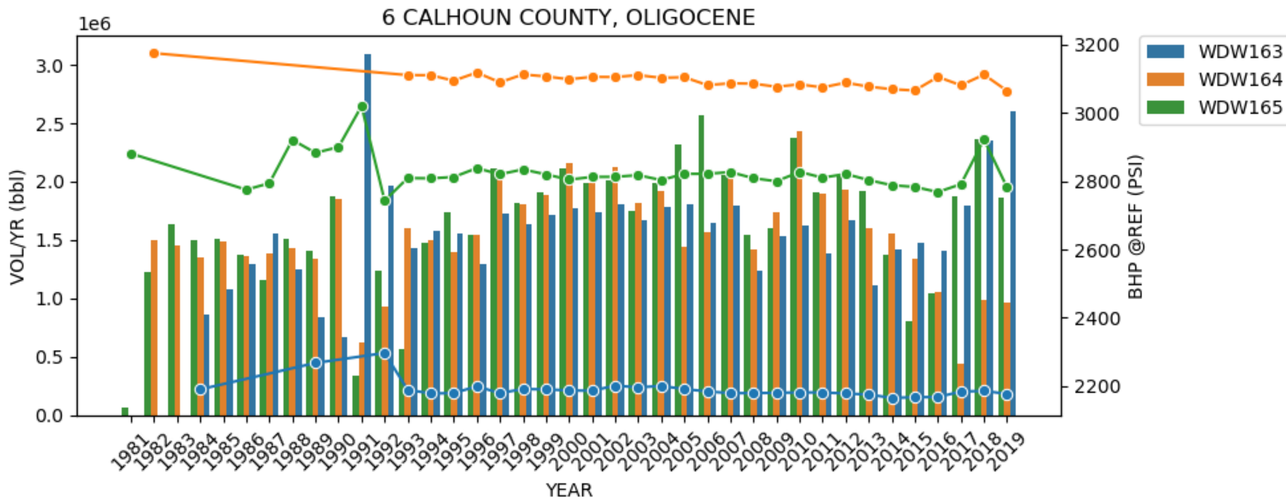

Figure 4.13 INEOS wells into Oligocene sands. Volume (bar chart) and measured static bottomhole pressures (line plot) are shown to visualize the pressure change caused by injection. The maximum pressure buildup ever recorded between the wells is 277 psi from WDW165, representing around a 10% increase.

At the BASF facility, a single well was in operation, injecting an average of 874 Mbbl per year, for nearly 20 years before a new one was added around 1990 when they began regularly injection around a million bbls/yr (see Table 4.8 for summary on total volume and pressure increase). The pressure difference between the original static pressure and recorded pressure reached a maximum of 54 psi (a 1.91 % increase) for WDW051 and 43 psi (a 1.31 % increase) for WDW099. The most recent pressure recorded however, indicated an increase of 20 psi (a 0.71 % increase) and 32 psi (a 0.98 % increase) showing very minimal pressure build up over their lifespan ('recent' is arbitrary based on data collection). Results are summarized in Table 4.8. Additionally, no vertical pressure communication is noticed between these two sand intervals. The gaps in data seen in the 2010s are a result of not being able to view the specific documents with the needed information, but the wells were injecting during these times.

Table 4.8 BASF wells Summary for Volume and Pressure Increase

PERMIT NO.	YEARS	CUM V (bbl)	CUM CO2 (Mton)	Max Δ P (psi)	Ending Δ P (psi)	Max Inc %	End Inc %
WDW051	46	4.36E+07	4.85	54	20	1.91	0.71
WDW099	37	3.52E+07	3.92	43	32	1.31	0.98

At the INEOS facility, all three wells started injected within 4 years of each other and have been injecting for nearly 40 years. Table 4.9 summarizes the maximum and most recently recorded pressure buildup.

Table 4.9 INEOS wells Summary for Volume and Pressure Increase

PERMIT NO.	YEARS	CUM V (bbl)	CUM CO2 (Mton)	Max Δ P (psi)	Ending Δ P (psi)	Max Inc %	End Inc %
WDW163	36	5.72E+07	6.36	131	11	6.05	0.51
WDW164	38	5.89E+07	6.56	110	0	3.59	0
WDW165	39	6.35E+07	7.07	277	39	10.1	1.42

Looking at just the maximum pressure buildup, it is high compared to the Miocene wells up above, but it also shows significant pressure dissipation. Plots showing injected volumes and measured pressure per year are included in Appendix N. Appendix O lists the pressure increases recorded from the static bottomhole pressure measurements.

4.2.4.2 INVISTA S.à r. l (previously E. I. Dupont de Nemours & Co.) in Orange, TX

This site had 11 different wells, though they were not all in operation at the same time. Many of the wells in this location were also discontinued some time ago, and information about them were not found. The currently injecting wells are WDW191 and WDW282 which inject into the S-Sand and T-Sand shown in Figure 4.14 (Geostock Sandia, 2018).

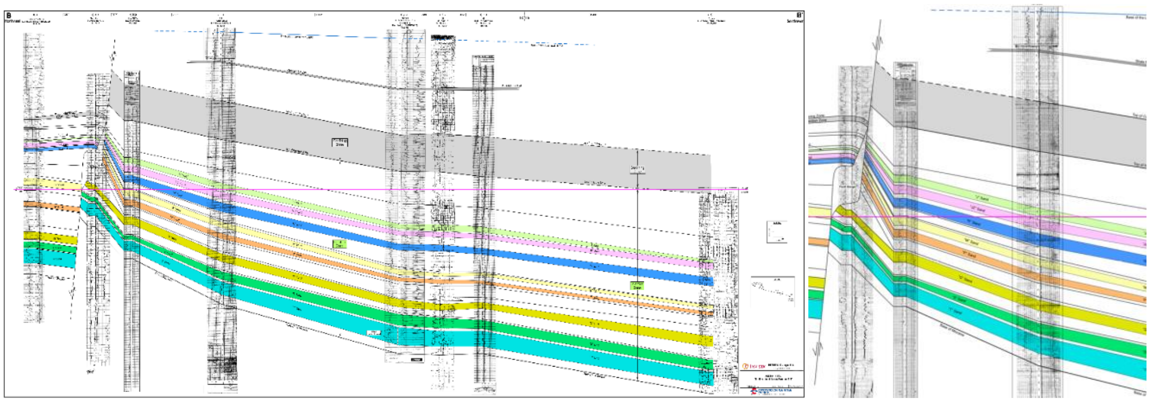

Figure 4.14 Northwest to Southwest structural cross section in the Geology Section of the permit for INVISTA S.à r.l., showing the multiple sand intervals permitted within the zone. Figure is created by ESSJ and Geology interpreted by WGK, PWP and included in Appendix 2-20 (Geostock Sandia, 2018).

Figure 4.15 shows pressure and volume plots for INVISTA S.à r. l and Table 4.10 summarizes the volume and pressure responses from the wells found.

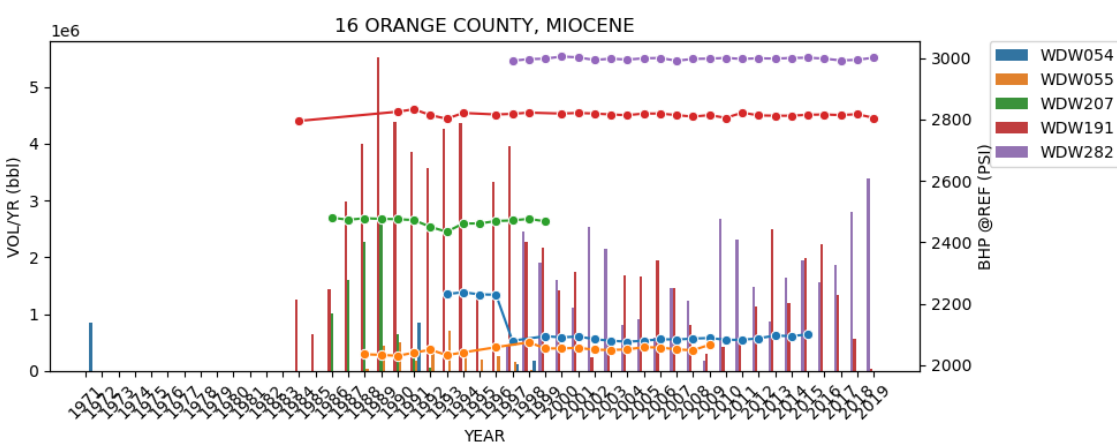

Figure 4.15 Annual Volume and Pressure in Orange, Texas, Miocene injection wells. The drop in WDW054 is from the move in sand zones (from K-Sand to J2-Sand) discussed previously in Section 4.2.1.

Table 4.10 INVISTA S.à r. l wells Summary for Volume and Pressure Increase

PERMIT NO.	YEARS	CUM V (bbl)	CUM CO2 (Mton)	Max Δ P (psi)	Ending Δ P (psi)	Max Inc %	End Inc %
WDW054	26	2.22E+07	2.72	161	24	7.76	1.16
WDW055	11	3.24E+06	0.36	44	36	2.17	1.77
WDW207	14	8.60E+06	1.01	46	34	1.89	1.4
WDW191	36	7.32E+07	8.15	38	10	1.36	0.36
WDW282	23	3.79E+07	4.22	14	10	0.47	0.33

Falloff tests for the two currently active wells, WDW191 and WDW282, show that they have similar injectivities at around 40 bbl/day/psi, which have not declined much since they began injection in 1984 and 1997. Data for WDW054 and WDW055 were limited, but from the available data, it is evident that use of the two wells were discontinued due to their drop in injectivity in 1999 (WDW054) and 1988 (WDW055).

WDW054 switched from its previous injection into the K-Sand, which to date, cumulatively had 76 MMbbl from multiple wells injected into it, into the J2-Sand, which had lower than expected permeability and injectivity. WDW055 injected into the J-Sand, for less than 10 years, and during that time, the injectivity decreased by ~ 90% of the original value, from 16 to 1.7 bbl/day/psi.

Looking at the cross section, a possible explanation is the presence of the fault nearby which acted as a partial barrier. The sand thickness for the two sand zones are also thinner than that for the currently active zones, which may have made it more sensitive to pressure increases. WDW054 and WDW055 were put in a temporary abandonment status for nearly 20 years rather than closing immediately (Lonquist & Co., 2021), and it is likely that the high performance of the two active wells into the bottom most sands made it unnecessary to try to continue operations in the thinner sands.

One additional interesting find in these locations were the issues studied during the Phase I Report of Class I wells conducted by the Underground Injection Practices Council in 1986. A well in this location, WDW012, injected around 8.3 million barrels between 1965 and 1971 into an unknown sand before injection had to be stopped due to sanding issues caused by the unconsolidated sandstone. (UIPC, 1986). However, this issue of the loose grains entering the well is an engineering issue, and the lack of any repeat incidents points to improved construction standards.

4.2.4.3 Mitsubishi/Lucite International in Nederland, TX

This site stands out because the permeability values from the falloff tests were +10000 md, but the injectivity is not correspondingly high. In this location, WDW100 and WDW101 inject into the same injection interval into the Lower Oakville sands. Looking at the workover history of this well, it was noted that throughout the years, they had issues with ‘elevated high pressures’ which resulted in decreased injectivity (Geostock Sandia, LLC, 2015). The Lower Oakville sand is around 4200-4350 ft bgl, with an initial pressure 1920.7 psia, which is a typical pressure that follows the hydrostatic gradient.

Under this permit, four sand intervals are identified and are referred to as: (1) Upper Oakville Sand, (2) Lower Oakville Sand, (3) Lower Lower Oakville Sand, and (4) Catahoula Sand. Both WDW100 and WDW101 initially injected into the deepest Catahoula Sand, moved to the Upper Oakville, then settled with the Lower Oakville Sand, due to injectivity issues related to high pressures in the sands (Geostock Sandia, 2015). WDW188, which injected into the Catahoula Sand, is no longer in use.

These two wells are used intermittently in alternation. Figure 4.16 details some of the workover activities done to try and increase the injectivity of the well. As shown, remediation efforts are frequent (more so than others), and they show that they were successful in each attempt to increase injectivity.

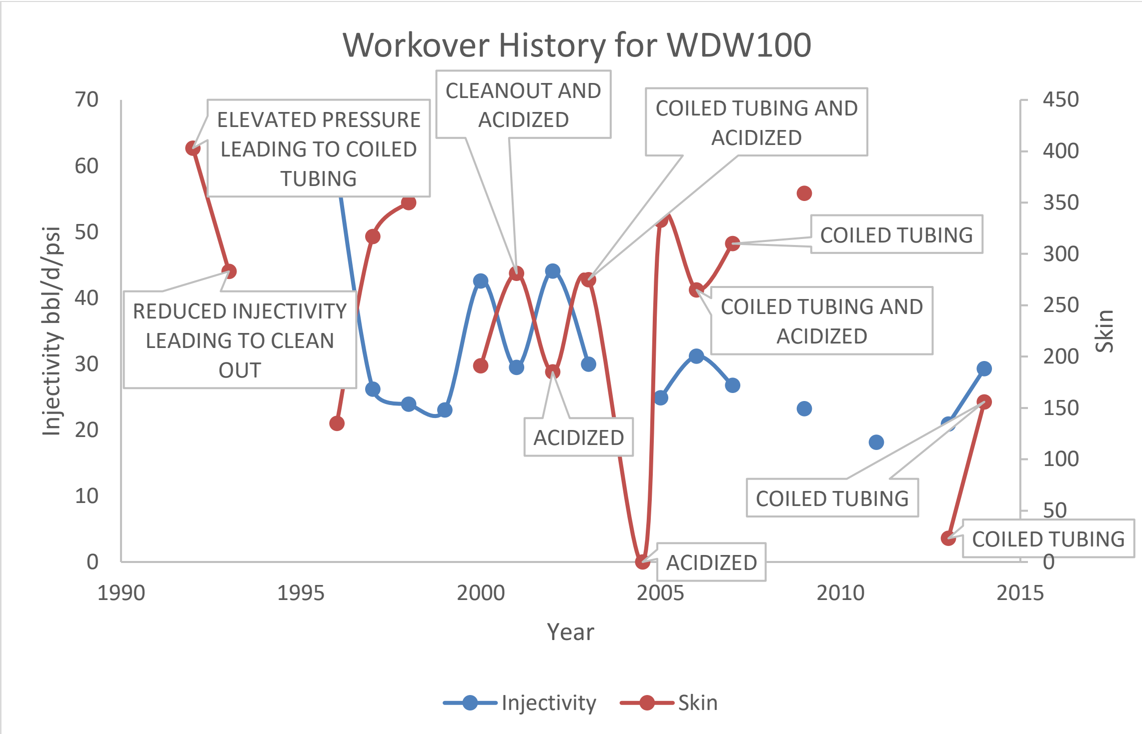

Figure 4.16 Workover history of WDW100 as noted in Appendix VI-9 (Geostock Sandia, LLC, 2015) for Mitsubishi/Lucite International Beaumont Site.

Figure 4.17 shows a structure map (photo taken on phone) which shows that this site lies between two salt domes to the West and East as well as two faults, referred to as 'Fault A' and 'Fault H', North and South of the wells. The sands pinch out in the West towards the Spindletop Salt Dome and meets a fault that lies above the Port Neches Salt Dome to the East. Fault A is in the up-dip of the fault block, North of the wells. However, as stated in the Section V of the permit, there was no indication of the presence of a boundary in the falloff tests. Usually, an exponential increase in pressure and a change in the slope of the semi-log graph is expected when in proximity to a closed boundary, which was not observed. Additionally, there was no significant observed pressure buildup throughout the previous volume injected, so this fault was deemed to most likely be a laterally transmissive fault (Geostock Sandia, 2015, Section V-Page 38). Fault H is interpreted as a no-flow-boundary.

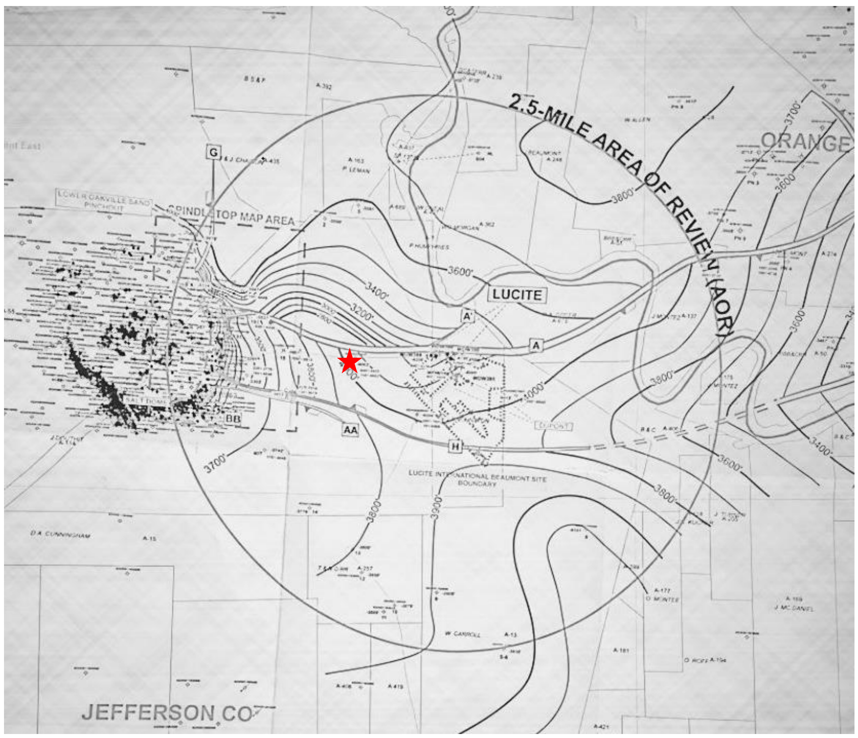

Figure 4.17 Edited Structure Map Top of Lower Oakville. Mapping illustration by ESSJ and geology by WGK, PWP, NM as included in Appendix V-31 (Geostock Sandia, 2015) for Lucite International Beaumont Site. Red Star added in to better show location of wells.

As one of the few permits with well-defined boundaries allowing for an estimation of a reservoir area, EASiTool was used to see if there was a close match between the estimation provided by the program and values predicted in this study. EASiTool is a program made by the GCCC which allows a fast and easy estimation of storage capacity, injection rates, and more, given pressure limitations under different boundary conditions

(Wang & Hosseini, 2023; Gandjanesh & Hosseini, 2019). Closed and Open boundary conditions were assessed, and well rates of ~0.115 Million Metric Tons (MMT)/year and ~30 MMT/year were estimated under the two cases.

The results from Section 4.2.3 regarding predictions of equivalent CO_2 injection rates for WDW100 and WDW 101 are in Table 4.11. To refresh, q1 is the rate estimated from the cumulative injected volume, q2 is the maximum value recorded during the falloff test (or annual injection), q3 is the max allowed rate estimated from the average injectivity index, and q4 is the max allowed rate if the pressure drop caused by skin were not included.

Table 4.11 CO_2 injection rates for Mitsubishi/Lucite Beaumont estimated from this thesis as reported in Appendix M. CO_2 injection rates are calculated from a volumetric conversion of water to million tons of CO_2

PERMIT NO.	q1(Mton/yr)	q2(Mton/yr)	q3(Mton/yr)	q4(Mton/yr)
WDW100	0.18	0.82	1.10	29.56
WDW101	0.21	0.81	1.47	19.55

The values estimated by the closed boundary case (0.115 MMT/yr) using EASiTool is quite close to the observed values from the wells under Case 1 (q1 in Table 4.11). The predicted maximum rate in Case 4 (q4 - no skin considered) is a surprisingly close match to the open boundary condition (30 MMT/yr). One way to interpret this is that this location behaves like an open boundary reservoir, and really does just suffer from a lot of near wellbore damage, indicated by the good match between EASiTool and the q4 estimation.

Another interpretation is that this is a partially-sealed, partially-opened boundary which can dissipate pressure given the time, but shows an immediate response in pressure increase due to being closed on three sides which leads to injection rates that are higher than what a completely closed boundary would allow, but is still more restricted compared to an open boundary scenario. Still, as shown in Table 4.12, the maximum increase was only high as 6% when compared to the original static reservoir pressure

Table 4.12 Mitsubishi/Lucite Beaumont Volume and Pressure Increase

PERMIT NO.	YEARS	CUM V (bbl)	CUM CO2 (Mton)	Max Δ P (psi)	Ending Δ P (psi)	Max Inc %	End Inc %
WDW100	47	7.79E+07	8.67	35	22	1.89	1.19
WDW101	47	9.01E+07	10.02	112	19	6.02	1.02

4.2.4.4 Environmental Processing Systems in Dayton, Texas

Environmental Processing Systems (EPS), operates WDW316 and WDW317, where both wells inject into the same interval around 7330-8180 ft bgl. The text of the permit referenced multiple salt domes in the area (no image from permit), as well as two salt water disposal wells near the edge of the area of review (could not find depth of injection for these wells). This site was particularly eye-catching because of the rather drastic drop in injectivity that never recovered despite remediation efforts (see Figure 4.18)

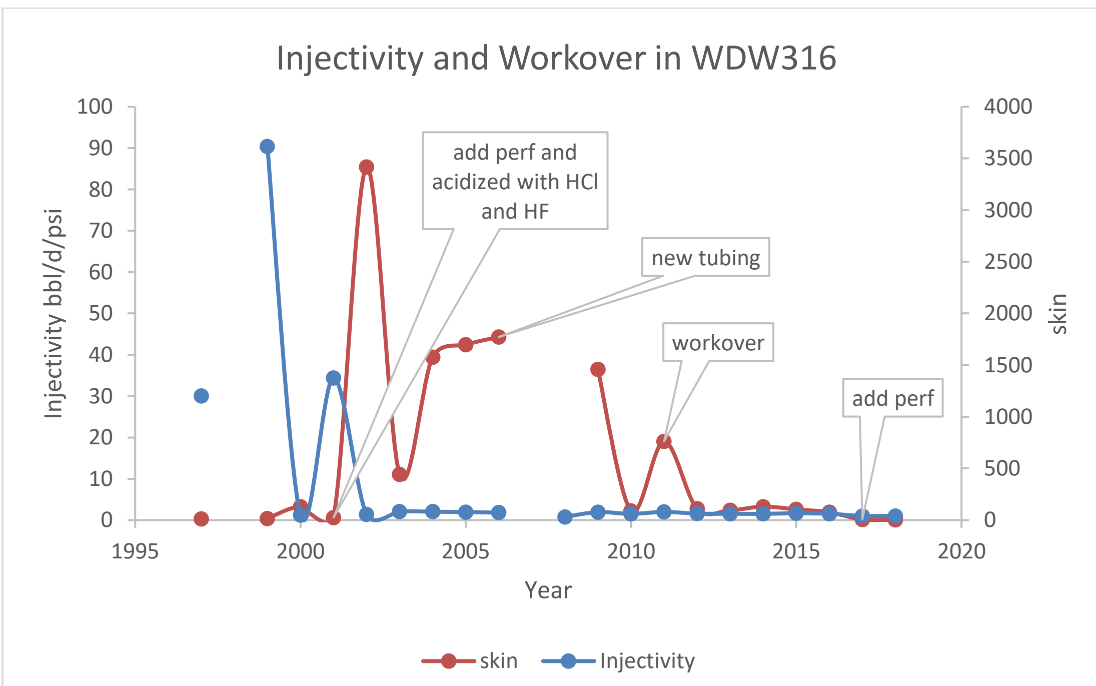

Figure 4.18 Injectivity and workover history as noted in Section VI (Intera, 2019; Daniel B. Stephens & Associates, Inc., 2018).

Therefore, it was believed that the injectivity loss was caused by pressure related restrictions caused either by the salt domes and faults or by the presence of the SWD wells. Figure 4.19 and Figure 4.20 show the volume and pressures noted in the permit including and excluding the volumes injected by the Enterprise SWD wells. Figure 4.21 shows the location of the wells and suspected boundary locations.

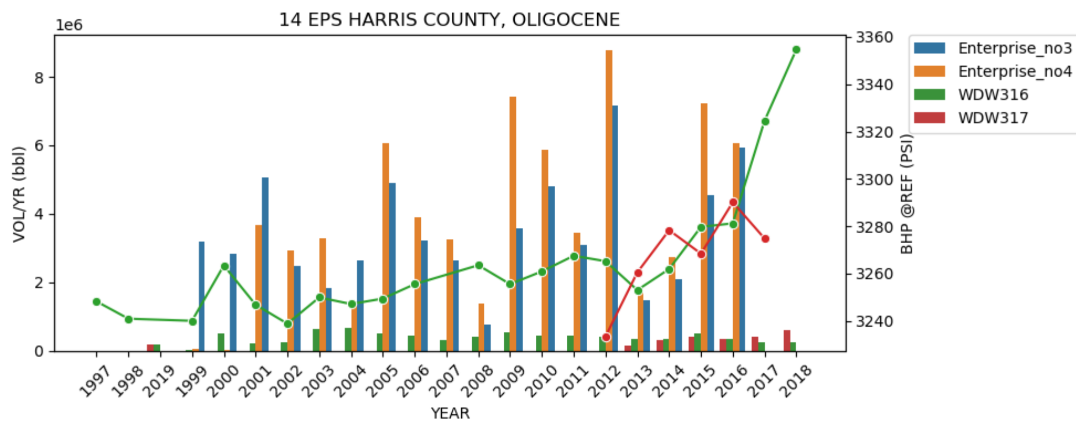

Figure 4.19 Plot of the two EPS wells and two SWD wells. The SWD wells are injecting at much greater volumes that the EPS wells, but pressure response at EPS does not seem to be caused by SWD wells.

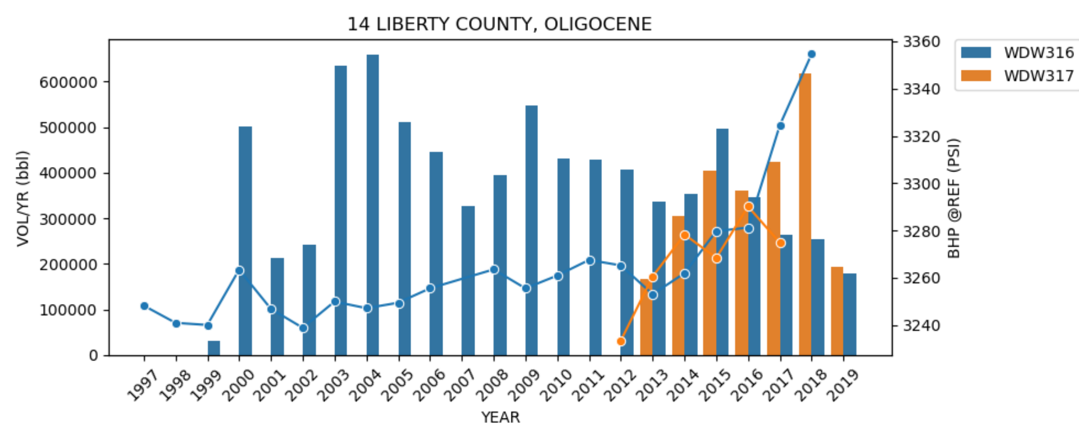

Figure 4.20 Plot of volumes and pressures of just the EPS wells. SWD stopped injecting in 2016, pressure spike in WDW316 seen after in 2017-2018.

Looking at the plots, there is little to no indication that the injection from the SWD wells increased the pressure at this location, so they are not considered as a cause for injectivity loss. The mechanical integrity testing and ambient pressure monitoring of WDW316 in 2000 reported a belief of the loss in transmissivity to be caused by "significant permeability impairment in the near well bore regions of the well" (Terra Dynamics, INC, 2000) i.e. skin, but given the continuously low injectivity in 2012-2018 despite reduced skin, this is also most likely not entirely true.

Table 4.13 Environmental Processing Systems Summary of Volume and Pressure

PERMIT NO.	YEARS	CUM V bbl	CUM CO2 Mton	Max Δ P (psi)	Ending Δ P (psi)	Max Inc %	End Inc %
WDW316	21	8.01E+06	0.89	115	115	3.55	3.55
WDW317	7	2.47E+06	0.28	56	41	1.73	1.27

Replicating the process for Lucite International, EASiTool was used to see if the observed values in operation match a closed or open boundary scenario. Figure 4.21 shows the salt domes and faults that are considered to be the extent of the reservoir area. The permit mentioned a fault related to the Barbers Hill Dome (South East of the wells) but not the Esperson Dome (North of the well) within the injection zone, so the fault in Figure 4.21 located North West to the wells was ignored.

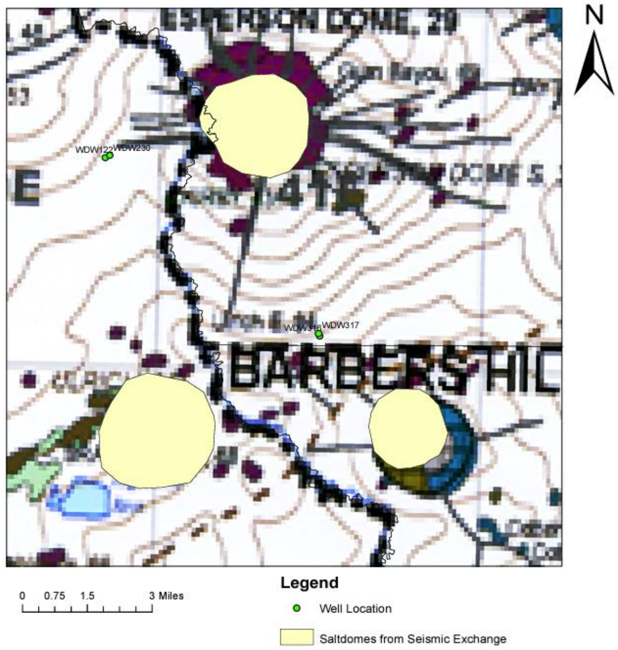

Figure 4.21 EPS site with basemap from GCCC georeferenced (Geomap, 2009). Overlaid are the well locations and salt dome locations downloaded from Seismic Exchange. The faults and salt domes indicate this is a relatively closed reservoir.

The closed boundary prediction from EASiTool estimates the rate to be ~0.165 MMT/year and the open boundary case predicts a rate of ~17.5 MMT/year. Table 4.14 summarizes the estimations made in this thesis. The closed boundary case closely matches the estimations for q2 and q3 (which is the max rate from operations, and the max rate predicted from the average injectivity index, respectively), lending confidence to the theory that the injectivity issues in this location are caused by the boundary conditions.

Table 4.14 CO_2 injection rates for EPS estimated from this thesis as reported in Appendix M. CO_2 injection rates are calculated from a volumetric conversion of water to million tons of CO_2

PERMIT NO.	q1(Mton/yr)	q2(Mton/yr)	q3(Mton/yr)	q4(Mton/yr)
WDW316	0.04	0.13	0.63	7.28
WDW317	0.04	0.12	0.24	4.69

4.2.4.5 Multiple Facilities in Houston, TX

This area near the Houston Ship Channel operates many wells from various facilities which includes TM Deer Park, Vopak, Geo Specialty Chemicals, Sasol Chemicals, Exxon, and Lyondell Chemical. While they were all clustered together in this thesis since they all injected into the Frio formation within the same general area, they are broken down by sand intervals to show some pressure interactions between these wells. Figure 4.22 shows these wells.

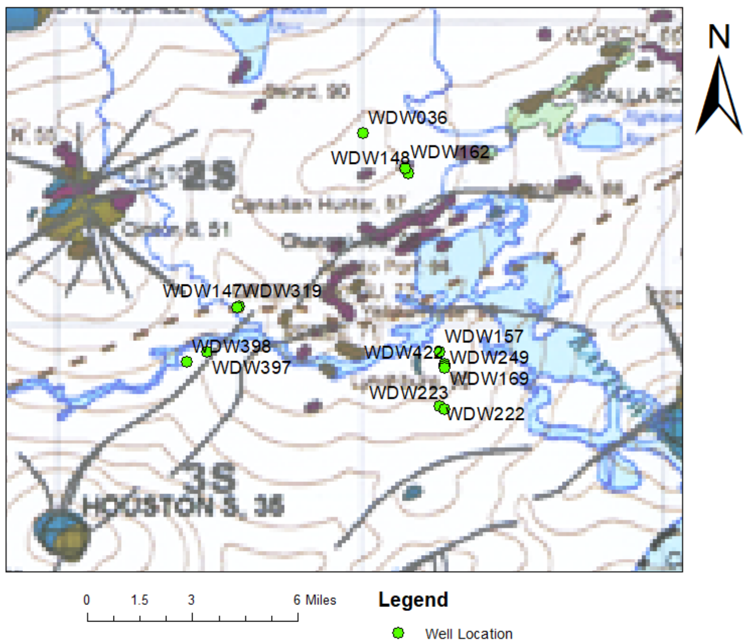

Figure 4.22 Oligocene-Frio Injection wells in Houston, Texas. This location is one of the most densely populated areas for Class I wells. Presence of several faults serve as a pressure seal between wells further up North and to the West.

Within the permits for these wells, applicants frequently referenced each other and included those wells in their cross sections, providing reasonable certainty that the sand one applicant calls ‘Frio A’ or ‘Frio B’ are in fact the same sands as the ones another applicant calls ‘A’ or ‘B’. Figure 4.23 shows a portion of the cross sections from WDW162.

As shown, E&F are the upper most injection sand and Frio A, B, C are often referred to and is lumped together as the ‘comingled Frio ABC’ sands.

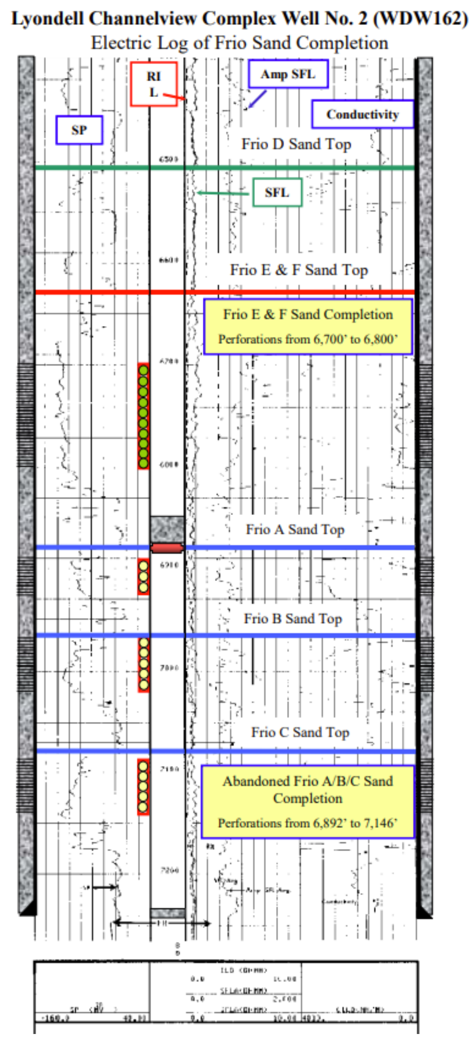

Figure 4.23 Shows Frio names as discussed in Permits (Geostock Sandia, LLC, 2021).

Table 4.15 summarizes the historic injection rates for each well. For the most part, many of these wells inject about similar rates, but the wells operated by Exxon (WDW397 and WDW398) have very high injection volumes. Some records of the pressures were not found.

Table 4.15 Houston area Oligocene-Frio injection rates of water and pressure buildup

PERMIT NO.	YEARS	CUM V (bbl)	CUM CO2 (Mton)	Max Δ P (psi)	Ending Δ P (psi)	Max Inc %	End Inc %
WDW148	37	7.69E+07	8.56	78	78	2.7	2.7
WDW162	33	5.96E+07	6.64				
WDW147	22	5.19E+07	5.77	54	54	1.92	1.92
WDW319	15	2.87E+07	3.19	28	28	0.94	0.94
WDW222	35	1.23E+07	1.37	84	83	2.84	2.8
WDW223	35	8.31E+06	0.93	57	57	1.8	1.8
WDW169	38	2.55E+07	2.84	93	93	3.18	3.18
WDW249	26	1.82E+07	2.02	91	91	3.11	3.11
WDW422	4	8.73E+05	0.10				
WDW157	38	2.48E+07	2.76	57	57	1.93	1.93
WDW397	7	2.98E+07	3.32				
WDW398	4	1.86E+07	2.07				

Figure 4.24 shows the pressure and volume interactions into Frio E&F. WDW147 was on standby since 2000 and was mostly unused, and as mentioned in the permit, the pressure increase shown for that well (in blue) is from the activity in WDW397 and WDW398 which started injection in 2006. These wells are around 1.5 mi from each other and show that they are laterally communicative.

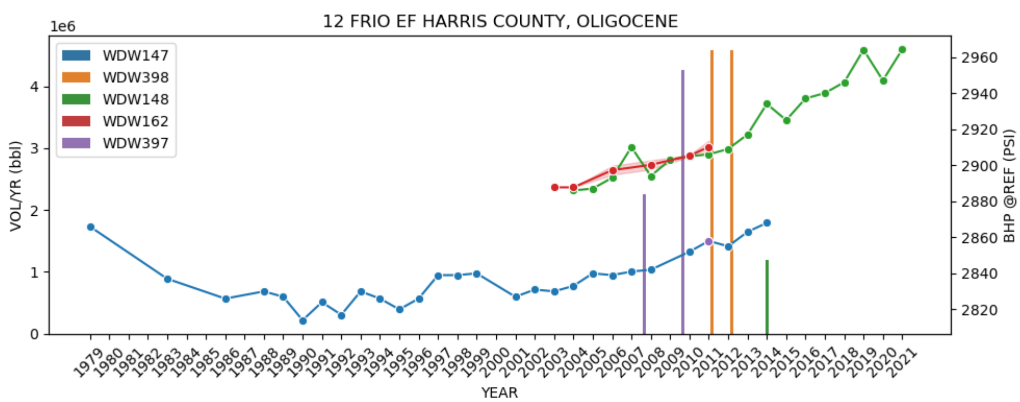

Figure 4.24 Volume and Pressure in Frio EF for wells in Houston. WDW 147 on standby since 2000. Pressure increase is speculated to be caused by WDW397.

WDW162 and WDW 148 are more than 7 miles away, and although they were injecting fluid during that time, given the similarity in the increase of pressure for each of the wells injecting into Frio EF, it is assumed that they are also communicating.

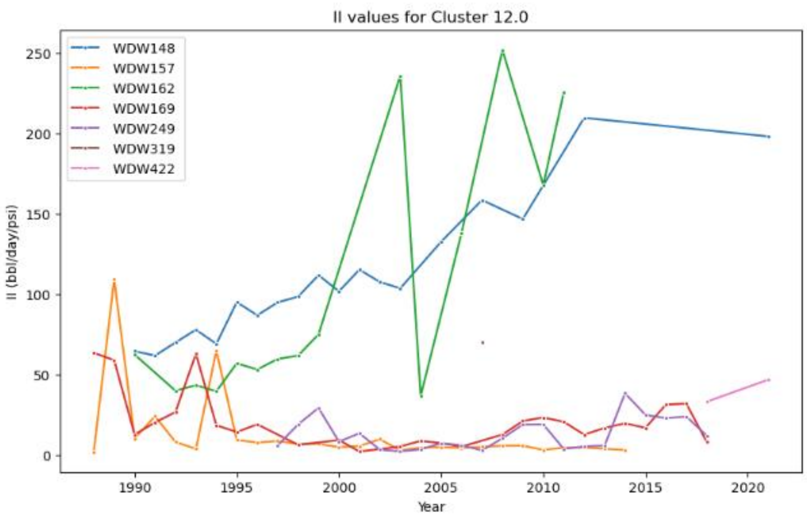

Figure 4.25 Injectivity Index from falloff tests for all wells in Cluster 12, WDW162 and WDW148 are increasing in injectivity.

Looking at Figure 4.25, this increase in pressure does not seem to have affected the injectivity of WDW 162 and WDW148, rather, the injectivity is increasing. It is unclear why and there is not enough data to make a guess. The only information available is that WDW148 recompleted into Frio E&F from Frio ABC in 2004 and WDW162 recompleted into Frio E&F from Frio ABC in 2003, but that does not explain why the increasing trend for the injectivity persists.

Likewise, Lower Frio Injections show similar increasing pressure trends even with WDW157 (green line/bar in Figure 4.26), which has reduced the injection volume year after year since the mid-2000s. These wells are separated from the Exxon wells with multiple faults, and those faults are believed to prevent lateral pressure communication.

The pressure increase seen in Figure 4.26 are cause by these specific wells. These wells show typical injectivity behaviors – initial decrease in injectivity that either plateaus or, in this case, increases later likely due to well stimulation (See Figure 4.25).

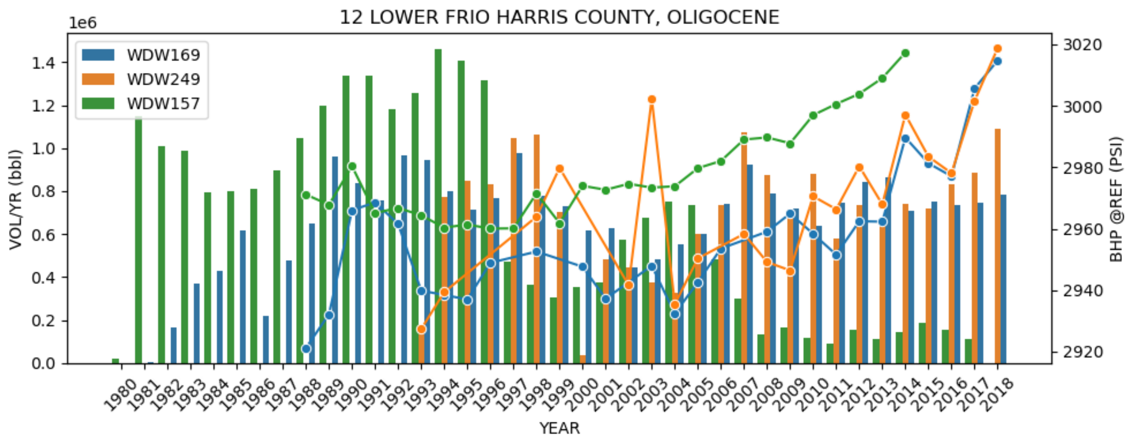

Figure 4.26 Lower Frio Injection Wells in Houston, TX where volume is plotted as bar charts and pressure is plotted as a line. All three wells show similar increase in pressure despite varying volumes.

4.2.4.6 South Texas

In the examples above, and in general, pressure increase is minimal and doesn't increase drastically in response to the waste injected. However, in South Texas, where the wells all injected into the Oligocene formation sands, the pressure increases year after year, not able to easily dissipate, and has a stronger response to fluid injection. Table 4.16 summarizes the volume and pressure response in these wells.

This is not unexpected as the geology in the Oligocene formation sands in this region tend to have poorer quality rocks due to the presence of feldspar, carbonate rocks, and volcanic grains (Loucks et al., 1977). Figure 4.27 – Figure 4.29 shows examples of several facilities which demonstrate this trend.

Table 4.16 South Texas Volume and Pressure Increase

PERMIT NO.	YEARS	CUM V (bbl)	CUM CO2 (Mton)	Max Δ P (psi)	Ending Δ P (psi)	Max Inc %	End Inc %
WDW248	28	3.12E+07	3.48	217	90	11.57	4.8
WDW278	29	4.62E+06	0.51	98	94	4.72	4.53
WDW070	52	1.41e+07	1.57	140	136	7.24	7.03
WDW210	35	2.94E+07	3.275	361	75	18.59	3.86
WDW211	31	1.57E+07	1.749	426	153	23.27	8.36
WDW212	38	3.12E+07	3.472	367	49	19	2.54

As shown in Table 4.16, the wells with the highest pressure buildup are seen in WDW210, WDW211, and WDW212, which are all operated by the same facility. Ticona Polymers, Inc. injects into thick sequences of barrier-bars between the depths of 4160 – 4680 ft in the Anahuac formation in Nueces, Texas and the historical static bottomhole pressure measurements are shown in Figure 4.27. Data on injection volumes were not found.

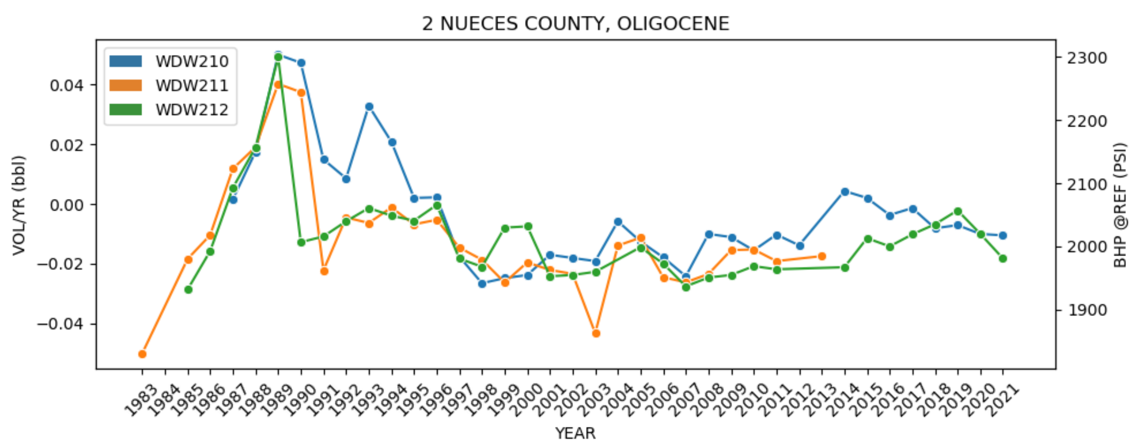

Figure 4.27 Ticona Polymers Bishop Plant. The maximum pressure buildup (for WDW211) is 426 psi (23.27 % increase). By the most recent measurement, it has decreased to a buildup of 153 psi (8.36 % increase).

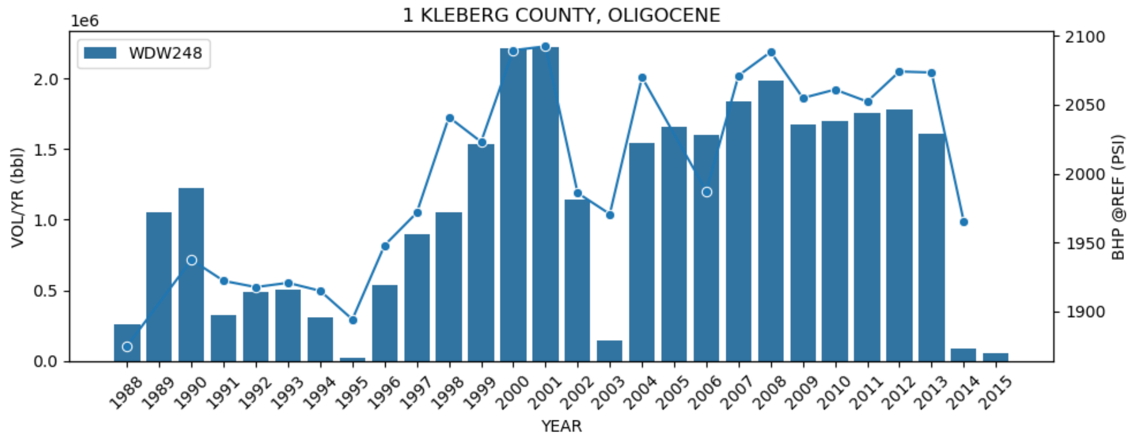

Figure 4.28 Kingsville Dome Uranium Mine. The maximum pressure buildup is at 217 psi (11% increase), though at the end when the pressure drops due to a drop in injected volume, the pressure buildup is at 90 psi (5% increase).

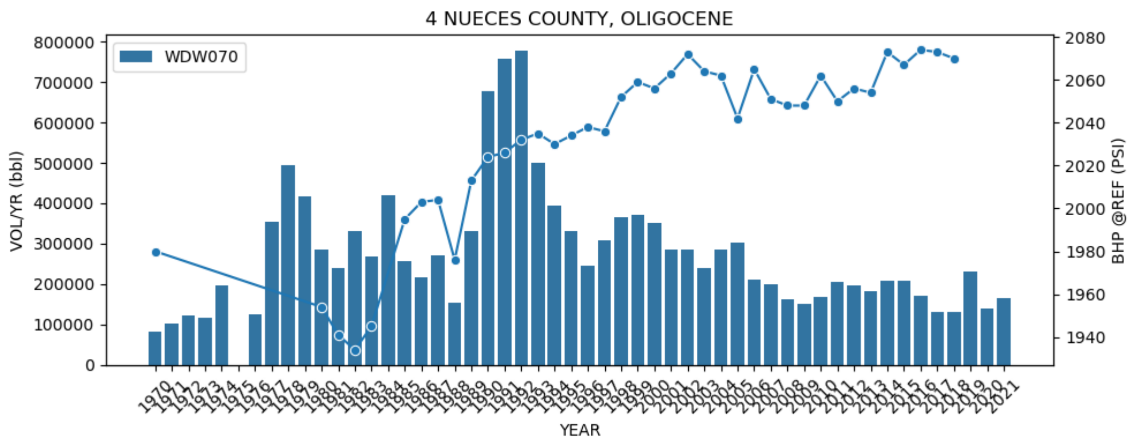

Figure 4.29 TM Corpus Christi. The maximum pressure buildup is at 140 psi (7% increase) and the ending pressure is 136 psi greater than the minimum (7% increase).

5. Discussion

Information pertaining to permeability was gathered from core test reports, which were upscaled using well logs, and was compared to the values derived from the falloff tests. The values calculated for the Injectivity Index were gathered from the flowing bottomhole pressure, rate, and static pressure measured from falloff tests. These tests were conducted over extended periods, spanning many years up to decades. As a result, the collected data encompasses a wide range of permeability and Injectivity Index values, and is believed to be well representative of the formations.

Permeability was upscaled from the data available in 23 wells. All the upscaled values fell within range of the field-scale permeabilities derived from the falloff tests though there was a preference for falling into the upper range (higher than the 50th percentile), and when just comparing the average permeability values, there was an error of around 35% (either over- or underestimating). There were many uncertainties in the porosity estimations of the well logs due to using substitutions from gamma ray and resistivity logs rather than porosity logs and in the relatively small sample size.

Still, the results are believed to be fairly representative given the good match between the log porosity and core porosity values. Notably, there were examples where specific sand intervals were proven to be much lower in permeability when compared to what was predicted through upscaling methods. In these examples however, there were other sand intervals in which the field-scale permeability and upscaled permeability matched well, indicating that errors were due to heterogeneities that could not be captured in this simple upscaling process.

Through analyzing the Injectivity Index from the falloff tests, it was observed that one of the most significant factors impacting the injectivity was the skin factor, which controls near wellbore properties, but that the influence of skin on the injectivity more often than not decreased with time. This indicates that although many wells experienced a decline in injectivity, they eventually plateaued and maintained the ability to accept fluid (see Appendix J). However, skin can be remediated through engineered practices, most often through adding perforations or injecting acid, to bring injectivity up though they may not return to the desired original high-performance value. In the case noted in Section 4.3.5, where remediation efforts made little impact, boundary conditions are suspected to be the cause for the sharp decline in injectivity.

While examining the permits, problematic wells experiencing unexpected issues with injection operations were of particular interest. However, no such wells were identified in this study. This lack of identification can be attributed to the fact that the analysis was mostly limited to current injection wells, which by definition means they are and have been successfully injecting, leading to a survivorship bias. Another likely explanation however, is that the in-depth analysis and site characterization required for these permits were effective for operators to inject into formations that suited their needs.

In the few cases where drops in injectivity were observed, they were caused by pressure issues caused by boundary conditions, near wellbore damage, and well design issues in the early days of injection (1960s). These issues can be resolved with good engineering and management strategies.

Most of these facilities utilized multiple wells, and were able to regulate their injections by alternating between multiple wells or by injecting at lower volumes in every well. Additionally, while permit holders can inject all wells into a single injection interval, more often than not, multiple sand layers are used. This allows injection operations to commence in different layers that do not see vertical communication and allows wells to move to different sand zones if their current sand zone is no longer preferable.

Using the Injectivity Index values as well as historic injected volumes and rates, predictions were made for potential injection rates for CO_2. In the assumptions, only volumetric and density (700 kg/m^3) considerations were made, which is a simplified conversion that does not consider any multiphase flow or consider the efficiency factor in the CO_2 displacing the brine. The uniqueness of the Class VI program not considered is the buoyancy and viscosity of the fluid compared to that of water which would greatly affect the saturation plume of the waste, which would have to be addressed with sophisticated modeling and monitoring practices.

5.1 Policy

CCS and Class VI are still in early development in the United States and face many uncertainties. However, as discussed, a majority of the guidelines have been shaped after pre-existing regulations and have drawn upon the advice and recommendations of experts of established UIC programs to formulate the rules for Class VI (B. Knape, personal communication, August 7, 2023). As the technology and regulations surrounding it continue to update, it is worth considering the evolution of past policies which impacted UIC wells in order to anticipate potential regulatory changes specific to Class VI.

Building on the driving theme of this thesis, which is to leverage the precedents set from previous deep well injections, this section will explore implications for Class VI given the history and development of regulatory standards for other UIC wells.

5.1.1 Historical Overview

Two major regulations governing UIC wells are the Safe Water Drinking Act of 1974 and the Resource Conservation Recovery Act (RCRA) of 1976, which established standards for protecting the drinking water and for disposing waste, respectively. The RCRA defined hazardous waste as any "solid waste" (RCRA § 1004(5), 1976) which is:

> "any garbage, refuse, sludge from a waste treatment plant, water supply treatment plant, or air pollution control facility and other discarded material, including solid, liquid, semisolid, or contained gaseous material resulting from industrial, commercial, mining, and agricultural operations, and from community activities…" (RCRA § 1004(27), 1976).

They also made a distinction in the governing framework for hazardous wastes to be under RCRA Subtitle C and for other 'State or Regional Solid Wastes' to be under

RCRA Subtitle D (RCRA, 1976). The main distinction being that the regulations under Subtitle D were (and still are) more flexible and permissive than those under Subtitle C. However, identifying which wastes belonged under which framework was much contested.

Two years later, the EPA issued Hazardous Waste Guidelines and Regulations (1978) which further described characteristics of these wastes to have ignitability, corrosivity, reactivity, and toxicity. They also aside certain 'special wastes' which shared characteristics of occurring "in very large volumes …[with] potential hazards… [that are] relatively low, and … not amenable to the control techniques developed in Subpart D". These included: (1) Cement Kiln Dust, (2) Utility Waste, (3) Phosphate Mining, Beneficiation, and Processing Waste, (4) Uranium Mining, (5) Other Mining Waste, and (6) Gas and Oil Drilling Muds and Oil Production Brines (43 CFR 58992; 40 CFR § 261.20 –261.24). They were deferred till further study could be conducted as the EPA was not yet clear on the amount of hazardous waste within the materials.

5.1.1.1 Bevill and Bentsen Amendments

Two significant cases were found in searching for past amendments regarding UIC wastes. Congress passed the Solid Waste Disposal Act Amendments of 1980 which exempted wastes from mining and oil & gas related activities from being subject to Subtitle C standards till further analysis was conducted. Specifically, the Bevill Amendment, led by Representative Thomas Bevill, exempted solid wastes from mining related activities, fossil fuel combustions, and cement kiln dust (42 U.S.C. §6921(b)(3)(A)(i)-(iii)). The Bentsen amendment, led by Senator Lloyd Bentsen, exempted wastes related to the energy industry, which included drilling fluids and produced waters (42 U.S.C. §6921(b)(2)(A)).

Ultimately, the EPA concluded that both wastes were not hazardous and would not warrant regulation under Subtitle C. However, they each offer different insights into how these conclusions were made.

In regards to the Bevill Amendment studies on mining materials, though a portion of the waste was found to contain hazardous materials out of the 1.3 billion metric tons of mining waste analyzed, it was concluded to not be need to be regulated under Subtitle C for being "environmentally unnecessary, technically infeasible, [and] economically impractical" (51 FR 24496, 1986). Later, in Environmental Defense Fund (EDF) v. U.S.E.P.A., the court ruled in favor of EPA's decision and noted that Congress indicated studies on the waste should evaluate both the economic and environmental aspects of existing and alternative disposal options, and that the economic evaluations in EPA's study was in line with Congress' goal to "relieve the mining industry of the onerous economic burden of stringent Subtitle C controls if at all possible" (EDF v. U.S.E.P.A, 1988).

Following this, the Bentsen Amendments for "drilling fluids, produced water, and other wastes associated with the exploration, development, or production of crude oil or natural gas" (42 U.S.C. §6921(b)(2)(A)) were similarly analyzed. Though these wastes also contained hazardous constituents, lobbying efforts, concerns for national and energy security, and the large volumes of waste with 1000s of wells made strict regulations for these wastes particularly burdensome (B. Knape, personal communication, August 7, 2023; Cox, 2003). Ultimately, the EPA noted that although there were cases of damage from oil and gas wastes, they were done in violation of existing requirements and concluded that these wastes were unsuited for Subtitle C (hazardous waste management) as it offers little flexibility for regulating these waste products, which are generated from different ecological settings with a "wide variety of hazardous constituents" (53 FR 25446). However, the EPA also conceded to the notion of needing better regulations and sought to work closely with states to improve standards under Subtitle D, the Clean Water Act, and the Safe Drinking Water Act.

One thing made clear was the legislative definition of "other wastes associated", which in this case, refers specifically to primary field operations related to E&P which is specific to substances derived from operation, not those from manufacturing or transportation (EPA, 2002). There is an emphasis here that the exempted wastes depend on how it was generated, not on the actual content of that waste.

In more recent years, with the shale and fracking boom, the applicability of past exemptions to these wastes were brought back to scrutiny as new waste types were utilized in tandem with horizontal drilling practices. After analysis of more current violations and waste releases from these wells, it was found that the primary causes for those incidents were due to human error and lack of compliance with the existing regulations that ultimately did not provide any indication that new regulations were warranted (EPA, 2019, p. 9-4).

What these two cases highlight is the precedent set by the EPA in determining regulatory standards which were ultimately influenced by a number of different of factors which included (but not limited to): business/economic needs, source of waste, quantity of waste, and ability of state authorities to meet federal standards.

5.1.2 Current Applications

As exemplified in the cases above, prominent regulatory alterations within UIC programs were made through various exemptions and considerations of factors like classification of the definition of the waste, business needs, and site exemptions.

This approach of making amendments have already been implemented with EPA's *Hazardous Waste Management System: Conditional Exclusion for Carbon Dioxide (CO2)* in 2014. In this Final Rule, the EPA classified the CO_2 stream captured from an emission source intended for Class VI to be a solid waste, as it fits the hazardous waste description for 'discarded material', but made a conditional exclusion of regulating it under Subtitle C which depends on the fulfillment of the following: (1) Meet the restrictions set by the Department of Transportation, (2) Be compliant with Class VI rules, (3) Should not be mixed with wastes that are considered to be hazardous, and (4) Sign a certification under penalty of law (79 FR 350). However, on the opposing side, there is disagreement that CO_2 used for EOR is viewed as a transactional commodity, not a discarded, abandoned, or recycled material, bringing questions forward questions about why CO_2 for storage is considered a contained, discarded material.

As the program develops and waste management strategies incorporate the usage of hubs for transportation, it becomes essential to delve deeper into the precise characterization of a carbon dioxide stream. The existing definition encompasses 'incidental associated substances', yet in light of the diverse purities originating from different sources, along with the uncertainty surrounding potential chemical interactions and the potential harm certain streams might pose to pipelines, considerations remain for in-depth discussions during the evaluation process.

A current example of the nuances involved in the different types of sources and qualifications for receiving credit for a carbon dioxide stream involves an acid gas recovery unit. A methanol plant installed an acid gas removal (AGR) unit which had already separated CO2 from its gas stream since 2017, just to be released, in order to purify their stream of hydrogen sulfide. Later in 2021, an investor installed new parts to capture this CO_2 that would have otherwise been released to the atmosphere in a 'single process train. The question arose of whether or not an AGR unit which separated CO_2 at its site qualified for the 45Q credit (Rev. Rul. 2021-13; Righetti, 2023).

The intricacy of the matter extends beyond the Class VI Underground Injection Control (UIC) program's criteria for carbon dioxide stream eligibility. It also adds the complexity of broader 45Q credit qualifications, which encompasses waste disposal through a Class II well, and in this case, it was ultimately decided that this investor qualifies for the higher credit.

While the 45Q credit differentiates between CO_2 injected for enhanced oil recovery vs. geologic storage (where the credit for EOR is lower) the distinction was made that disposing of the *waste* from oil and gas can take the higher credit, which reemphasizes the significance of the waste's origin. Furthermore, this case also established that investors claiming credit for 45Q only need to own "at least one component… of a single process train" (Rev. Rul. 2021-13) as long as they are the ones physically ensuring the capture and disposal of the carbon oxide.

In making this a precedent, the Revenue Ruling helps open the doors for more investors to participate in carbon dioxide storage without necessarily going through the process of acquiring a Class VI while also presenting a pathway for Class II wells to transition to Class VI.

Additionally, it is worth mentioning some of the biggest perceived risks of CCS operations: risk of seismic activity and risk of leakage (Warner et al., 2020). Historically, much of these were caused by Class II injection wells, which have older standards and regulations when compared to those for Class VI and Class I. As observed through reading these Class I permits, the monitoring and mechanical integrity testing programs were effective in preventing major issues not necessarily because they never happened, but because problems were caught before they became a major issue leading to a leakage.

On the other hand, while Class II wells do have testing and monitoring requirements (mechanical integrity tests), requirements for testing are less frequent, less stringent, and more time can pass before detecting anomalies. Though regulation in itself is not enough to fully prevent issues, the history of regulatory standards between Class I and Class II wells suggest that the stricter standards set for Class VI are adequate in being able to better monitor, detect, and mitigate major issues commonly associated with injection wells.

5.1.3 Other Considerations

A prominent argument in opposition towards injection practices stems from environmental concerns, but they also stem from the lack of ease in finding or even accessing data with deep well injections. Additionally, as reported by ProPublica when questioned about injection wells, the EPA acknowledged it has done little with the data that it has collected and mentioned a previous attempt to create a national database for injection wells which generated minimal participation from states and regulating bodies (Lustgarten, 2012). Others have noted that though there are some sources of data from the EPA such as the Toxics Release Inventory - which provides data on the quantities and characteristics of emitted wastes - and the Biennial Hazardous Waste Report - which reports the submitted data from large hazardous waste generators - they are not complete and are sometimes contradictory (Simpson & Lester, 2009).

This lack of data availability affects public perception and leaves room for much skepticism. Given the influence of public engagement, communication, and acceptance on the success of CCS projects, a prudent first step to encouraging confidence with the practice would be to make these permits - particularly Class I permits upon which Class VI was built - easier to access. Encouraging actions to increase transparency will not only help with public perception, but will also help Class VI investors, operators, and other stakeholders better understand UIC programs, expectations, and proof of historic success in injection operations.

Furthermore, while reading these permits, it was observed that issues with the wellbore is not an uncommon occurrence, but the frequency of the mechanical integrity tests allowed the operator to remediate the situation before it led to a leakage or well failure. This points to the effectiveness of the regulations for Class I not in necessarily making sure complications never occur, but in ensuring that the measures put in place are able to recognize and prevent problems before they become a risk to human health and the environment. Additionally, a commonly noticed practice in reading these permits were the citation of other Class I wells to describe and defend the assumptions for model inputs such as permeability, porosity, injectivity, etc., which would be beneficial for Class VI permit creators to reference as they take first steps for site characterization.

5.2 FUTURE WORK

The resolution of datasets for the variables analyzing injectivity were limited to annual values. While enlightening, they can often mask the finer details seen in operation. Current research with the GCCC however, includes analysis of Class II SWD disposal wells which have datasets with better resolution of pressure and volume in monthly reports. This will allow for more in-depth analysis of how predictive models for injectivity hold up against real operational data. It would be worthwhile to see how this study can augment those studies and if a similar approach can be taken with Class I data.

It should also be noted that the primary motivation for Class I disposals is to simply dispose of the waste that was generated on site, so they have not been significantly stress tested. Additionally, fall off tests, which were the primary source for injectivity analysis in this thesis, are designed to show a sufficient pressure buildup for analysis, and would likewise, not show a maximum possible rate (E. Gallagher, personal communication, August 18, 2022). However, to see high volume sites with Class I, a good starting point may be to look at commercial Treatment, Storage, and Disposal Facilities (TSDF). These commercial TSDF sites are designed to both treat and store hazardous wastes and are in operation in order to make a profit, accepting wastes from other facilities and generators of waste, and would have more incentive to inject as much as possible (EPA, 2005).

Also, looking more into the details of remediation activities would be interesting to see what the break point seems to be when the operator decides to act. It would be worth knowing if these decisions are driven more by cost or by loss of injectivity. Studying over time would also shed light on whether there are diminishing returns for each stimulation job and if there is a point at which one would choose to abandon the well.

Finally, finding and analyzing older, plugged wells would be needed to see if any of them discontinued due to a loss of injectivity. Understanding what caused the reservoir to not accept fluids will help prepare Class VI operators for potential problems.

6. Conclusion

In this preliminary analysis of Class I wells, permits and associated documents were studied to extract data from these long-term, large-volume, wastewater injection wells, which have established safe practices and strong precedents for the UIC program. The material in each of these permits is data dense and includes details applicable to Class VI injection wells for carbon dioxide storage.

Assuming injectivity to be a transferrable property between water vs. carbon dioxide injection, the collected information focuses on any data describing the permeability or pressure response caused by injection. These included data from core test reports, well logs, fall off tests, and historical information detailing injection volume, rate, or pressure.

From the comparison of core-scale, log-scale, and field-scale permeabilities, it was concluded that values from core samples provide reasonable estimations of the observed field-scale permeabilities derived from the falloff tests. The upscaled values fell within the whole range of ‘real’ permeability values but had a preference to overestimate the average permeability value, falling in the upper half of the entire range. There was an error of 36% in wells that overestimated and an error of 34 % in the wells that underestimated the field-scale permeability value, averaging at a 35% error above or below the real permeability.

Additionally, it was found that these formations can maintain sufficient injectivity even after decades of injection and can store large volumes of waste without endangering the underground source of drinking water. Analysis of different locations show trends which show higher permeability and injectivity in Miocene formations as well as in Oligocene formations further East along the Texas Gulf Coast. Predictions for these injection rates of CO_2 showed they have the ability to injection over 1 Million Metric Ton a year, with exceptions in South Texas where there are poorer quality rocks.

Issues interfering with injectivity were mostly limited problems caused by near wellbore damage and pressure management issues caused by the proximity to sealed boundaries. These are all things that can be addressed with engineering solutions and good well management strategies.

Looking at the historic data, most wells show a minimal increase in total pressure buildup, with some (in Miocene formations) showing a low of a 0% increase. Wells in South Texas saw a maximum pressure buildup of 426 psi (23% increase) which at the most recent static pressure measurement, was down to 153 psi (8% increase). For most other wells not in South Texas, pressure buildup stayed well below a 10% increase.

This data is representative of decades worth of operational history which not only builds confidence in the validity of the long-term impacts of large volume injections, but also builds confidence in the regulatory compliance of the programs through the mere fact that these old documents were able to be found and reported after all these years.

Using the lessons learned from Class I wells and leveraging the data available in these permits, measures can be taken to ensure a degree of certainty in the Class VI program's success and help stakeholders utilize the data to help make assessments early in the permitting process.

Appendices

APPENDIX A: PERMIT AND WELL DETAILS

The following table shows details for the wells viewed in this study. The 'PERMITEE' is relevant when analyzing injection rates and pressure buildup over time since many sites operate multiple wells simultaneously at lower rates or switch between wells as a way to moderate pressure buildup. The permit holder listed here may not necessarily be the most recent owner of the permit as these wells can be transferred. The 'O' and 'M' under column 'FM' stands for Oligocene and Miocene and the 'Injection FM' shows the specific sands as defined by the permittees.

CLUSTER	FM	INJECTION SAND	NO.	LAT(N)	LONG(W)	PERMITTEE	STATUS
			TEXAS WELLS				
1	O	FRIO	WDW248	27.39194	-97.77028	KINGSVILLE DOME URANIUM MINE	ACTIVE
2	O	ANAHUAC	WDW210	27.57139	-97.82944	TICONA POLYMERS INC.	ACTIVE
2	O	ANAHUAC	WDW211	27.56750	-97.82917	TICONA POLYMERS INC.	ACTIVE
2	O	ANAHUAC	WDW212	27.56611	-97.82972	TICONA POLYMERS INC.	ACTIVE
3	O	FRIO	WDW152	27.81167	-97.59500	EQUISTAR CHEMICALS	ACTIVE
3	O	FRIO	WDW153	27.81139	-97.59500	EQUISTAR CHEMICALS	ACTIVE
3	O	FRIO	WDW278	27.73028	-97.65778	US ECOLOGY TEXAS INC	ACTIVE
3	O	FRIO	WDW279	27.73083	-97.65778	US ECOLOGY TEXAS INC	ACTIVE
4	O	CATAHOULA	WDW070	27.71353	-97.46073	TM CORPUS CHRISTI SERVICES	ACTIVE
5	O	MAIN/LOWER CATAHOULA	WDW004	28.67444	-96.95139	INVISTA S. a r.l., LLC - VICTORIA SITE	ACTIVE

CLUSTER	FM	INJECTION SAND	NO.	LAT(N)	LONG(W)	PERMITTEE	STATUS
5	O	MAIN/LOWER CATAHOULA	WDW028	28.67056	-96.95833	INVISTA S. a r.l., LLC - VICTORIA SITE	ACTIVE
5	O	MAIN/LOWER CATAHOULA	WDW029	28.66889	-96.96083	INVISTA S. a r.l., LLC - VICTORIA SITE	ACTIVE
5	O	MAIN CATAHOULA	WDW030	28.67250	-96.95389	INVISTA S. a r.l., LLC - VICTORIA SITE	ACTIVE
5	O	LOWER CATAHOULA	WDW105	28.67611	-96.95778	INVISTA S. a r.l., LLC - VICTORIA SITE	ACTIVE
5	O	MAIN CATAHOULA	WDW106	28.67556	-96.95333	INVISTA S. a r.l., LLC - VICTORIA SITE	ACTIVE
5	O	MAIN CATAHOULA	WDW142	28.67111	-96.96250	INVISTA S. a r.l., LLC - VICTORIA SITE	ACTIVE
5	O	LOWER CATAHOULA	WDW143	28.67639	-96.95222	INVISTA S. a r.l., LLC - VICTORIA SITE	ACTIVE
5	O	LOWER CATAHOULA	WDW144	28.67361	-96.95750	INVISTA S. a r.l., LLC - VICTORIA SITE	ACTIVE
5	O	LOWER CATAHOULA/GRETA	WDW145	28.67806	-96.95472	INVISTA S. a r.l., LLC - VICTORIA SITE	EXPIRED
5	O	LOWER CATAHOULA/GRETA	WDW271	28.67806	-96.95472	INVISTA S. a r.l., LLC - VICTORIA SITE	CANCELLED
6	O	FRIO	WDW163	28.56583	-96.83722	INEOS NITRILES USA LLC	ACTIVE
6	O	FRIO	WDW164	28.56681	-96.83719	INEOS NITRILES USA LLC	ACTIVE
6	O	FRIO	WDW165	28.56758	-96.83556	INEOS NITRILES USA LLC	ACTIVE
7	M	UPPER MIOCENE	WDW014	28.87194	-96.02083	HOECHST CELANESE CHEMICAL GROUP	CANCELLED
7	M	UPPER MIOCENE	WDW032	28.85806	-96.02028	HOECHST CELANESE CHEMICAL GROUP	CANCELLED
7	M	UPPER MIOCENE	WDW049	28.85667	-96.01639	HOECHST CELANESE CHEMICAL GROUP	CANCELLED
7	M	UPPER MIOCENE	WDW110	28.86333	-96.02083	HOECHST CELANESE CHEMICAL GROUP	CANCELLED
8	M	OAKVILLE	WDW051	29.00361	-95.40028	BASF CORPORATION	ACTIVE
8	M	OAKVILLE	WDW099	29.00361	-95.39917	BASF CORPORATION	ACTIVE
8	M	OAKVILLE	WDW408	29.00444	-95.39944	BASF CORPORATION	ACTIVE
8	M	MIOCENE	WDW435	28.95318	-95.30769	HUNTSMAN ETHYLENEAMINES LLC	ACTIVE

CLUSTER	FM	INJECTION SAND	NO.	LAT(N)	LONG(W)	PERMITTEE	STATUS
8	M	MIOCENE	WDW436	28.95319	-95.30762	HUNTSMAN ETHYLENEAMINES LLC	ACTIVE
9	M	OAKVILLE	WDW013	29.25889	-95.20306	ASCEND PERFORMANCE MATERIALS LLC	ACTIVE
9	M	OAKVILLE	WDW224	29.24667	-95.20944	ASCEND PERFORMANCE MATERIALS LLC	ACTIVE
9	M	OAKVILLE	WDW318	29.25722	-95.20222	ASCEND PERFORMANCE MATERIALS LLC	ACTIVE
9	M	OAKVILLE	WDW326	29.25028	-95.20583	ASCEND PERFORMANCE MATERIALS LLC	ACTIVE
9	M	OAKVILLE	WDW359	29.24531	-95.21125	ASCEND PERFORMANCE MATERIALS LLC	ACTIVE
10	M	OAKVILLE	WDW091	29.37598	-94.89772	STERLING CHEMICALS INC	EXPIRED
10	M	OAKVILLE	WDW196	29.37621	-94.89776	STERLING CHEMICALS INC	EXPIRED
10	M	OAKVILLE	WDW314	29.37545	-94.89610	STERLING CHEMICALS INC	EXPIRED
10	M	OAKVILLE	WDW034	29.42583	-94.97083	ISP TECHNOLOGIES INC	ACTIVE
10	M	OAKVILLE	WDW113	29.42250	-94.96417	ISP TECHNOLOGIES INC	ACTIVE
10	M	OAKVILLE	WDW114	29.42889	-94.97578	ISP TECHNOLOGIES INC	ACTIVE
10	M	OAKVILLE	WDW080	29.37528	-94.92306	BLANCHARD REFINING COMPANY	ACTIVE
10	M	OAKVILLE	WDW127	29.3775	-94.92083	BLANCHARD REFINING COMPANY	PLUGGED
10	M	OAKVILLE	WDW128	29.37694	-94.92083	BLANCHARD REFINING COMPANY	ACTIVE
11	O	FRIO	WDW111	29.58000	-95.43000	AKZO NOBEL INDUSTRIAL SPECIALTIES	PLUGGED
11	O	FRIO	WDW139	29.58222	-95.43278	AKZO NOBEL INDUSTRIAL SPECIALTIES	ACTIVE
11	O	FRIO	WDW343	29.58333	-95.43528	AKZO NOBEL INDUSTRIAL SPECIALTIES	ACTIVE
12	O	FRIO	WDW148	29.81447	-95.10681	LYONDELL CHEMICAL COMPANY	ACTIVE
12	O	FRIO	WDW162	29.81680	-95.10787	LYONDELL CHEMICAL COMPANY	ACTIVE
12	O	FRIO	WDW147	29.75972	-95.17639	SASOL CHEMICALS USA	ACTIVE
12	O	FRIO	WDW319	29.75936	-95.17719	SASOL CHEMICALS USA	ACTIVE
12	O	FRIO	WDW222	29.71861	-95.09361	GEO SPECIALTY CHEMICALS	ACTIVE
12	O	FRIO	WDW223	29.71750	-95.09167	GEO SPECIALTY CHEMICALS	ACTIVE
12	O	FRIO	WDW169	29.73614	-95.09173	TM DEER PARK SERVICES LLC	ACTIVE
12	O	FRIO	WDW249	29.73540	-95.09193	TM DEER PARK SERVICES LLC	ACTIVE

CLUSTER	FM	INJECTION SAND	NO.	LAT(N)	LONG(W)	PERMITTEE	STATUS
12	O	FRIO	WDW422	29.73424	-95.09168	TM DEER PARK SERVICES LLC	ACTIVE
12	O	FRIO	WDW157	29.74083	-95.09389	VOPAK LOGISTICS SERVICES USA DEER PARK	ACTIVE
12	O	FRIO	WDW397	29.74083	-95.18972	EXXONMOBIL	ACTIVE
12	O	FRIO	WDW398	29.73667	-95.19806	EXXONMOBIL	ACTIVE
12	O	FRIO	WDW036	29.83111	-95.12556	EQUISTAR CHEMICALS	PLUGGED
13	M	OAKVILLE	WDW082	29.69972	-95.03861	E I DU PONT DE NEMOURS	ACTIVE
13	M	OAKVILLE	WDW083	29.70222	-95.04028	E I DU PONT DE NEMOURS	ACTIVE
13	M	OAKVILLE	WDW149	29.70139	-95.04306	E I DU PONT DE NEMOURS	ACTIVE
13	M	MIOCENE	WDW033	29.62611	-95.06389	CELANESE CLEAR LAKE PLANT	PLUGGED
14	O	FRIO	WDW316	29.88868	-94.93851	ENVIRONMENTAL PROCESSING SYSTEMS, L.C.	ACTIVE
14	O	FRIO	WDW317	29.88962	-94.93908	ENVIRONMENTAL PROCESSING SYSTEMS, L.C.	ACTIVE
14	O	FRIO/VICKSBURG	WDW122	29.94944	-95.02250	ARKEMA INC. CROSBY PLANT	ACTIVE
14	O	FRIO/VICKSBURG	WDW230	29.95028	-95.02083	ARKEMA INC. CROSBY PLANT	ACTIVE
15	M	OAKVILLE	WDW160	29.85389	-94.09806	VEOLIA ES TECHNICAL SOLUTIONS	ACTIVE
15	M	OAKVILLE	WDW358	29.85438	-94.09717	VEOLIA ES TECHNICAL SOLUTIONS	ACTIVE
15	M	OAKVILLE	WDW125	29.96917	-94.06083	BASF CORPORATION	PLUGGED
15	M	OAKVILLE	WDW155	29.96861	-94.05917	BASF CORPORATION	ACTIVE
15	M	OAKVILLE	WDW201	29.96750	-94.05917	BASF CORPORATION	ACTIVE
15	O	FRIO	WDW301	29.96778	-94.06111	BASF CORPORATION	ACTIVE
15	O	FRIO	WDW302	29.97056	-94.05861	BASF CORPORATION	ACTIVE
15	M	OAKVILLE	WDW100	30.01922	-94.03079	LUCITE INTERNATIONAL	ACTIVE
15	M	OAKVILLE	WDW101	30.01895	-94.02861	LUCITE INTERNATIONAL	ACTIVE
15	O	FRIO	WDW188	30.01685	-94.02801	THE DOW CHEMICAL COMPANY	ACTIVE
16	M	OAKVILLE	WDW054	30.05174	-93.75946	INVISTA S.ar.1. SABINE RIVER WORKS	ABANDONED
16	M	OAKVILLE	WDW055	30.05093	-93.75819	INVISTA S.ar.1. SABINE RIVER WORKS	PLUGGED
16	M	OAKVILLE	WDW191	30.05025	-93.75775	INVISTA S.ar.1. SABINE RIVER WORKS	ACTIVE

CLUSTER	FM	INJECTION SAND	NO.	LAT(N)	LONG(W)	PERMITTEE	STATUS
16	M	OAKVILLE	WDW282	30.05000	-93.75809	INVISTA S.ar.1. SABINE RIVER WORKS	ACTIVE
LOUISIANA WELLS							
17	M	MIOCENE	970903	30.17521	-93.32794	KEN E. DAVIS	plugged (1993)
17	M	MIOCENE	970904	30.17521	-93.32694	KEN E. DAVIS	plugged (1993)
17	M	MIOCENE	971123	30.17333	-93.32694	KEN E. DAVIS	plugged (1993)
17	M	MIOCENE	971124	30.17417	-93.33083	KEN E. DAVIS	plugged (1993)
18	M	MIOCENE	975072	30.21848	-91.05113	INNOPHOS, INC. (60042)	ACTIVE
18	M	MIOCENE	975071	30.21829	-91.05120	INNOPHOS, INC. (60042)	ACTIVE
19	M	MIOCENE	974237	30.04277	-90.80803	MOSAIC FERTILIZER, LLC (M338)	ACTIVE
19	M	MIOCENE	974238	30.04144	-90.82428	MOSAIC FERTILIZER, LLC (M338)	ACTIVE
20	M	MIOCENE	972060	29.98128	-90.45385	GALATA CHEMICALS, LLC (G198)	ACTIVE
20	M	MIOCENE	970802	30.00407	-90.42627	SHELL NMC (5386)	plugged (1989)
20	M	MIOCENE	970801	29.95457	-90.26959	SHELL NMC (5386)	
0*	E	COCKFIELD	WDW315	30.29288	-97.99361	TEXCOM GULF DISPOSAL	EXPIRED
0*	E	WILCOX	WDW168	28.94666	-97.99361	SOUTH TEXAS MINING VENTURE LLP	ACTIVE

** Cluster ‘0’ wells were not studied further, but core data was recorded and included in Appendix C.*

APPENDIX B: DATA AVAILABILITY

The following table summarizes which datasets were available for each well. The column 'INTERVAL (ft) BGL' shows the specific depths authorized for injection, not the entire injection zone, in feet below ground level (BGL). Depths from Louisiana's permits were from Mean Sea Level, but were altered by adding in the ground elevation. The 'CORE PLUGS' shows the number of individual data points reported in the core test results. 'WELL TEST YEARS' shows the number of years of falloff tests found. The 'X' indicates that logs or cumulative injected volumes were available.

CLUSTER	NO.	INTERVAL (ft) BGL		CORE	LOG	WELL TEST	CUMVOL
		TOP	BASE	PLUGS		YEARS	
1	WDW248	4198	5288	41	X	29	X
2	WDW210	4150	4670			25	X
2	WDW211	4200	4500			22	X
2	WDW212	4170	4700			22	X
3	WDW152	7115	7453	27		17	X
3	WDW153	7115	7435	77		18	X
3	WDW278	4720	5110	99		26	X
3	WDW279	4680	5130			1	X
4	WDW070	4525	4722	41	X	29	X
5	WDW004	3724	4626				X
5	WDW028	3742	4137				X
5	WDW029	3778	4162				X
5	WDW030	3745	4124				X
5	WDW105	3702	4105			5	X
5	WDW106	3706	4137				X
5	WDW142	3725	4162			23	X
5	WDW143	3708	4607				X
5	WDW144	3713	4628			16	X
5	WDW145	3782	4169			7	X
5	WDW271	4384	4650				X
6	WDW163	5352	5692	46	X	28	X
6	WDW164	7413	7983	74		32	X
6	WDW165	6578	7478	46	X	32	X

CLUSTER	NO.	INTERVAL (ft) BGL TOP	BASE	CORE PLUGS	LOG	WELL TEST YEARS	CUMVOL
7	WDW014	3350	3600			3	X
7	WDW032	3350	3600			4	X
7	WDW049	3350	3600			5	X
7	WDW110	3350	3600			5	X
8	WDW051	5886	6186		X	17	X
8	WDW099	6845	7367	7		13	X
8	WDW408	5877	7377			1	X
8	WDW435	5150	6450	12		1	X
8	WDW436	5150	6450			1	X
9	WDW013	6229	6911			27	X
9	WDW224	5835	6161				X
9	WDW318	4053	4615				X
9	WDW326	5762	6086	8			X
9	WDW359	5109	5165			20	X
10	WDW091	6678	7053	56		11	X
10	WDW196	6587	7056	35		12	X
10	WDW314	6610	7170	57		10	X
10	WDW034	3660	6000	10			X
10	WDW113	3723	6000	55			X
10	WDW114	3550	6000	76			X
10	WDW080	5750	6402			31	X
10	WDW127	5800	6482			32	X
10	WDW128	5799	6453	126	X	31	X
11	WDW111	5515	7435			3	X
11	WDW139	5523	7440			3	X
11	WDW343	5509	7426	66		15	X
12	WDW148	6494	7162	128		19	X
12	WDW162	6488	7155			15	X
12	WDW147	6548	7270	65	X	20	X
12	WDW319	6564	7274			15	X
12	WDW222	5584	7634	20		4	X
12	WDW223	5602	7634	12		5	X
12	WDW169	6853	7355	33	X	27	X
12	WDW249	6854	7354	27		22	X
12	WDW422	6862	7341		X	2	X
12	WDW157	5513	7488	85	X	27	X
12	WDW397	6613	6642	141	X	4	X
12	WDW398	6966	7130	20		2	X

CLUSTER	NO.	INTERVAL (ft) BGL TOP	BASE	CORE PLUGS	LOG	WELL TEST YEARS	CUMVOL
12	WDW036	6315	6885	30			
13	WDW082	4788	5438			1	X
13	WDW083	4788	5438			31	X
13	WDW149	4785	5435			18	X
13	WDW033	5250	5400	42		2	
14	WDW316	7332	8182	42	X	18	X
14	WDW317	7334	8184		X	5	X
14	WDW122	5083	6683	46		4	X
14	WDW230	5080	6680	36		4	X
15	WDW160	6981	7190	24	X	32	X
15	WDW358	6975	7271	12		6	X
15	WDW125	3830	6800				X
15	WDW155	3830	6800				X
15	WDW201	3830	6800				X
15	WDW301	7400	8250	129			X
15	WDW302	7400	8250	25		1	X
15	WDW100	4153	4208	81	X	17	X
15	WDW101	4148	4208			4	X
15	WDW188	7339	7543	34			
16	WDW054	4609	4739	56	X	6	X
16	WDW055	4513	4538			3	X
16	WDW191	6163	6361	51	X	25	X
16	WDW282	6410	6450	105	X	19	X
17	970903	4639	4859				X
17	970904	4782	4812			2	X
17	971123	5500	5946	48	X		X
17	971124	5832	6265	46		2	X
18	975071	4705	5050	46		1	X
18	975072	4745	5087	40		1	X
19	974237	6434	6643			1	
19	974238	6621	6990			1	
20	972060	6600	6731	36		1	X
20	970802	2830	2850	17	X		X

APPENDIX C: CORES

Cores divided by ‘Type’ is between SWC (sidewall core) vs FC (full core), and ‘Fluid’ injected for test is between air and liquid. Last plot shows regression equation for the logarithm of permeability vs porosity.

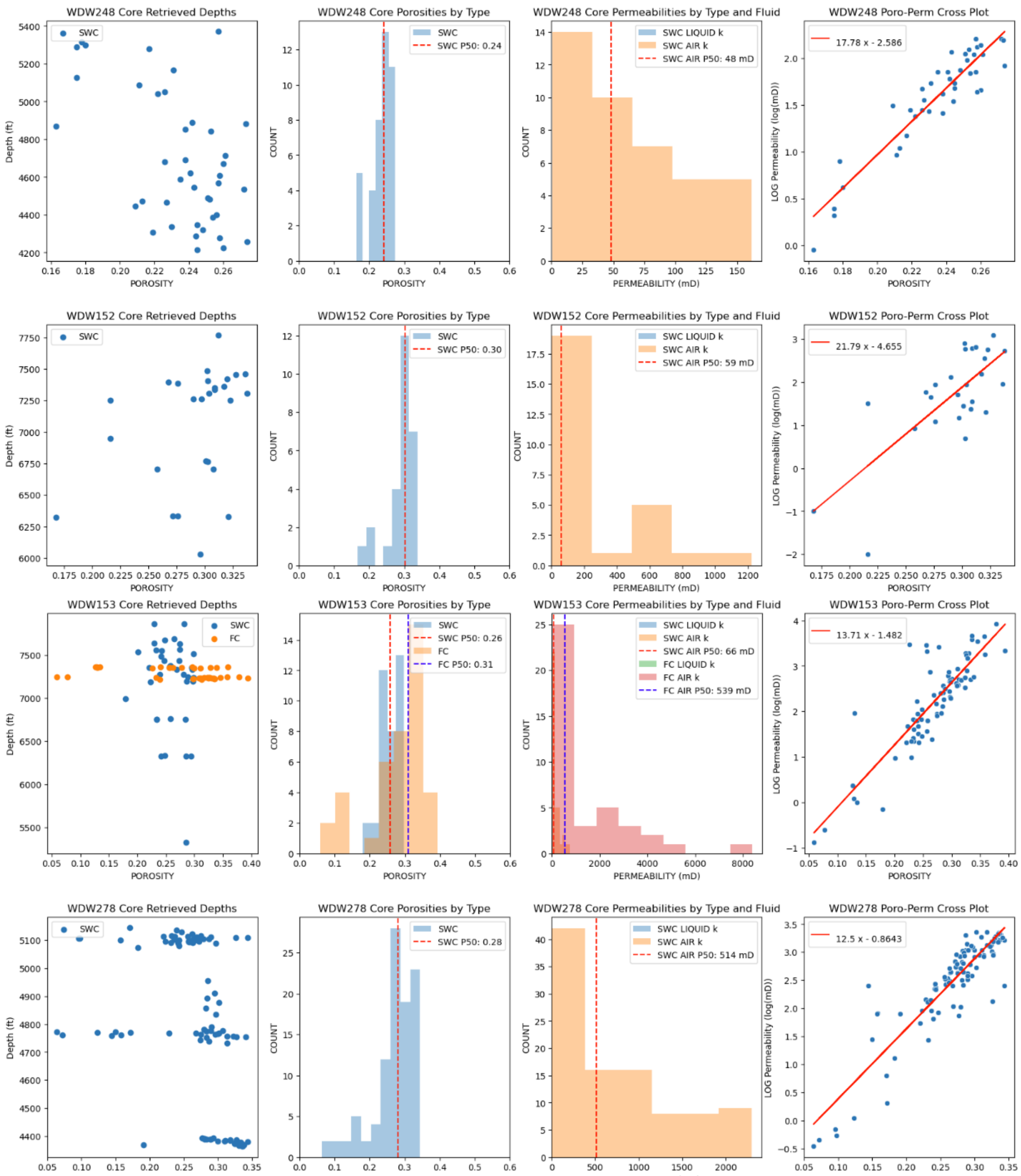

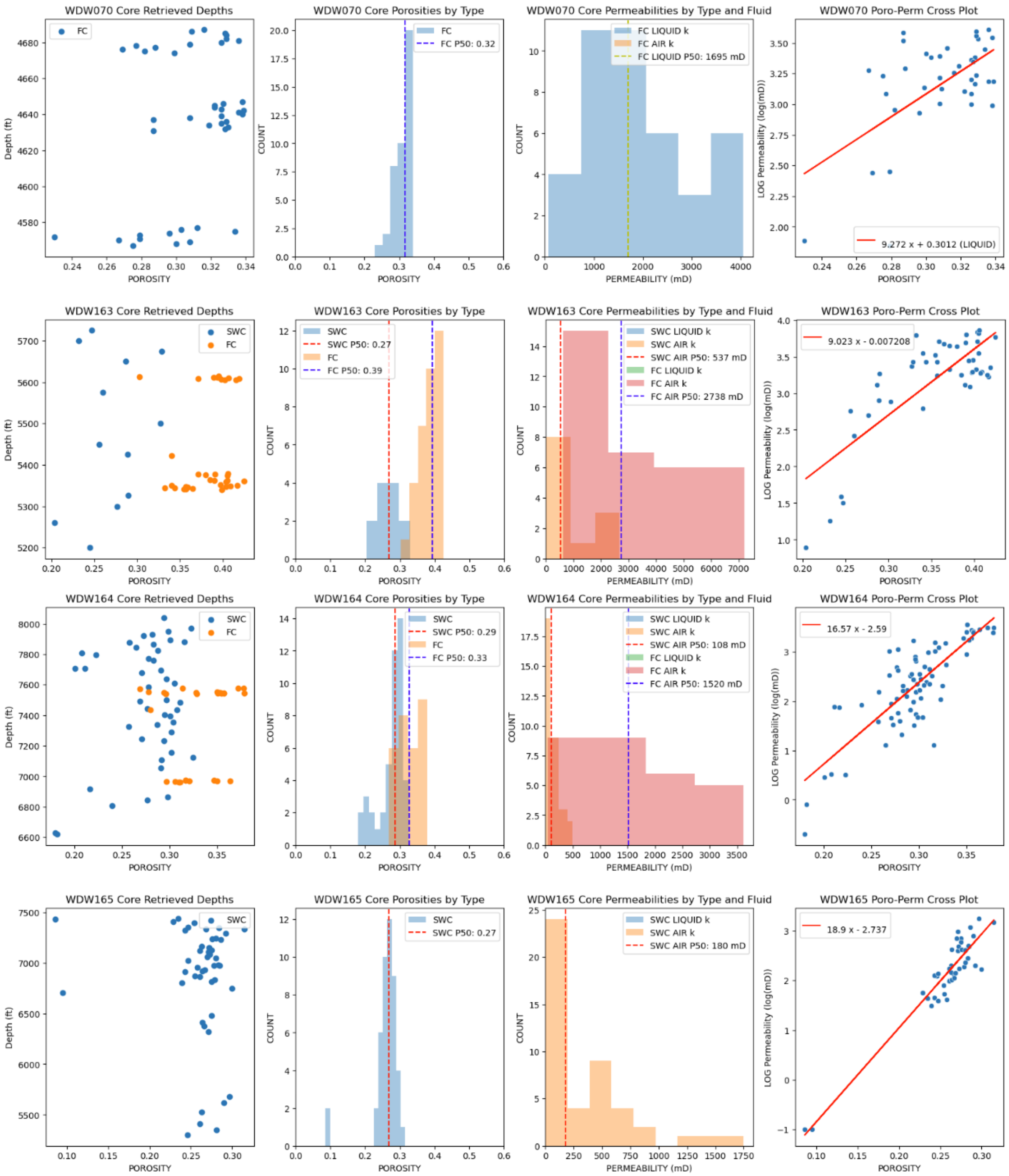
WDW070 Core Retrieved Depths
FC
Depth (ft)
POROSITY
WDW070 Core Porosities by Type
FC
FC P50: 0.32
COUNT
POROSITY
WDW070 Core Permeabilities by Type and Fluid
FC LIQUID k
FC AIR k
FC LIQUID P50: 1695 mD
COUNT
PERMEABILITY (mD)
WDW070 Poro-Perm Cross Plot
LOG Permeability (log(mD))
9.272 x + 0.3012 (LIQUID)
POROSITY
WDW163 Core Retrieved Depths
SWC
FC
Depth (ft)
POROSITY
WDW163 Core Porosities by Type
SWC
SWC P50: 0.27
FC
FC P50: 0.39
COUNT
POROSITY
WDW163 Core Permeabilities by Type and Fluid
SWC LIQUID k
SWC AIR k
SWC AIR P50: 537 mD
FC LIQUID k
FC AIR k
FC AIR P50: 2738 mD
COUNT
PERMEABILITY (mD)
WDW163 Poro-Perm Cross Plot
9.023 x - 0.007208
LOG Permeability (log(mD))
POROSITY
WDW164 Core Retrieved Depths
SWC
FC
Depth (ft)
POROSITY
WDW164 Core Porosities by Type
SWC
SWC P50: 0.29
FC
FC P50: 0.33
COUNT
POROSITY
WDW164 Core Permeabilities by Type and Fluid
SWC LIQUID k
SWC AIR k
SWC AIR P50: 108 mD
FC LIQUID k
FC AIR k
FC AIR P50: 1520 mD
COUNT
PERMEABILITY (mD)
WDW164 Poro-Perm Cross Plot
16.57 x - 2.59
LOG Permeability (log(mD))
POROSITY
WDW165 Core Retrieved Depths
SWC
Depth (ft)
POROSITY
WDW165 Core Porosities by Type
SWC
SWC P50: 0.27
COUNT
POROSITY
WDW165 Core Permeabilities by Type and Fluid
SWC LIQUID k
SWC AIR k
SWC AIR P50: 180 mD
COUNT
PERMEABILITY (mD)
WDW165 Poro-Perm Cross Plot
18.9 x - 2.737
LOG Permeability (log(mD))
POROSITY

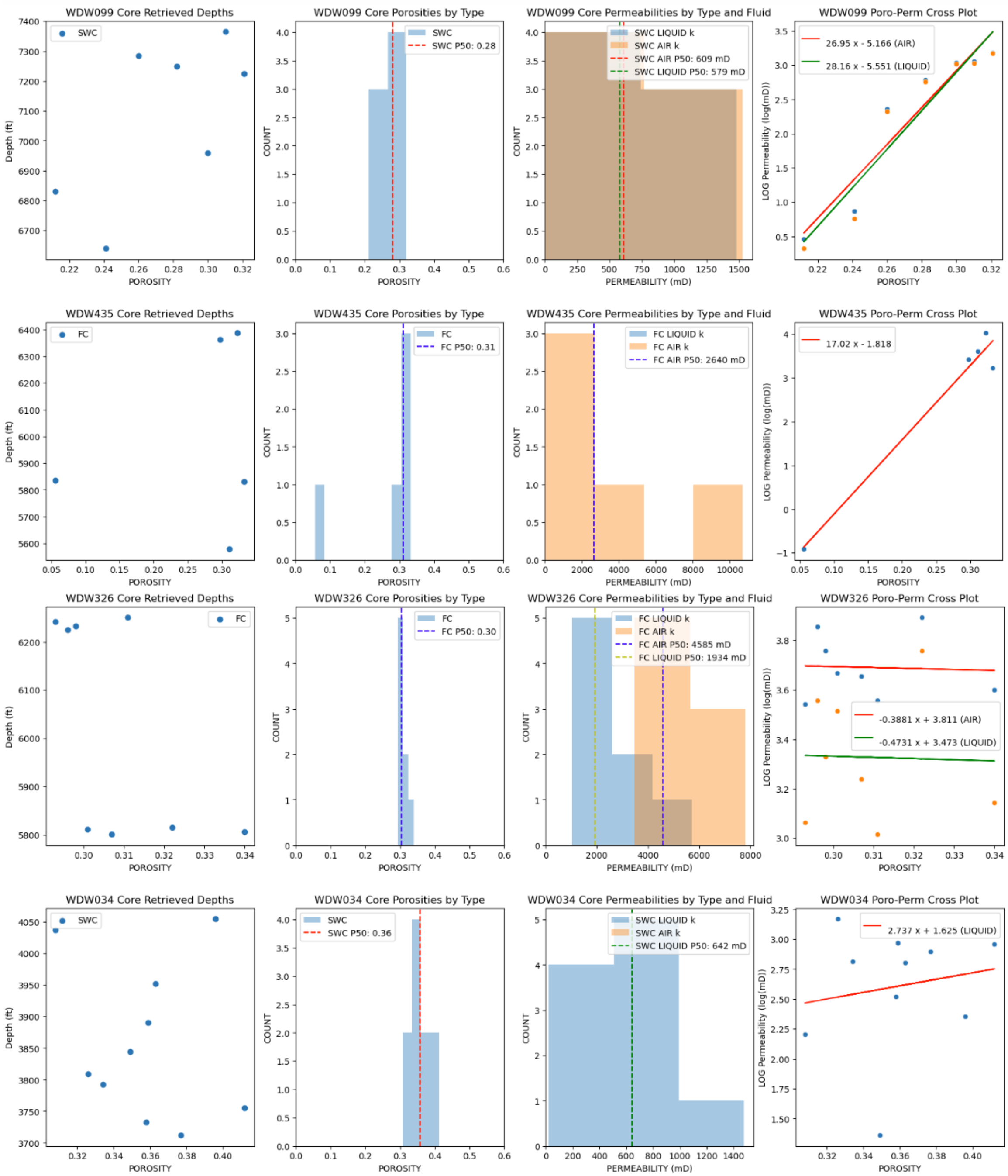
WDW099 Core Retrieved Depths
SWC
Depth (ft)
POROSITY
WDW099 Core Porosities by Type
SWC
SWC P50: 0.28
COUNT
POROSITY
WDW099 Core Permeabilities by Type and Fluid
SWC LIQUID k
SWC AIR k
SWC AIR P50: 609 mD
SWC LIQUID P50: 579 mD
COUNT
PERMEABILITY (mD)
WDW099 Poro-Perm Cross Plot
26.95 x - 5.166 (AIR)
28.16 x - 5.551 (LIQUID)
LOG Permeability (log(mD))
POROSITY
WDW435 Core Retrieved Depths
FC
Depth (ft)
POROSITY
WDW435 Core Porosities by Type
FC
FC P50: 0.31
COUNT
POROSITY
WDW435 Core Permeabilities by Type and Fluid
FC LIQUID k
FC AIR k
FC AIR P50: 2640 mD
COUNT
PERMEABILITY (mD)
WDW435 Poro-Perm Cross Plot
17.02 x - 1.818
LOG Permeability (log(mD))
POROSITY
WDW326 Core Retrieved Depths
FC
Depth (ft)
POROSITY
WDW326 Core Porosities by Type
FC
FC P50: 0.30
COUNT
POROSITY
WDW326 Core Permeabilities by Type and Fluid
FC LIQUID k
FC AIR k
FC AIR P50: 4585 mD
FC LIQUID P50: 1934 mD
COUNT
PERMEABILITY (mD)
WDW326 Poro-Perm Cross Plot
-0.3881 x + 3.811 (AIR)
-0.4731 x + 3.473 (LIQUID)
LOG Permeability (log(mD))
POROSITY
WDW034 Core Retrieved Depths
SWC
Depth (ft)
POROSITY
WDW034 Core Porosities by Type
SWC
SWC P50: 0.36
COUNT
POROSITY
WDW034 Core Permeabilities by Type and Fluid
SWC LIQUID k
SWC AIR k
SWC LIQUID P50: 642 mD
COUNT
PERMEABILITY (mD)
WDW034 Poro-Perm Cross Plot
2.737 x + 1.625 (LIQUID)
LOG Permeability (log(mD))
POROSITY

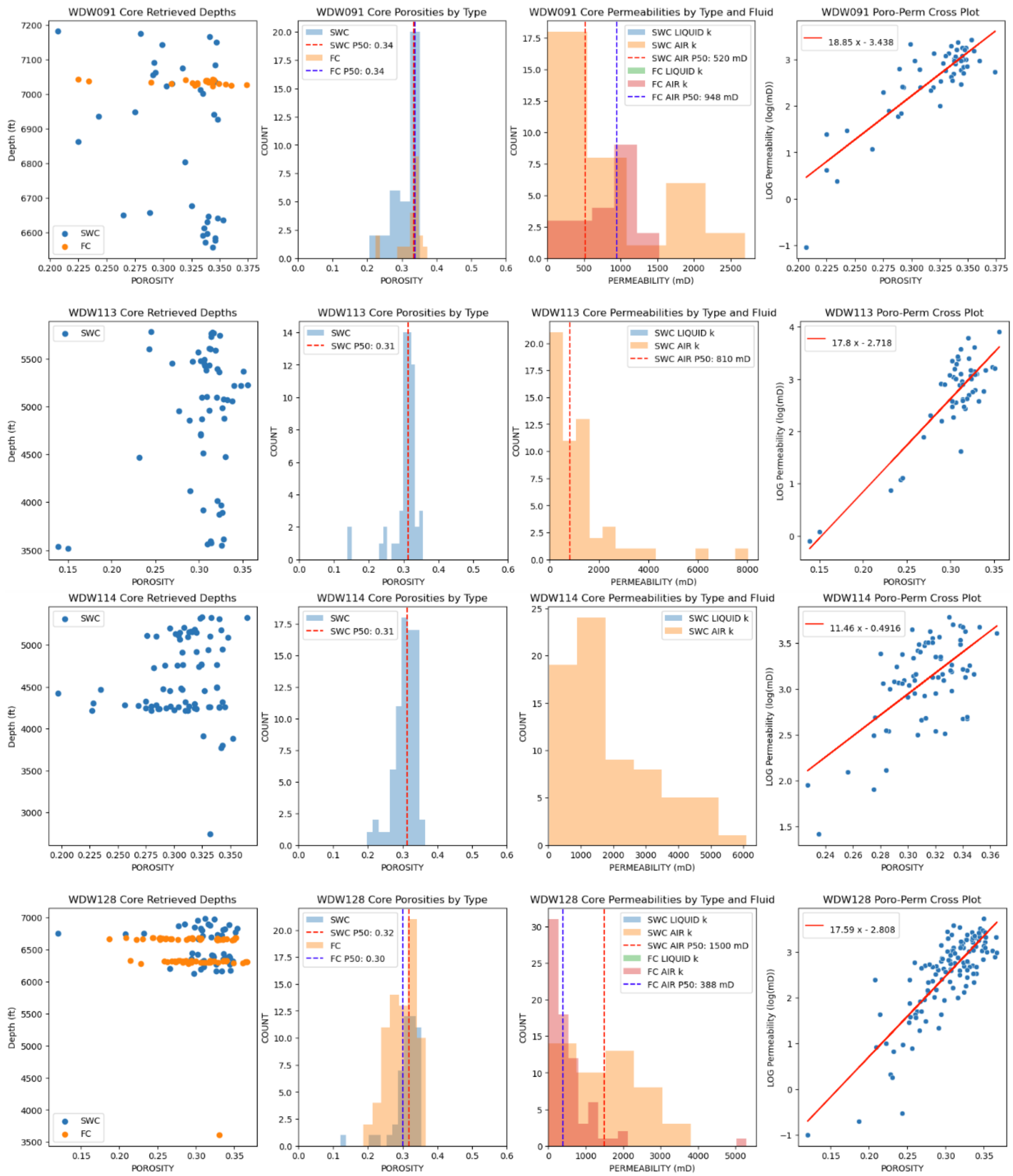
WDW091 Core Retrieved Depths
Depth (ft)
POROSITY
SWC
FC
WDW091 Core Porosities by Type
COUNT
SWC
SWC P50: 0.34
FC
FC P50: 0.34
WDW091 Core Permeabilities by Type and Fluid
SWC LIQUID k
SWC AIR k
SWC AIR P50: 520 mD
FC LIQUID k
FC AIR k
FC AIR P50: 948 mD
PERMEABILITY (mD)
WDW091 Poro-Perm Cross Plot
18.85 x - 3.438
LOG Permeability (log(mD))
WDW113 Core Retrieved Depths
WDW113 Core Porosities by Type
SWC P50: 0.31
WDW113 Core Permeabilities by Type and Fluid
SWC AIR P50: 810 mD
WDW113 Poro-Perm Cross Plot
17.8 x - 2.718
WDW114 Core Retrieved Depths
WDW114 Core Porosities by Type
SWC P50: 0.31
WDW114 Core Permeabilities by Type and Fluid
WDW114 Poro-Perm Cross Plot
11.46 x - 0.4916
WDW128 Core Retrieved Depths
WDW128 Core Porosities by Type
SWC P50: 0.32
FC P50: 0.30
WDW128 Core Permeabilities by Type and Fluid
SWC AIR P50: 1500 mD
FC AIR P50: 388 mD
WDW128 Poro-Perm Cross Plot
17.59 x - 2.808

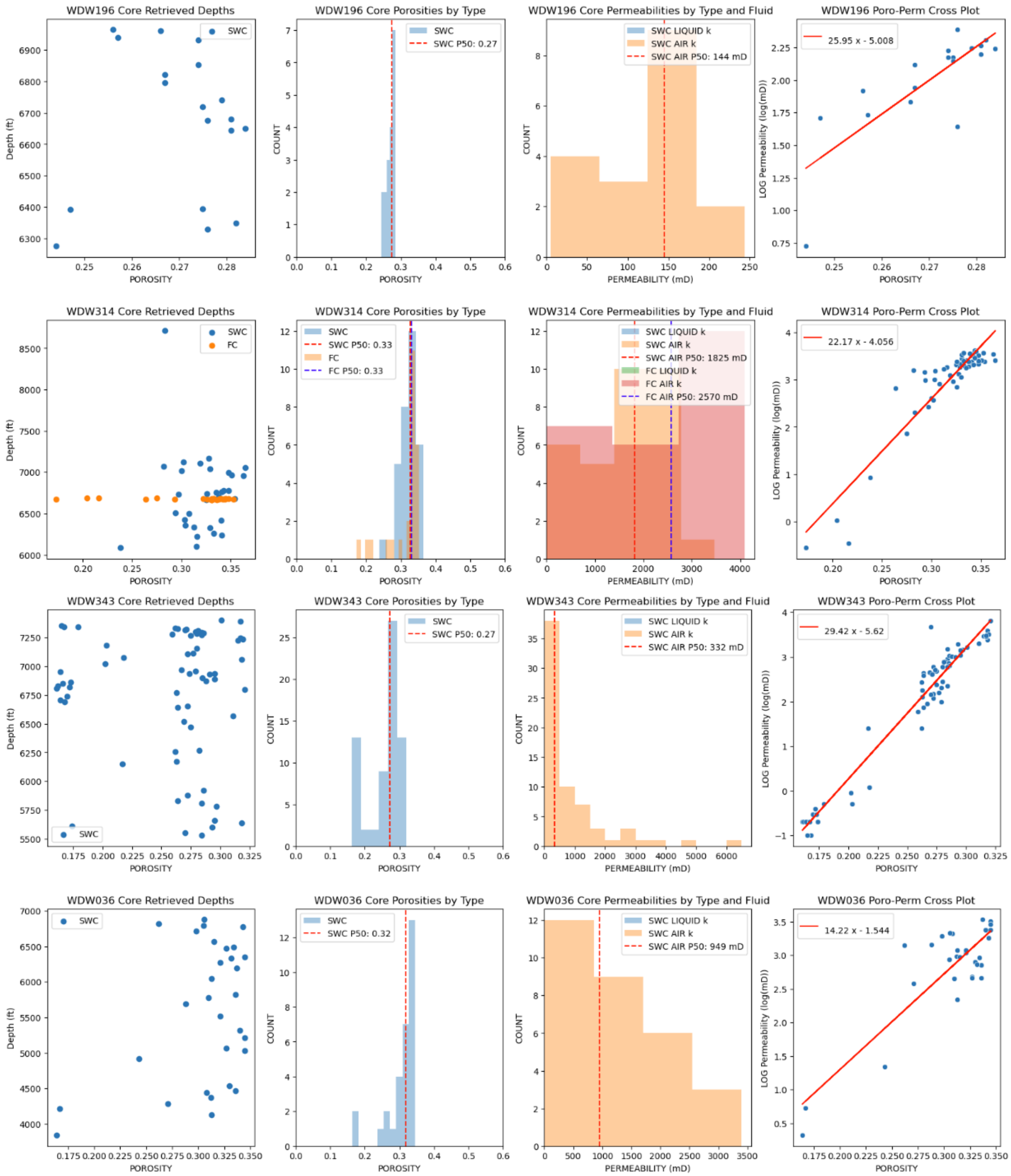
WDW196 Core Retrieved Depths
SWC
Depth (ft)
POROSITY
WDW196 Core Porosities by Type
SWC
SWC P50: 0.27
COUNT
POROSITY
WDW196 Core Permeabilities by Type and Fluid
SWC LIQUID k
SWC AIR k
SWC AIR P50: 144 mD
COUNT
PERMEABILITY (mD)
WDW196 Poro-Perm Cross Plot
25.95 x - 5.008
LOG Permeability (log(mD))
POROSITY
WDW314 Core Retrieved Depths
SWC
FC
Depth (ft)
POROSITY
WDW314 Core Porosities by Type
SWC
SWC P50: 0.33
FC
FC P50: 0.33
COUNT
POROSITY
WDW314 Core Permeabilities by Type and Fluid
SWC LIQUID k
SWC AIR k
SWC AIR P50: 1825 mD
FC LIQUID k
FC AIR k
FC AIR P50: 2570 mD
COUNT
PERMEABILITY (mD)
WDW314 Poro-Perm Cross Plot
22.17 x - 4.056
LOG Permeability (log(mD))
POROSITY
WDW343 Core Retrieved Depths
SWC
Depth (ft)
POROSITY
WDW343 Core Porosities by Type
SWC
SWC P50: 0.27
COUNT
POROSITY
WDW343 Core Permeabilities by Type and Fluid
SWC LIQUID k
SWC AIR k
SWC AIR P50: 332 mD
COUNT
PERMEABILITY (mD)
WDW343 Poro-Perm Cross Plot
29.42 x - 5.62
LOG Permeability (log(mD))
POROSITY
WDW036 Core Retrieved Depths
SWC
Depth (ft)
POROSITY
WDW036 Core Porosities by Type
SWC
SWC P50: 0.32
COUNT
POROSITY
WDW036 Core Permeabilities by Type and Fluid
SWC LIQUID k
SWC AIR k
SWC AIR P50: 949 mD
COUNT
PERMEABILITY (mD)
WDW036 Poro-Perm Cross Plot
14.22 x - 1.544
LOG Permeability (log(mD))
POROSITY

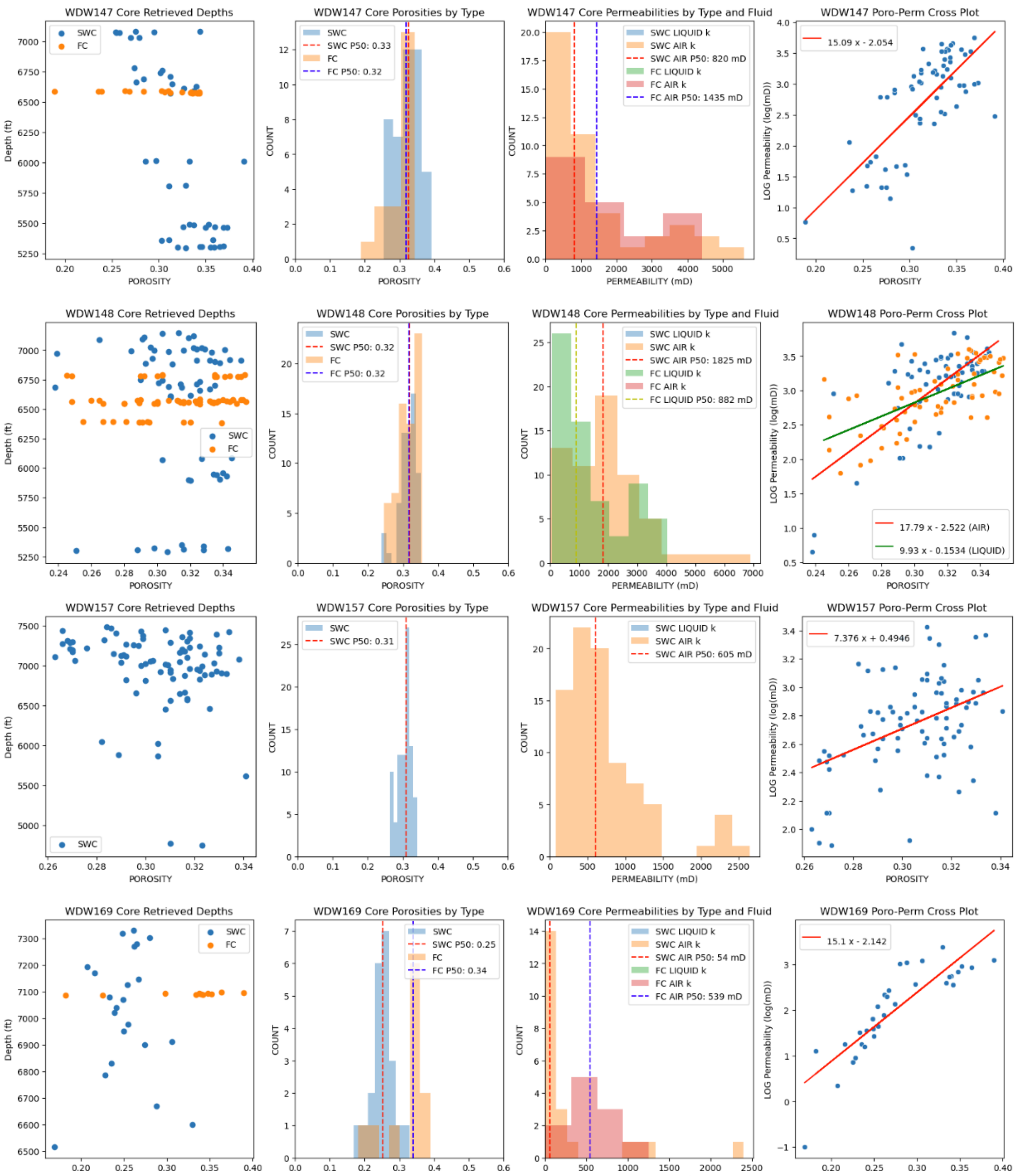

WDW147 Core Retrieved Depths
SWC
FC
Depth (ft)
POROSITY
WDW147 Core Porosities by Type
SWC
SWC P50: 0.33
FC
FC P50: 0.32
COUNT
POROSITY
WDW147 Core Permeabilities by Type and Fluid
SWC LIQUID k
SWC AIR k
SWC AIR P50: 820 mD
FC LIQUID k
FC AIR k
FC AIR P50: 1435 mD
COUNT
PERMEABILITY (mD)
WDW147 Poro-Perm Cross Plot
15.09 x - 2.054
LOG Permeability (log(mD))
POROSITY
WDW148 Core Retrieved Depths
SWC
FC
Depth (ft)
POROSITY
WDW148 Core Porosities by Type
SWC
SWC P50: 0.32
FC
FC P50: 0.32
COUNT
POROSITY
WDW148 Core Permeabilities by Type and Fluid
SWC LIQUID k
SWC AIR k
SWC AIR P50: 1825 mD
FC LIQUID k
FC AIR k
FC LIQUID P50: 882 mD
COUNT
PERMEABILITY (mD)
WDW148 Poro-Perm Cross Plot
17.79 x - 2.522 (AIR)
9.93 x - 0.1534 (LIQUID)
LOG Permeability (log(mD))
POROSITY
WDW157 Core Retrieved Depths
SWC
Depth (ft)
POROSITY
WDW157 Core Porosities by Type
SWC
SWC P50: 0.31
COUNT
POROSITY
WDW157 Core Permeabilities by Type and Fluid
SWC LIQUID k
SWC AIR k
SWC AIR P50: 605 mD
COUNT
PERMEABILITY (mD)
WDW157 Poro-Perm Cross Plot
7.376 x + 0.4946
LOG Permeability (log(mD))
POROSITY
WDW169 Core Retrieved Depths
SWC
FC
Depth (ft)
POROSITY
WDW169 Core Porosities by Type
SWC
SWC P50: 0.25
FC
FC P50: 0.34
COUNT
POROSITY
WDW169 Core Permeabilities by Type and Fluid
SWC LIQUID k
SWC AIR k
SWC AIR P50: 54 mD
FC LIQUID k
FC AIR k
FC AIR P50: 539 mD
COUNT
PERMEABILITY (mD)
WDW169 Poro-Perm Cross Plot
15.1 x - 2.142
LOG Permeability (log(mD))
POROSITY

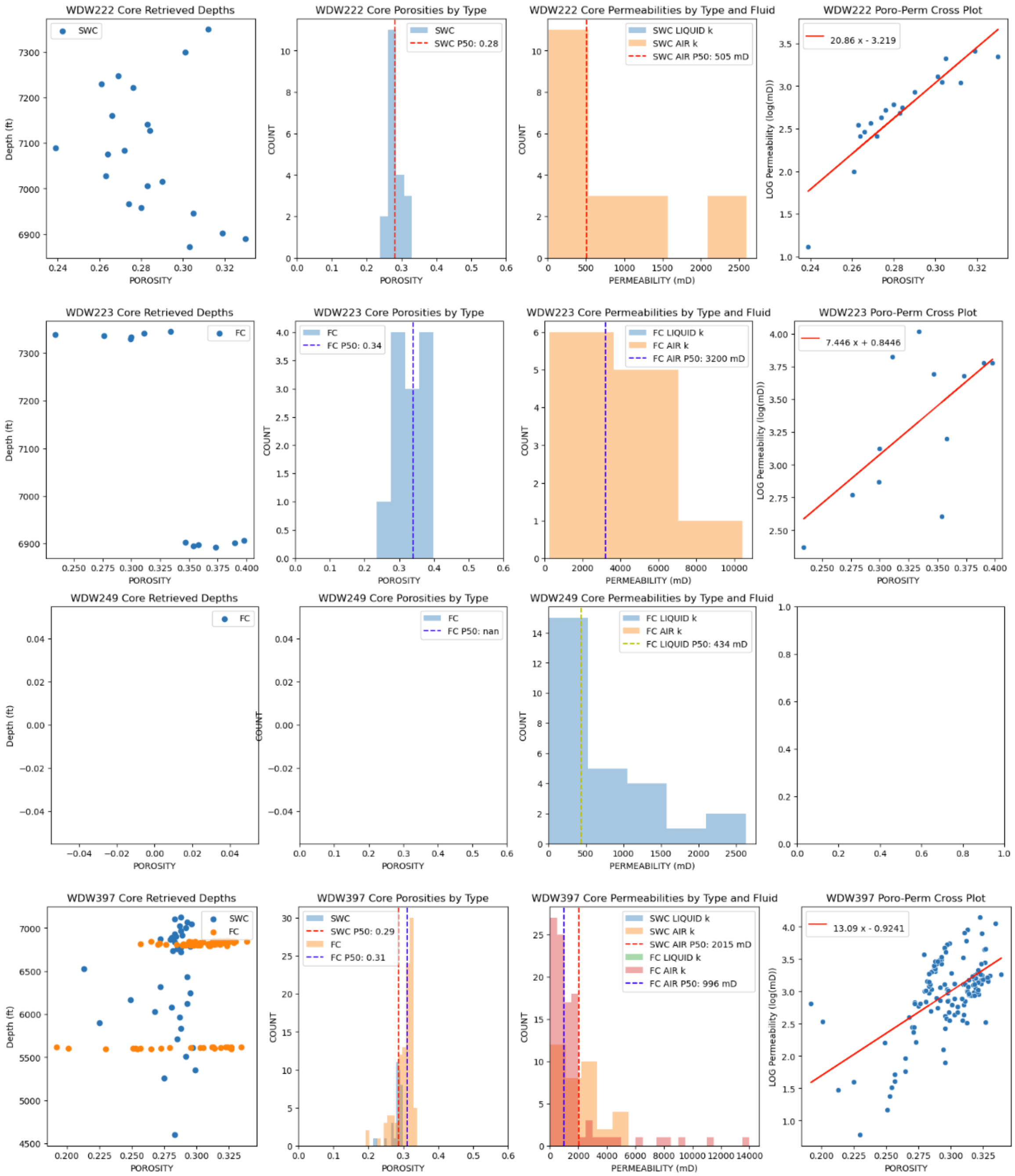
WDW222 Core Retrieved Depths
SWC
Depth (ft)
POROSITY
WDW222 Core Porosities by Type
SWC
SWC P50: 0.28
COUNT
POROSITY
WDW222 Core Permeabilities by Type and Fluid
SWC LIQUID k
SWC AIR k
SWC AIR P50: 505 mD
COUNT
PERMEABILITY (mD)
WDW222 Poro-Perm Cross Plot
20.86 x - 3.219
LOG Permeability (log(mD))
POROSITY
WDW223 Core Retrieved Depths
FC
Depth (ft)
POROSITY
WDW223 Core Porosities by Type
FC
FC P50: 0.34
COUNT
POROSITY
WDW223 Core Permeabilities by Type and Fluid
FC LIQUID k
FC AIR k
FC AIR P50: 3200 mD
COUNT
PERMEABILITY (mD)
WDW223 Poro-Perm Cross Plot
7.446 x + 0.8446
LOG Permeability (log(mD))
POROSITY
WDW249 Core Retrieved Depths
FC
Depth (ft)
POROSITY
WDW249 Core Porosities by Type
FC
FC P50: nan
COUNT
POROSITY
WDW249 Core Permeabilities by Type and Fluid
FC LIQUID k
FC AIR k
FC LIQUID P50: 434 mD
COUNT
PERMEABILITY (mD)
WDW397 Core Retrieved Depths
SWC
FC
Depth (ft)
POROSITY
WDW397 Core Porosities by Type
SWC
SWC P50: 0.29
FC
FC P50: 0.31
COUNT
POROSITY
WDW397 Core Permeabilities by Type and Fluid
SWC LIQUID k
SWC AIR k
SWC AIR P50: 2015 mD
FC LIQUID k
FC AIR k
FC AIR P50: 996 mD
COUNT
PERMEABILITY (mD)
WDW397 Poro-Perm Cross Plot
13.09 x - 0.9241
LOG Permeability (log(mD))
POROSITY

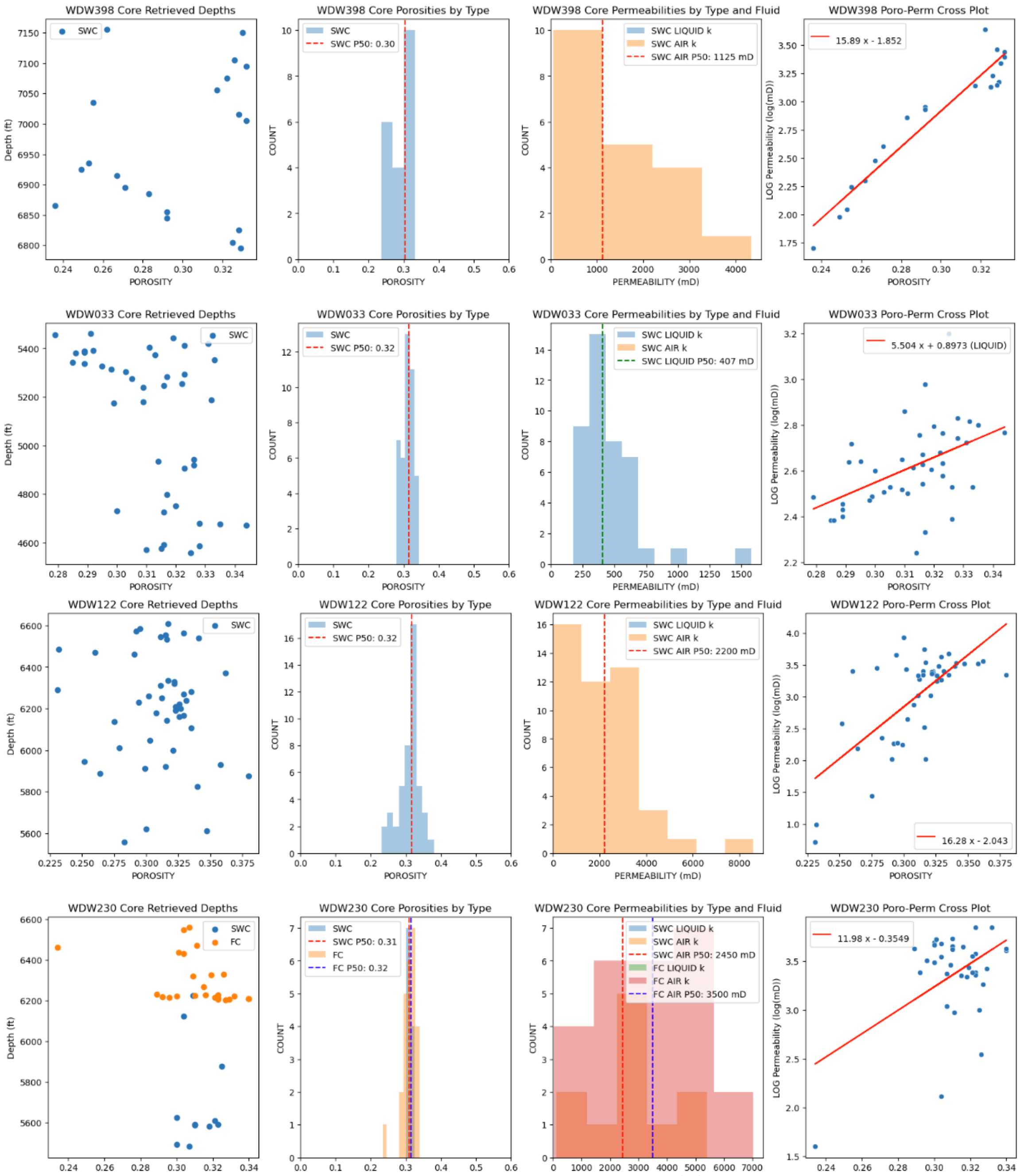
WDW398 Core Retrieved Depths
SWC
Depth (ft)
POROSITY
WDW398 Core Porosities by Type
SWC
SWC P50: 0.30
COUNT
POROSITY
WDW398 Core Permeabilities by Type and Fluid
SWC LIQUID k
SWC AIR k
SWC AIR P50: 1125 mD
COUNT
PERMEABILITY (mD)
WDW398 Poro-Perm Cross Plot
15.89 x - 1.852
LOG Permeability (log(mD))
POROSITY
WDW033 Core Retrieved Depths
SWC
Depth (ft)
POROSITY
WDW033 Core Porosities by Type
SWC
SWC P50: 0.32
COUNT
POROSITY
WDW033 Core Permeabilities by Type and Fluid
SWC LIQUID k
SWC AIR k
SWC LIQUID P50: 407 mD
COUNT
PERMEABILITY (mD)
WDW033 Poro-Perm Cross Plot
5.504 x + 0.8973 (LIQUID)
LOG Permeability (log(mD))
POROSITY
WDW122 Core Retrieved Depths
SWC
Depth (ft)
POROSITY
WDW122 Core Porosities by Type
SWC
SWC P50: 0.32
COUNT
POROSITY
WDW122 Core Permeabilities by Type and Fluid
SWC LIQUID k
SWC AIR k
SWC AIR P50: 2200 mD
COUNT
PERMEABILITY (mD)
WDW122 Poro-Perm Cross Plot
16.28 x - 2.043
LOG Permeability (log(mD))
POROSITY
WDW230 Core Retrieved Depths
SWC
FC
Depth (ft)
POROSITY
WDW230 Core Porosities by Type
SWC
SWC P50: 0.31
FC
FC P50: 0.32
COUNT
POROSITY
WDW230 Core Permeabilities by Type and Fluid
SWC LIQUID k
SWC AIR k
SWC AIR P50: 2450 mD
FC LIQUID k
FC AIR k
FC AIR P50: 3500 mD
COUNT
PERMEABILITY (mD)
WDW230 Poro-Perm Cross Plot
11.98 x - 0.3549
LOG Permeability (log(mD))
POROSITY

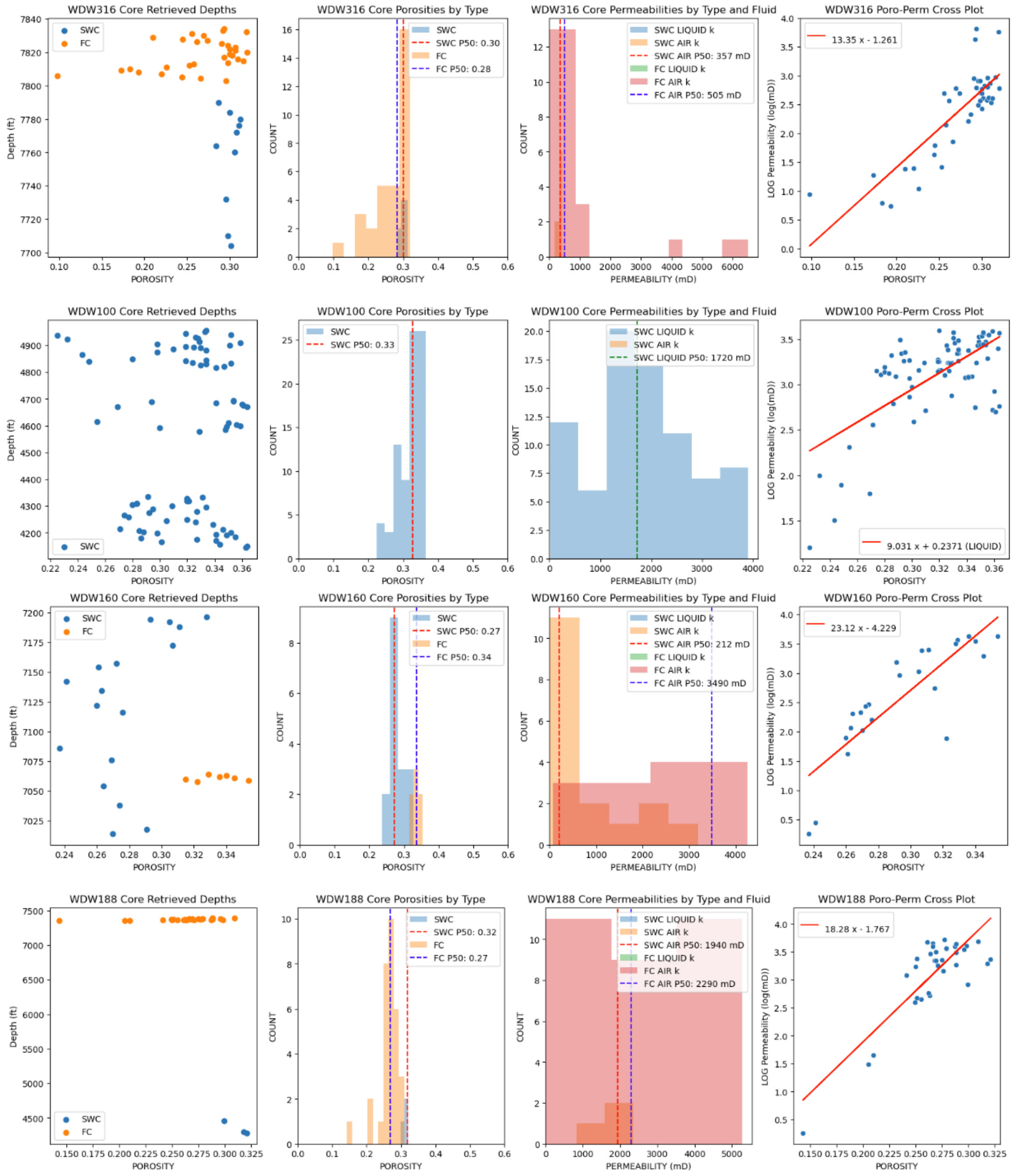
WDW316 Core Retrieved Depths
SWC
FC
Depth (ft)
POROSITY
WDW316 Core Porosities by Type
SWC
SWC P50: 0.30
FC
FC P50: 0.28
COUNT
POROSITY
WDW316 Core Permeabilities by Type and Fluid
SWC LIQUID k
SWC AIR k
SWC AIR P50: 357 mD
FC LIQUID k
FC AIR k
FC AIR P50: 505 mD
COUNT
PERMEABILITY (mD)
WDW316 Poro-Perm Cross Plot
13.35 x - 1.261
LOG Permeability (log(mD))
POROSITY
WDW100 Core Retrieved Depths
SWC
Depth (ft)
POROSITY
WDW100 Core Porosities by Type
SWC
SWC P50: 0.33
COUNT
POROSITY
WDW100 Core Permeabilities by Type and Fluid
SWC LIQUID k
SWC AIR k
SWC LIQUID P50: 1720 mD
COUNT
PERMEABILITY (mD)
WDW100 Poro-Perm Cross Plot
9.031 x + 0.2371 (LIQUID)
LOG Permeability (log(mD))
POROSITY
WDW160 Core Retrieved Depths
SWC
FC
Depth (ft)
POROSITY
WDW160 Core Porosities by Type
SWC
SWC P50: 0.27
FC
FC P50: 0.34
COUNT
POROSITY
WDW160 Core Permeabilities by Type and Fluid
SWC LIQUID k
SWC AIR k
SWC AIR P50: 212 mD
FC LIQUID k
FC AIR k
FC AIR P50: 3490 mD
COUNT
PERMEABILITY (mD)
WDW160 Poro-Perm Cross Plot
23.12 x - 4.229
LOG Permeability (log(mD))
POROSITY
WDW188 Core Retrieved Depths
SWC
FC
Depth (ft)
POROSITY
WDW188 Core Porosities by Type
SWC
SWC P50: 0.32
FC
FC P50: 0.27
COUNT
POROSITY
WDW188 Core Permeabilities by Type and Fluid
SWC LIQUID k
SWC AIR k
SWC AIR P50: 1940 mD
FC LIQUID k
FC AIR k
FC AIR P50: 2290 mD
COUNT
PERMEABILITY (mD)
WDW188 Poro-Perm Cross Plot
18.28 x - 1.767
LOG Permeability (log(mD))
POROSITY

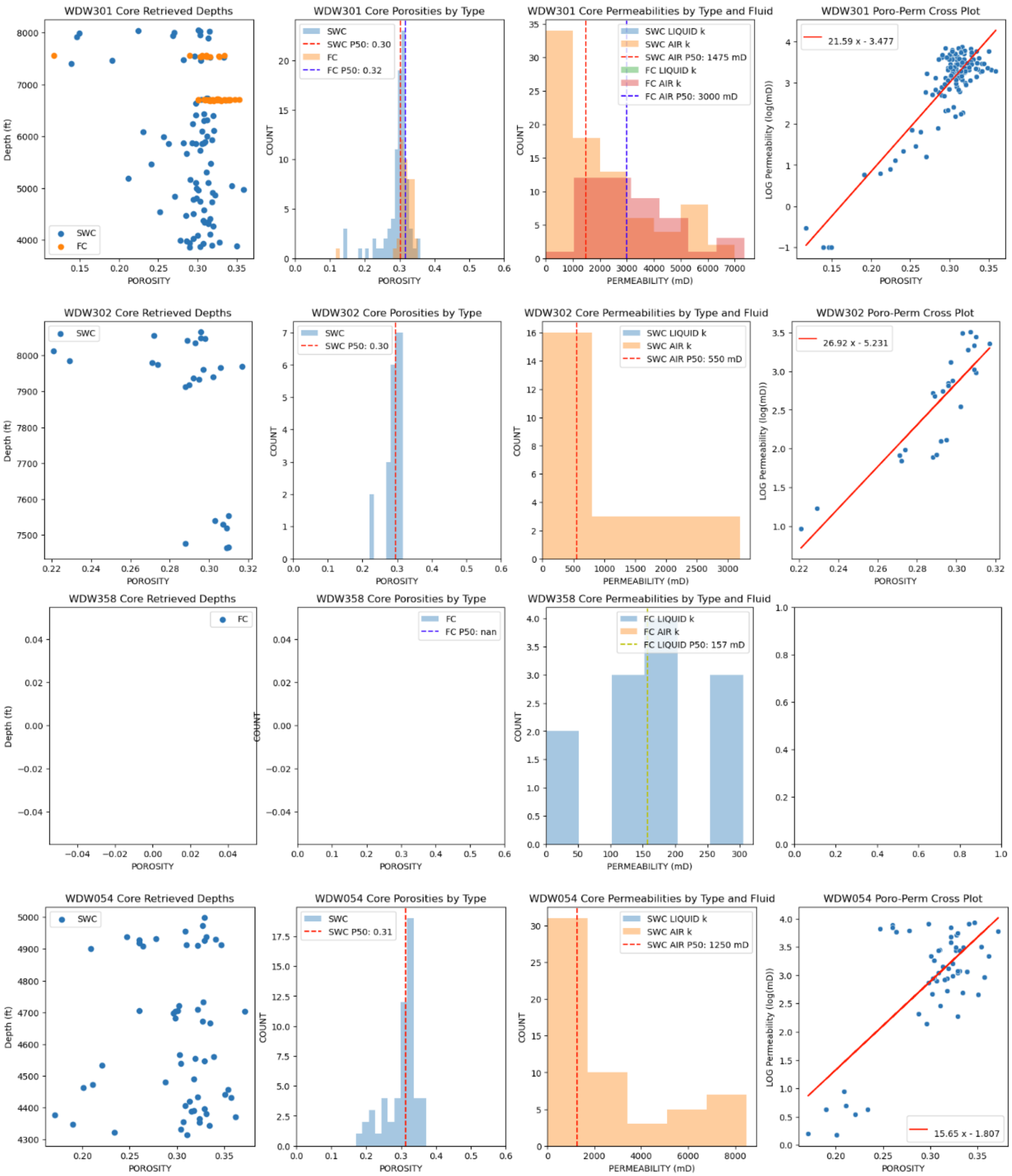
WDW301 Core Retrieved Depths
Depth (ft)
POROSITY
SWC
FC
WDW301 Core Porosities by Type
COUNT
POROSITY
SWC
SWC P50: 0.30
FC
FC P50: 0.32
WDW301 Core Permeabilities by Type and Fluid
COUNT
PERMEABILITY (mD)
SWC LIQUID k
SWC AIR k
SWC AIR P50: 1475 mD
FC LIQUID k
FC AIR k
FC AIR P50: 3000 mD
WDW301 Poro-Perm Cross Plot
LOG Permeability (log(mD))
POROSITY
21.59 x - 3.477
WDW302 Core Retrieved Depths
Depth (ft)
POROSITY
SWC
WDW302 Core Porosities by Type
COUNT
POROSITY
SWC
SWC P50: 0.30
WDW302 Core Permeabilities by Type and Fluid
COUNT
PERMEABILITY (mD)
SWC LIQUID k
SWC AIR k
SWC AIR P50: 550 mD
WDW302 Poro-Perm Cross Plot
LOG Permeability (log(mD))
POROSITY
26.92 x - 5.231
WDW358 Core Retrieved Depths
Depth (ft)
POROSITY
FC
WDW358 Core Porosities by Type
COUNT
POROSITY
FC
FC P50: nan
WDW358 Core Permeabilities by Type and Fluid
COUNT
PERMEABILITY (mD)
FC LIQUID k
FC AIR k
FC LIQUID P50: 157 mD
WDW054 Core Retrieved Depths
Depth (ft)
POROSITY
SWC
WDW054 Core Porosities by Type
COUNT
POROSITY
SWC
SWC P50: 0.31
WDW054 Core Permeabilities by Type and Fluid
COUNT
PERMEABILITY (mD)
SWC LIQUID k
SWC AIR k
SWC AIR P50: 1250 mD
WDW054 Poro-Perm Cross Plot
LOG Permeability (log(mD))
POROSITY
15.65 x - 1.807

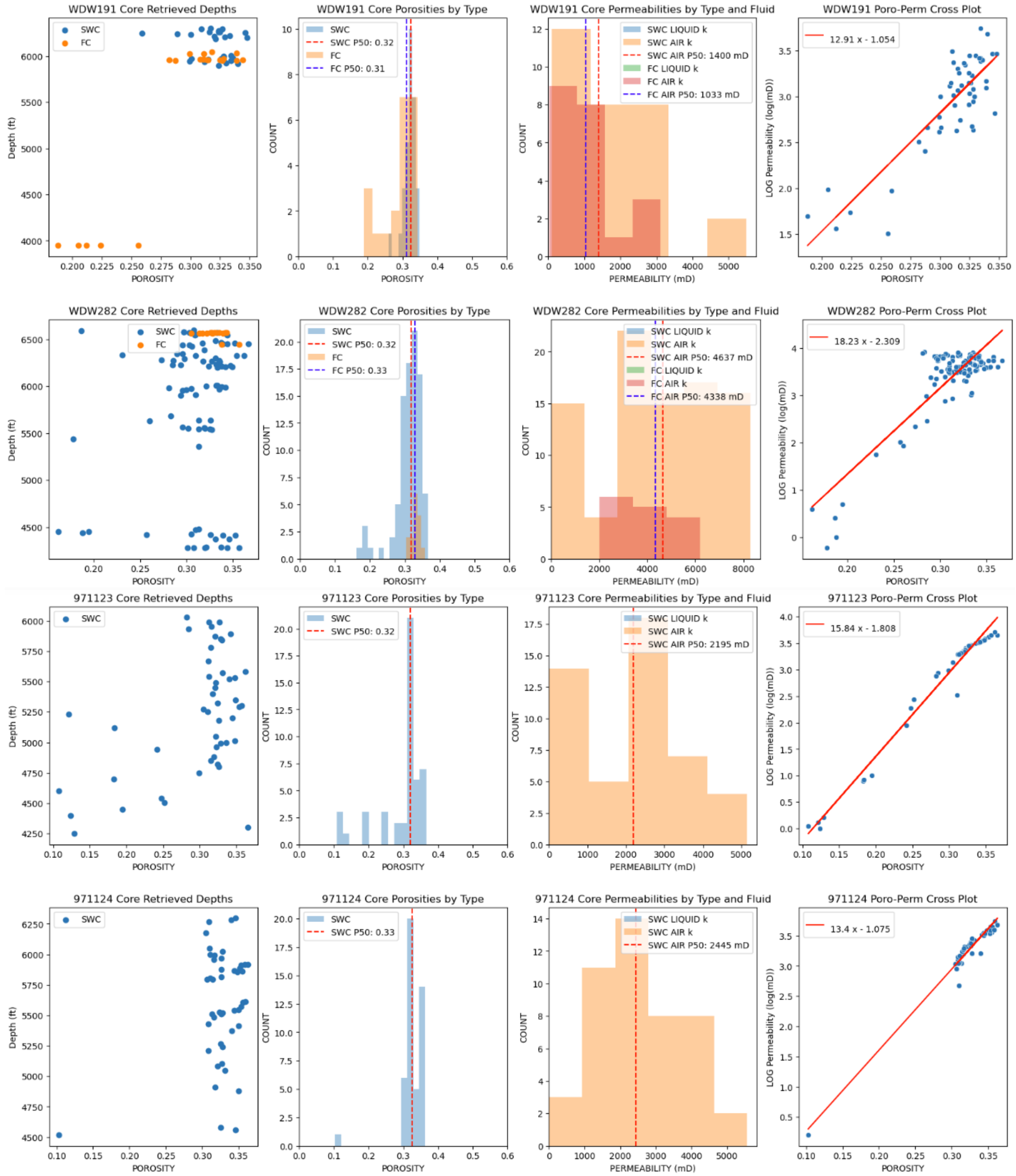
WDW191 Core Retrieved Depths
SWC
FC
Depth (ft)
POROSITY
WDW191 Core Porosities by Type
SWC
SWC P50: 0.32
FC
FC P50: 0.31
COUNT
POROSITY
WDW191 Core Permeabilities by Type and Fluid
SWC LIQUID k
SWC AIR k
SWC AIR P50: 1400 mD
FC LIQUID k
FC AIR k
FC AIR P50: 1033 mD
COUNT
PERMEABILITY (mD)
WDW191 Poro-Perm Cross Plot
12.91 x - 1.054
LOG Permeability (log(mD))
POROSITY
WDW282 Core Retrieved Depths
SWC
FC
Depth (ft)
POROSITY
WDW282 Core Porosities by Type
SWC
SWC P50: 0.32
FC
FC P50: 0.33
COUNT
POROSITY
WDW282 Core Permeabilities by Type and Fluid
SWC LIQUID k
SWC AIR k
SWC AIR P50: 4637 mD
FC LIQUID k
FC AIR k
FC AIR P50: 4338 mD
COUNT
PERMEABILITY (mD)
WDW282 Poro-Perm Cross Plot
18.23 x - 2.309
LOG Permeability (log(mD))
POROSITY
971123 Core Retrieved Depths
SWC
Depth (ft)
POROSITY
971123 Core Porosities by Type
SWC
SWC P50: 0.32
COUNT
POROSITY
971123 Core Permeabilities by Type and Fluid
SWC LIQUID k
SWC AIR k
SWC AIR P50: 2195 mD
COUNT
PERMEABILITY (mD)
971123 Poro-Perm Cross Plot
15.84 x - 1.808
LOG Permeability (log(mD))
POROSITY
971124 Core Retrieved Depths
SWC
Depth (ft)
POROSITY
971124 Core Porosities by Type
SWC
SWC P50: 0.33
COUNT
POROSITY
971124 Core Permeabilities by Type and Fluid
SWC LIQUID k
SWC AIR k
SWC AIR P50: 2445 mD
COUNT
PERMEABILITY (mD)
971124 Poro-Perm Cross Plot
13.4 x - 1.075
LOG Permeability (log(mD))
POROSITY

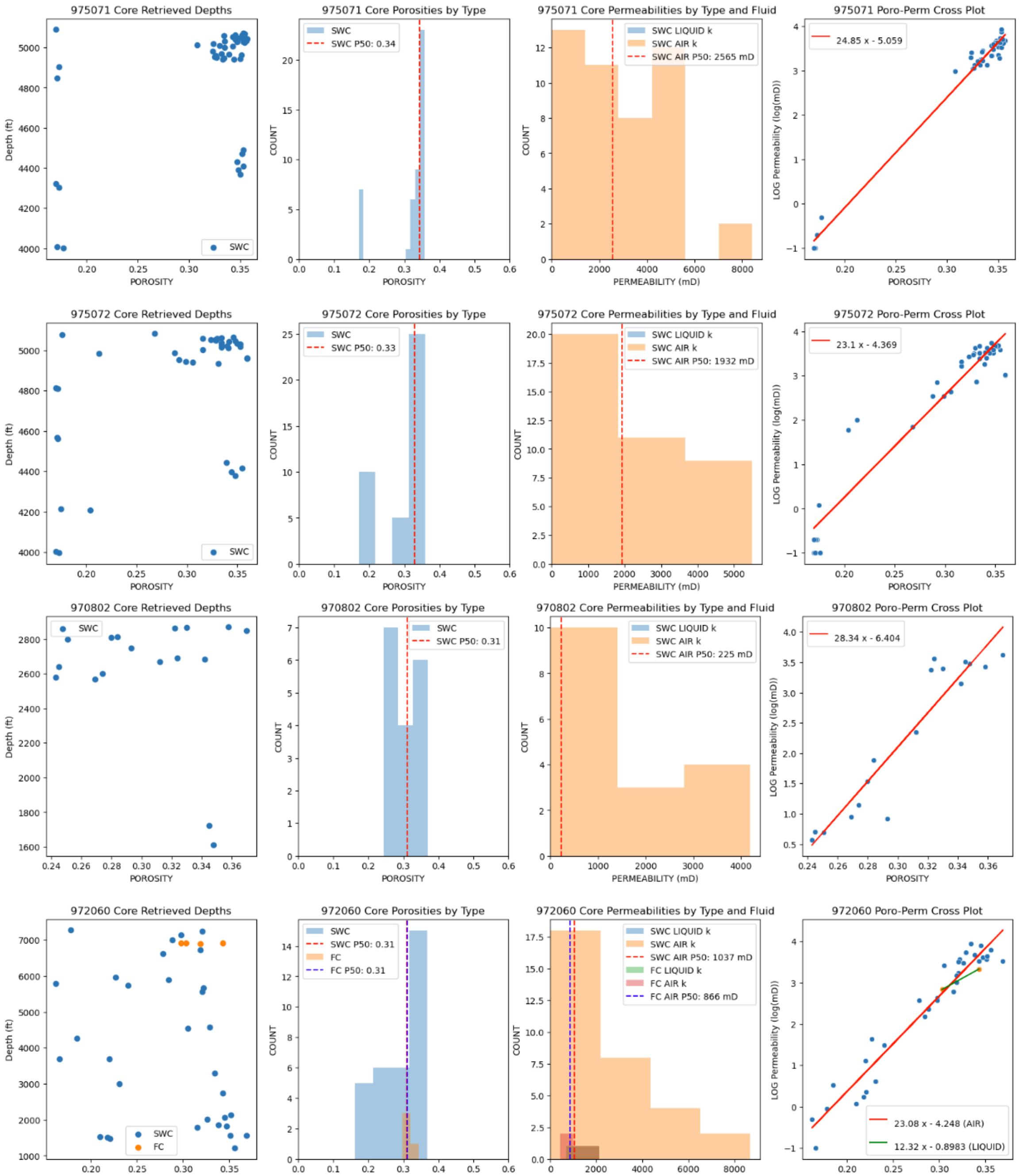
975071 Core Retrieved Depths
Depth (ft)
POROSITY
SWC
975071 Core Porosities by Type
SWC
SWC P50: 0.34
COUNT
POROSITY
975071 Core Permeabilities by Type and Fluid
SWC LIQUID k
SWC AIR k
SWC AIR P50: 2565 mD
COUNT
PERMEABILITY (mD)
975071 Poro-Perm Cross Plot
24.85 x - 5.059
LOG Permeability (log(mD))
POROSITY
975072 Core Retrieved Depths
Depth (ft)
POROSITY
SWC
975072 Core Porosities by Type
SWC
SWC P50: 0.33
COUNT
POROSITY
975072 Core Permeabilities by Type and Fluid
SWC LIQUID k
SWC AIR k
SWC AIR P50: 1932 mD
COUNT
PERMEABILITY (mD)
975072 Poro-Perm Cross Plot
23.1 x - 4.369
LOG Permeability (log(mD))
POROSITY
970802 Core Retrieved Depths
SWC
Depth (ft)
POROSITY
970802 Core Porosities by Type
SWC
SWC P50: 0.31
COUNT
POROSITY
970802 Core Permeabilities by Type and Fluid
SWC LIQUID k
SWC AIR k
SWC AIR P50: 225 mD
COUNT
PERMEABILITY (mD)
970802 Poro-Perm Cross Plot
28.34 x - 6.404
LOG Permeability (log(mD))
POROSITY
972060 Core Retrieved Depths
Depth (ft)
SWC
FC
POROSITY
972060 Core Porosities by Type
SWC
SWC P50: 0.31
FC
FC P50: 0.31
COUNT
POROSITY
972060 Core Permeabilities by Type and Fluid
SWC LIQUID k
SWC AIR k
SWC AIR P50: 1037 mD
FC LIQUID k
FC AIR k
FC AIR P50: 866 mD
COUNT
PERMEABILITY (mD)
972060 Poro-Perm Cross Plot
LOG Permeability (log(mD))
23.08 x - 4.248 (AIR)
12.32 x - 0.8983 (LIQUID)
POROSITY

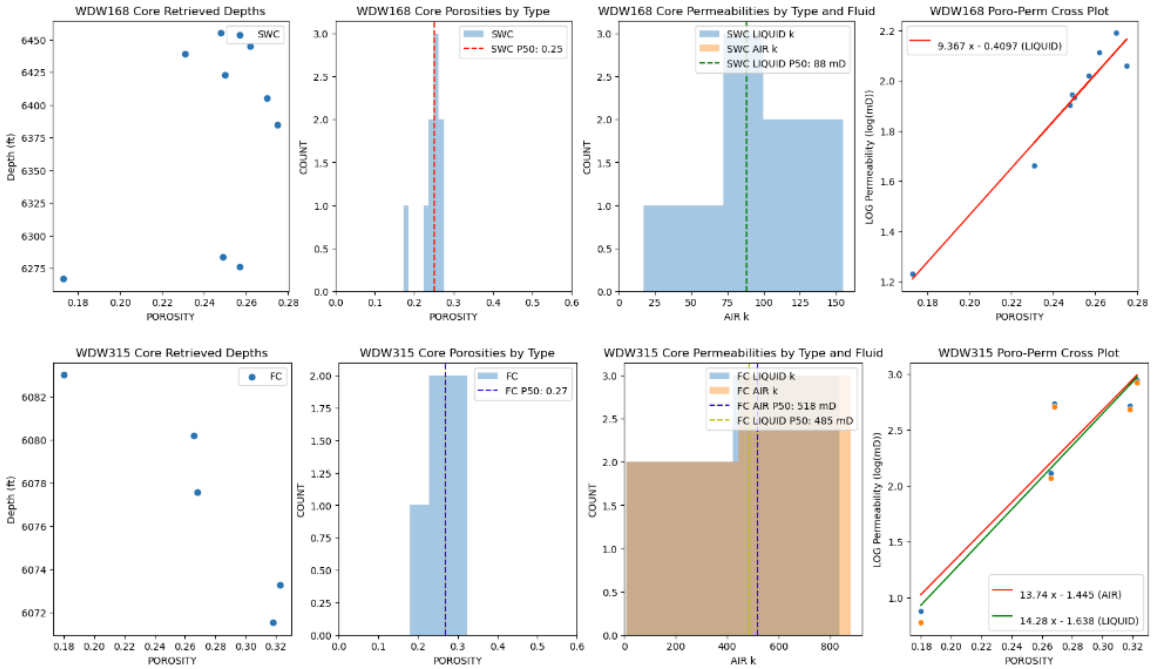
WDW168 Core Retrieved Depths
SWC
Depth (ft)
POROSITY
WDW168 Core Porosities by Type
SWC
SWC P50: 0.25
COUNT
POROSITY
WDW168 Core Permeabilities by Type and Fluid
SWC LIQUID k
SWC AIR k
SWC LIQUID P50: 88 mD
COUNT
AIR k
WDW168 Poro-Perm Cross Plot
9.367 x - 0.4097 (LIQUID)
LOG Permeability (log(mD))
POROSITY
WDW315 Core Retrieved Depths
FC
Depth (ft)
POROSITY
WDW315 Core Porosities by Type
FC
FC P50: 0.27
COUNT
POROSITY
WDW315 Core Permeabilities by Type and Fluid
FC LIQUID k
FC AIR k
FC AIR P50: 518 mD
FC LIQUID P50: 485 mD
COUNT
AIR k
WDW315 Poro-Perm Cross Plot
13.74 x - 1.445 (AIR)
14.28 x - 1.638 (LIQUID)
LOG Permeability (log(mD))
POROSITY

APPENDIX D: REPORTS FROM NON-PERMEABLE CORES

Core samples from the confining zone (CZ) or from shale samples. Samples from the confining zone do not tend to have porosity values.

CLUSTER	NO.	CZ por	CZ k md	(KB)	CLUSTER	NO.	CZ por	CZ k md	(KB)
3	WDW278	0.114	0.0014	3875.2	10	WDW314		7.47E-06	6566
3	WDW278	0.113	0.0028	3875.5	10	WDW299	0.305	4.1	2580
3	WDW278	0.104	0.0044	3877.5	10	WDW299	0.284	118	2581
3	WDW278	0.145	0.0097	3879.9	10	WDW299	0.279	87.5	2582
3	WDW278	0.146	0.0063	3879.8	10	WDW299	0.276	72.6	2583
3	WDW278	0.14	0.0056	3881.4	10	WDW299	0.286	15.49	2584
3	WDW278	0.139	0.0014	3881.5	10	WDW299	0.279	69.9	2585
3	WDW278	0.151	0.0055	3883.4	10	WDW299	0.275	51.23	2586
3	WDW278	0.11	0.0019	3883.7	10	WDW299	0.271	1.98	2587
3	WDW278	0.131	0.0062	3885.3	10	WDW299	0.259	0.06	2588
3	WDW278	0.129	0.0047	3885.8	10	WDW299	0.167		5082
3	WDW278	0.117	0.0019	3887.3	10	WDW299	0.176		5083
3	WDW278	0.126	0.0034	3887.4	10	WDW299	0.182		5084
3	WDW278	0.116	0.0026	3889.1	10	WDW299	0.172		5085
3	WDW278	0.122	0.0009	3889.3	10	WDW299	0.189	2.74	5086
3	WDW278	0.1	0.0032	3891.2	10	WDW299	0.193		5086.5
3	WDW278	0.075	0.0008	3891.3	10	WDW299	0.182	4.3	5087
3	WDW278	0.123	0.0021	3893.3	10	WDW299	0.274		5087.5
3	WDW278	0.129	0.0014	3893.5	10	WDW299	0.203		5088
3	WDW278	0.113	0.0064	3895.2	10	WDW299	0.226		5089
3	WDW278	0.098	0.0014	3894.9	10	WDW299	0.233	14.94	5090
3	WDW278	0.079	0.0029	3897.1	10	WDW299	0.218		5091
3	WDW278	0.121	0.0021	3897.6	10	WDW127		1.46E-06	
3	WDW278	0.175	0.0584	3899.8	11	WDW343	0.202	1.2	4990
3	WDW278	0.148	0.0118	3899.9	11	WDW343	0.181	0.9	5020
3	WDW278	0.161	0.0201	3901.9	11	WDW343	0.238	9.5	5050
3	WDW278	0.17	0.0091	3901.8	11	WDW343	0.191	1	5080
5	WDW142		1.27E-06		11	WDW343	0.217	2.5	5110
5	WDW271		1.46E-06		11	WDW343	0.176	1	5140
8	WDW051		0.0374	6041	11	WDW343	0.179	0.5	5170
10	WDW196		0.000535	6553	11	WDW343	0.184	1.4	5200
10	WDW314		4.58E-06	5682	11	WDW343	0.182	0.8	5230
10	WDW314		4.24E-06	5684	11	WDW343	0.175	0.7	5260
10	WDW314		4.67E-06	5688	11	WDW343	0.16	0.1	5290

CLUSTER	NO.	CZ por	CZ k md	(KB)	CLUSTER	NO.	CZ por	CZ k md	(KB)
11	WDW343	0.179	0.5	5320					
11	WDW343	0.168	0.1	5350	14	WDW316	0.128	0.7	5760
11	WDW343	0.194	1.5	5402	14	WDW316	0.121	0.2	5770
11	WDW343	0.167	0.1	5404	14	WDW316	0.142	2.6	5780
11	WDW343	0.18	0.2	5406	14	WDW316	0.117	0.1	5870
11	WDW343	0.163	0.1	5408	14	WDW316	0.136	1.4	5880
11	WDW343	0.18	0.2	5410	14	WDW316	0.127	0.5	5890
11	WDW343	0.179	0.3	5414	14	WDW316	0.146	3.3	5900
11	WDW343	0.169	0.1	5416	14	WDW316	0.139	1.8	5910
11	WDW343	0.177	0.2	5418	14	WDW230	0.295	<0.001	3830.4
11	WDW343	0.163	0.1	5420	14	WDW230	0.274	<0.001	3843.3
12	WDW148	0.093	1.5	4890	14	WDW230	0.299	<0.001	3846.3
12	WDW148	0.055	<0.1	4896	14	WDW230	0.218	<0.001	4536.8
12	WDW148	0.123	<0.1	4897	15	WDW358		0.00031	4566.2
12	WDW148	0.052	<0.1	4898	15	WDW358		9.30E-05	4567.7
12	WDW148	0.075	<0.1	4899	15	WDW358		0.0036	4568
12	WDW148	0.083	<0.1	4900	15	WDW301		1.10E-06	3603.2
12	WDW148	0.102	<0.1	4901	15	WDW301		5.60E-07	3609.1
12	WDW148	0.081	<0.1	4902	15	WDW301		2.60E-06	7143.1
12	WDW148	0.088	<0.1	4903	15	WDW301		1.60E-06	7152.1
12	WDW148	0.084	<0.1	4904	15	WDW188		5.10E-06	3595
12	WDW148	0.101	1	4905	15	WDW188		1.10E-05	3602
12	WDW148	0.067	0.1	4906	15	WDW188		1.70E-05	4055
12	WDW148	0.056	<0.1	4907	15	WDW188		2.80E-05	5949
12	WDW148	0.099	1.5	4908	15	WDW188		5.90E-05	6688
12	WDW148	0.05	<0.1	4909	15	WDW188		1.80E-05	6698
12	WDW148	0.061	<0.1	4910	15	WDW188		8.00E-05	7356
12	WDW148	0.083	3	4929	16	WDW054	0.161	0.6	
12	WDW148	0.055	<0.1	4935	16	WDW191		1.10E-05	3602
12	WDW148	0.061	0.1	4937	16	WDW191		5.10E-06	3595
12	WDW148	0.052	<0.1	4939	16	WDW191		1.70E-05	4055
12	WDW148	0.068	<0.1	4941	16	WDW282	0.304	165	6394.8
12	WDW249		1.62E-06	5403.7	16	WDW282	0.269	68.4	6395.6
12	WDW249		1.47E-06	5405.1	16	WDW282	0.325	667	
12	WDW397		0.000506	5075	16	WDW282	0.09	15.5	
12	WDW397		0.00231	5076	20	972060	0.216	0.01896	6885.5
12	WDW397		0.000618	5077	20	972060	0.232	0.1789	6889.2
14	WDW316	0.125	0.4	5750	20	972060	0.21	0.000667	6896.8

APPENDIX E: POROSITY - PERMEABILITY CROSS PLOTS BY CLUSTER

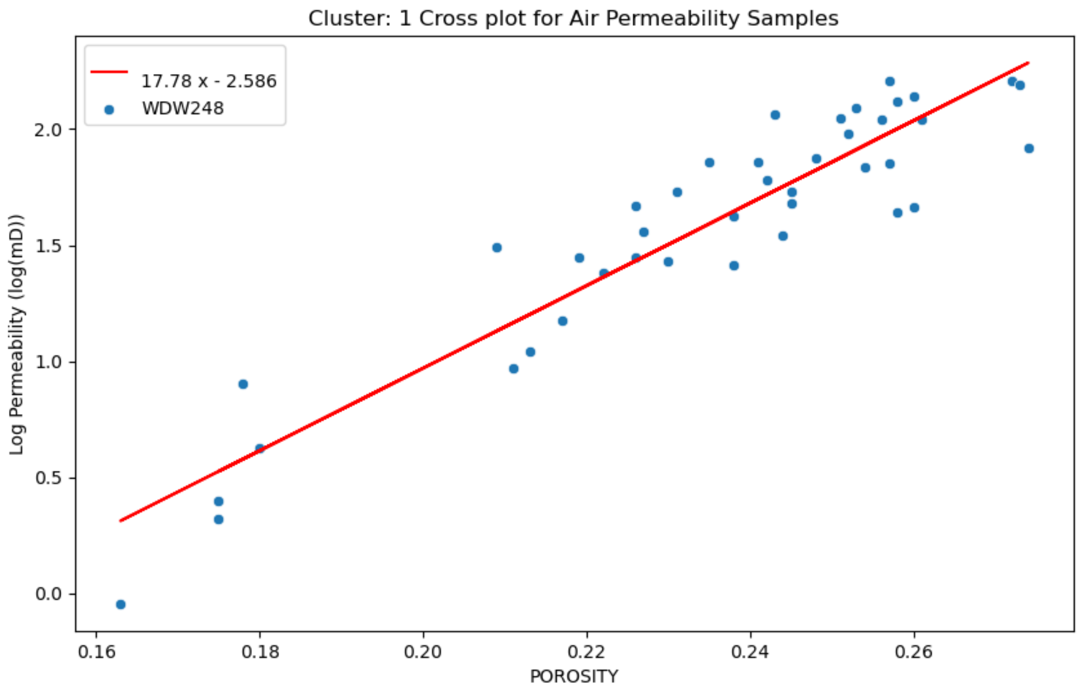

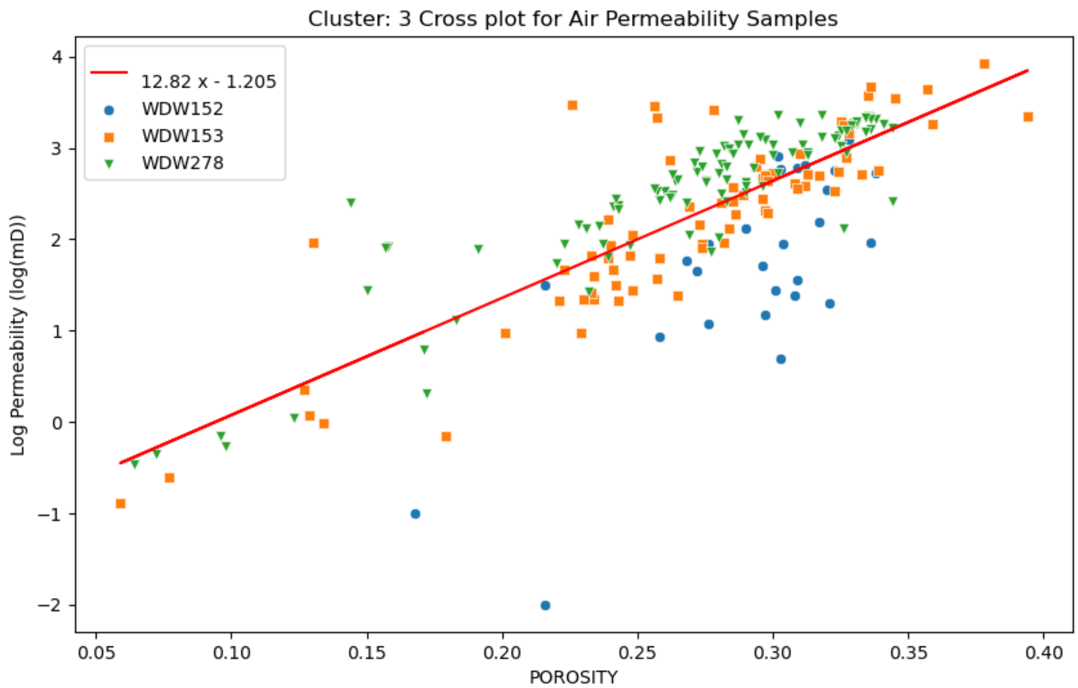

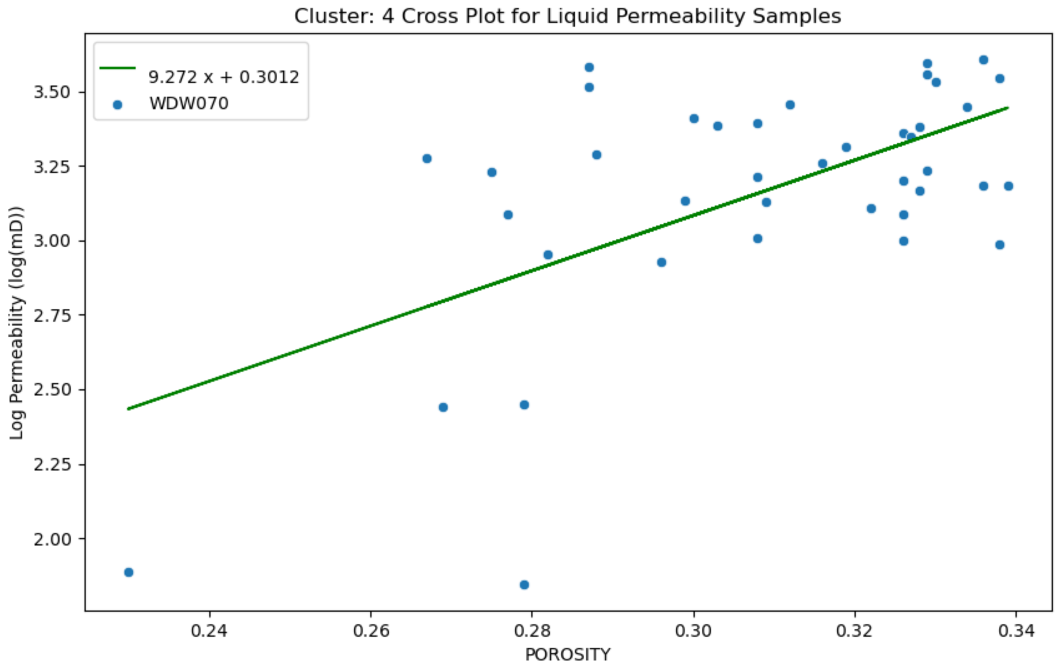
Cluster: 4 Cross Plot for Liquid Permeability Samples
9.272 x + 0.3012
WDW070
Log Permeability (log(mD))
POROSITY

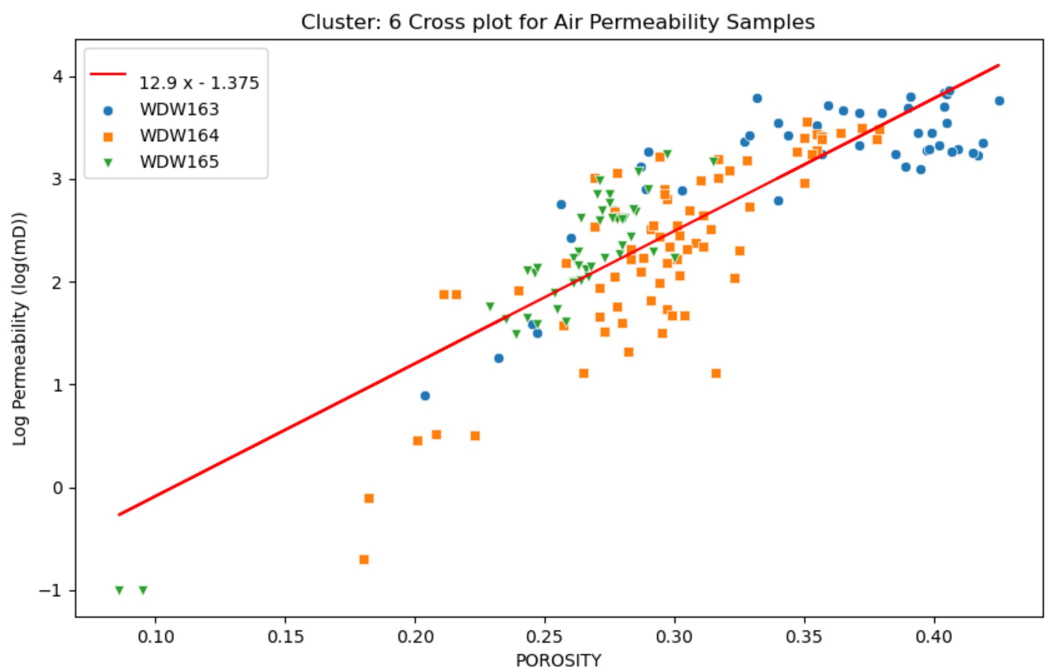
Cluster: 6 Cross plot for Air Permeability Samples
12.9 x - 1.375
WDW163
WDW164
WDW165
Log Permeability (log(mD))
POROSITY

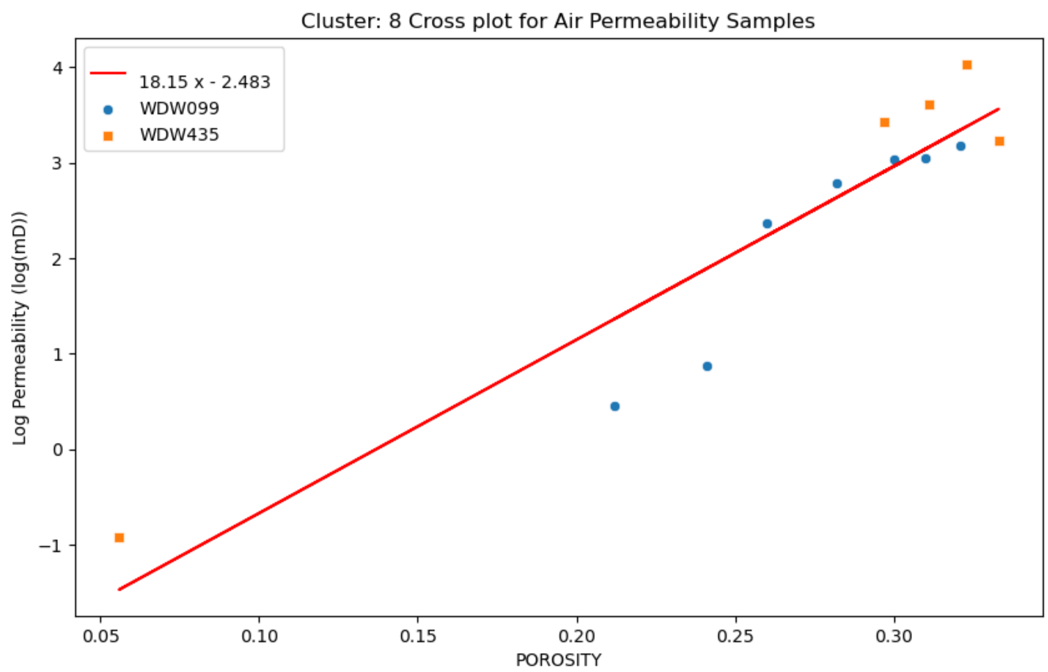

Cluster: 8 Cross plot for Air Permeability Samples
18.15 x - 2.483
WDW099
WDW435
Log Permeability (log(mD))
POROSITY
4
3
2
1
0
−1
0.05
0.10
0.15
0.20
0.25
0.30

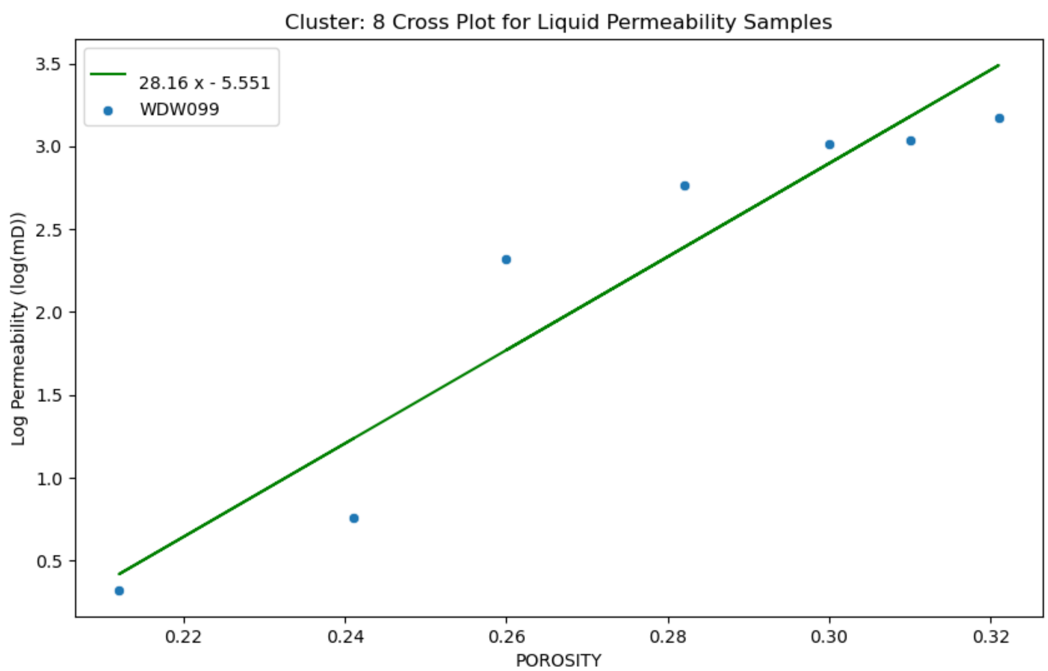

Cluster: 8 Cross Plot for Liquid Permeability Samples
28.16 x - 5.551
WDW099
Log Permeability (log(mD))
POROSITY
3.5
3.0
2.5
2.0
1.5
1.0
0.5
0.22
0.24
0.26
0.28
0.30
0.32

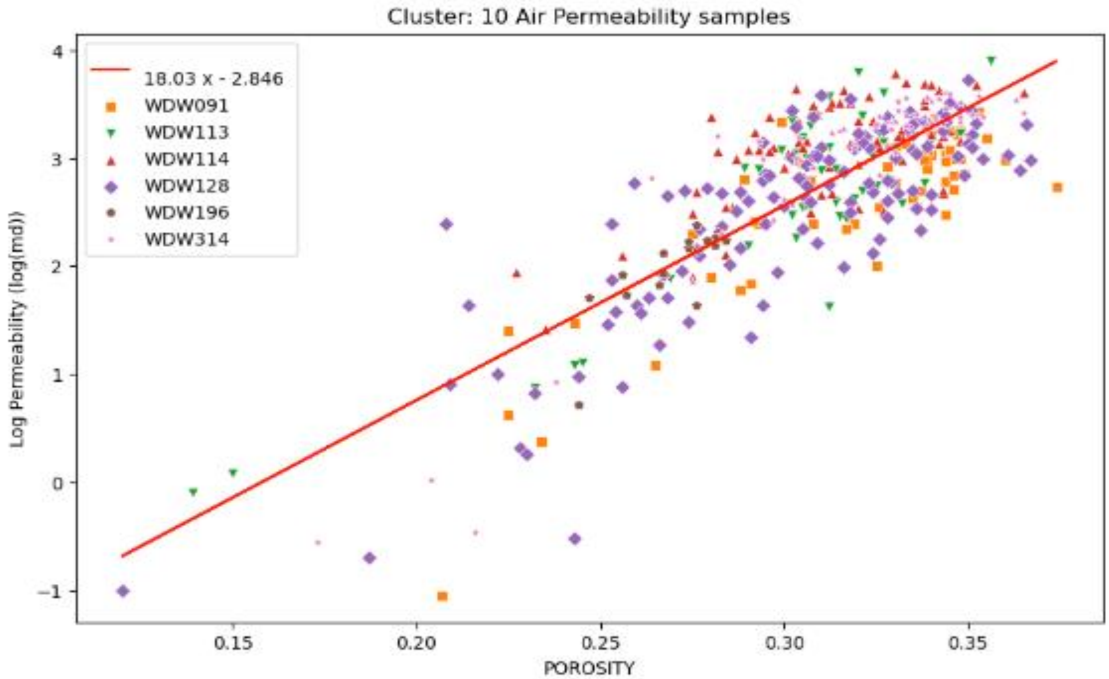

Cluster: 10 Air Permeability samples
18.03 x - 2.846
WDW091
WDW113
WDW114
WDW128
WDW196
WDW314
Log Permeability (log(md))
POROSITY
4
3
2
1
0
−1
0.15
0.20
0.25
0.30
0.35

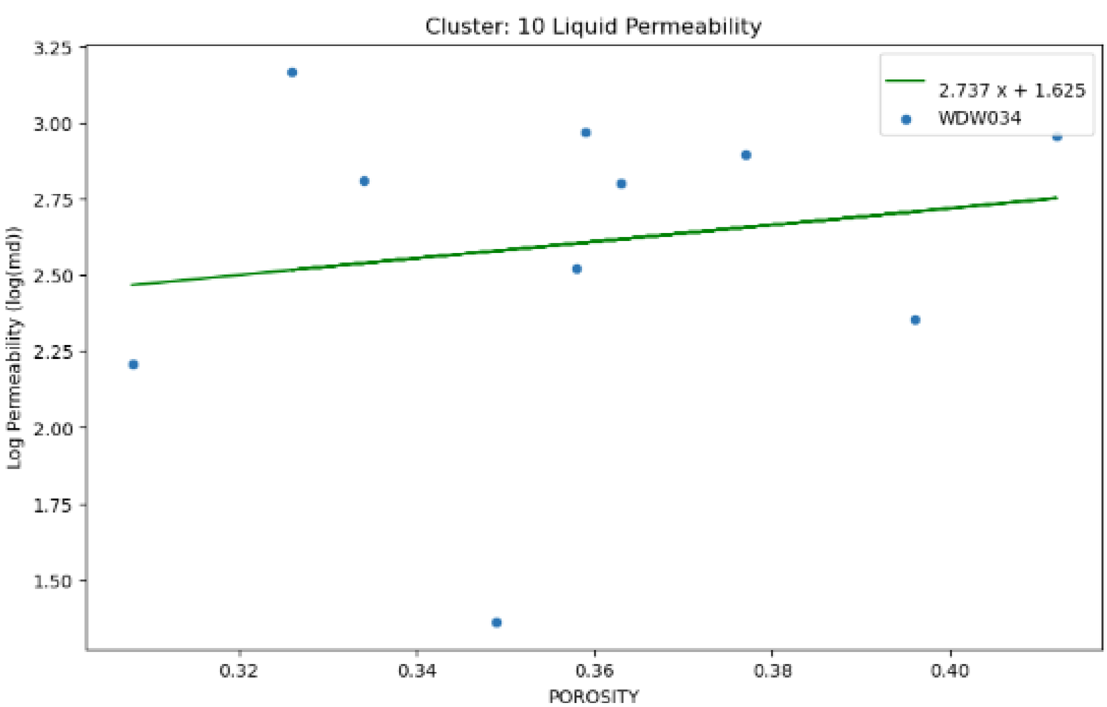

Cluster: 10 Liquid Permeability
2.737 x + 1.625
WDW034
Log Permeability (log(md))
POROSITY
3.25
3.00
2.75
2.50
2.25
2.00
1.75
1.50
0.32
0.34
0.36
0.38
0.40

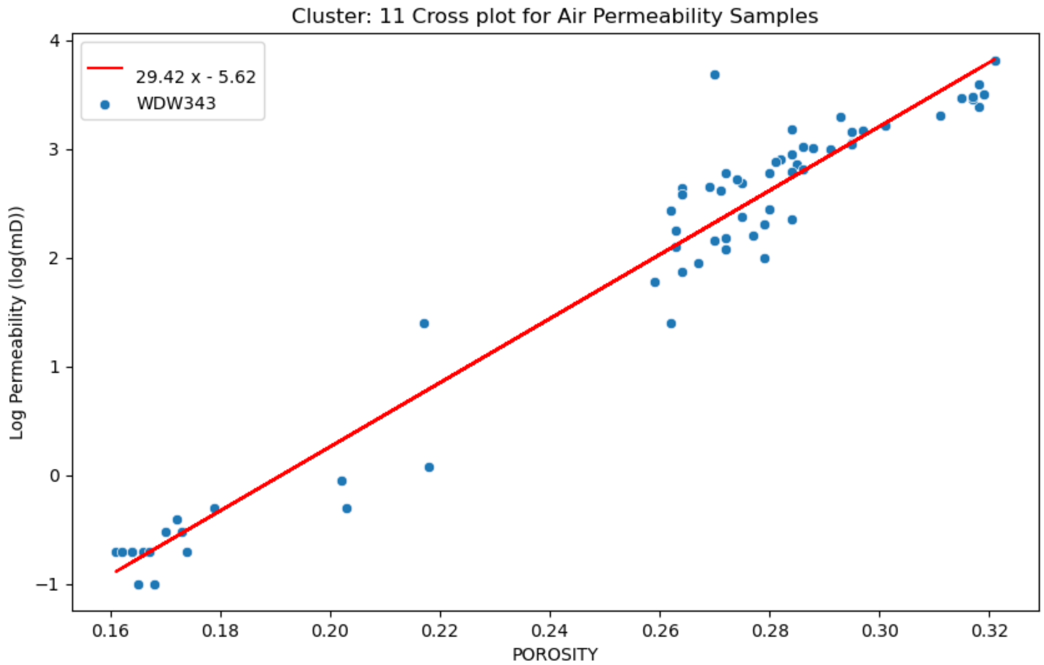

Cluster: 11 Cross plot for Air Permeability Samples
29.42 x - 5.62
WDW343
Log Permeability (log(mD))
POROSITY

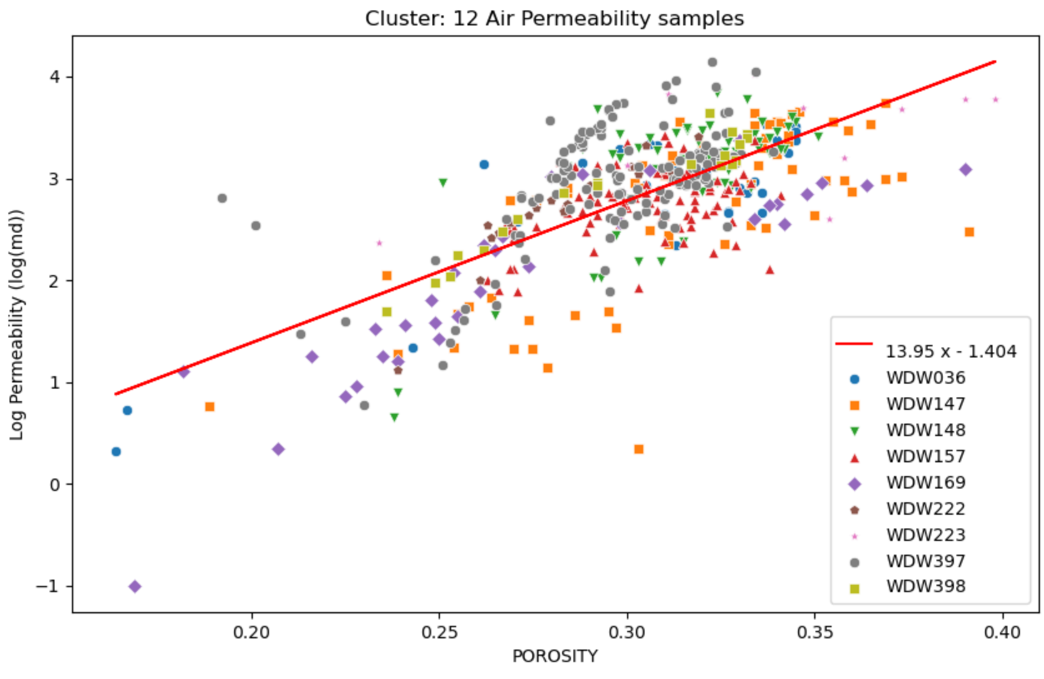

Cluster: 12 Air Permeability samples
13.95 x - 1.404
WDW036
WDW147
WDW148
WDW157
WDW169
WDW222
WDW223
WDW397
WDW398
Log Permeability (log(md))
POROSITY

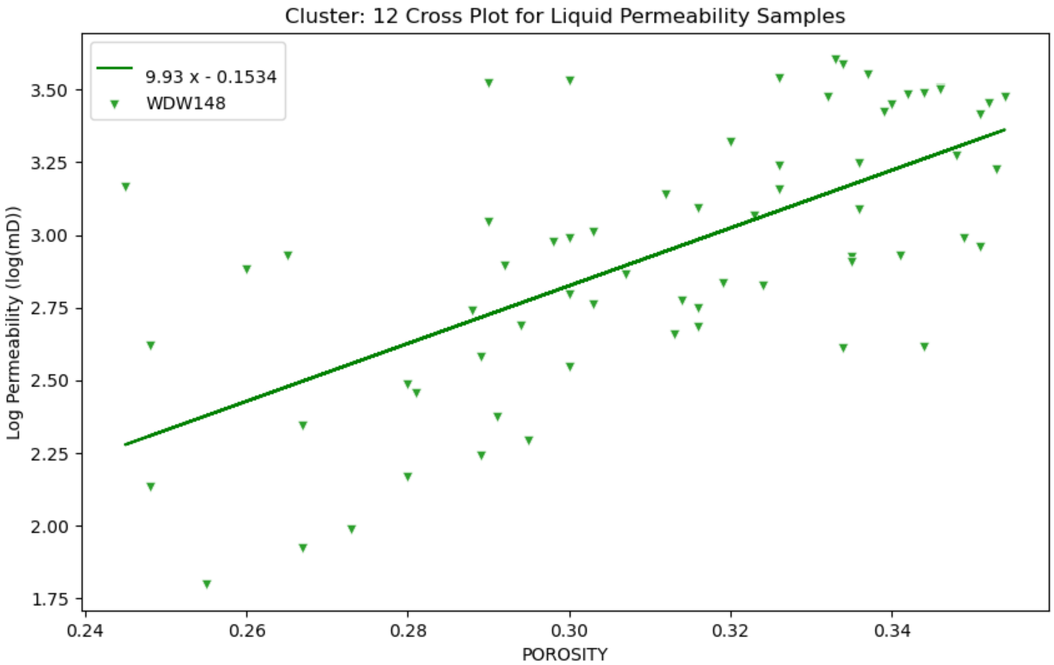
Cluster: 12 Cross Plot for Liquid Permeability Samples
9.93 x - 0.1534
WDW148
Log Permeability (log(mD))
POROSITY
3.50
3.25
3.00
2.75
2.50
2.25
2.00
1.75
0.24
0.26
0.28
0.30
0.32
0.34

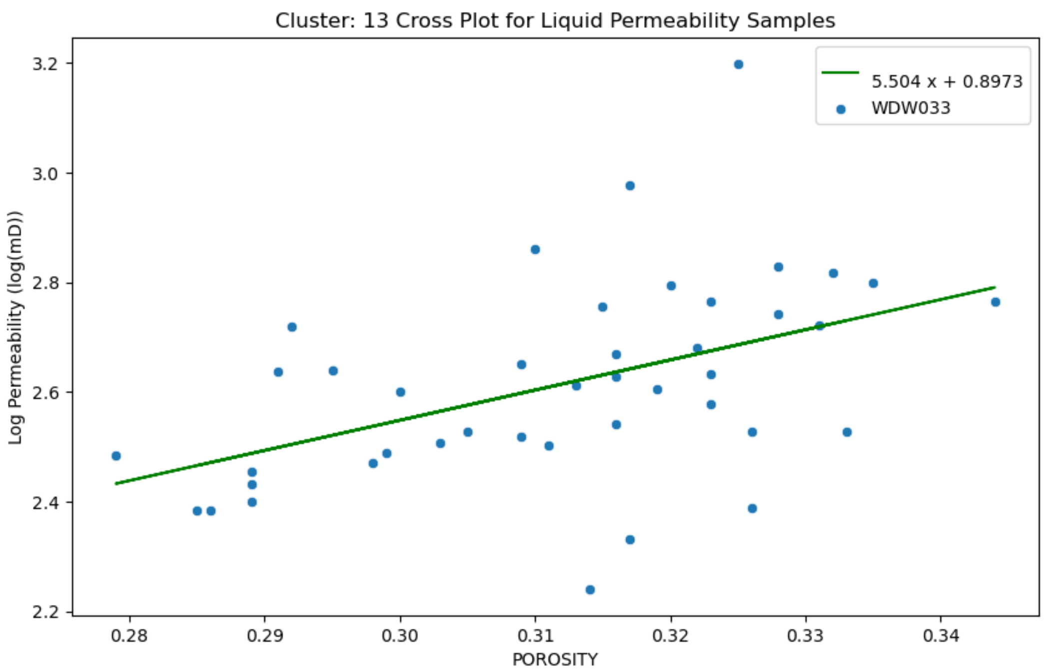
Cluster: 13 Cross Plot for Liquid Permeability Samples
5.504 x + 0.8973
WDW033
Log Permeability (log(mD))
POROSITY
3.2
3.0
2.8
2.6
2.4
2.2
0.28
0.29
0.30
0.31
0.32
0.33
0.34

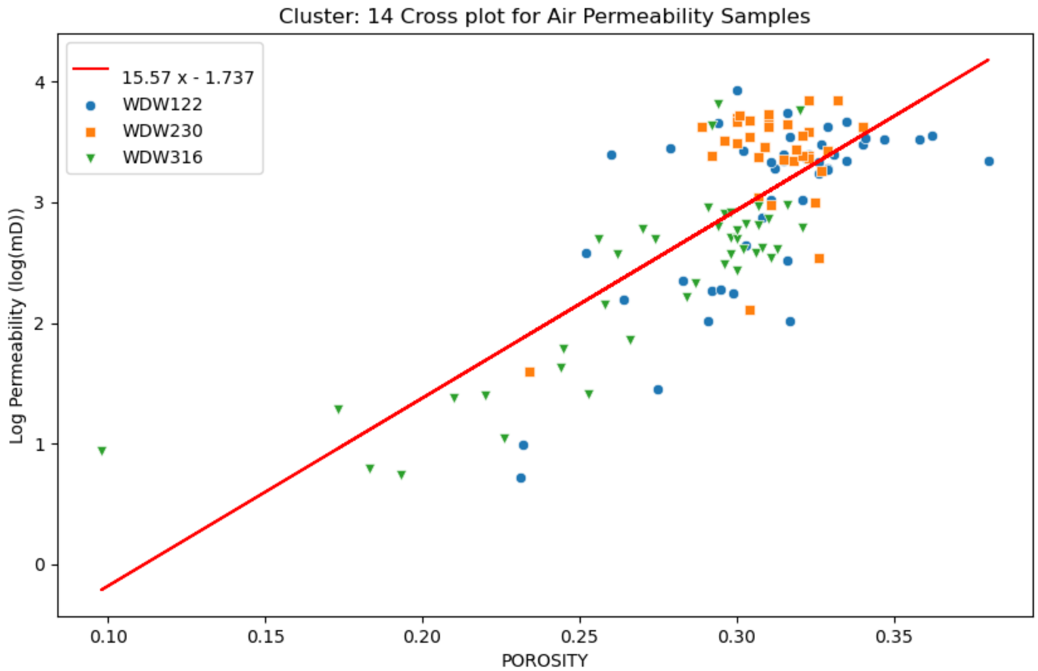
Cluster: 14 Cross plot for Air Permeability Samples
15.57 x - 1.737
WDW122
WDW230
WDW316
Log Permeability (log(mD))
POROSITY
0.10
0.15
0.20
0.25
0.30
0.35
0
1
2
3
4

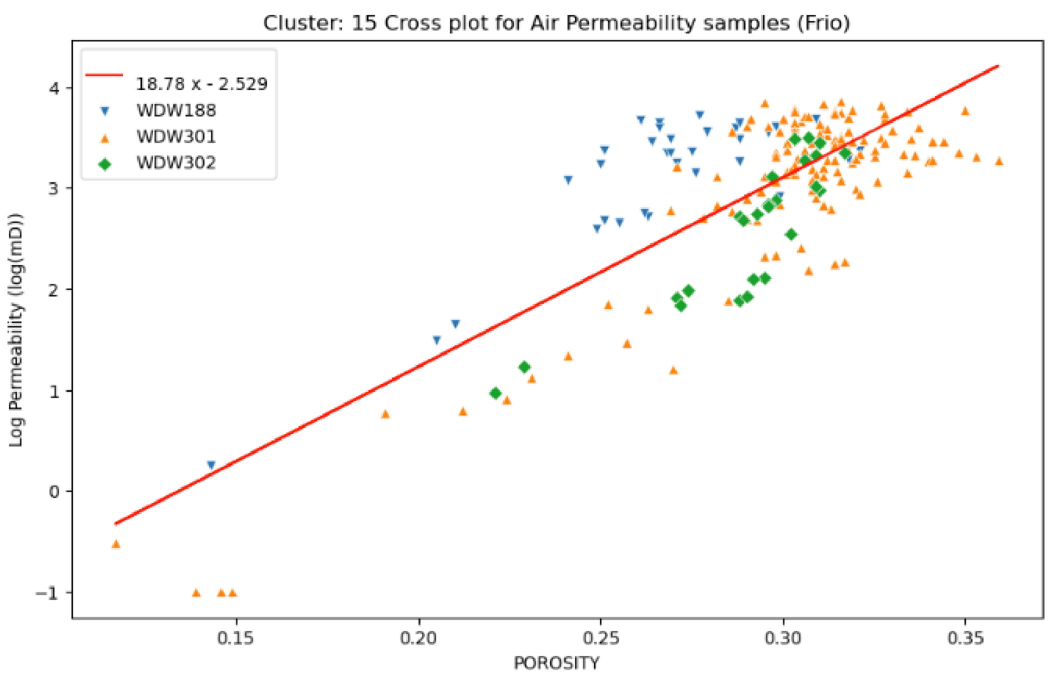
Cluster: 15 Cross plot for Air Permeability samples (Frio)
18.78 x - 2.529
WDW188
WDW301
WDW302
Log Permeability (log(mD))
POROSITY
0.15
0.20
0.25
0.30
0.35
−1
0
1
2
3
4

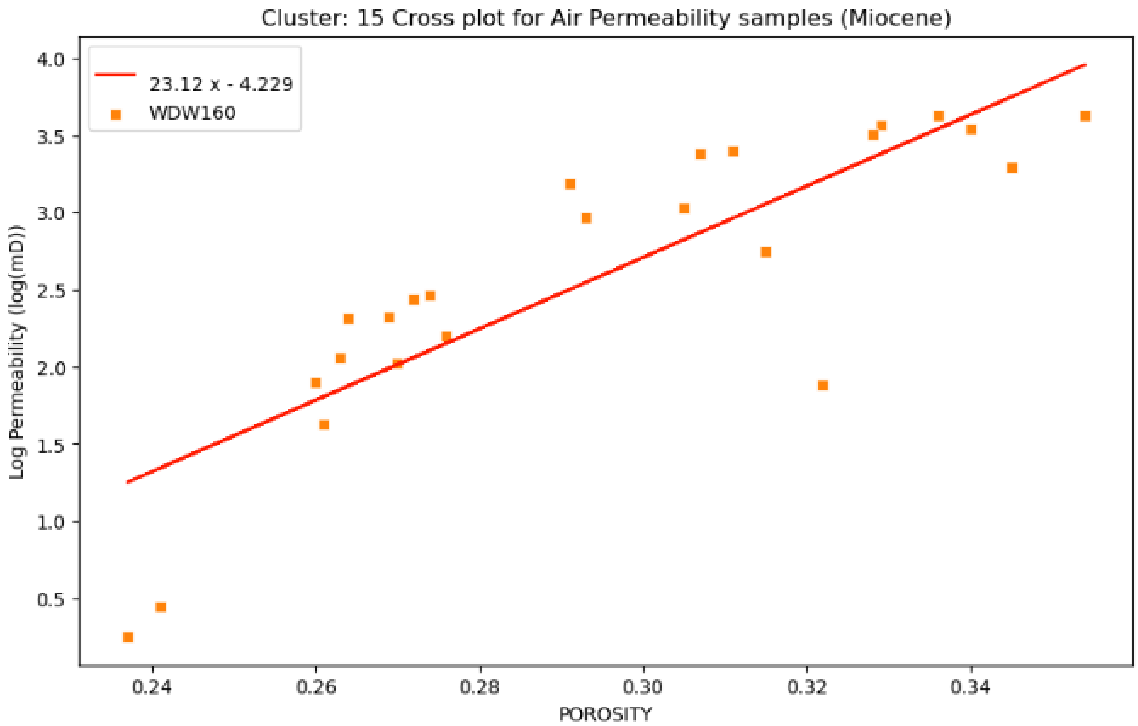
Cluster: 15 Cross plot for Air Permeability samples (Miocene)
23.12 x - 4.229
WDW160
Log Permeability (log(mD))
POROSITY
4.0
3.5
3.0
2.5
2.0
1.5
1.0
0.5
0.24
0.26
0.28
0.30
0.32
0.34

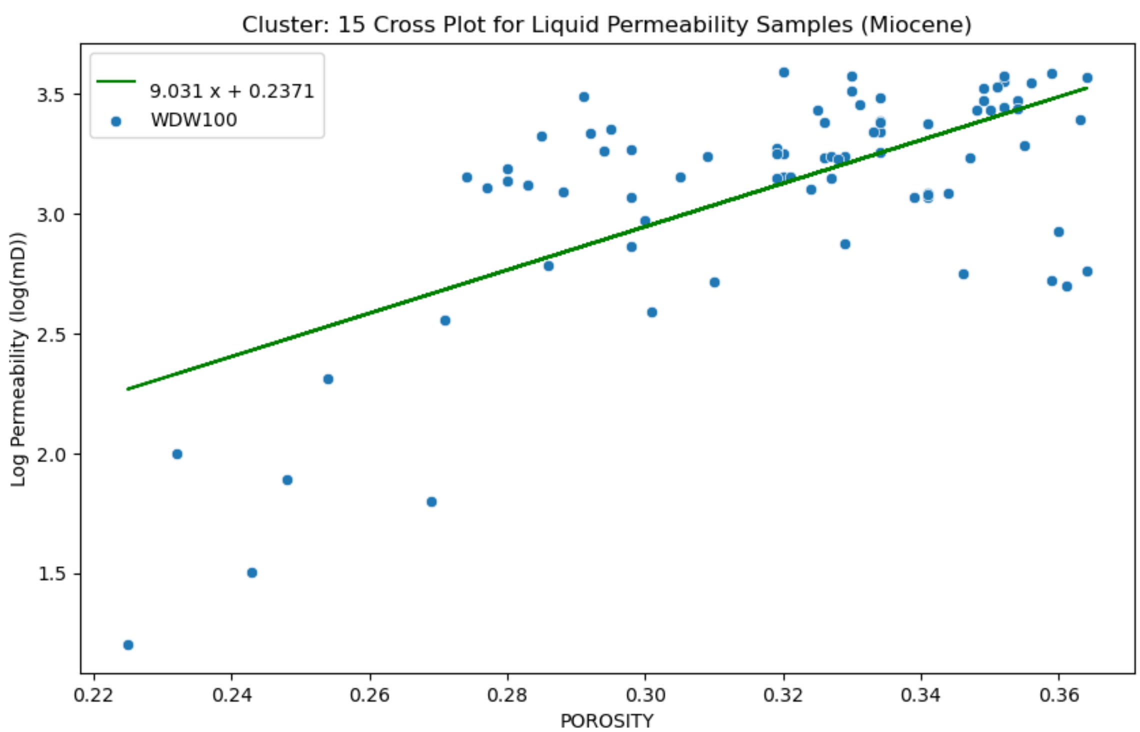
Cluster: 15 Cross Plot for Liquid Permeability Samples (Miocene)
9.031 x + 0.2371
WDW100
Log Permeability (log(mD))
POROSITY
3.5
3.0
2.5
2.0
1.5
0.22
0.24
0.26
0.28
0.30
0.32
0.34
0.36

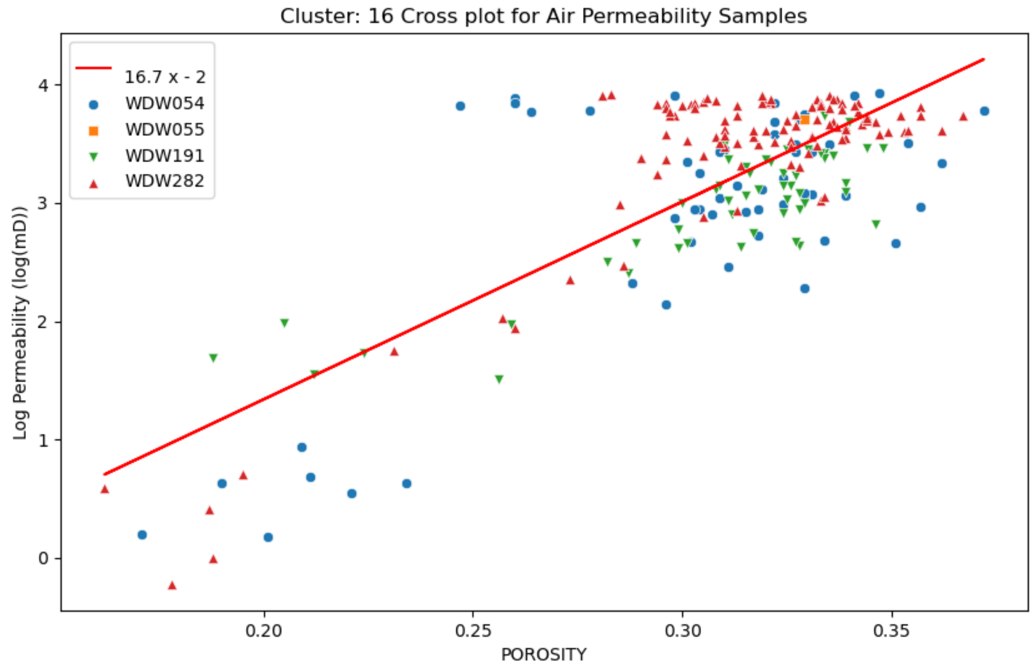
Cluster: 16 Cross plot for Air Permeability Samples
16.7 x - 2
WDW054
WDW055
WDW191
WDW282
Log Permeability (log(mD))
POROSITY
0
1
2
3
4
0.20
0.25
0.30
0.35

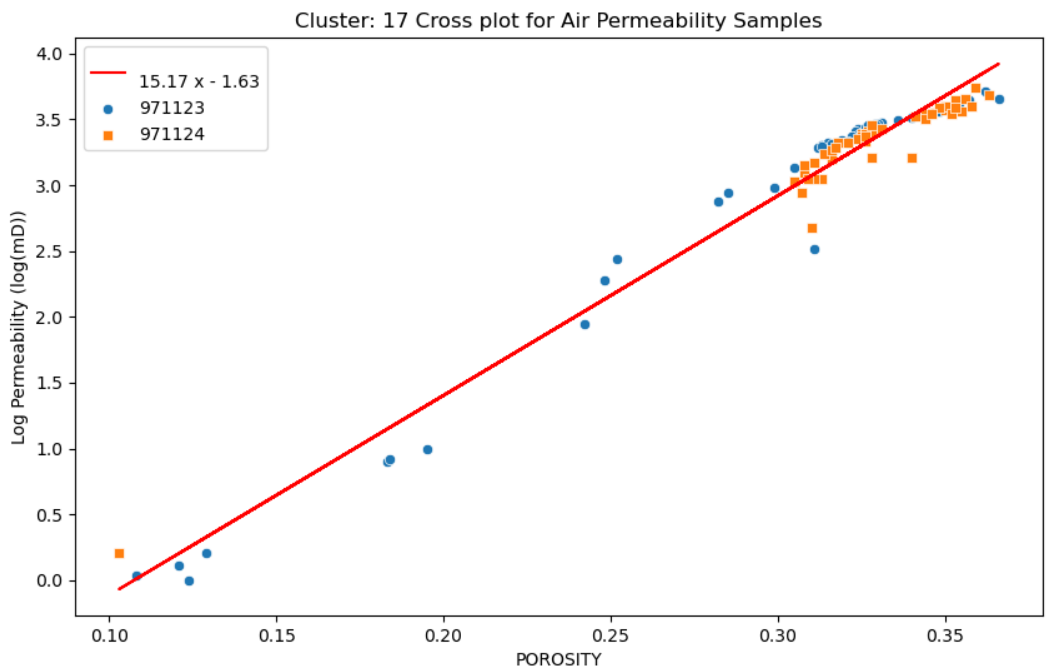
Cluster: 17 Cross plot for Air Permeability Samples
15.17 x - 1.63
971123
971124
Log Permeability (log(mD))
POROSITY
0.0
0.5
1.0
1.5
2.0
2.5
3.0
3.5
4.0
0.10
0.15
0.20
0.25
0.30
0.35

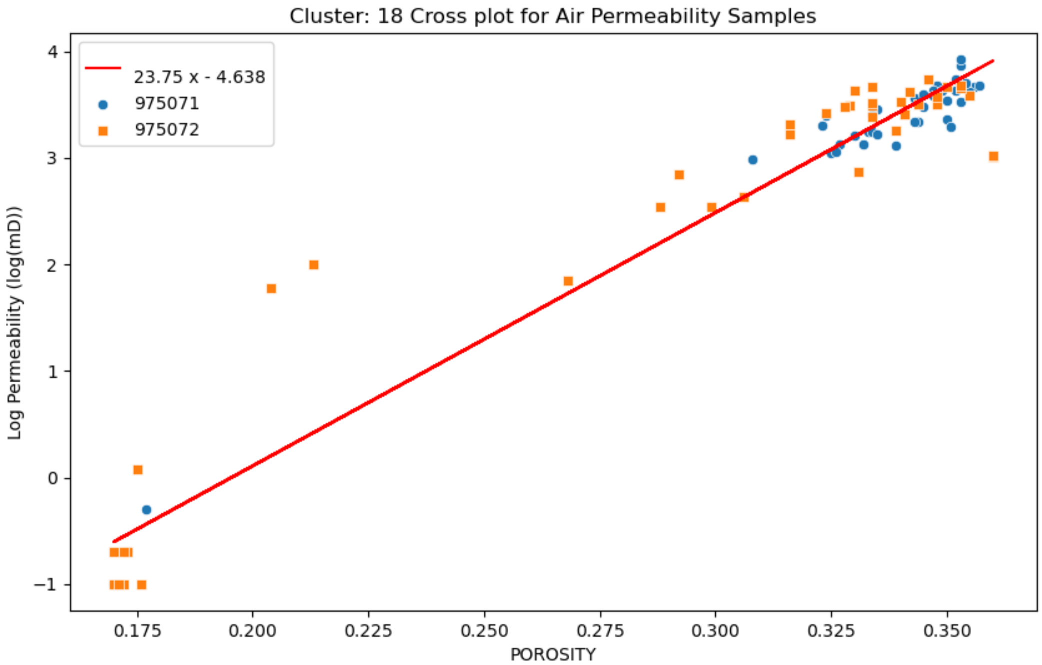
Cluster: 18 Cross plot for Air Permeability Samples
23.75 x - 4.638
975071
975072
Log Permeability (log(mD))
POROSITY
4
3
2
1
0
−1
0.175
0.200
0.225
0.250
0.275
0.300
0.325
0.350

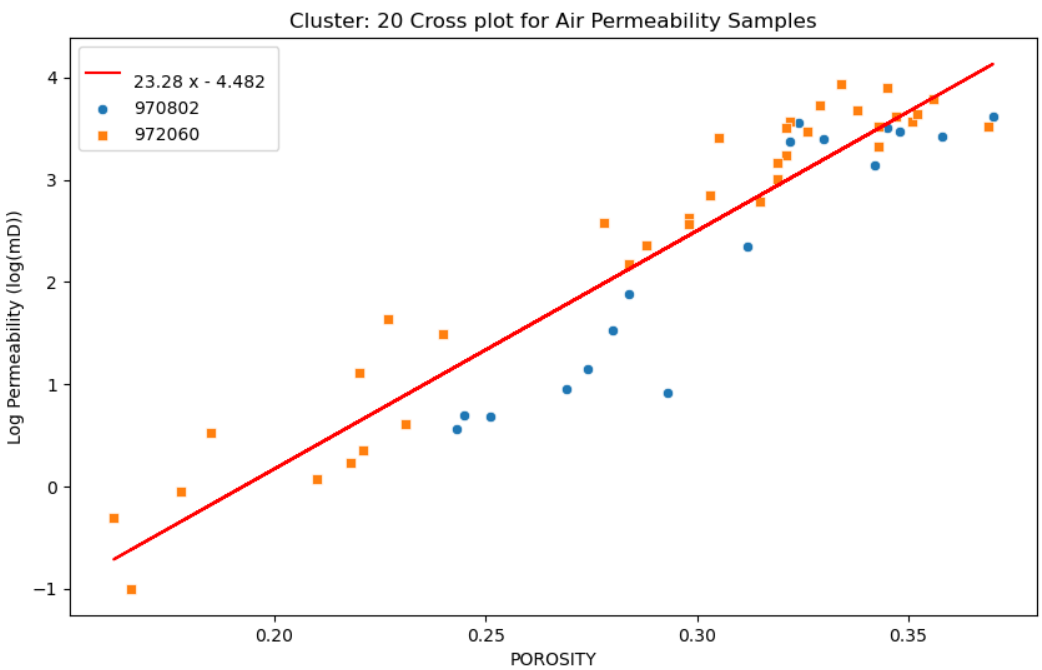
Cluster: 20 Cross plot for Air Permeability Samples
23.28 x - 4.482
970802
972060
Log Permeability (log(mD))
POROSITY
4
3
2
1
0
−1
0.20
0.25
0.30
0.35

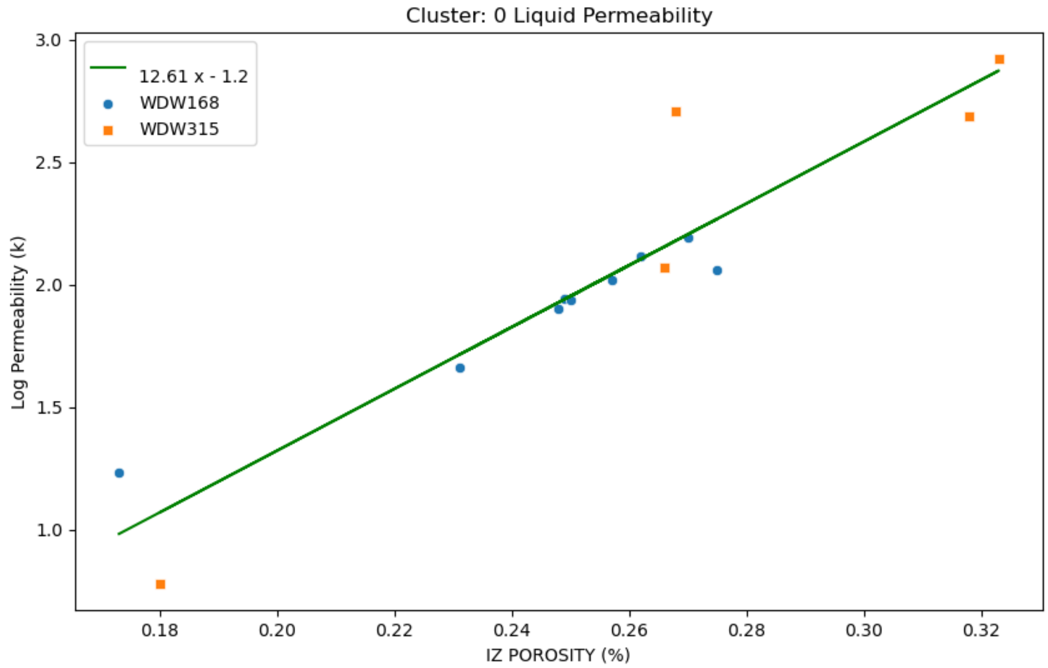
Cluster: 0 Liquid Permeability
12.61 x - 1.2
WDW168
WDW315
Log Permeability (k)
IZ POROSITY (%)
3.0
2.5
2.0
1.5
1.0
0.18
0.20
0.22
0.24
0.26
0.28
0.30
0.32

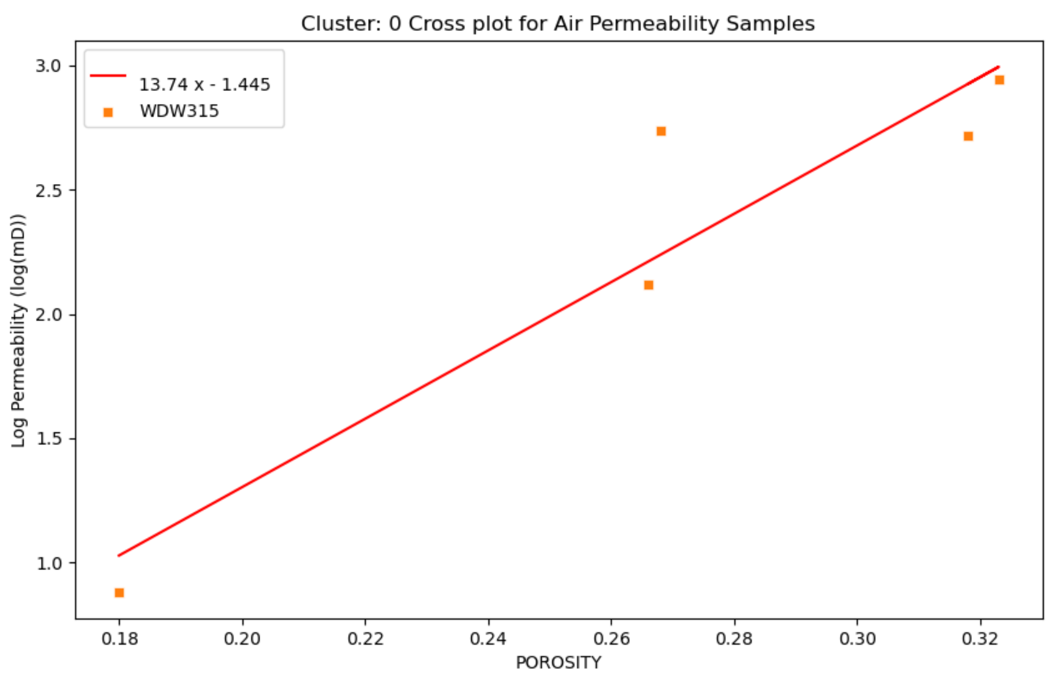
Cluster: 0 Cross plot for Air Permeability Samples
13.74 x - 1.445
WDW315
Log Permeability (log(mD))
POROSITY
3.0
2.5
2.0
1.5
1.0
0.18
0.20
0.22
0.24
0.26
0.28
0.30
0.32

APPENDIX F: FORMATION FLUID ANALYSIS

Chemical analysis of formation fluid reports each ion in concentrations of milligrams per Liter (MPL). The total dissolved solids (TDS), also in MPL, reports the value as found in the permit.

Legend for Column names of Ions

Table Label	Name of Ion	Units	Table Label	Name of Ion	Units
Na	*Sodium*	mg/L	Ba	*Barium*	mg/L
Cl	*Chloride*	mg/L	Sr	*Strontium*	mg/L
Ca	*Calcium*	mg/L	HCO3	*Bicarbonate*	mg/L
Mg	*Magnesium*	mg/L	K	*Potassium*	mg/L
SO4	*Sulfate*	mg/L	Br	*Bromide*	mg/L
Iron	*Iron*	mg/L	CaCo3	*Calcium Carbonate*	mg/L

CLUSTER	NO.	TDS (mg/L)	Na	Cl	Ca	Mg	SO4	Iron	Ba	Sr	HCO3	K	Br	CaCo3
6	WDW163	86700	28130	50700	2160	220	87		16	272	177	150		
9	WDW224	213201	51000	101777	3500	1100	235	3				450		
9	WDW318	135993	46550	83425	4350	1370	240	56					1	
9	WDW359	119763	39859	4140	4140	1383	7	0.065			1380		71	
8	WDW051*	182000	61800*	107000*	1700*	430*	31*	30*	5.8*	180*	48*	230*	23*	
12	WDW148	109025	39200	63548	2700	340	18	5	44	160	115			
10	WDW091	162820	49000	86200	3200	890		1.5	22		134			110
10	WDW196	99000	25000	59000	1800	580	640	9			230	3390	9	
16	WDW055	88600	32700	5410	1760	493	70	9.42	41.3	124		598	250	
16	WDW191	108000	36500	68700	295	1120	3.5	15.9	39	134	87	3980	100	122

CLUSTER	NO.	TDS (mg/L)	Na	Cl	Ca	Mg	SO4	Iron	Ba	Sr	HCO3	K	Br	CaCo3
16	WDW282	87500	33700	4070	2470	761	98.8	28.2	28.6	117		666		
1	WDW248	71233	20700	3666	6543	112.3	178	2.7	8.3		43.3	97.2		
10	WDW034	116832	40330	71000	3400	986	0				126			
10	WDW113	123500	43000	75500	3600	974	99	0.04			23			
10	WDW114	134000	47100	81000	3180	985	40	6.2			183			
15	WDW301		41000	67900	2700	440	82		10	185	289	200		
3	WDW278	92000	41600	87500	2480	193	33					154		6987
2	WDW211	63300	19961	38560	4080	300	350				88			
14	WDW316	146000	45930	71850	2930	450	35	4	70	120	200	300	30	
15	WDW100	99000	27000	56000		58	200	36	41	180		8250		
15	WDW188	73080	21500	26771			432	2.4						
12	WDW147	128000	55664	60247	2250	475	18		66	150				
12	WDW319	135000	45700	82000	1610	214	654	1170	49	85				
4	WDW070	87400	28600	53600	4650	540	2274				49	7.99		277
10	WDW127	147000	52136	87900	2920	830	43	30			132			108
12	WDW222	113400	39400	70520	2200	457	99	60.5	63	112	135	360		80.1
12	WDW223	115400	41200	70872	2160	455	99	53.4	46	113	12	368		109.1
12	WDW422		12820	17229	626	123		7408		1.2	5	2318	108	5
12	WDW036		43000	63548	6400	1440	18	5	190		99			
14	WDW122	120924	44214	73605	2476	403	98	13.3	0		111			
14	WDW230		44000											
13	WDW033	120721	41377	74000	4280	888	78				98			
17	970904	132700	167531											
17	971124		167531											
20	972060		40000	67350	2270	746	68	4	64	86	240	120		
20	970802	101219	28400	58800	3400	1670	3	91.5	130	61.8	13	134		

** concentration is reported in PPM, not milligram/Liter*

APPENDIX G: LOG MATCH TO CORES

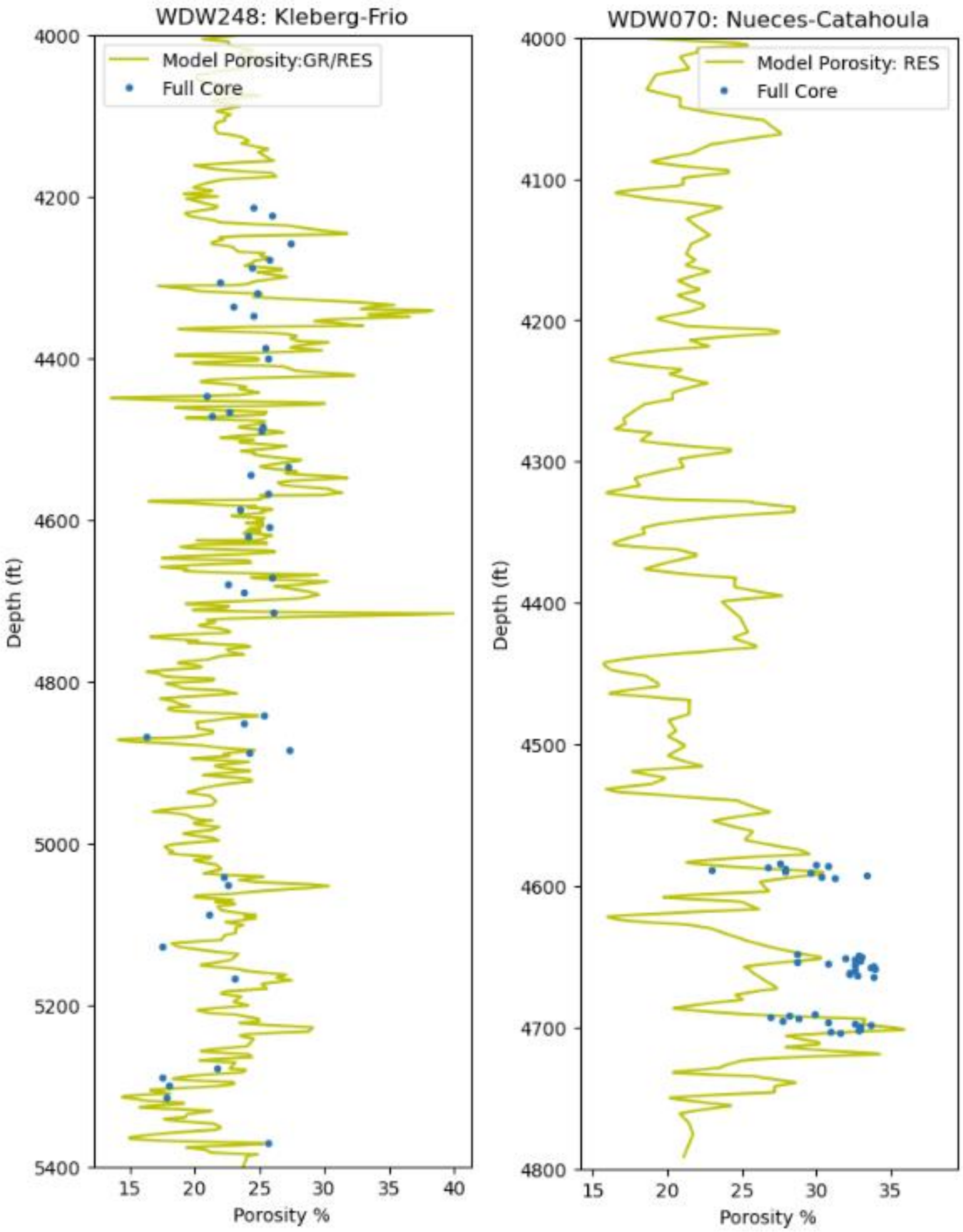

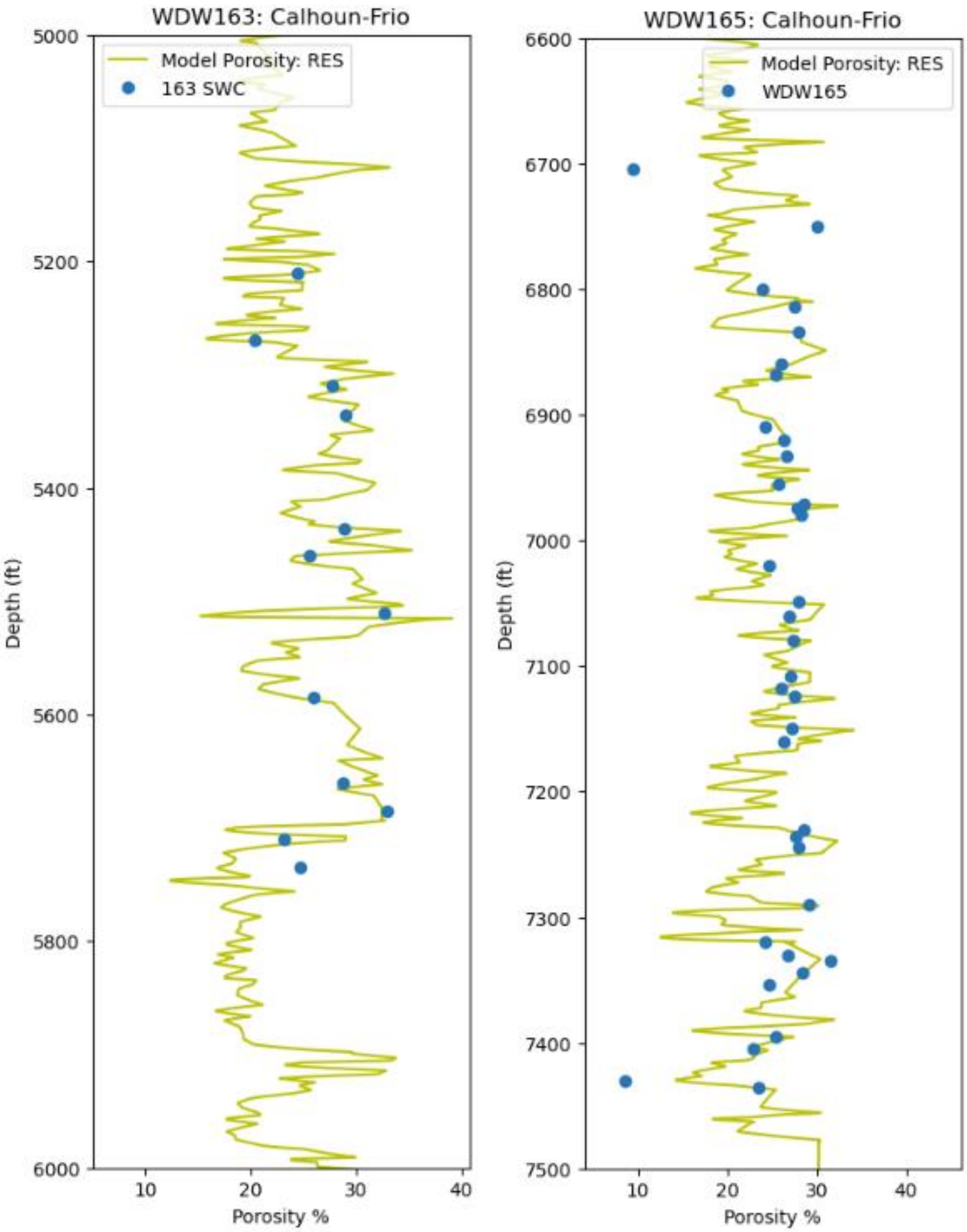
WDW163: Calhoun-Frio
Model Porosity: RES
163 SWC
Depth (ft)
Porosity %
5000
5200
5400
5600
5800
6000
10
20
30
40
WDW165: Calhoun-Frio
Model Porosity: RES
WDW165
6600
6700
6800
6900
7000
7100
7200
7300
7400
7500

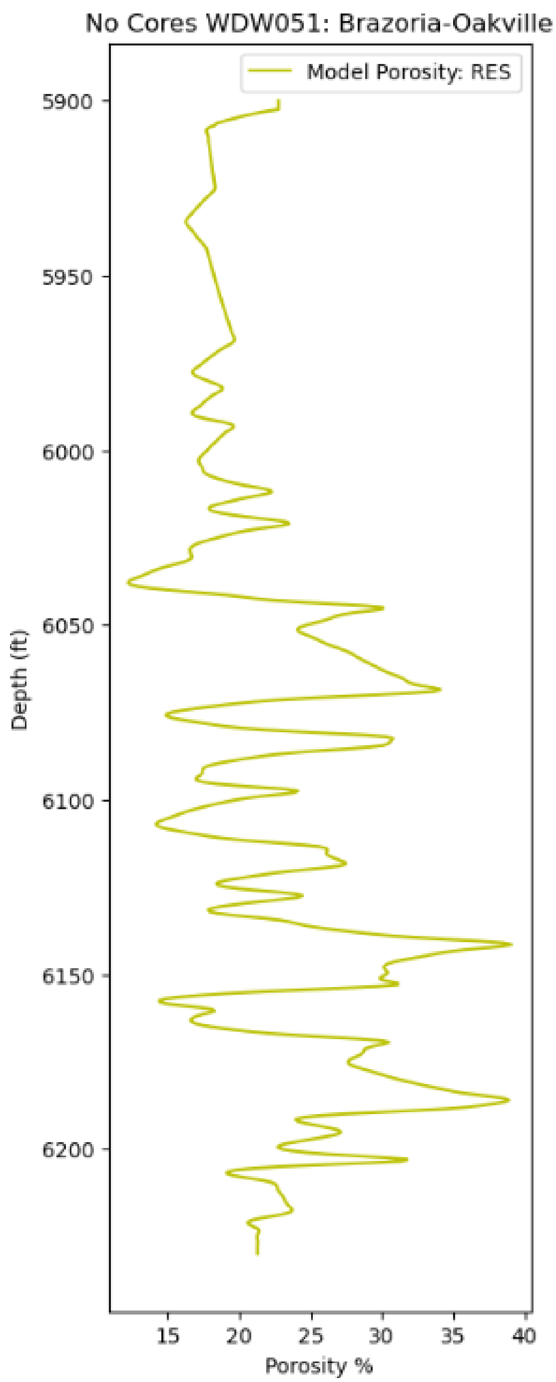
No Cores WDW051: Brazoria-Oakville
Model Porosity: RES
Depth (ft)
Porosity %
5900
5950
6000
6050
6100
6150
6200
15
20
25
30
35
40

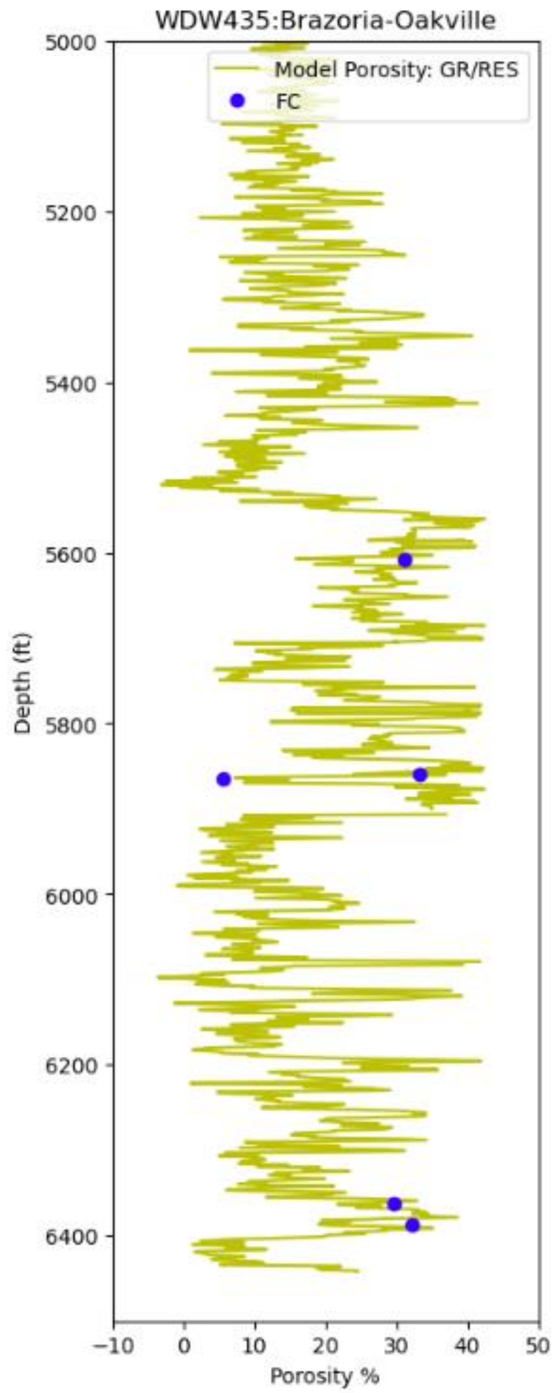
WDW435:Brazoria-Oakville
Model Porosity: GR/RES
FC
Depth (ft)
Porosity %
5000
5200
5400
5600
5800
6000
6200
6400
−10
0
10
20
30
40
50

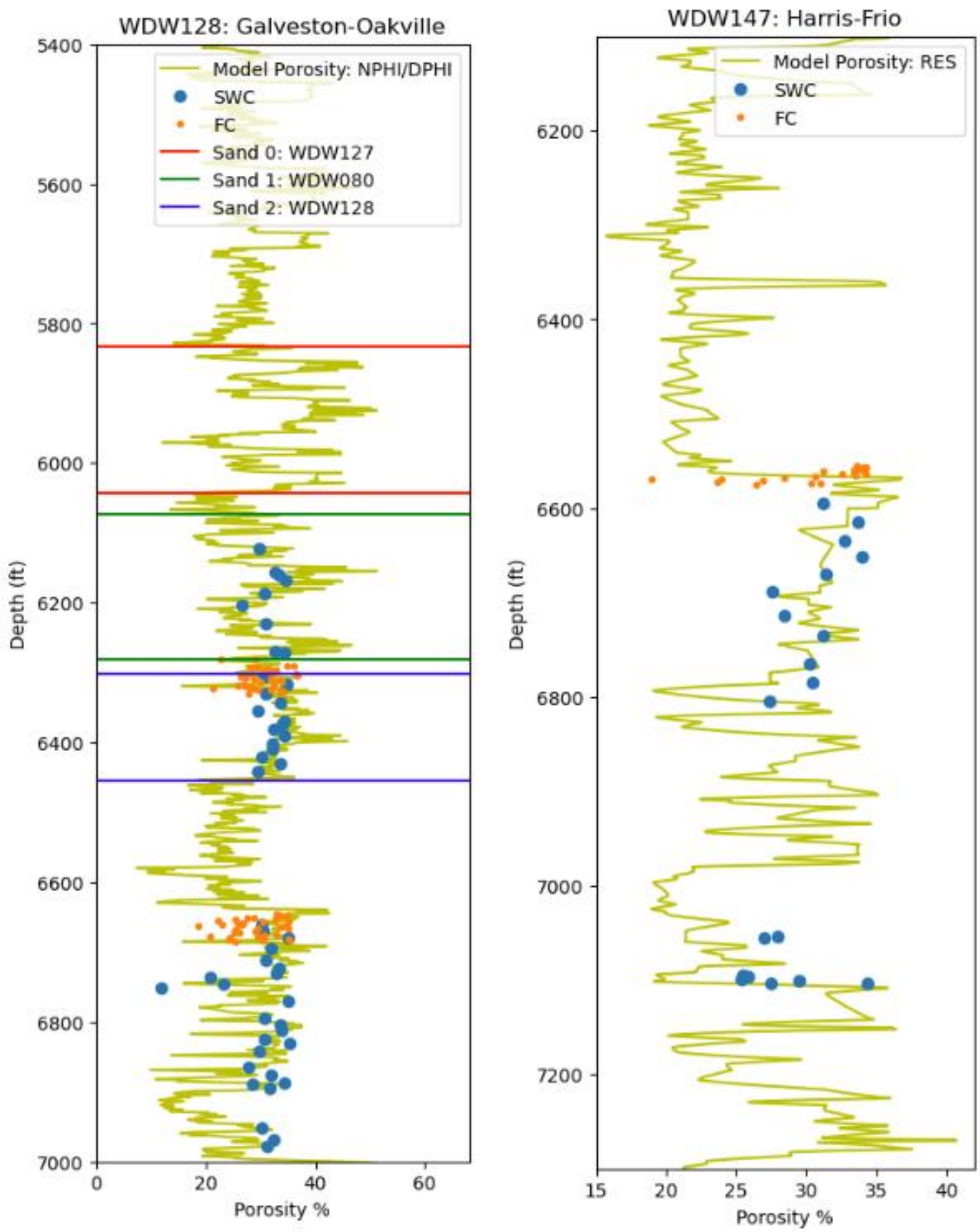
WDW128: Galveston-Oakville
Model Porosity: NPHI/DPHI
SWC
FC
Sand 0: WDW127
Sand 1: WDW080
Sand 2: WDW128
Depth (ft)
Porosity %
WDW147: Harris-Frio
Model Porosity: RES
SWC
FC
Depth (ft)
Porosity %

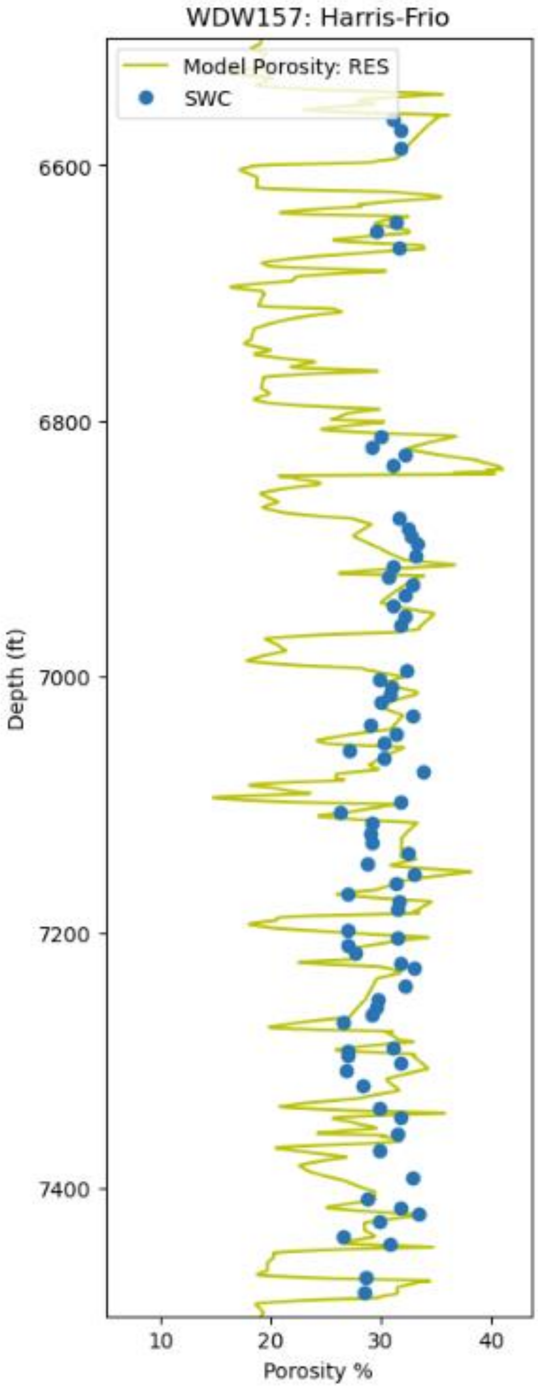

WDW157: Harris-Frio
Model Porosity: RES
SWC
Depth (ft)
6600
6800
7000
7200
7400
10
20
30
40
Porosity %

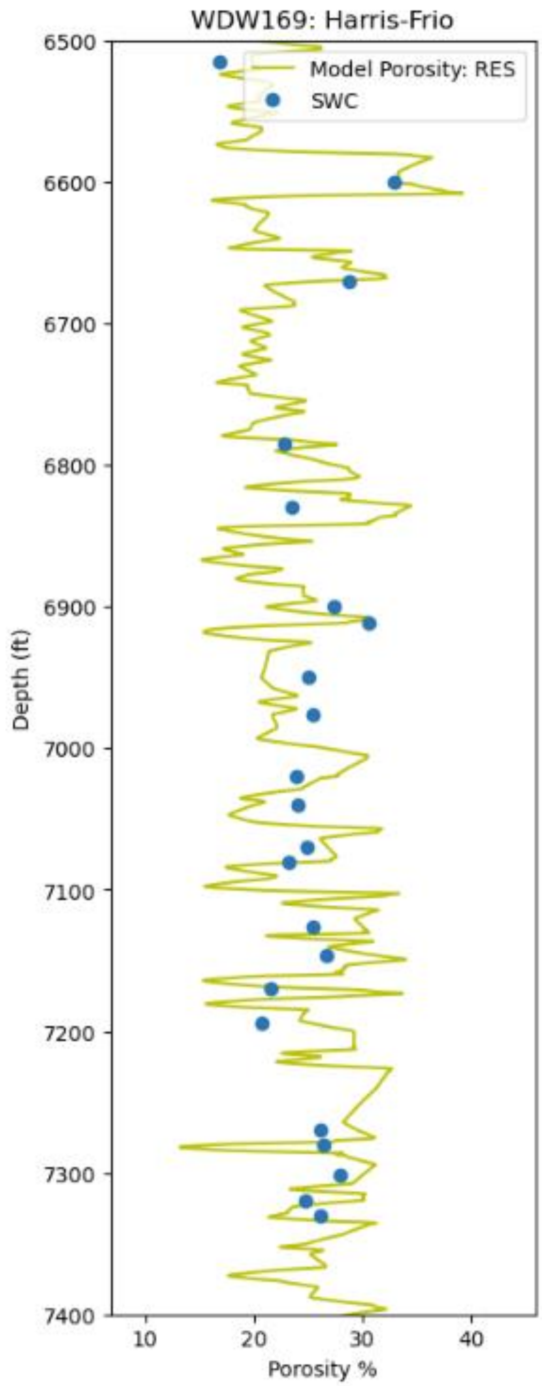

WDW169: Harris-Frio
Model Porosity: RES
SWC
Depth (ft)
6500
6600
6700
6800
6900
7000
7100
7200
7300
7400
10
20
30
40
Porosity %

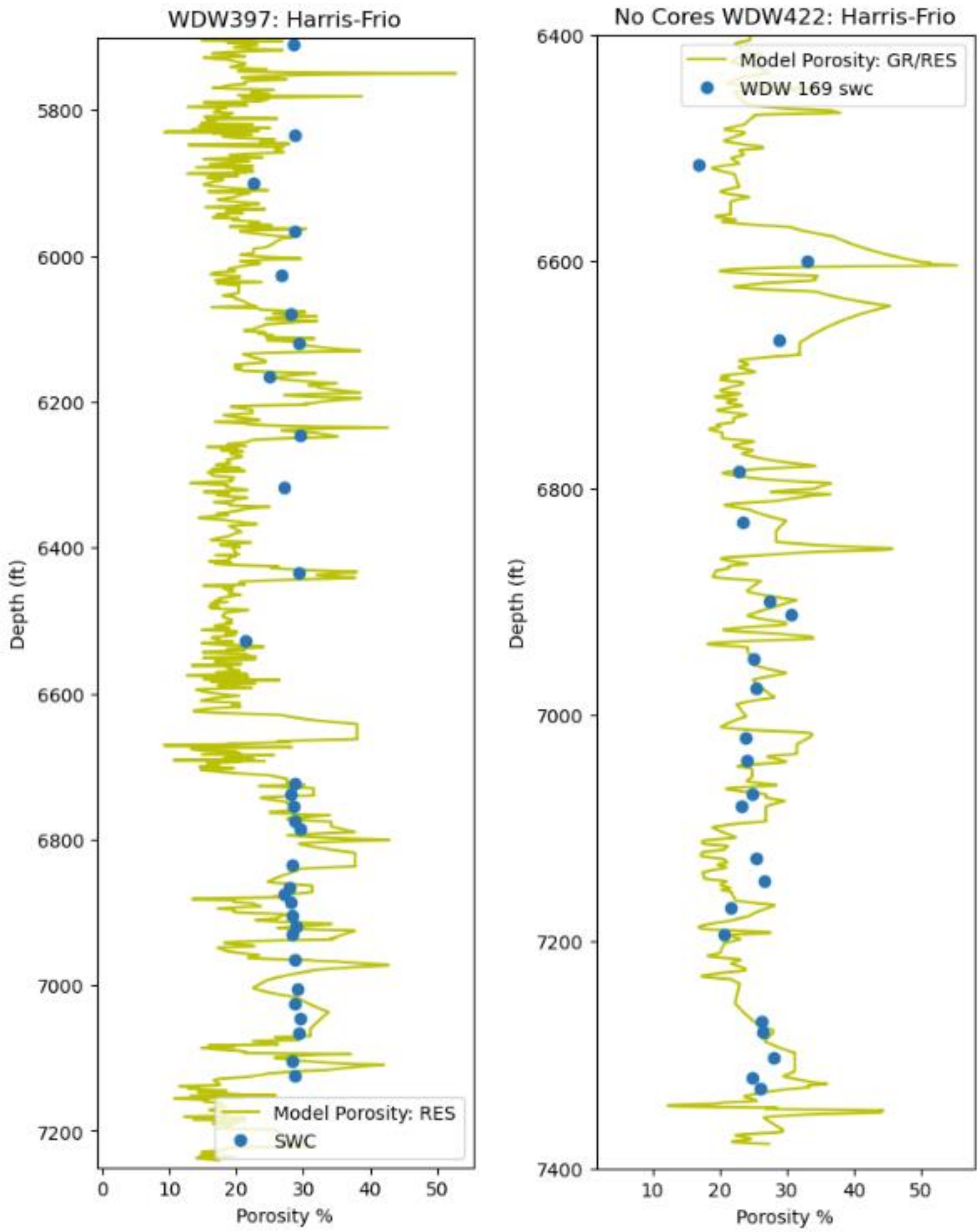

WDW397: Harris-Frio
Depth (ft)
Porosity %
Model Porosity: RES
SWC
No Cores WDW422: Harris-Frio
Model Porosity: GR/RES
WDW 169 swc

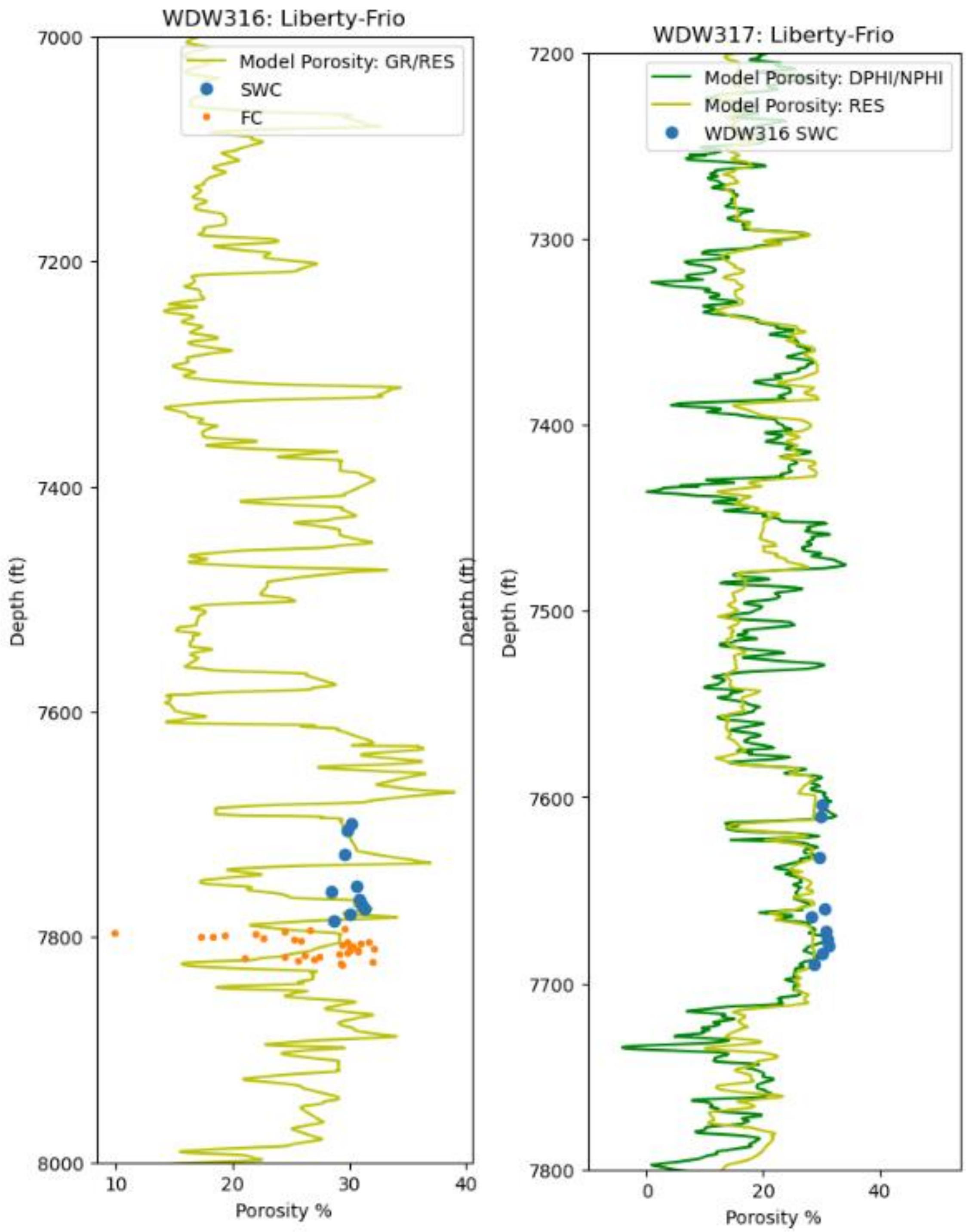
WDW316: Liberty-Frio
Model Porosity: GR/RES
SWC
FC
Depth (ft)
Porosity %
7000
7200
7400
7600
7800
8000
10
20
30
40
WDW317: Liberty-Frio
Model Porosity: DPHI/NPHI
Model Porosity: RES
WDW316 SWC
Depth (ft)
Porosity %
7200
7300
7400
7500
7600
7700
7800
0
20
40

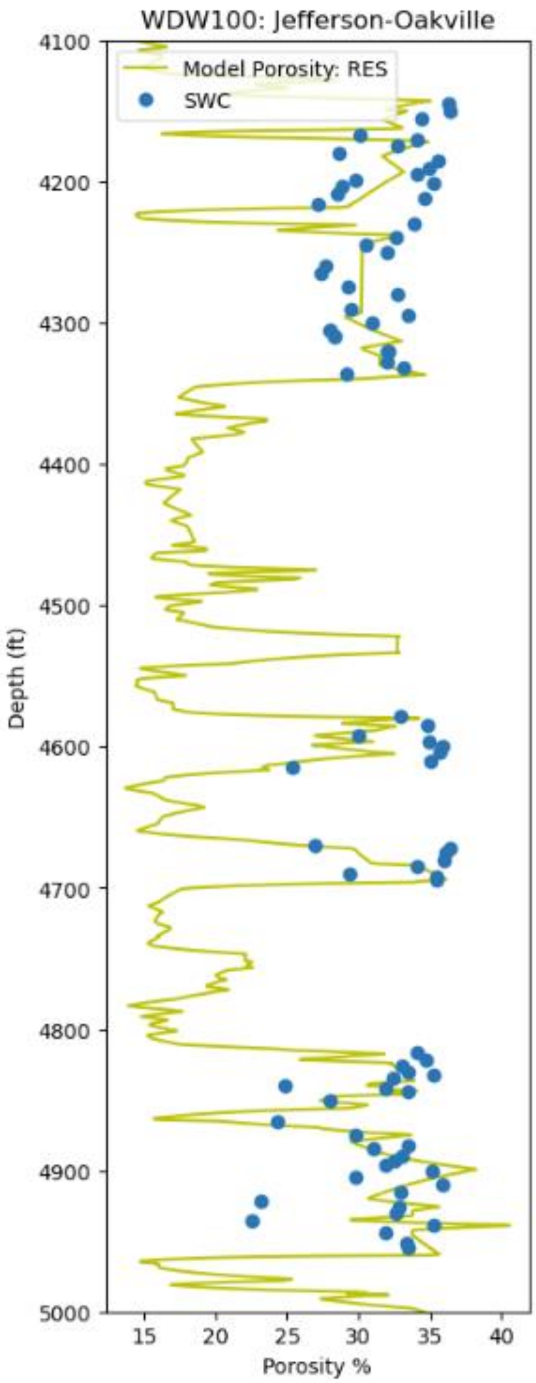
WDW100: Jefferson-Oakville
Model Porosity: RES
SWC
Depth (ft)
Porosity %
4100
4200
4300
4400
4500
4600
4700
4800
4900
5000
15
20
25
30
35
40
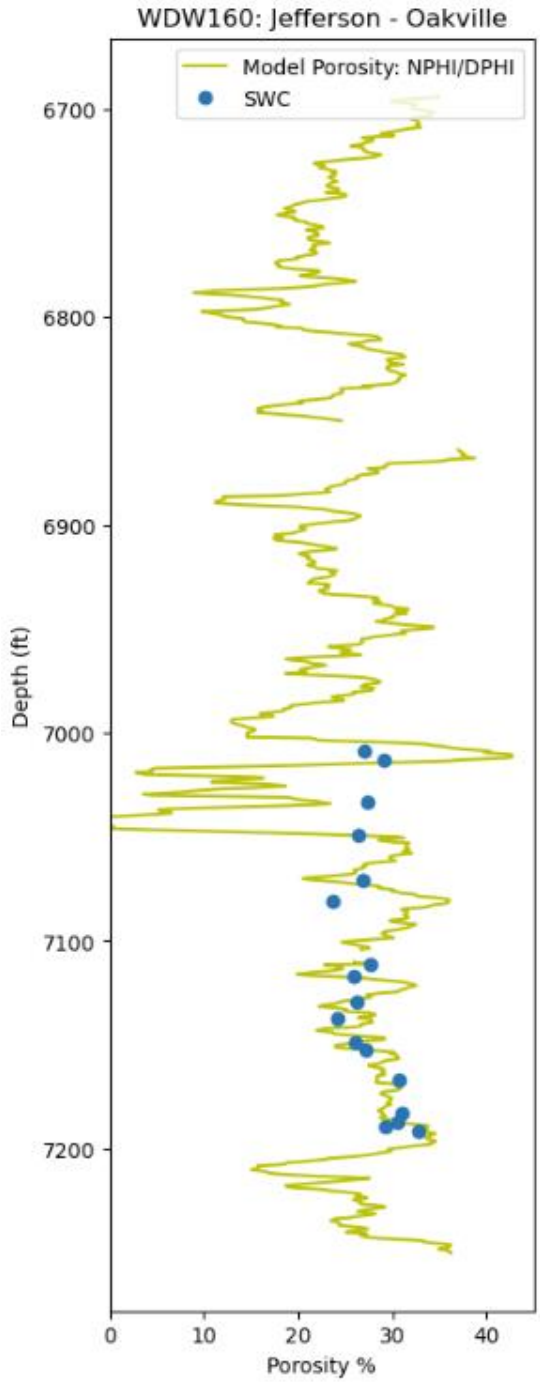
WDW160: Jefferson - Oakville
Model Porosity: NPHI/DPHI
SWC
Depth (ft)
Porosity %
6700
6800
6900
7000
7100
7200
0
10
20
30
40

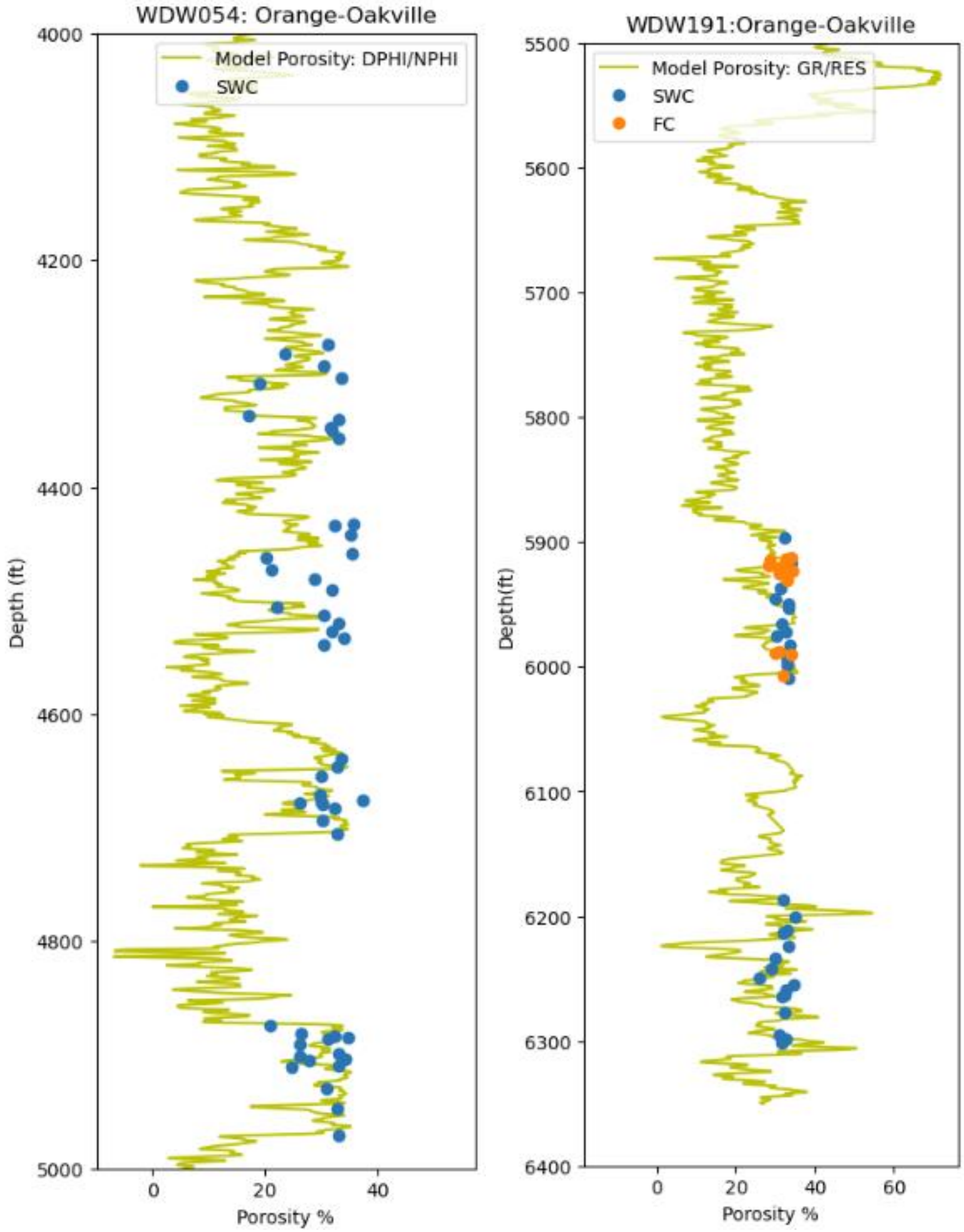

WDW054: Orange-Oakville
Model Porosity: DPHI/NPHI
SWC
Depth (ft)
Porosity %
4000
4200
4400
4600
4800
5000
0
20
40
WDW191:Orange-Oakville
Model Porosity: GR/RES
SWC
FC
Depth(ft)
Porosity %
5500
5600
5700
5800
5900
6000
6100
6200
6300
6400
0
20
40
60

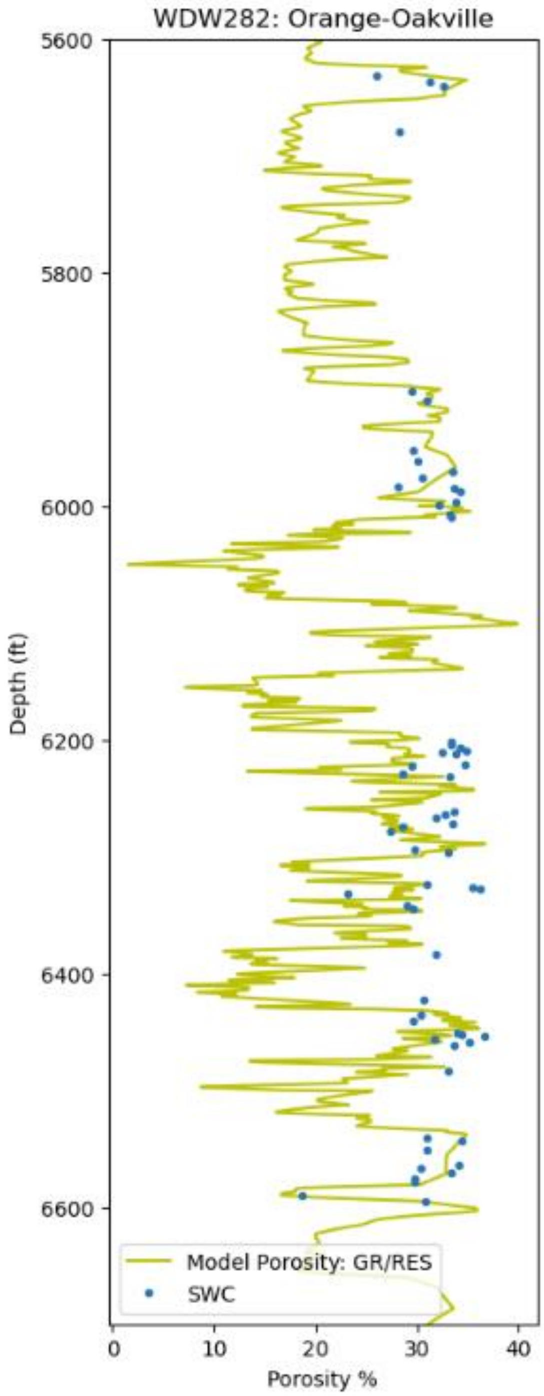
WDW282: Orange-Oakville
Depth (ft)
5600
5800
6000
6200
6400
6600
Model Porosity: GR/RES
SWC
0
10
20
30
40
Porosity %

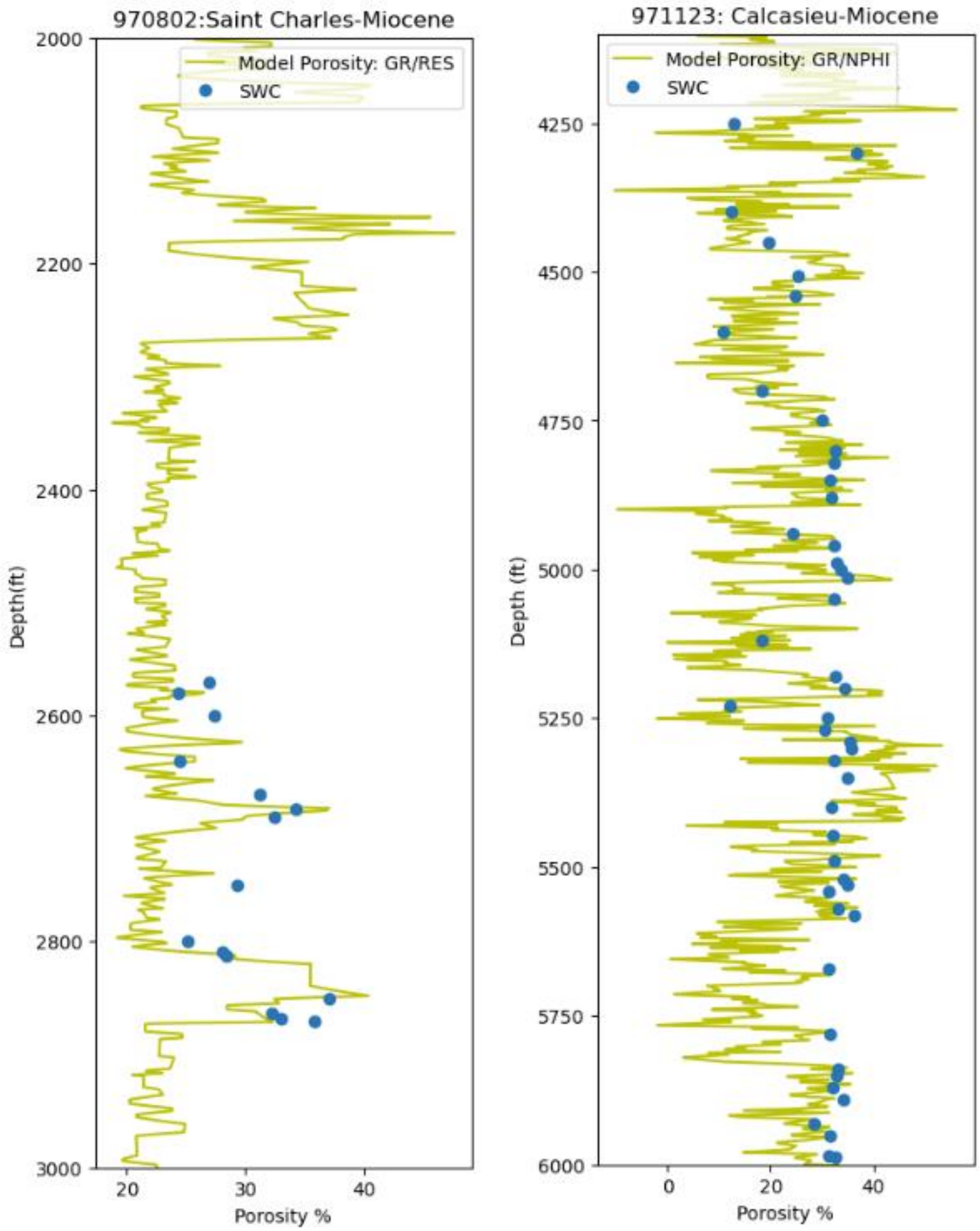
970802:Saint Charles-Miocene
Model Porosity: GR/RES
SWC
Depth(ft)
2000
2200
2400
2600
2800
3000
20
30
40
Porosity %
971123: Calcasieu-Miocene
Model Porosity: GR/NPHI
SWC
Depth (ft)
4250
4500
4750
5000
5250
5500
5750
6000
0
20
40
Porosity %

APPENDIX H: HISTOGRAMS OF PERMEABILITY AT DIFFERENT SCALES

X-axis limits and some Y-axis limits were set at arbitrary values that often excluded the total ranges to better show core and falloff test values.

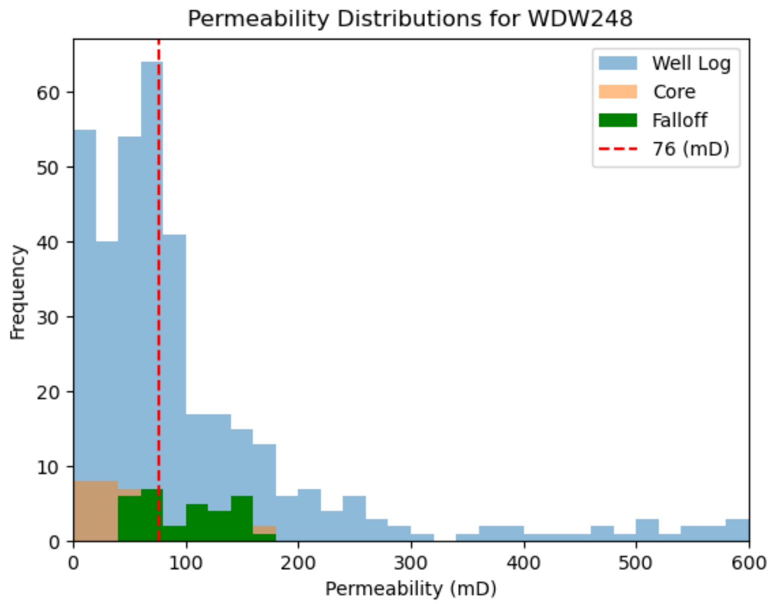

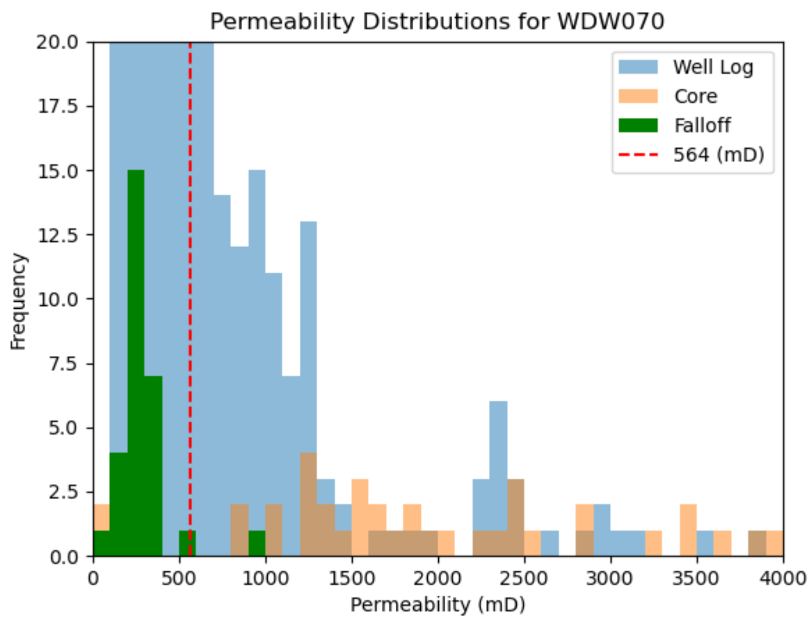

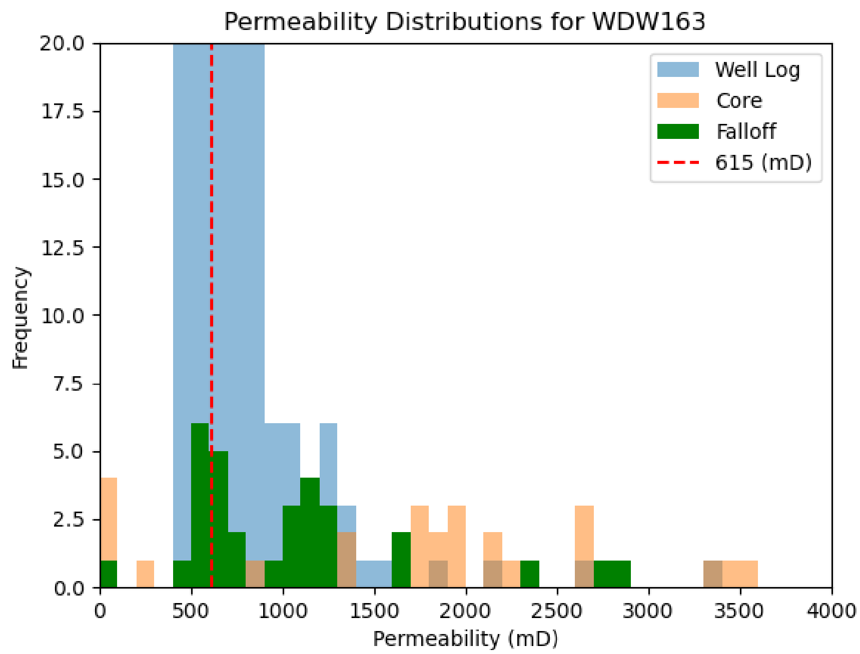
Permeability Distributions for WDW163
Frequency
Permeability (mD)
Well Log
Core
Falloff
615 (mD)
0.0
2.5
5.0
7.5
10.0
12.5
15.0
17.5
20.0
0
500
1000
1500
2000
2500
3000
3500
4000

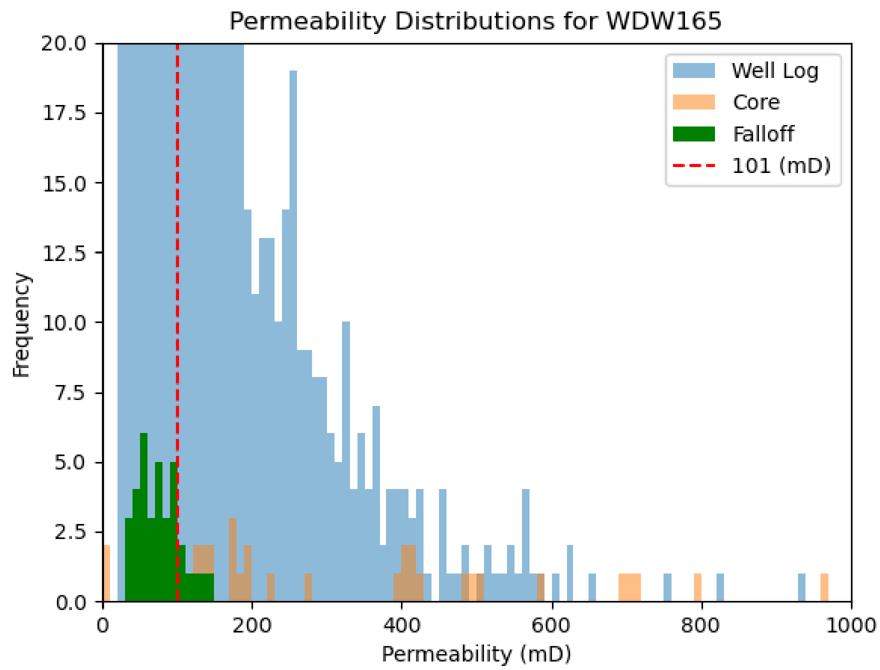
Permeability Distributions for WDW165
Frequency
Permeability (mD)
Well Log
Core
Falloff
101 (mD)
0.0
2.5
5.0
7.5
10.0
12.5
15.0
17.5
20.0
0
200
400
600
800
1000

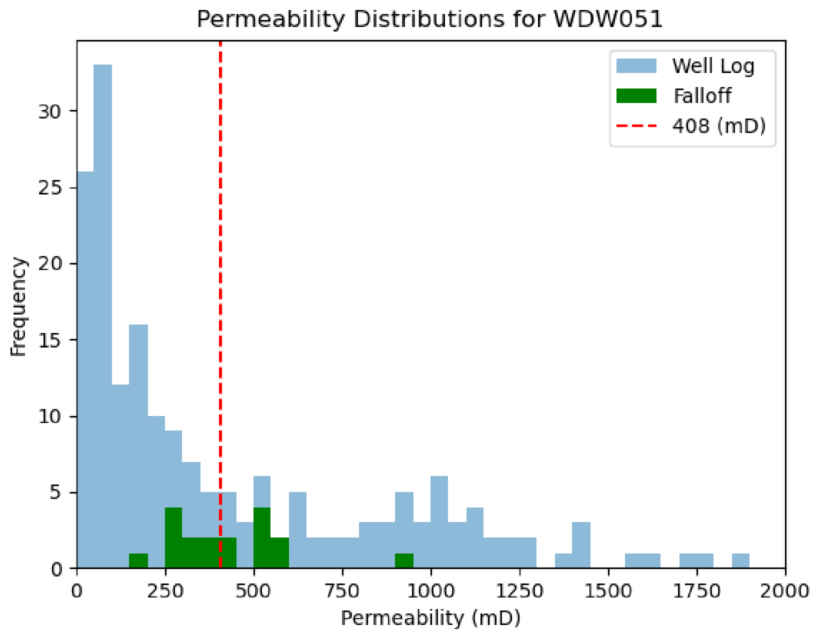

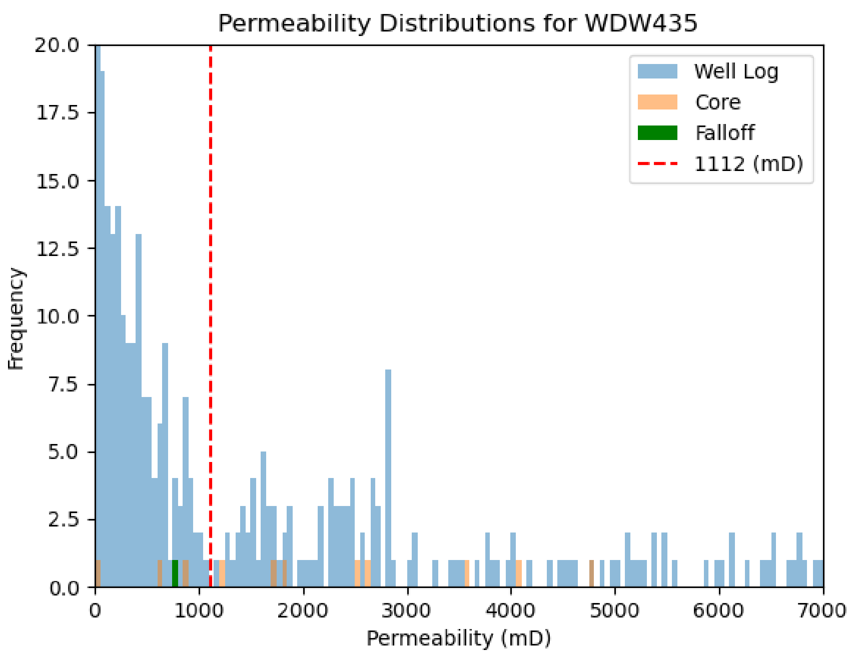

- Only one year for falloff test for WDW435 k=753

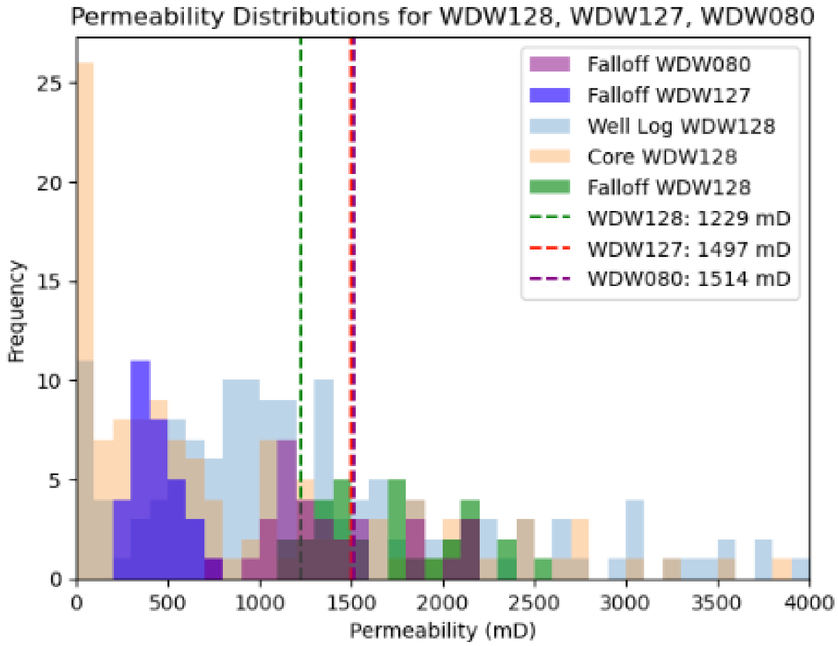

- Only 1 log and 1 core test report were available from WDW128. Upscaling of WDW080 and WDW127 was done from this single log.

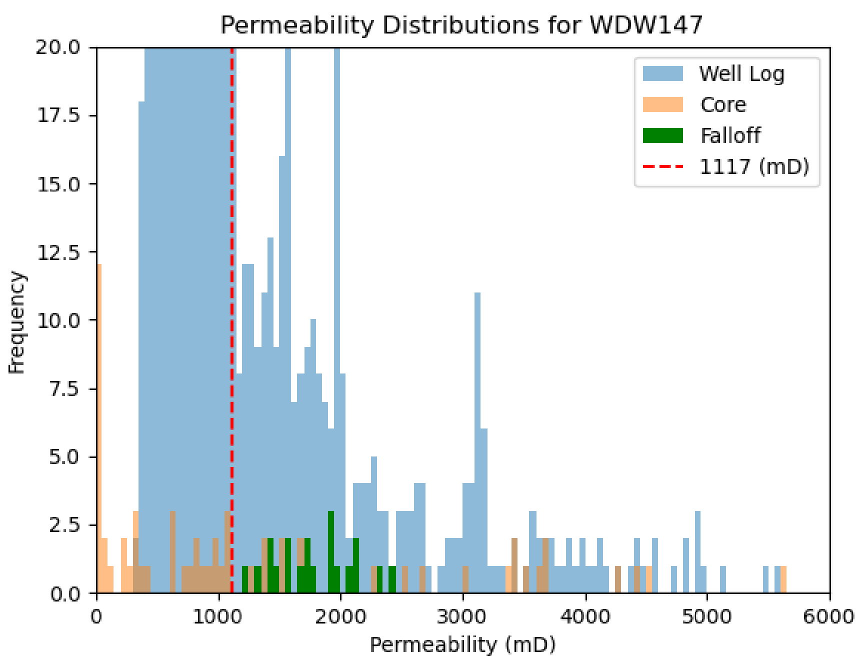

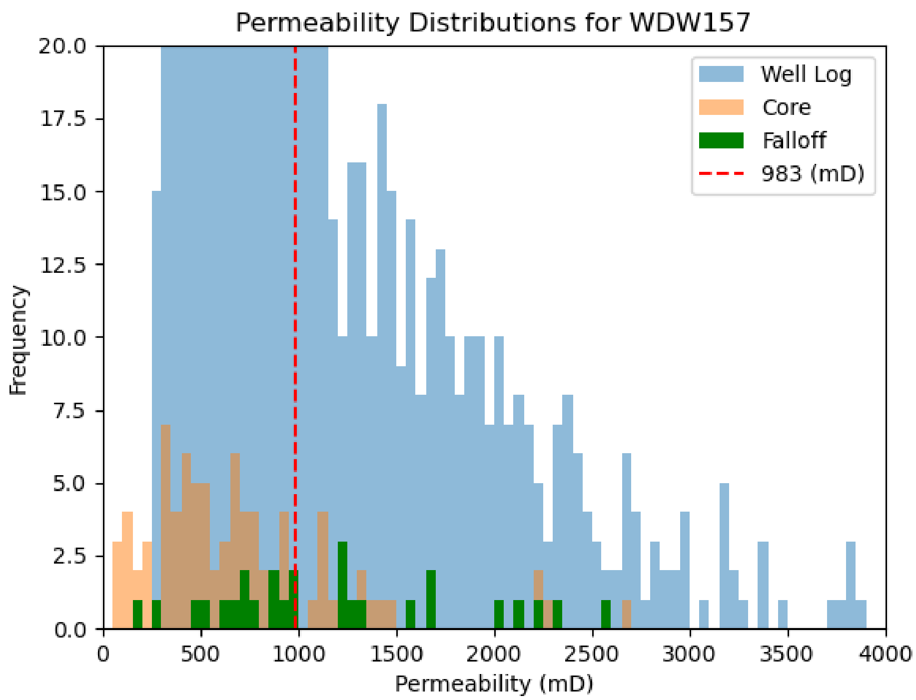
Permeability Distributions for WDW157
Well Log
Core
Falloff
983 (mD)
Frequency
Permeability (mD)
0.0
2.5
5.0
7.5
10.0
12.5
15.0
17.5
20.0
0
500
1000
1500
2000
2500
3000
3500
4000

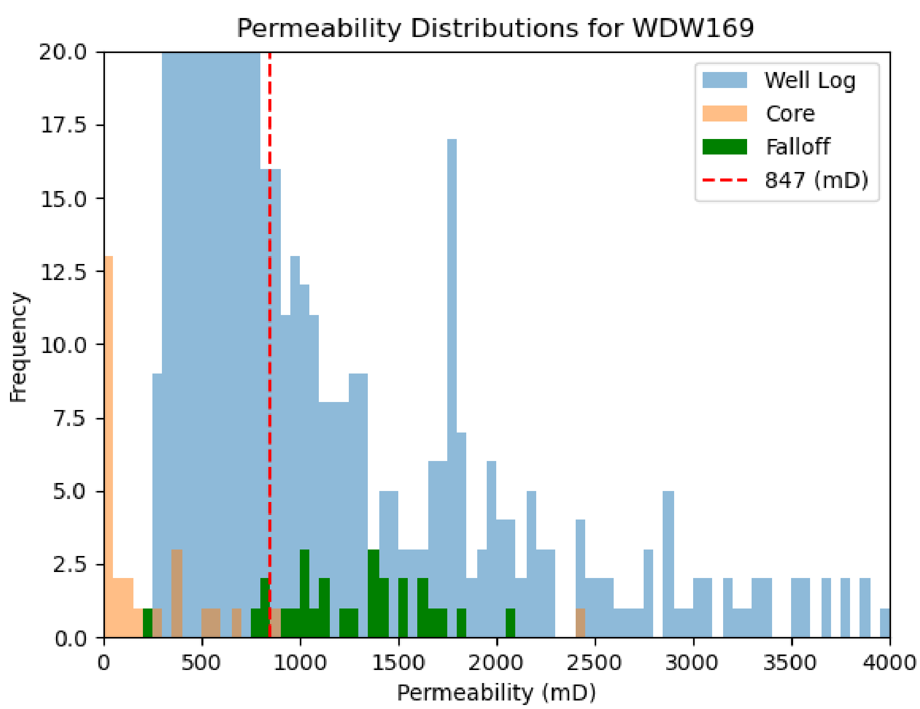
Permeability Distributions for WDW169
Well Log
Core
Falloff
847 (mD)
Frequency
Permeability (mD)
0.0
2.5
5.0
7.5
10.0
12.5
15.0
17.5
20.0
0
500
1000
1500
2000
2500
3000
3500
4000

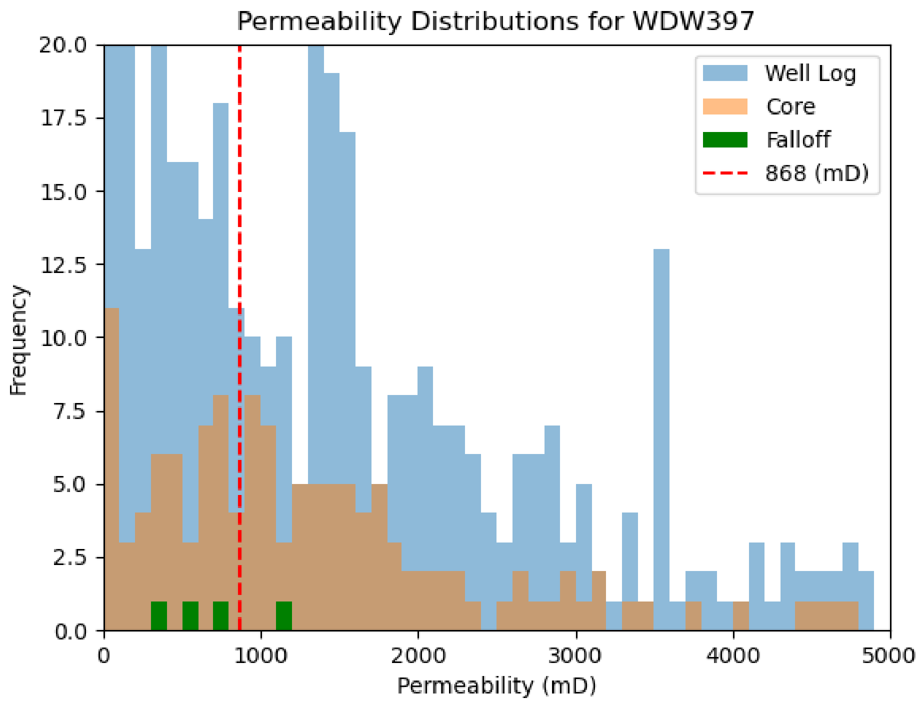
Permeability Distributions for WDW397
Well Log
Core
Falloff
868 (mD)
Frequency
Permeability (mD)
0.0
2.5
5.0
7.5
10.0
12.5
15.0
17.5
20.0
0
1000
2000
3000
4000
5000

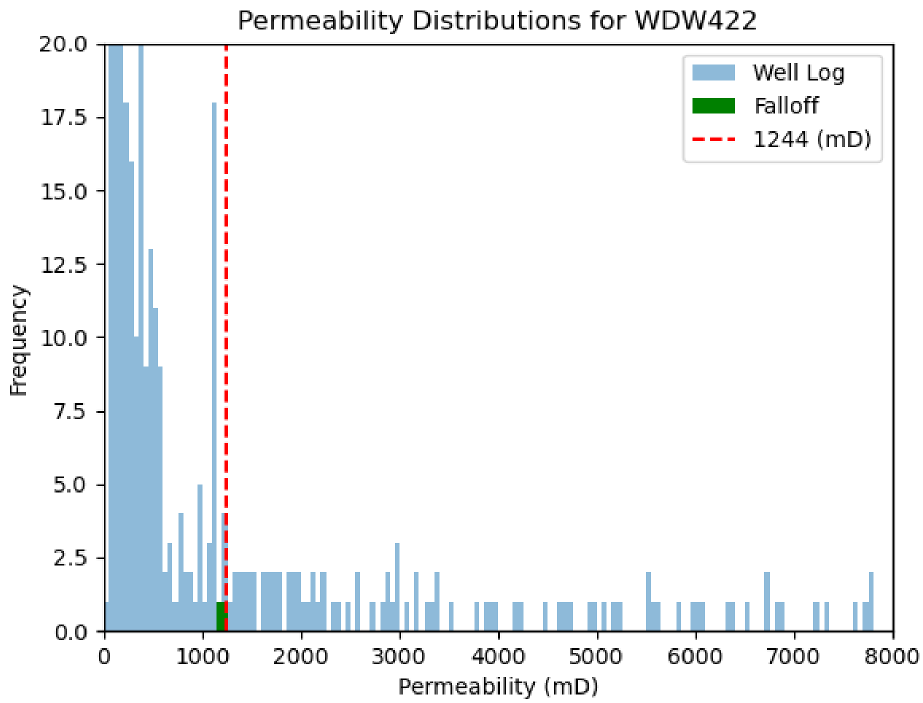
Permeability Distributions for WDW422
Well Log
Falloff
1244 (mD)
Frequency
Permeability (mD)
0.0
2.5
5.0
7.5
10.0
12.5
15.0
17.5
20.0
0
1000
2000
3000
4000
5000
6000
7000
8000

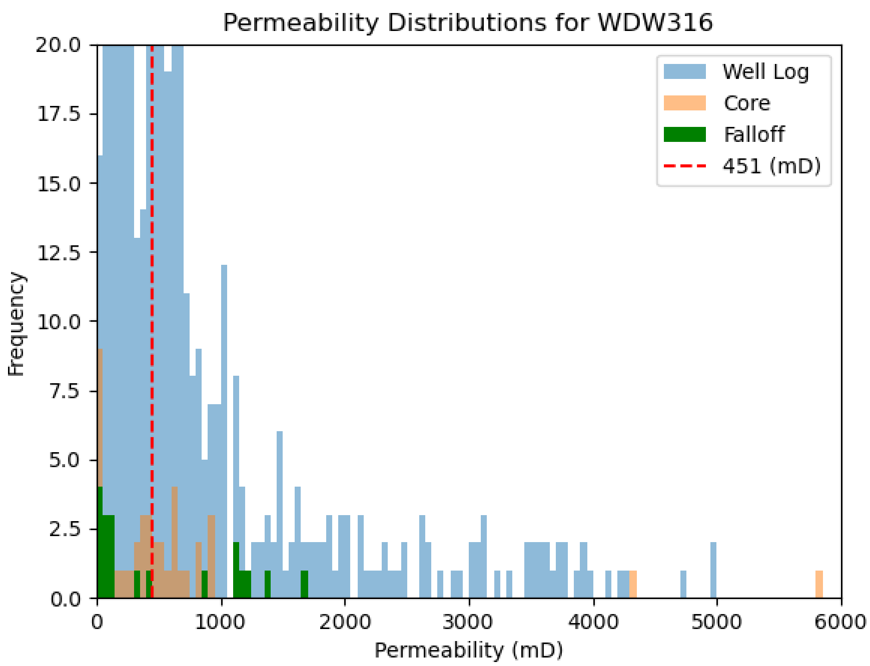
Permeability Distributions for WDW316
Frequency
Permeability (mD)
Well Log
Core
Falloff
451 (mD)
0.0
2.5
5.0
7.5
10.0
12.5
15.0
17.5
20.0
0
1000
2000
3000
4000
5000
6000

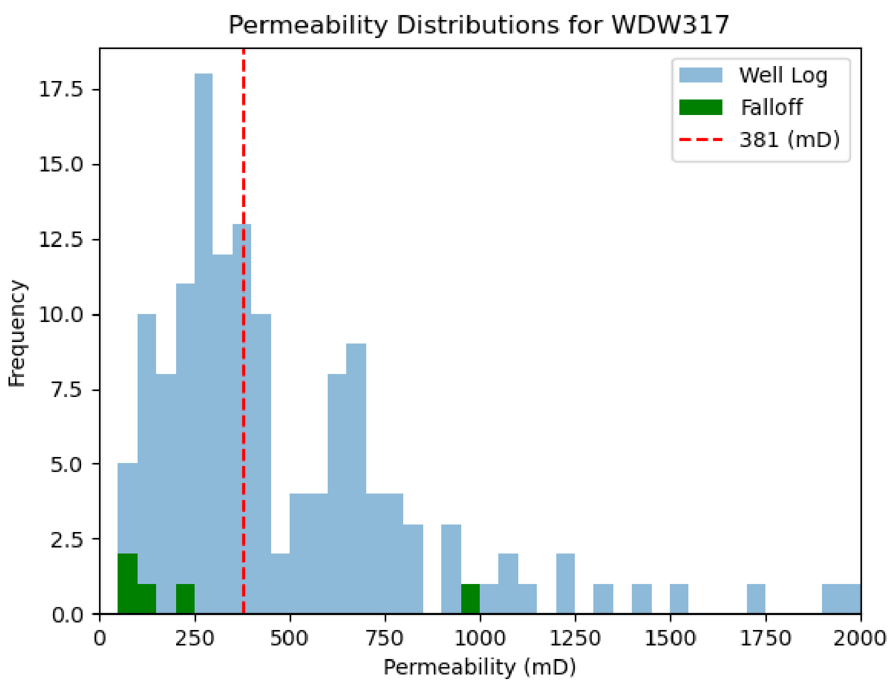
Permeability Distributions for WDW317
Frequency
Permeability (mD)
Well Log
Falloff
381 (mD)
0.0
2.5
5.0
7.5
10.0
12.5
15.0
17.5
0
250
500
750
1000
1250
1500
1750
2000

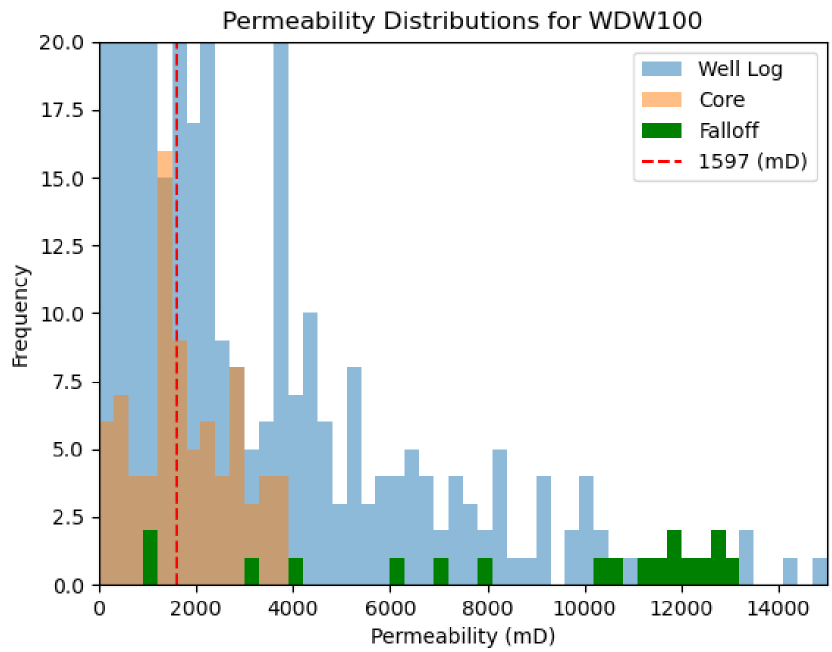
Permeability Distributions for WDW100
Well Log
Core
Falloff
1597 (mD)
Frequency
Permeability (mD)
0.0
2.5
5.0
7.5
10.0
12.5
15.0
17.5
20.0
0
2000
4000
6000
8000
10000
12000
14000

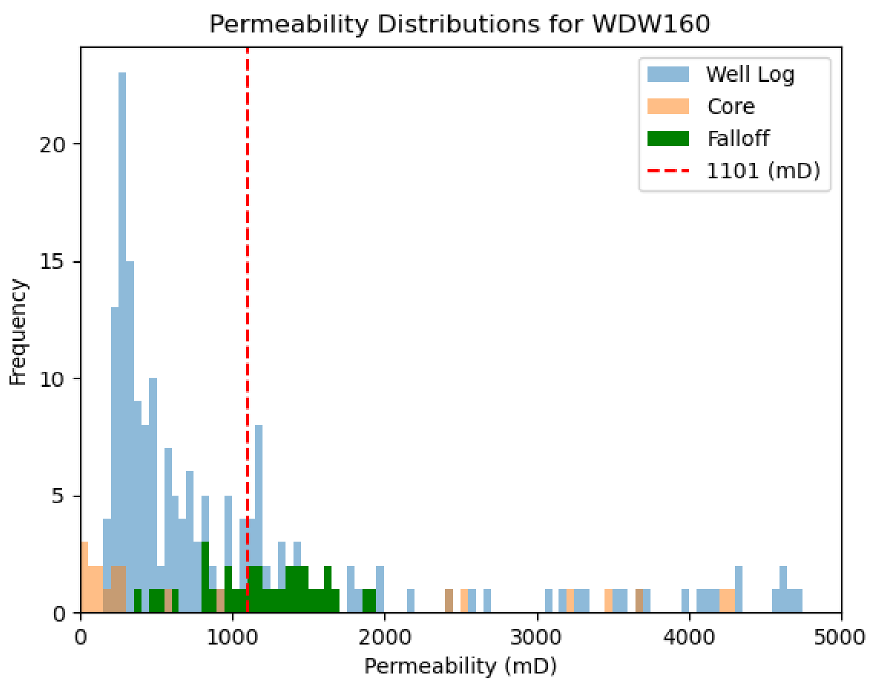
Permeability Distributions for WDW160
Well Log
Core
Falloff
1101 (mD)
Frequency
Permeability (mD)
0
5
10
15
20
0
1000
2000
3000
4000
5000

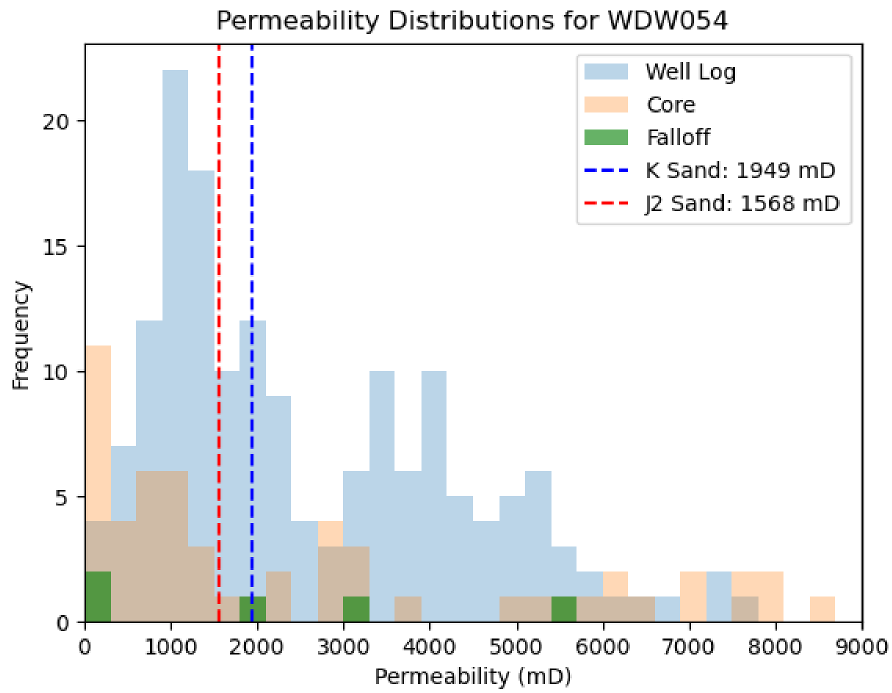
Permeability Distributions for WDW054
Well Log
Core
Falloff
K Sand: 1949 mD
J2 Sand: 1568 mD
Frequency
Permeability (mD)
0
5
10
15
20
0
1000
2000
3000
4000
5000
6000
7000
8000
9000

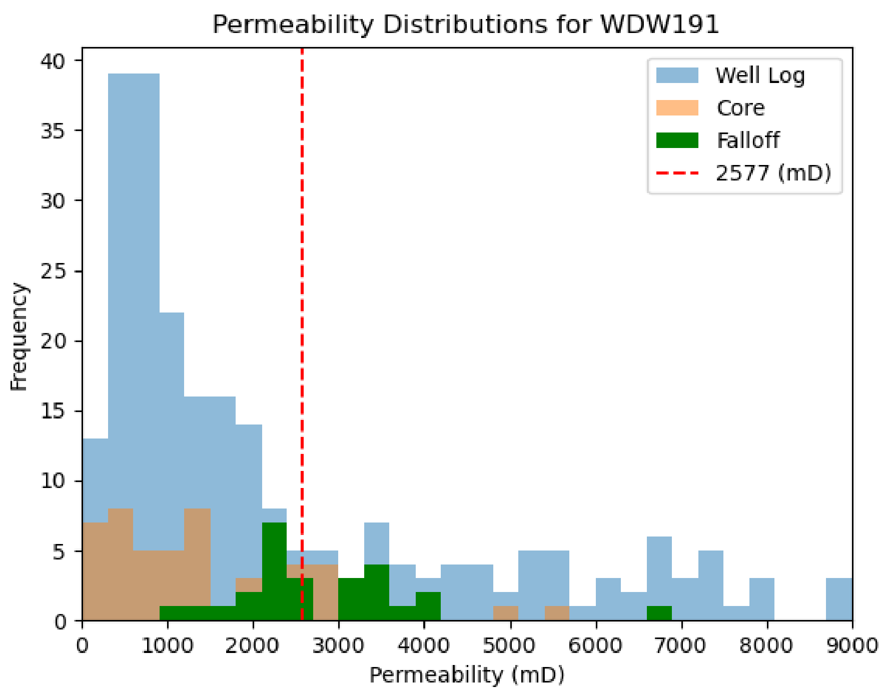
Permeability Distributions for WDW191
Well Log
Core
Falloff
2577 (mD)
Frequency
Permeability (mD)
0
5
10
15
20
25
30
35
40
0
1000
2000
3000
4000
5000
6000
7000
8000
9000

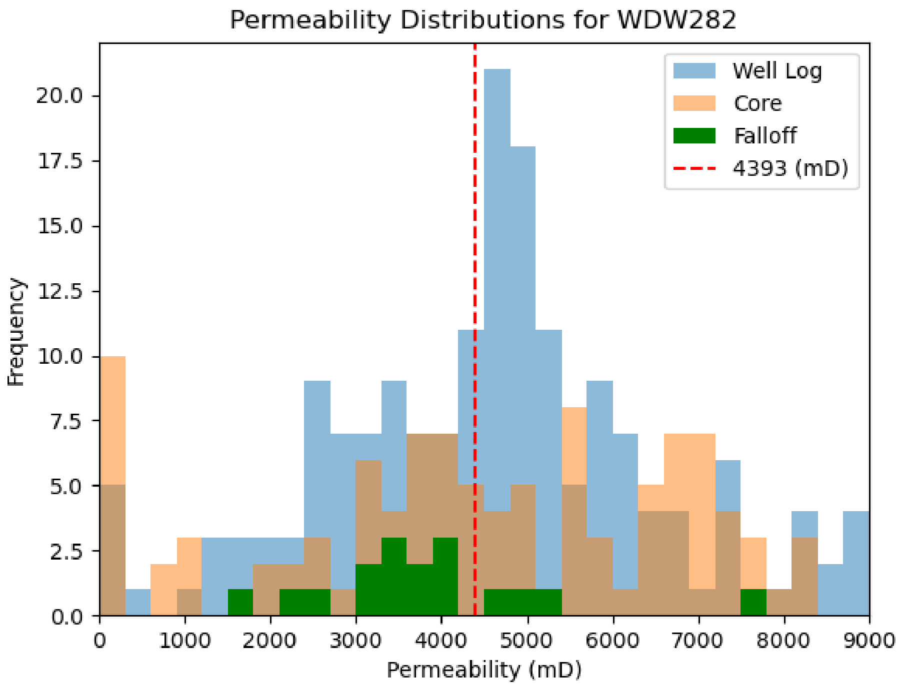

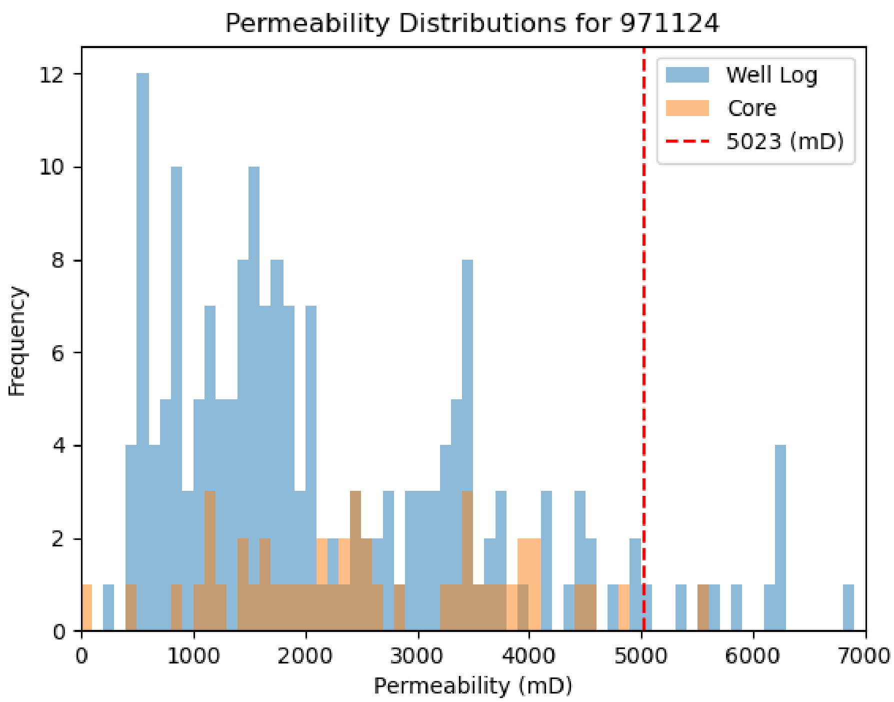

- Falloff test from nearby well came out to 3564 mD

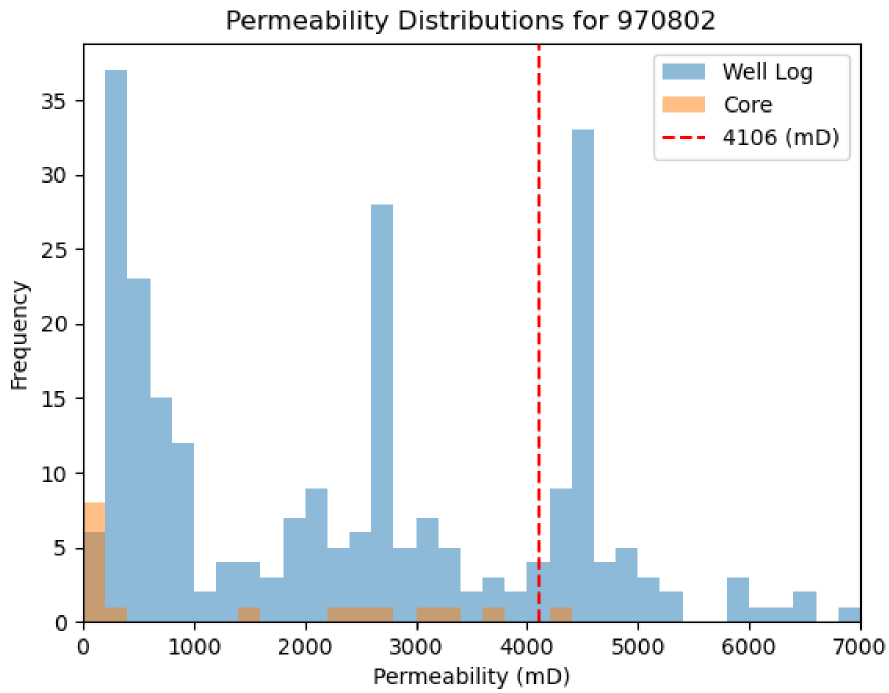

- Falloff test from nearby well came out to 3200 mD

APPENDIX I: PERMEABILITY TABLE

PERMIT NO.	Core-Scale Permeabilities (mD)				Log-Scale Permeabilities (mD)				Geometric Mean (mD)	Field-Scale Permeabilities (mD)			
	std	10%	50%	90%	std	10%	50%	90%		std	10%	50%	90%
WDW248	47	8	48	132	1157	14	74	492	76	38	52	102	151
WDW210										14	24	48	61
WDW211										70	8	50	127
WDW212										14	10	21	44
WDW152	314	5	59	655						49	134	175	273
WDW153	1381	10	255	2610						40	163	195	249
WDW278	675	28	514	1869						116	105	195	289
WDW279											61.4	61.4	61.4
WDW070	1047	845	1695	3495	682	232	519	1295	564	144	151	247	373
WDW105										354	672	740	1320
WDW142										286	656	937	1352
WDW144										173	367	634	821
WDW145										795	776	946	1922
WDW163	2004	265	2122	6196	275	452	571	834	615	633	558	944	1676
WDW164	935	21	232	2460						115	58	157	302
WDW165	383	41	180	795	125	35	100	299	101	28	42	73	116
WDW014										467	496	602	1189
WDW032										141	708	818	969
WDW049										591	484	1417	1498
WDW110										126	885	1050	1133

PERMIT NO.	Core-Scale Permeabilities (mD)				Log-Scale Permeabilities (mD)				Geometric Mean (mD)	Field-Scale Permeabilities (mD)			
WDW051					6311	46	343	4432	408	168	288	398	582
WDW099	545	2	579	1480						326	305	834	1181
WDW408										2146	920	2075	4298
WDW435	2734	622	2175	4790	31450	11	1617	56484	1112	0	753	753	753
WDW436											2950	2950	2950
WDW013										190	378	533	673
WDW359										604	357	664	1438
WDW326	1610	1120	1934	4242									
WDW080					53300	121	1987	11800	1514	372	1041	1280	2004
WDW091	649	30	704	1800						202	155	253	621
WDW127					68391	13	4256	62085	1497	134	261	418	649
WDW128	970	29	552	2250	9374	369	1320	6210	1229	383	1262	1706	2191
WDW196	260	51	169	590						70	192	277	360
WDW314	1134	200	2060	3530						224	87	339	650
WDW034	441	147	643	988									
WDW113	1475	56	810	2480									
WDW114	1474	325	1450	4300									
WDW111										830	166	356	1400
WDW139										127	9	19	190
WDW343	1254	0	333	2820						1284	201	1823	3807
WDW147	1399	22	925	3600	1266	518	1021	2669	1117	330	1409	1756	2164
WDW148	1289	175	1275	3300						1053	853	1604	3043
WDW157	546	190	605	1370	2276	384	938	2430	983	635	480	984	2217
WDW162										682	846	1644	2448
WDW169	529	9	138	1100	1203	379	705	2530	847	388	802	1299	1712

PERMIT NO.	Core-Scale Permeabilities (mD)				Log-Scale Permeabilities (mD)				Geometric Mean (mD)	Field-Scale Permeabilities (mD)			
WDW222	718	244	505	2110						410	280	585	1303
WDW223	3186	403	3200	6740						143	297	584	686
WDW249	679	52	434	1675						458	685	1368	1887
WDW319										232	634	822	1058
WDW397	2068	164	1150	3730	4869	44	1378	7015	868	303	350	611	1161
WDW398	1151	109	1125	2765						180	1225	1403	1580
WDW422					125973	117	596	34706	1244	12	1180	1192	1203
WDW036	949	200	950	2446									
WDW033	239	245	407	656						80	191	271	350
WDW082											851	851	851
WDW083										188	643	915	981
WDW149										663	151	245	1554
WDW122	1720	105	2200	4200						280	390	666	1149
WDW230	1706	950	3000	5300						223	634	1005	1170
WDW316	1381	19	408	920	1112	134	447	2043	451	559	7	124	1399
WDW317					360	146	365	922	381	2175	55	190	6071
WDW100	1036	500	1720	3350	10868	238	1768	8707	1597	4056	987	10873	12660
WDW101										11145	2560	11464	13876
WDW160	1470	42	426	3652	60950	264	710	9096	1101	389	602	1196	1646
WDW302	1016	69	550	2800						173	133	304	475
WDW358	87	40	158	290						209	443	564	1021
WDW188	1587	415	2260	4473									
WDW301	1873	77	2064	5180									
WDW054	2610	5	1250	7000	1734	792	2056	5105	1949	2017	246	2050	5689
WDW055	0	5125	5125	5125						941	762	2048	2083

PERMIT NO.	Core-Scale Permeabilities (mD)				Log-Scale Permeabilities (mD)				Geometric Mean (mD)	Field-Scale Permeabilities (mD)			
WDW056											2572	2572	2572
WDW057										1431	211	1021	1831
WDW191	1175	96	1200	2800	1069002	436	1783	17914	2577	1089	1695	2508	4039
WDW282	2292	767	4472	7200	2470	3002	4488	10203	4950	2980	2214	3837	12520
970904										92	1384	1436	1488
971124										88	3513	3563	3613
971123	1412	8	2195	3718									
971124	1231	1110	2445	4010	83649	821	3360	53881	5023				
975071											4825	4825	4825
975072											6969	6969	6969
975071	2015	0	2565	5000									
975072	1784	0	1933	4545									
974237											6691	6691	6691
974238										323	3237	3420	3603
972060											3200	3200	3200
970802	1512	5	225	3610	684762	373	3891	54270	4106				
972060	2395	1	857	5070									

APPENDIX J: INJECTIVITY VALUES

'Injectivity Index values as measured' is calculated from the gauge readings and measurements and $II = \left|\frac{q}{(P_{wf}-P_{BH})}\right|$ (rate/pressure buildup). 'Injectivity Index values if there were no skin effects' uses the calculated pressure drop due to skin effects found from the falloff test to find a new value where $II = \left|\frac{q}{(P_{wf}-P_{BH}-P_{Skin})}\right|$. The II water (bbl/day/psi) values are directly from the falloff tests. These values are converted to equivalent CO_2 values through simple unit conversions taking into consideration the supercritical density of CO_2 at 700 kg/m^3.

	Injectivity Index where $II = \left\|\frac{q}{(P_{wf}-P_{BH})}\right\|$							Injectivity Index where $II = \left\|\frac{q}{(P_{wf}-P_{BH}-P_{Skin})}\right\|$						
PERMIT NO.		**II water (bbl/day/psi)**			**II CO2 (Mton/yr/MPa)**				**II water (bbl/day/psi)**			**II CO2 (Mton/yr/MPa)**		
Well	**count**	**10%**	**50%**	**90%**	**10%**	**50%**	**90%**	**count**	**10%**	**50%**	**90%**	**10%**	**50%**	**90%**
WDW248	30	3	6	10	0.020	0.039	0.064	29	6	10	16	0.037	0.062	0.107
WDW210	25	4	11	16	0.029	0.070	0.106	25	14	29	35	0.094	0.189	0.230
WDW211	22	3	6	19	0.019	0.039	0.120	22	4	9	24	0.024	0.060	0.153
WDW212	22	5	9	14	0.033	0.057	0.091	22	6	12	23	0.039	0.078	0.148
WDW152	15	15	18	22	0.098	0.117	0.143	15	22	26	36	0.140	0.167	0.237
WDW153	18	10	15	25	0.068	0.096	0.165	18	25	29	38	0.162	0.187	0.246
WDW278	29	1	3	10	0.006	0.021	0.065	26	14	19	25	0.090	0.124	0.161
WDW070	29	4	5	9	0.026	0.032	0.057	29	28	56	76	0.181	0.367	0.492
WDW163	27	6	11	19	0.042	0.069	0.123	27	131	321	563	0.852	2.087	3.658
WDW164	32	5	8	18	0.030	0.054	0.114	32	29	90	162	0.186	0.588	1.052
WDW165	32	5	7	13	0.032	0.045	0.082	32	36	59	82	0.232	0.385	0.530

	Injectivity Index where $II = \left\lvert \frac{q}{(P_{wf} - P_{BH})} \right\rvert$							Injectivity Index where $II = \left\lvert \frac{q}{(P_{wf} - P_{BH} - P_{Skin})} \right\rvert$						
PERMIT NO.		**II water (bbl/day/psi)**			**II CO2 (Mton/yr/MPa)**				**II water (bbl/day/psi)**			**II CO2 (Mton/yr/MPa)**		
Well	**count**	**10%**	**50%**	**90%**	**10%**	**50%**	**90%**	**count**	**10%**	**50%**	**90%**	**10%**	**50%**	**90%**
WDW014	3	23	27	37	0.152	0.175	0.240	3	71	146	150	0.462	0.950	0.978
WDW032	4	10	13	14	0.068	0.085	0.089	4	115	137	154	0.749	0.890	0.999
WDW049	5	8	15	21	0.050	0.099	0.138	5	46	124	140	0.300	0.806	0.907
WDW110	5	20	36	52	0.131	0.233	0.339	5	163	191	216	1.057	1.244	1.401
WDW051	17	6	18	40	0.040	0.116	0.257	17	41	103	172	0.269	0.672	1.120
WDW099	13	10	20	69	0.068	0.132	0.451	13	346	643	975	2.248	4.179	6.339
WDW408	1	21	21	21	0.138	0.138	0.138	1	184	184	184	1.197	1.197	1.197
WDW435	1	227	227	227	1.473	1.473	1.473	1	396	396	396	2.571	2.571	2.571
WDW436	1	506	506	506	3.288	3.288	3.288	1	640	640	640	4.159	4.159	4.159
WDW013	27	54	84	104	0.354	0.544	0.673	27	157	217	315	1.023	1.411	2.045
WDW080	31	17	34	62	0.109	0.219	0.402	31	154	178	270	0.999	1.157	1.758
WDW091	11	11	13	19	0.070	0.081	0.124	11	18	21	32	0.115	0.136	0.211
WDW127	32	29	39	56	0.187	0.251	0.366	32	38	59	101	0.249	0.381	0.657
WDW128	31	20	41	106	0.129	0.268	0.686	31	250	297	377	1.624	1.930	2.447
WDW196	12	14	19	29	0.089	0.123	0.187	12	19	26	36	0.122	0.169	0.232
WDW314	10	10	28	46	0.064	0.179	0.296	10	24	72	113	0.154	0.468	0.734
WDW148	19	68	102	167	0.444	0.662	1.083	19	201	402	646	1.309	2.610	4.200
WDW157	27	3	6	16	0.021	0.037	0.104	27	102	235	402	0.665	1.529	2.615
WDW162	19	40	75	228	0.260	0.489	1.480	15	238	315	487	1.545	2.050	3.163
WDW169	27	6	17	43	0.039	0.110	0.279	27	62	185	322	0.405	1.205	2.093
WDW249	22	3	9	25	0.022	0.062	0.162	22	87	123	289	0.564	0.798	1.877
WDW319	1	70	70	70	0.456	0.456	0.456	1	219	219	219	1.421	1.421	1.421
WDW422	2	35	40	46	0.225	0.261	0.296	2	170	183	197	1.102	1.192	1.282

	Injectivity Index where $II = \left\lvert\frac{q}{(P_{wf}-P_{BH})}\right\rvert$							Injectivity Index where $II = \left\lvert\frac{q}{(P_{wf}-P_{BH}-P_{Skin})}\right\rvert$						
PERMIT NO.		II water (bbl/day/psi)			II CO2 (Mton/yr/MPa)				II water (bbl/day/psi)			II CO2 (Mton/yr/MPa)		
Well	count	10%	50%	90%	10%	50%	90%	count	10%	50%	90%	10%	50%	90%
WDW033	1	8	8	8	0.055	0.055	0.055	1	7	7	7	0.047	0.047	0.047
WDW082	1	9	9	9	0.059	0.059	0.059	1	93	93	93	0.602	0.602	0.602
WDW083	31	7	12	17	0.046	0.076	0.110	31	41	62	75	0.265	0.406	0.487
WDW149	18	5	16	93	0.035	0.105	0.607	18	24	42	251	0.159	0.270	1.628
WDW122	1	17	17	17	0.112	0.112	0.112	1	180	180	180	1.168	1.168	1.168
WDW230	1	16	16	16	0.104	0.104	0.104	1	88	88	88	0.573	0.573	0.573
WDW316	20	1	2	30	0.007	0.010	0.198	18	2	23	314	0.014	0.148	2.039
WDW317	6	1	2	8	0.008	0.012	0.049	5	18	35	149	0.116	0.225	0.970
WDW100	16	22	28	43	0.143	0.182	0.282	15	489	894	969	3.175	5.810	6.297
WDW101	6	21	26	73	0.138	0.170	0.477	4	233	533	834	1.514	3.461	5.421
WDW160	32	10	40	67	0.063	0.262	0.436	32	41	83	250	0.265	0.541	1.628
WDW302	2	9	14	18	0.056	0.088	0.120	1	18	18	18	0.120	0.120	0.120
WDW358	6	25	37	39	0.165	0.239	0.254	6	40	48	72	0.261	0.310	0.465
WDW054	5	2	3	33	0.011	0.020	0.212	5	17	39	498	0.113	0.256	3.240
WDW055	2	3	9	15	0.021	0.058	0.096	2	17	35	54	0.113	0.230	0.348
WDW191	26	21	38	62	0.136	0.250	0.400	25	353	515	775	2.296	3.350	5.034
WDW282	19	31	47	54	0.203	0.308	0.350	19	656	1008	3096	4.263	6.553	20.118
970904	2	2	2	2	0.011	0.012	0.013	2	290	310	329	1.888	2.012	2.136
971124	2	64	70	77	0.415	0.458	0.501	2	317	321	326	2.057	2.087	2.116
975072	1	364	364	364	2.365	2.365	2.365	1	1494	1494	1494	9.711	9.711	9.711
974237	1	8	8	8	0.054	0.054	0.054	1	1710	1710	1710	11.115	11.115	11.115
974238	2	101	106	112	0.655	0.692	0.728	1	858	858	858	5.578	5.578	5.578

APPENDIX K: INJECTIVITY AND SKIN

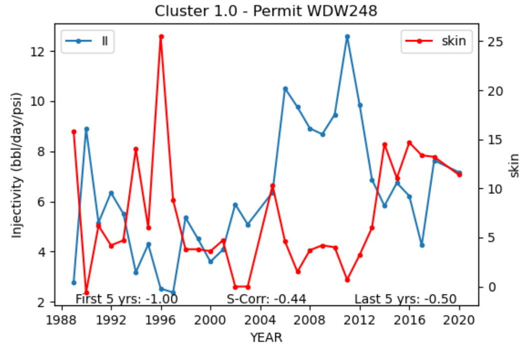

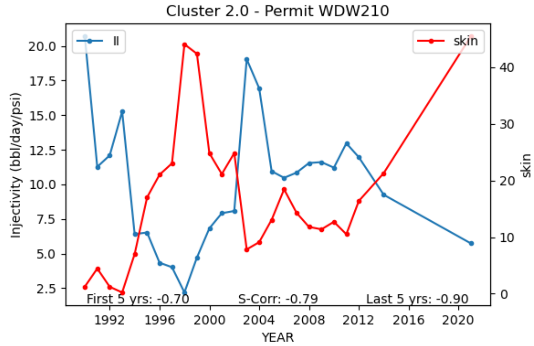

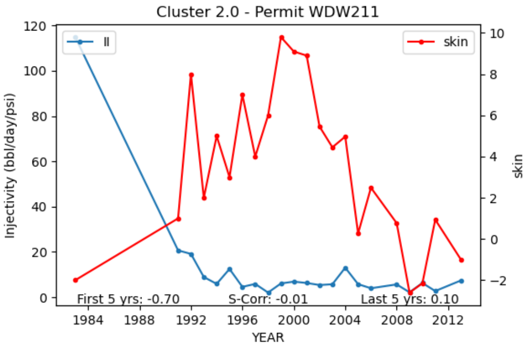

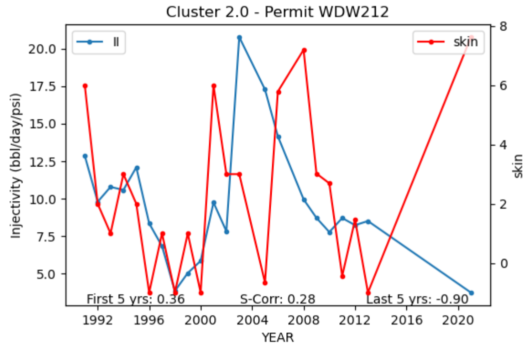

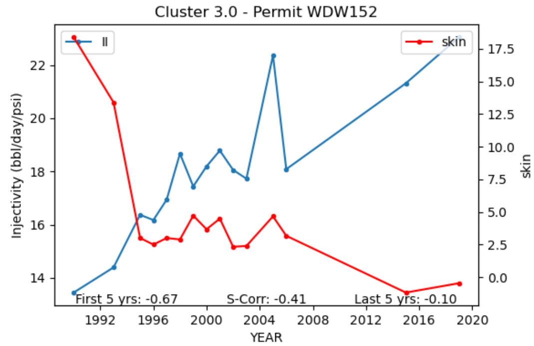

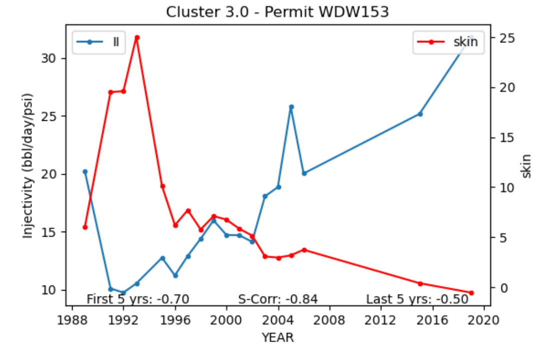

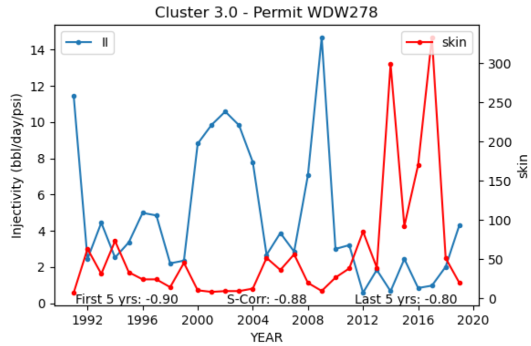

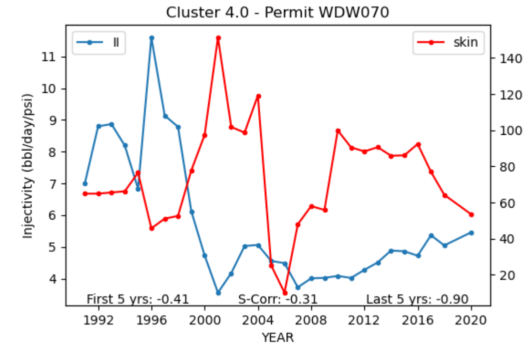

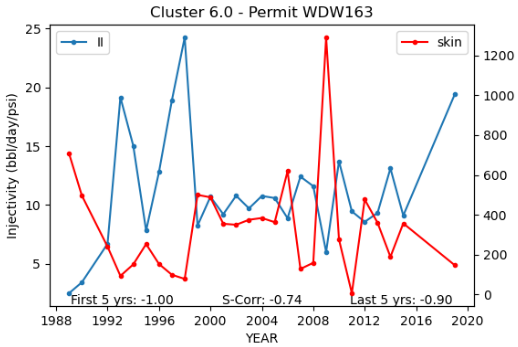
Cluster 6.0 - Permit WDW163
II
skin
Injectivity (bbl/day/psi)
skin
YEAR
First 5 yrs: -1.00
S-Corr: -0.74
Last 5 yrs: -0.90

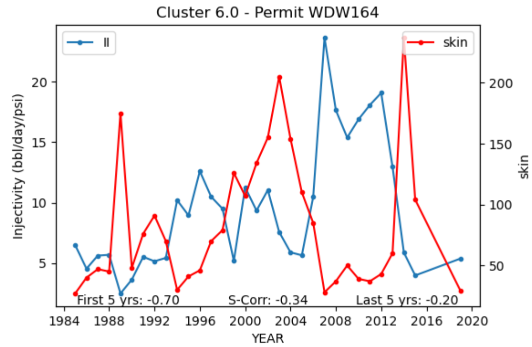
Cluster 6.0 - Permit WDW164
II
skin
Injectivity (bbl/day/psi)
skin
YEAR
First 5 yrs: -0.70
S-Corr: -0.34
Last 5 yrs: -0.20

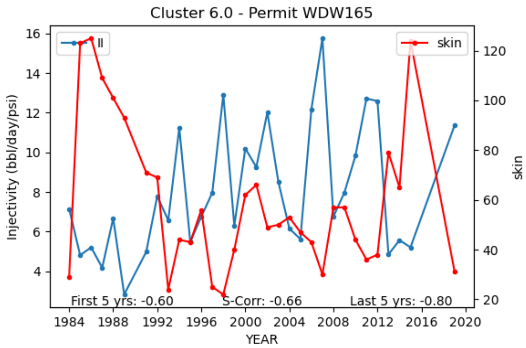
Cluster 6.0 - Permit WDW165
II
skin
Injectivity (bbl/day/psi)
skin
YEAR
First 5 yrs: -0.60
S-Corr: -0.66
Last 5 yrs: -0.80

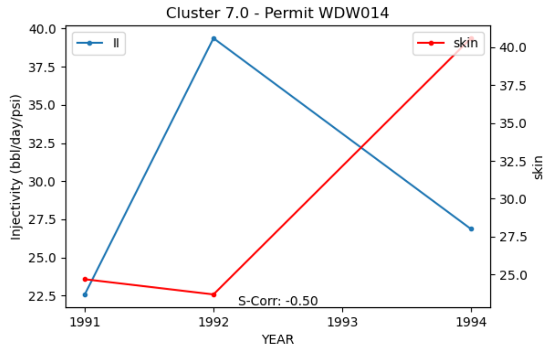
Cluster 7.0 - Permit WDW014
II
skin
Injectivity (bbl/day/psi)
skin
YEAR
S-Corr: -0.50

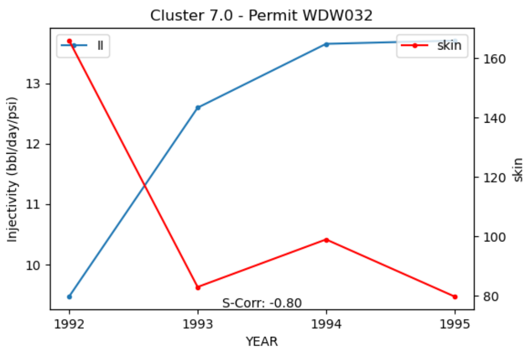
Cluster 7.0 - Permit WDW032
II
skin
Injectivity (bbl/day/psi)
skin
YEAR
S-Corr: -0.80

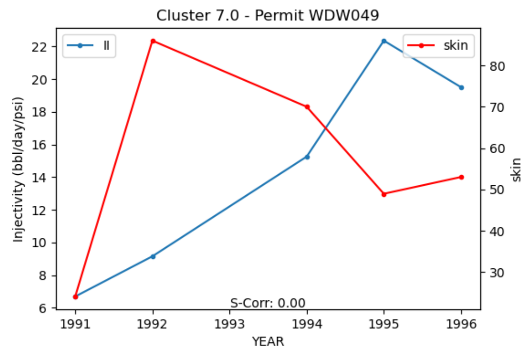
Cluster 7.0 - Permit WDW049
II
skin
Injectivity (bbl/day/psi)
skin
YEAR
S-Corr: 0.00

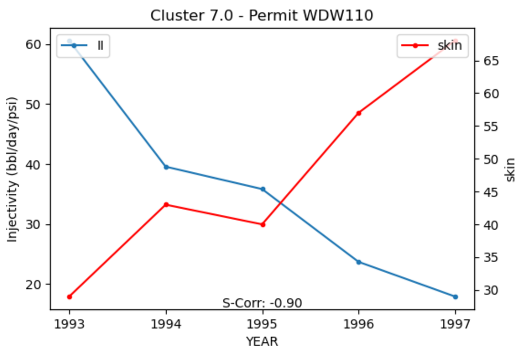
Cluster 7.0 - Permit WDW110
II
skin
Injectivity (bbl/day/psi)
skin
YEAR
S-Corr: -0.90

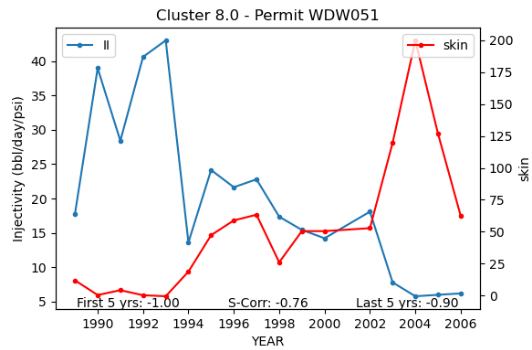
Cluster 8.0 - Permit WDW051
II
skin
Injectivity (bbl/day/psi)
skin
YEAR
First 5 yrs: -1.00
S-Corr: -0.76
Last 5 yrs: -0.90

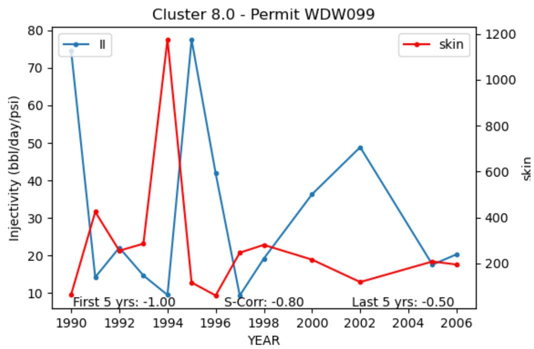
Cluster 8.0 - Permit WDW099
ll
skin
Injectivity (bbl/day/psi)
skin
YEAR
First 5 yrs: -1.00
S-Corr: -0.80
Last 5 yrs: -0.50

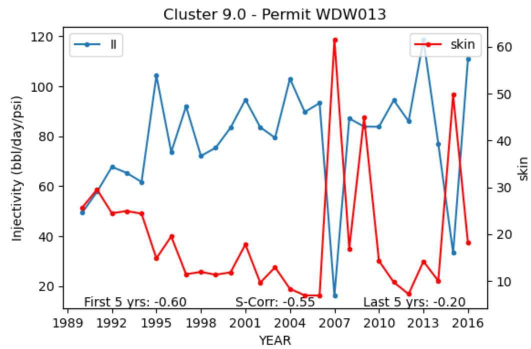
Cluster 9.0 - Permit WDW013
ll
skin
Injectivity (bbl/day/psi)
skin
YEAR
First 5 yrs: -0.60
S-Corr: -0.55
Last 5 yrs: -0.20

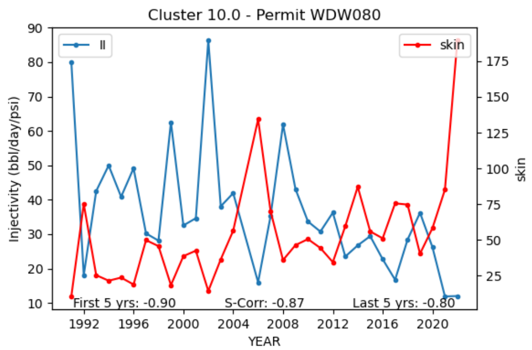
Cluster 10.0 - Permit WDW080
ll
skin
Injectivity (bbl/day/psi)
skin
YEAR
First 5 yrs: -0.90
S-Corr: -0.87
Last 5 yrs: -0.80

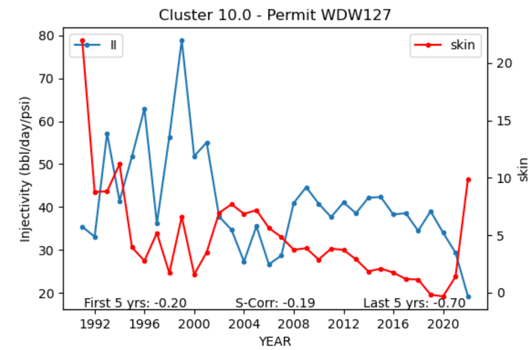
Cluster 10.0 - Permit WDW127
ll
skin
Injectivity (bbl/day/psi)
skin
YEAR
First 5 yrs: -0.20
S-Corr: -0.19
Last 5 yrs: -0.70

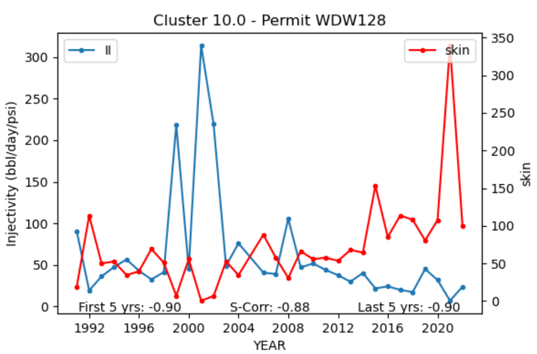
Cluster 10.0 - Permit WDW128
ll
skin
Injectivity (bbl/day/psi)
skin
YEAR
First 5 yrs: -0.90
S-Corr: -0.88
Last 5 yrs: -0.90

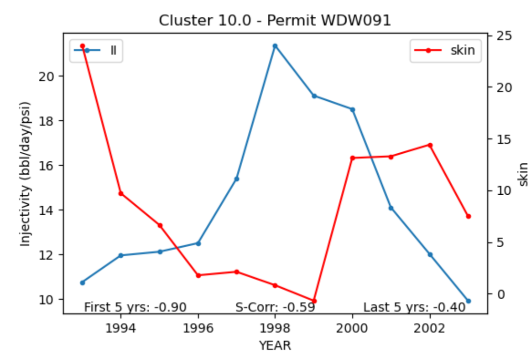
Cluster 10.0 - Permit WDW091
ll
skin
Injectivity (bbl/day/psi)
skin
YEAR
First 5 yrs: -0.90
S-Corr: -0.59
Last 5 yrs: -0.40

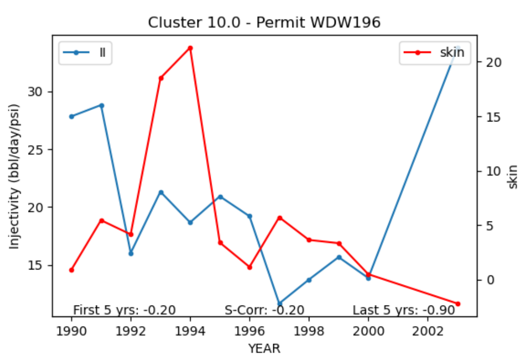
Cluster 10.0 - Permit WDW196
ll
skin
Injectivity (bbl/day/psi)
skin
YEAR
First 5 yrs: -0.20
S-Corr: -0.20
Last 5 yrs: -0.90

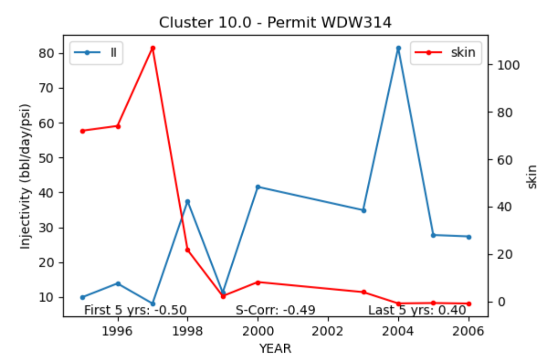
Cluster 10.0 - Permit WDW314
ll
skin
Injectivity (bbl/day/psi)
skin
YEAR
First 5 yrs: -0.50
S-Corr: -0.49
Last 5 yrs: 0.40

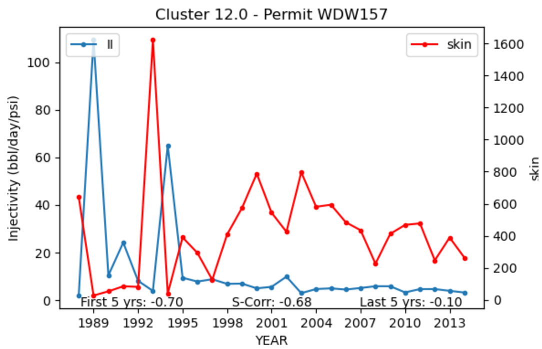
Cluster 12.0 - Permit WDW157
ll
skin
Injectivity (bbl/day/psi)
skin
First 5 yrs: -0.70
S-Corr: -0.68
Last 5 yrs: -0.10
YEAR

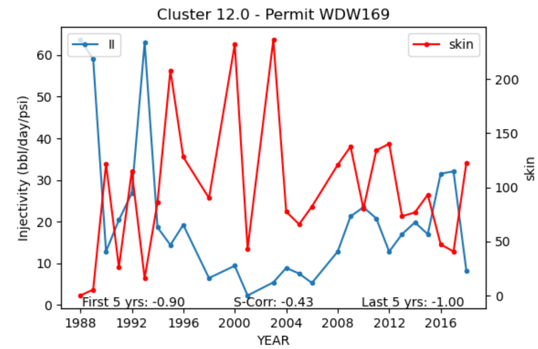
Cluster 12.0 - Permit WDW169
ll
skin
Injectivity (bbl/day/psi)
skin
First 5 yrs: -0.90
S-Corr: -0.43
Last 5 yrs: -1.00
YEAR

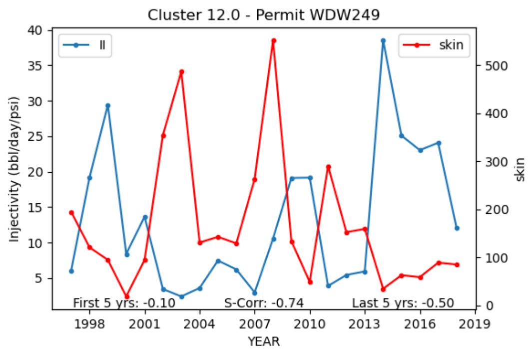
Cluster 12.0 - Permit WDW249
ll
skin
Injectivity (bbl/day/psi)
skin
First 5 yrs: -0.10
S-Corr: -0.74
Last 5 yrs: -0.50
YEAR

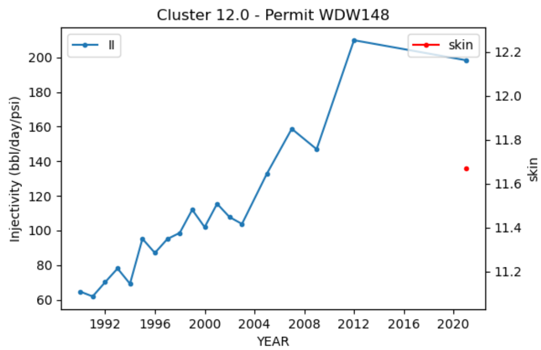
Cluster 12.0 - Permit WDW148
ll
skin
Injectivity (bbl/day/psi)
skin
YEAR

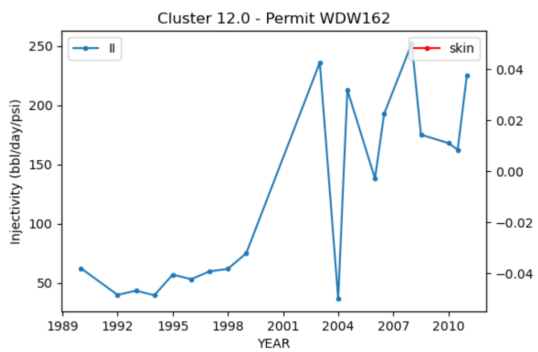
Cluster 12.0 - Permit WDW162
ll
skin
Injectivity (bbl/day/psi)
YEAR

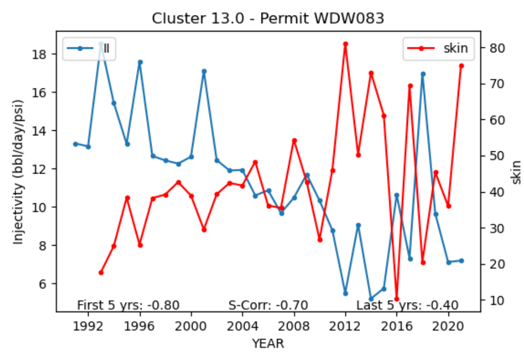
Cluster 13.0 - Permit WDW083
ll
skin
Injectivity (bbl/day/psi)
skin
First 5 yrs: -0.80
S-Corr: -0.70
Last 5 yrs: -0.40
YEAR

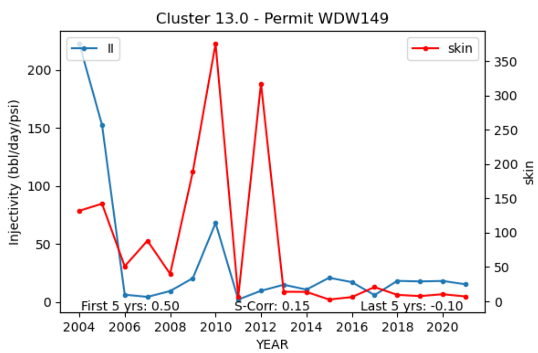
Cluster 13.0 - Permit WDW149
ll
skin
Injectivity (bbl/day/psi)
skin
First 5 yrs: 0.50
S-Corr: 0.15
Last 5 yrs: -0.10
YEAR

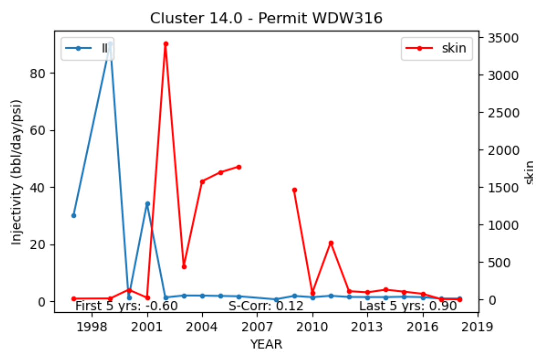
Cluster 14.0 - Permit WDW316
ll
skin
Injectivity (bbl/day/psi)
skin
First 5 yrs: -0.60
S-Corr: 0.12
Last 5 yrs: 0.90
YEAR

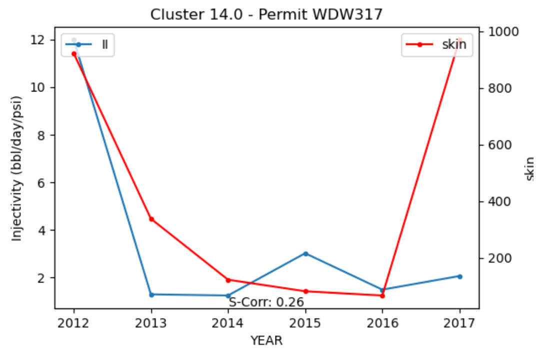
Cluster 14.0 - Permit WDW317
Injectivity (bbl/day/psi)
skin
II
skin
S-Corr: 0.26
YEAR

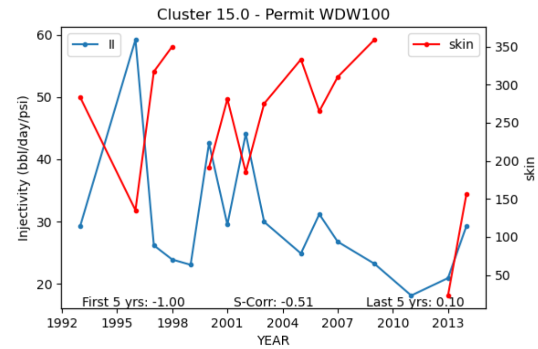
Cluster 15.0 - Permit WDW100
Injectivity (bbl/day/psi)
skin
II
skin
First 5 yrs: -1.00
S-Corr: -0.51
Last 5 yrs: 0.10
YEAR

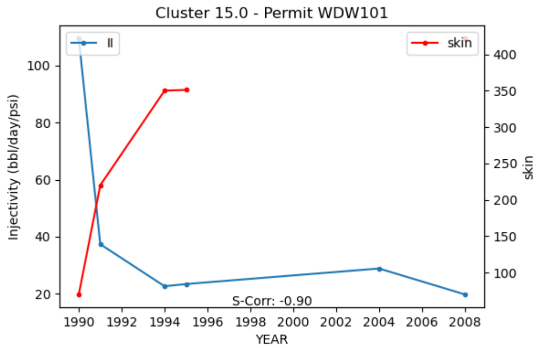
Cluster 15.0 - Permit WDW101
Injectivity (bbl/day/psi)
skin
II
skin
S-Corr: -0.90
YEAR

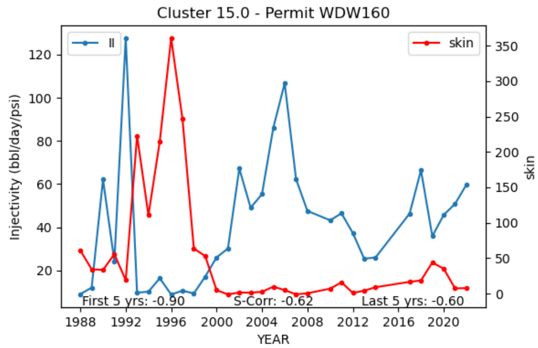
Cluster 15.0 - Permit WDW160
Injectivity (bbl/day/psi)
skin
II
skin
First 5 yrs: -0.90
S-Corr: -0.62
Last 5 yrs: -0.60
YEAR

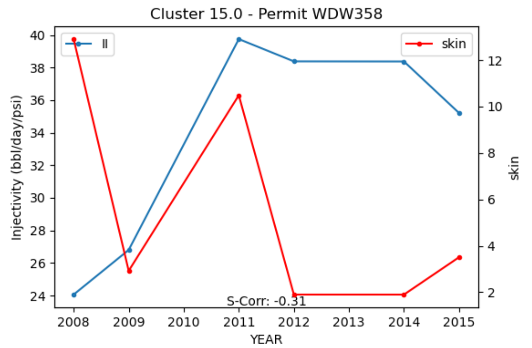
Cluster 15.0 - Permit WDW358
Injectivity (bbl/day/psi)
skin
II
skin
S-Corr: -0.31
YEAR

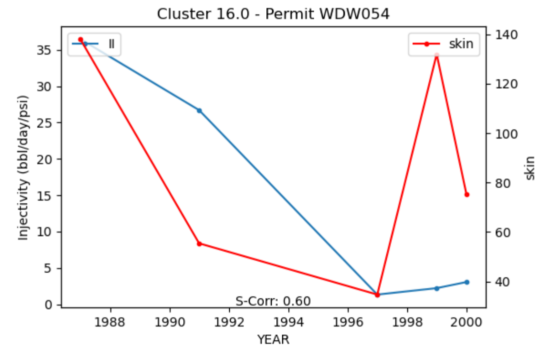
Cluster 16.0 - Permit WDW054
Injectivity (bbl/day/psi)
skin
II
skin
S-Corr: 0.60
YEAR

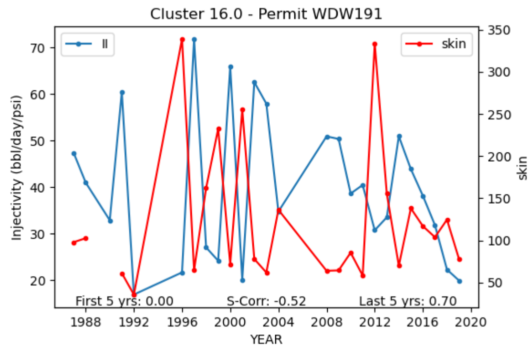
Cluster 16.0 - Permit WDW191
Injectivity (bbl/day/psi)
skin
II
skin
First 5 yrs: 0.00
S-Corr: -0.52
Last 5 yrs: 0.70
YEAR

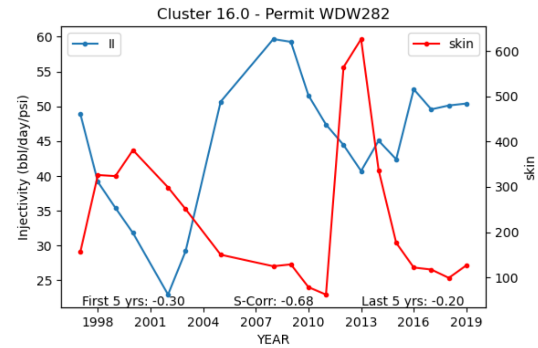
Cluster 16.0 - Permit WDW282
Injectivity (bbl/day/psi)
skin
II
skin
First 5 yrs: -0.30
S-Corr: -0.68
Last 5 yrs: -0.20
YEAR

APPENDIX L: INJECTIVITY RELATIONSHIP TO PERMEABILITY-THICKNESS

The following plots correlate the injectivity index to permeability-thickness to find an approximate linear relationship. II on the y-axis is based off the pressure differential which accounts for the pressure drop due to skin effects where $II = \left|\frac{q}{(P_{wf}-P_{BH}-P_{Skin})}\right|$. The II value of bbl/day/psi from the falloff tests are converted to ton $_{CO2}$/yr/MPa assuming a 700 kg/m^3 supercritical density. The points are colored by which well the data came from and the II value derived from $II = \left|\frac{q}{(P_{wf}-P_{BH})}\right|$ are labeled 'II with skin' showing in many cases, the II value with skin effects tends to constant regardless of increasing *kh.* Estimations of II made from some permeability-thickness from these relationships would be highly optimistic and more representative of the first few years of injection where there are little to no skin effects.

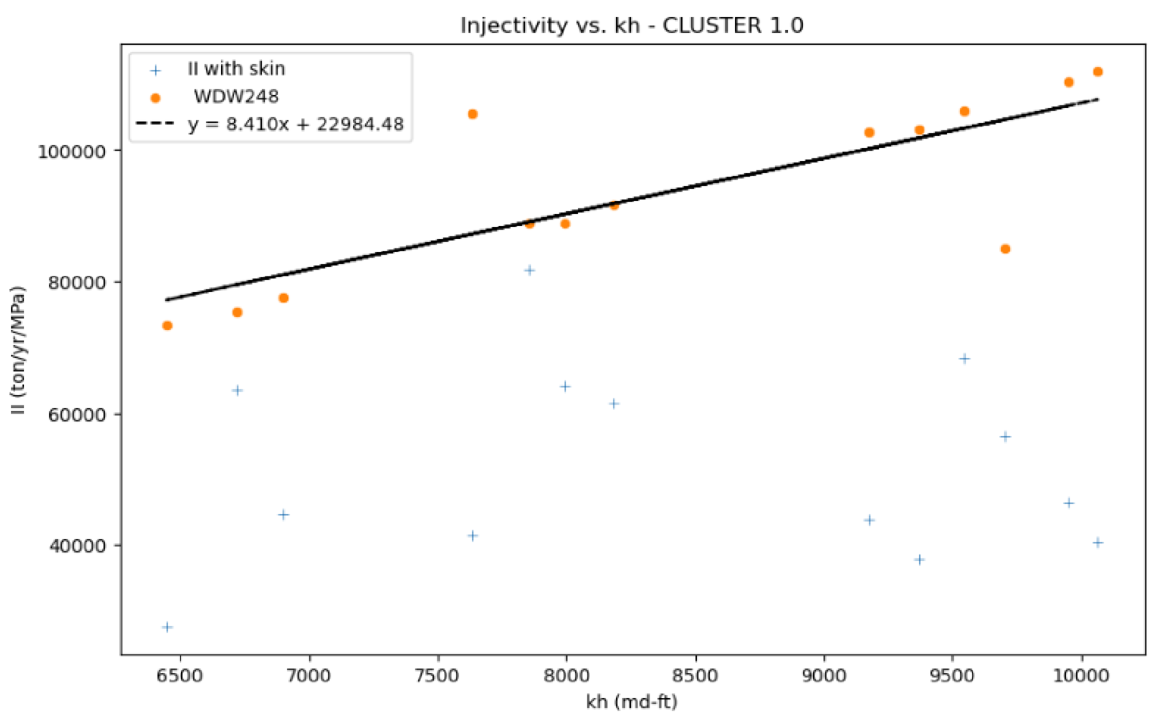

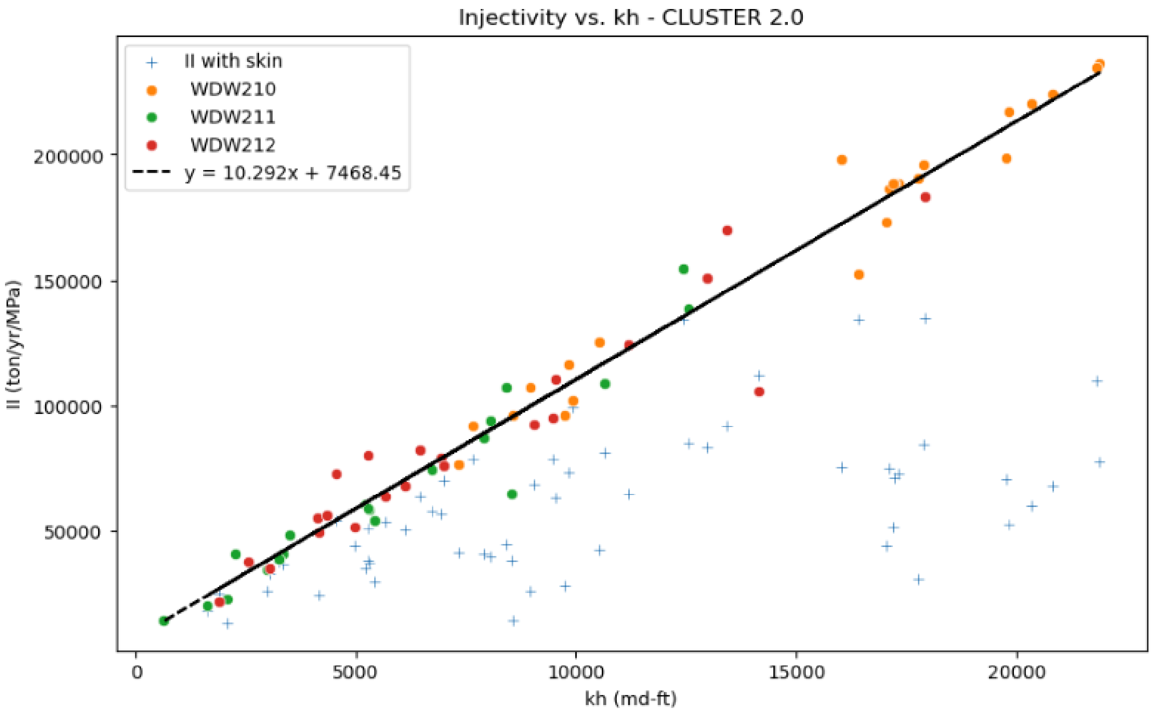

Injectivity vs. kh - CLUSTER 2.0
II with skin
WDW210
WDW211
WDW212
y = 10.292x + 7468.45
II (ton/yr/MPa)
kh (md-ft)

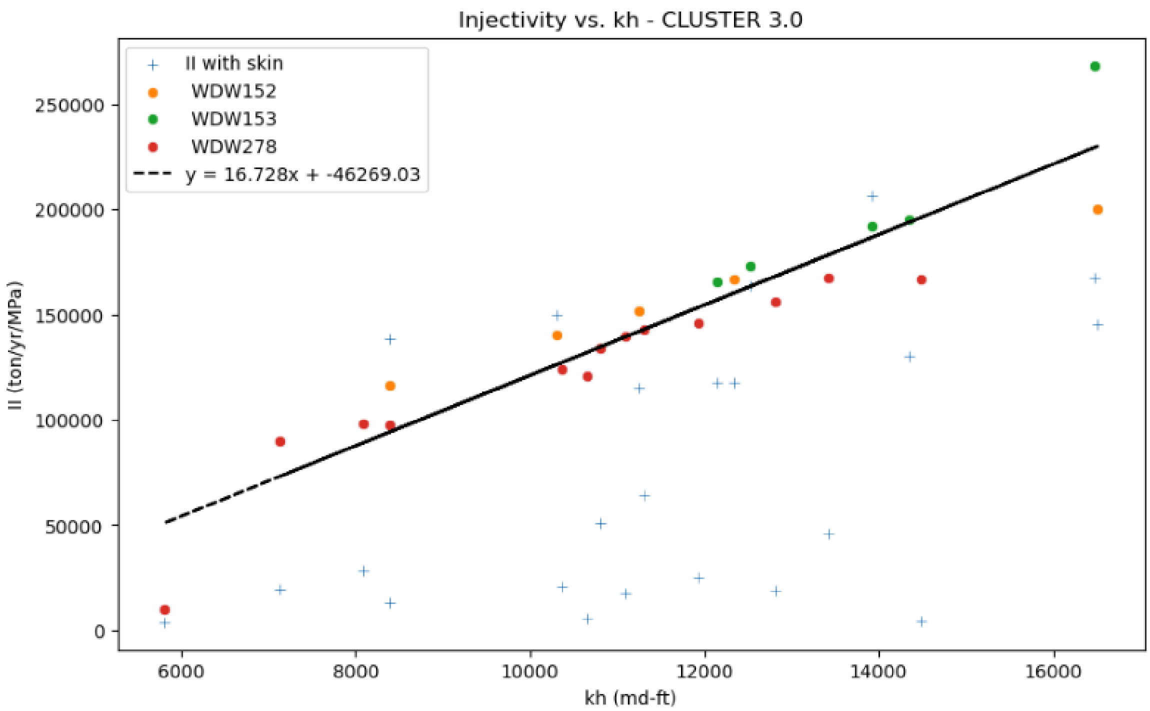

Injectivity vs. kh - CLUSTER 3.0
II with skin
WDW152
WDW153
WDW278
y = 16.728x + -46269.03
II (ton/yr/MPa)
kh (md-ft)

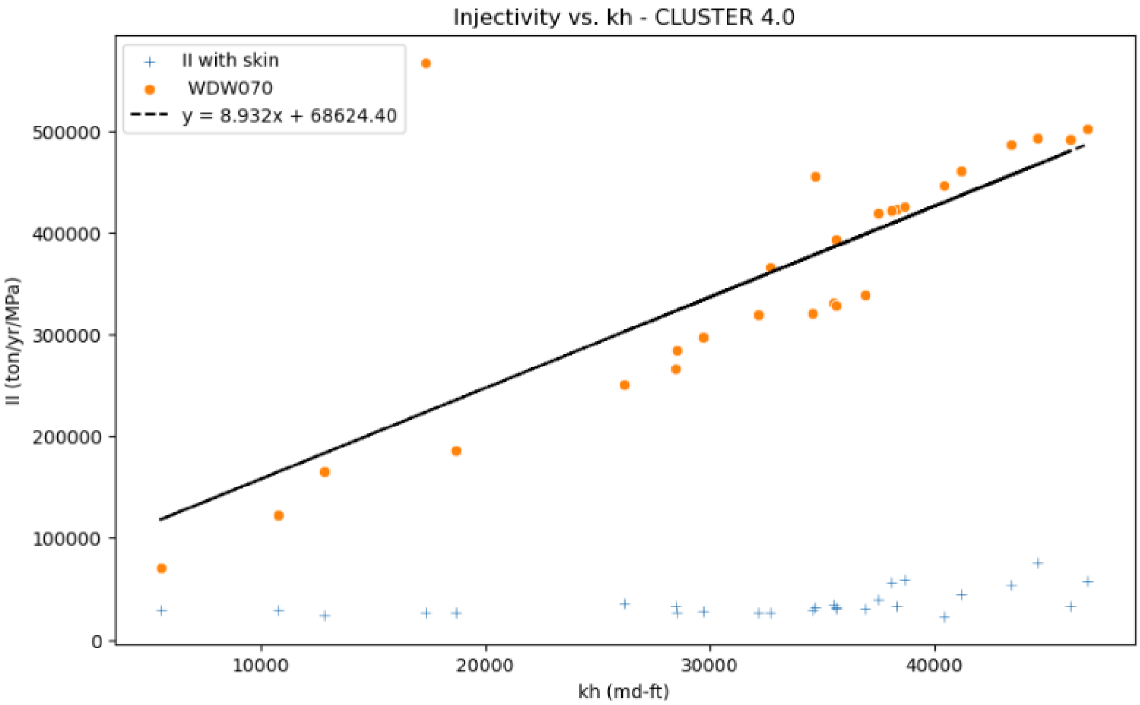
Injectivity vs. kh - CLUSTER 4.0
II with skin
WDW070
y = 8.932x + 68624.40
II (ton/yr/MPa)
kh (md-ft)
0
100000
200000
300000
400000
500000
10000
20000
30000
40000

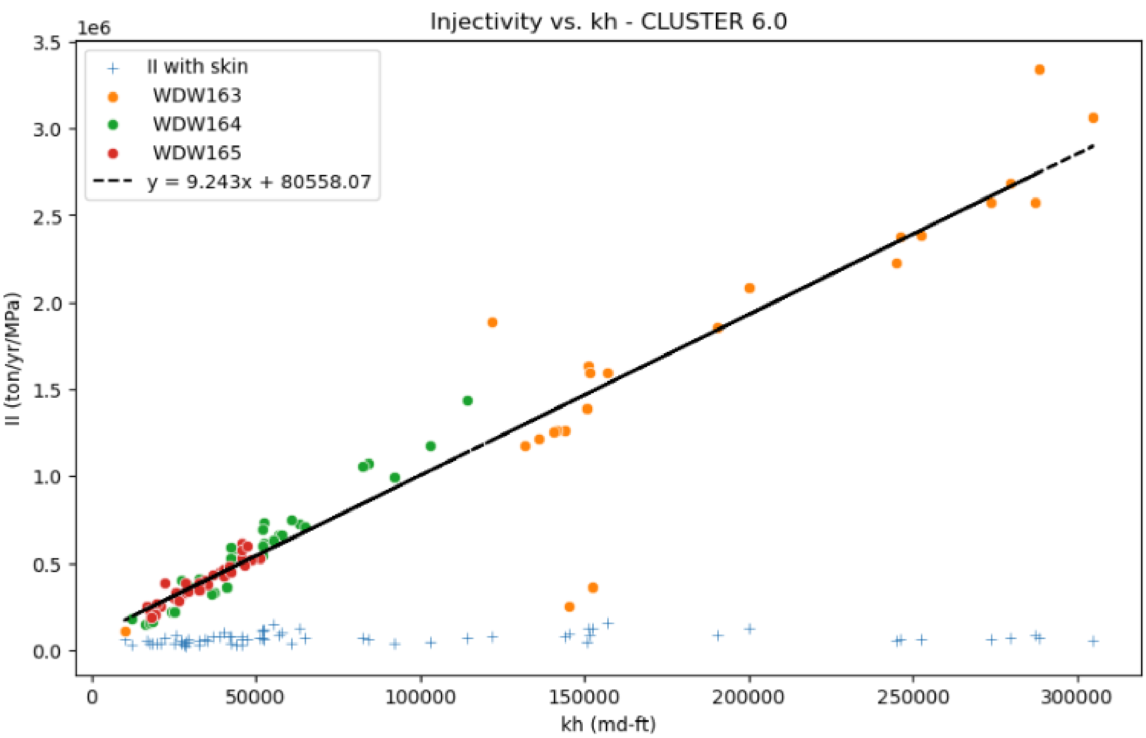
Injectivity vs. kh - CLUSTER 6.0
1e6
II with skin
WDW163
WDW164
WDW165
y = 9.243x + 80558.07
II (ton/yr/MPa)
kh (md-ft)
0.0
0.5
1.0
1.5
2.0
2.5
3.0
3.5
0
50000
100000
150000
200000
250000
300000

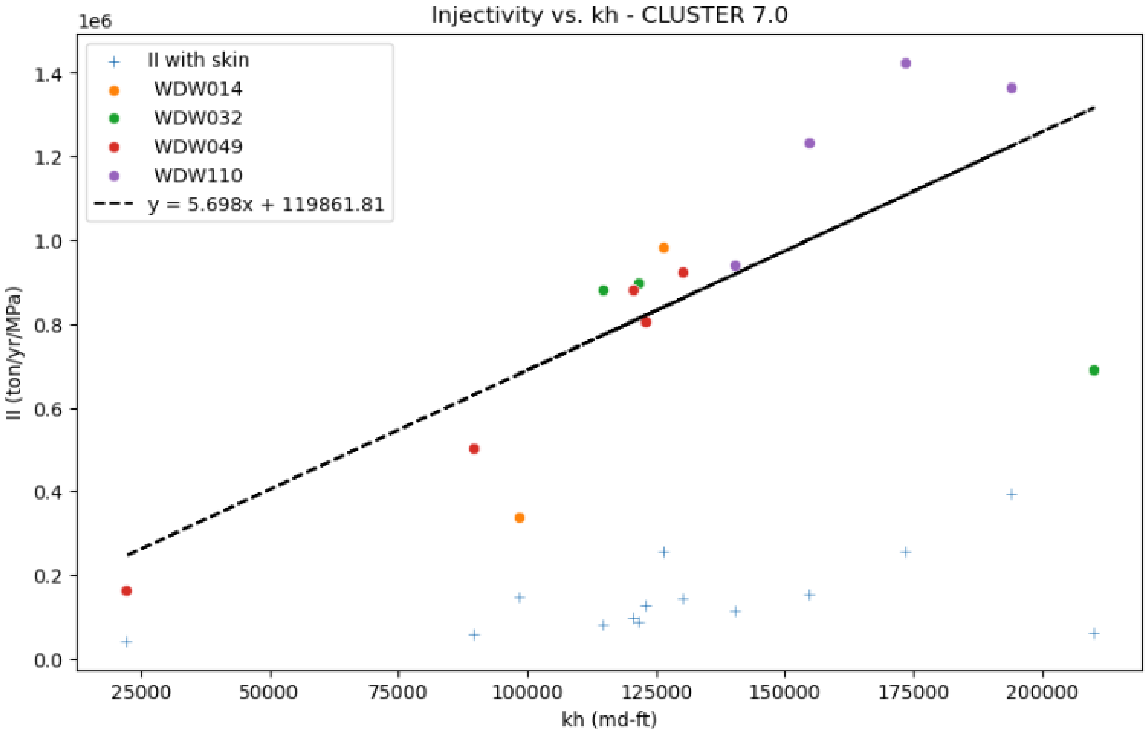

Injectivity vs. kh - CLUSTER 7.0
1e6
II with skin
WDW014
WDW032
WDW049
WDW110
y = 5.698x + 119861.81
II (ton/yr/MPa)
kh (md-ft)
0.0
0.2
0.4
0.6
0.8
1.0
1.2
1.4
25000
50000
75000
100000
125000
150000
175000
200000

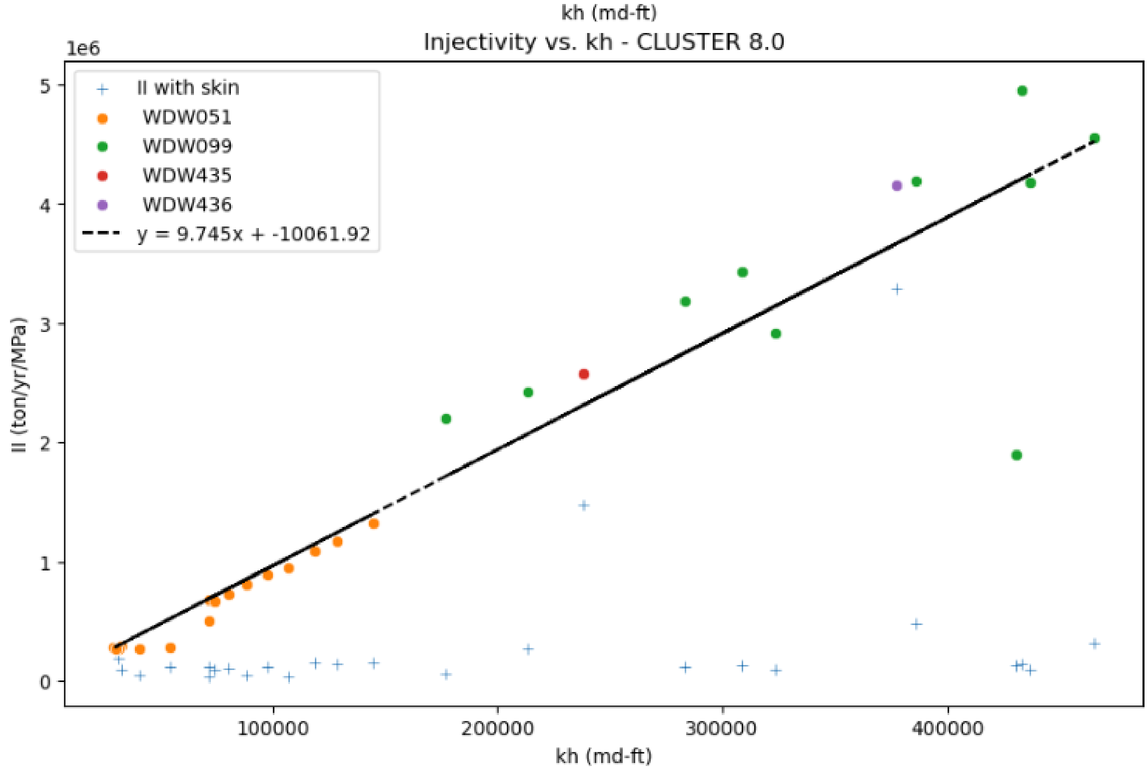

Injectivity vs. kh - CLUSTER 8.0
1e6
II with skin
WDW051
WDW099
WDW435
WDW436
y = 9.745x + -10061.92
II (ton/yr/MPa)
kh (md-ft)
0
1
2
3
4
5
100000
200000
300000
400000

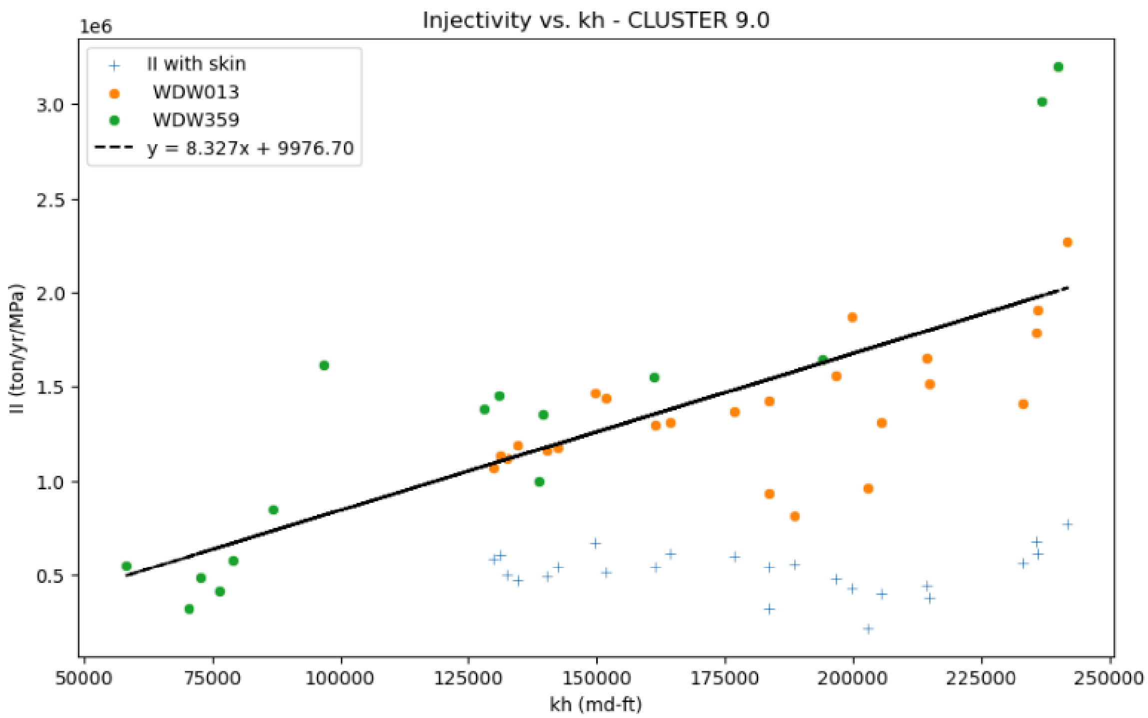
Injectivity vs. kh - CLUSTER 9.0
1e6
II with skin
WDW013
WDW359
y = 8.327x + 9976.70
II (ton/yr/MPa)
kh (md-ft)
0.5
1.0
1.5
2.0
2.5
3.0
50000
75000
100000
125000
150000
175000
200000
225000
250000

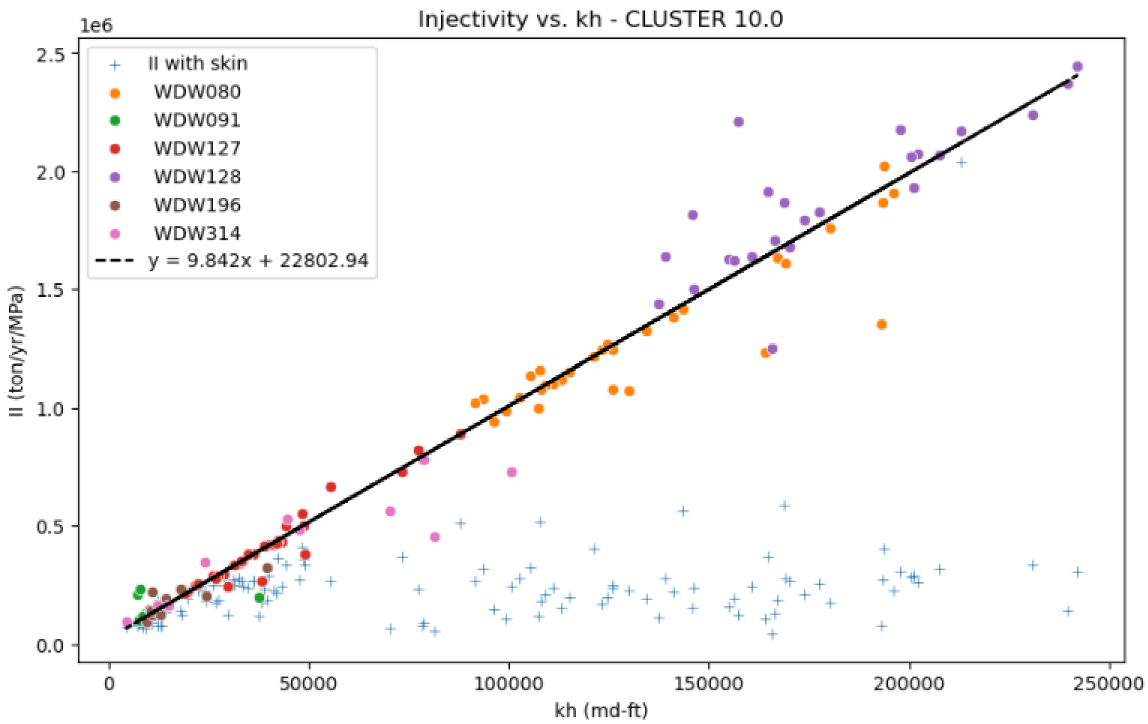
Injectivity vs. kh - CLUSTER 10.0
1e6
II with skin
WDW080
WDW091
WDW127
WDW128
WDW196
WDW314
y = 9.842x + 22802.94
II (ton/yr/MPa)
kh (md-ft)
0.0
0.5
1.0
1.5
2.0
2.5
0
50000
100000
150000
200000
250000

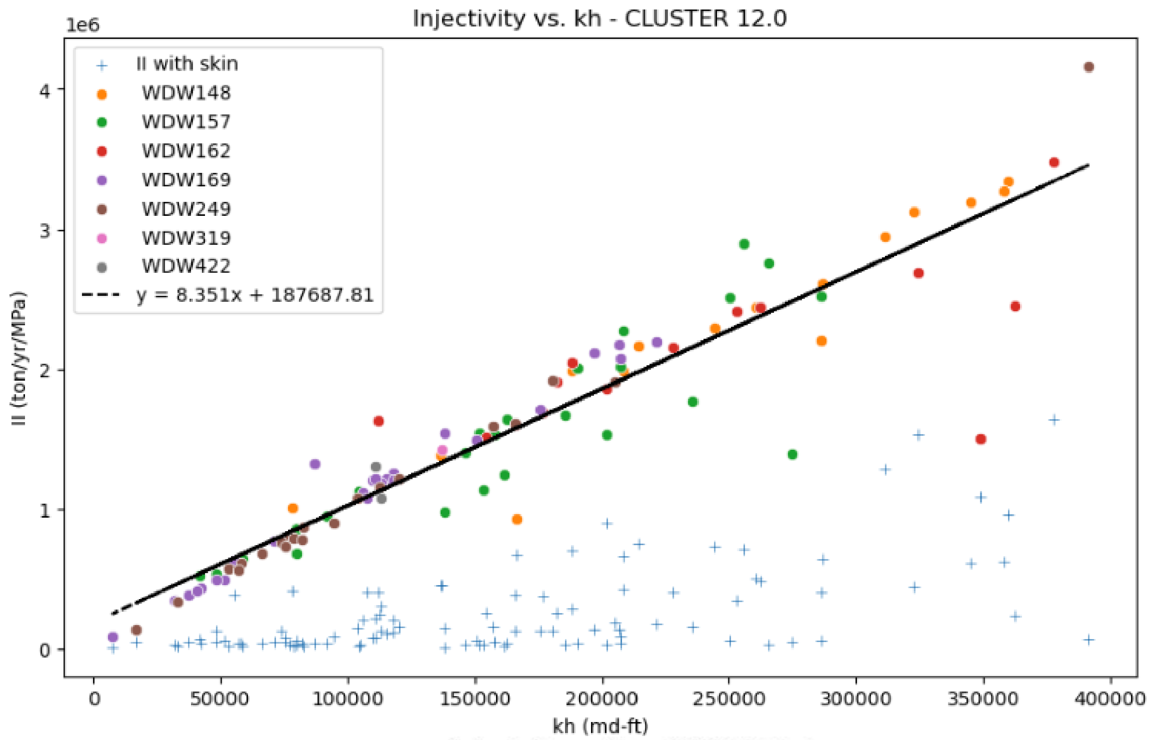
Injectivity vs. kh - CLUSTER 12.0
1e6
II with skin
WDW148
WDW157
WDW162
WDW169
WDW249
WDW319
WDW422
y = 8.351x + 187687.81
II (ton/yr/MPa)
kh (md-ft)
0
1
2
3
4
0
50000
100000
150000
200000
250000
300000
350000
400000

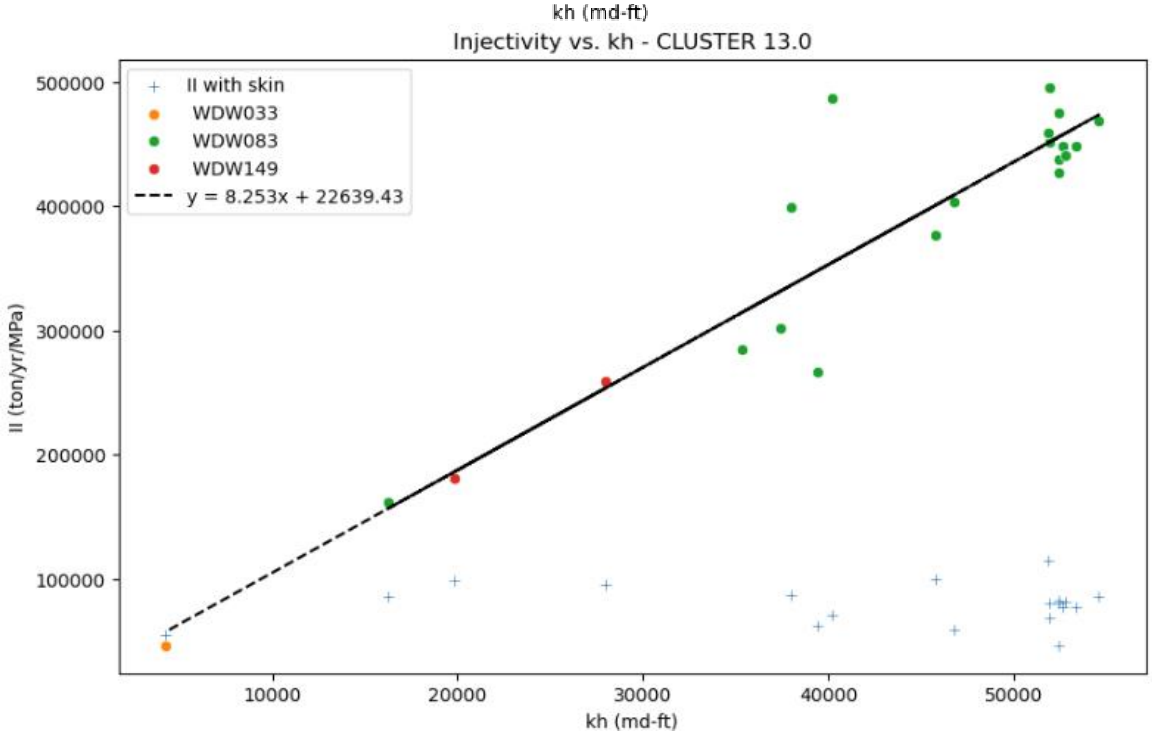
Injectivity vs. kh - CLUSTER 13.0
II with skin
WDW033
WDW083
WDW149
y = 8.253x + 22639.43
II (ton/yr/MPa)
kh (md-ft)
100000
200000
300000
400000
500000
10000
20000
30000
40000
50000

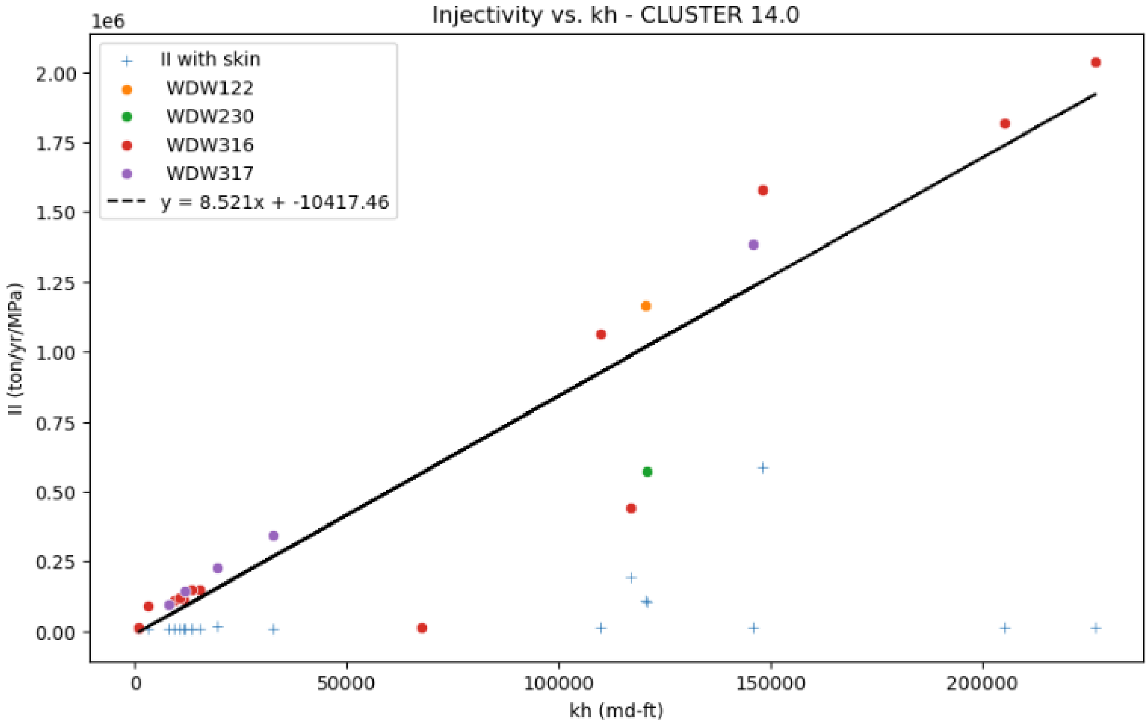
Injectivity vs. kh - CLUSTER 14.0
1e6
II with skin
WDW122
WDW230
WDW316
WDW317
y = 8.521x + -10417.46
II (ton/yr/MPa)
0.00
0.25
0.50
0.75
1.00
1.25
1.50
1.75
2.00
0
50000
100000
150000
200000
kh (md-ft)

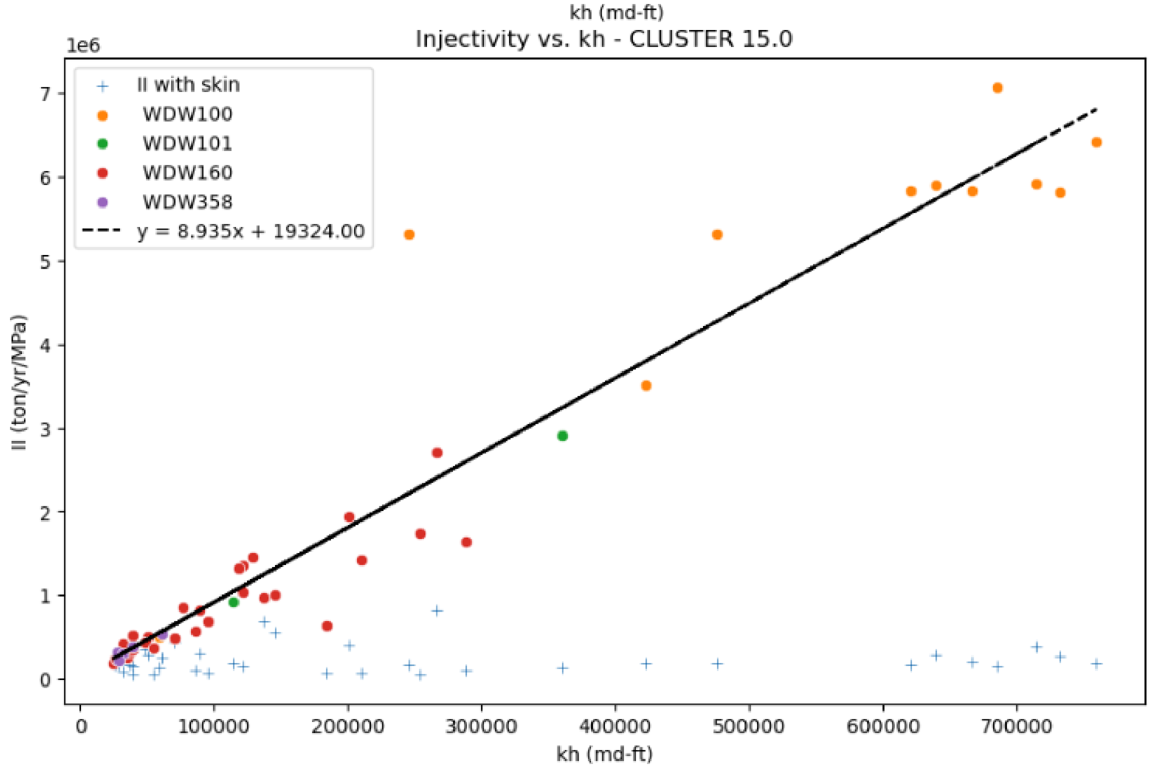
Injectivity vs. kh - CLUSTER 15.0
1e6
II with skin
WDW100
WDW101
WDW160
WDW358
y = 8.935x + 19324.00
II (ton/yr/MPa)
0
1
2
3
4
5
6
7
0
100000
200000
300000
400000
500000
600000
700000
kh (md-ft)

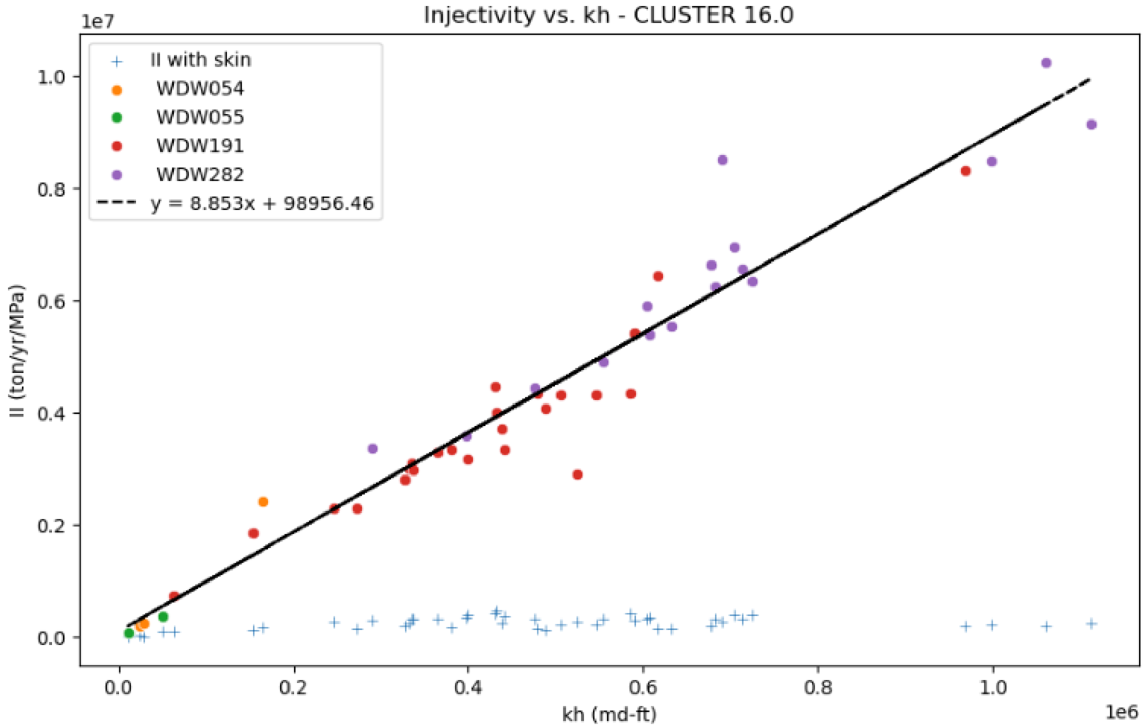
Injectivity vs. kh - CLUSTER 16.0
1e7
II with skin
WDW054
WDW055
WDW191
WDW282
y = 8.853x + 98956.46
II (ton/yr/MPa)
kh (md-ft)
1e6
0.0
0.2
0.4
0.6
0.8
1.0

APPENDIX M: HYPOTHETICAL CO_2 INJECTION RATES

Scenario 1 (q1) is the Cumulative Volume/Total number of Years. Scenario 2 (q2) is the maximum rate seen from falloff tests or annual volume reports. Scenario 3 (q3) is a hypothetical rate from pushing the average injectivity index to the max allowed bottomhole pressure. Scenario 4 (q4) is a hypothetical rate from the average injectivity index without skin effects pushed to the max allowed bottomhole pressure. Mton/year is for Million tons of CO_2/year.

CLUSTER	PERMIT NO.	LAT	LONG	START	LAST	CUM bbl	q1(Mton/yr)	q2(Mton/yr)	q3(Mton/yr)	q4(Mton/yr)
1	WDW248	27.39194	-97.7703	1988	2015	3.12E+07	0.12411	0.24743	0.24151	0.41311
2	WDW210	27.57139	-97.8294	1987	2021	2.94E+07	0.09358	0.41782	0.36949	0.9196
2	WDW211	27.5675	-97.8292	1983	2013	1.57E+07	0.05643	0.34818	0.46083	0.55658
2	WDW212	27.56611	-97.8297	1984	2021	3.12E+07	0.09136	0.29247	0.34647	0.46941
3	WDW152	27.81167	-97.595	1982	2005	6.07E+06	0.02814	0.18287	1.21446	1.79875
3	WDW153	27.81139	-97.595	1979	2005	6.07E+06	0.02501	0.22646	1.13826	2.05249
3	WDW278	27.73028	-97.6578	1991	2019	4.62E+06	0.01773	0.11281	0.21661	0.86113
3	WDW279	27.73083	-97.6578	2018	2019	1.88E+05	0.01046	0.03482		0.26466
4	WDW070	27.71353	-97.4607	1970	2021	1.41E+07	0.03021	0.19263	0.24342	2.33979
5	WDW004	28.67444	-96.9514	1963	2015	7.09E+07	0.14889			
5	WDW028	28.67056	-96.9583	1968	2015	6.16E+07	0.14281			
5	WDW029	28.66889	-96.9608	1964	2015	5.04E+07	0.10783			
5	WDW030	28.6725	-96.9539	1975	2015	6.26E+07	0.16997			
5	WDW105	28.67611	-96.9578	1972	2015	1.43E+08	0.36085			3.69747
5	WDW106	28.67556	-96.9533	1972	2015	1.16E+08	0.29425			
5	WDW142	28.67111	-96.9625	1953	2015	7.39E+07	0.13051			11.33233
5	WDW143	28.67639	-96.9522	1954	2015	4.73E+07	0.08488			
5	WDW144	28.67361	-96.9575	1957	2015	3.22E+07	0.06068			2.43397

CLUSTER	PERMIT NO.	LAT	LONG	START	LAST	CUM bbl	q1(Mton/yr)	q2(Mton/yr)	q3(Mton/yr)	q4(Mton/yr)
5	WDW145	28.67806	-96.9547	1979	2000	6.39E+07	0.32339			7.9758
5	WDW271	28.67806	-96.9547	1989	2000	3.32E+07	0.30826			
6	WDW163	28.56583	-96.8372	1984	2019	5.72E+07	0.17678	0.34426	0.56393	16.42275
6	WDW164	28.56681	-96.8372	1982	2019	5.89E+07	0.17252	0.51531	0.79167	7.43282
6	WDW165	28.56758	-96.8356	1981	2019	6.35E+07	0.18133	0.50138	0.526	3.89554
7	WDW014	28.87194	-96.0208	1965	1994	5.72E+07	0.21219	0.47961	0.84282	3.32063
7	WDW032	28.85806	-96.0203	1967	1995	4.40E+07	0.16895	0.38398	0.35176	3.84866
7	WDW049	28.85667	-96.0164	1969	1996	4.65E+07	0.18463	0.40574	0.42129	2.91359
7	WDW110	28.86333	-96.0208	1973	1991	4.81E+07	0.02466	0.4598	1.39725	7.51479
8	WDW051	29.00361	-95.4003	1970	2015	4.36E+07	0.10543	0.33878	1.1688	5.64181
8	WDW099	29.00361	-95.3992	1983	2019	3.52E+07	0.10593	0.34146	2.33921	48.28779
8	WDW408	29.00444	-95.3994					0.37741	1.36149	11.8347
8	WDW435	28.95318	-95.3077					0.81966	11.79621	20.58554
8	WDW436	28.95319	-95.3076					0.58856	26.62222	33.67758
9	WDW013	29.25889	-95.2031	1965	2016	4.28E+08	0.91581	1.92375	4.53232	13.17294
9	WDW224	29.24667	-95.2094	1985	2016	2.23E+07	0.07763			
9	WDW318	29.25722	-95.2022	1996	2016	1.54E+08	0.8149			
9	WDW326	29.25028	-95.2058	1997	2016	1.54E+07	0.0858			
9	WDW359	29.24531	-95.2113	2000	2019	1.43E+07	0.07952	1.08215		11.71286
10	WDW091	29.37598	-94.8977	1977	2007	8.76E+07	0.31445	0.82408	0.99445	1.63342
10	WDW196	29.37621	-94.8978	1982	2006	6.27E+07	0.27916	0.67547	1.37638	1.90182
10	WDW314	29.37545	-94.8961	1995	2005	1.25E+07	0.12612	0.50556	2.01762	4.54878
10	WDW034	29.42583	-94.9708	1968	2009	5.34E+07	0.14152			
10	WDW113	29.4225	-94.9642	1974	2009	2.80E+07	0.08638			
10	WDW114	29.42889	-94.9758	1975	1990	1.78E+07	0.12363			
10	WDW080	29.37528	-94.9231	1991	2021	1.11E+08	0.39752	0.97186	1.86361	10.00494

CLUSTER	PERMIT NO.	LAT	LONG	START	LAST	CUM bbl	q1(Mton/yr)	q2(Mton/yr)	q3(Mton/yr)	q4(Mton/yr)
10	WDW127	29.3775	-94.9208	1991	2022	1.18E+08	0.40955	0.96795	2.12179	3.25015
10	WDW128	29.37694	-94.9208	1991	2022	1.13E+08	0.39355	1.08076	3.19203	16.06143
11	WDW111	29.58	-95.43	1973	2007	8.89E+06	0.02828			3.00569
11	WDW139	29.58222	-95.4328	1979	2017	4.05E+07	0.11569	0.21345		1.77913
11	WDW343	29.58333	-95.4353	2003	2017	1.82E+07	0.13535	0.18636		14.9568
12	WDW148	29.81447	-95.1068	1978	2014	7.69E+07	0.23129	0.51561	8.60949	35.45728
12	WDW162	29.8168	-95.1079	1979	2011	5.96E+07	0.20106	0.4596	9.36132	26.53064
12	WDW147	29.75972	-95.1764	1979	2000	5.19E+07	0.2624	0		39.39876
12	WDW319	29.75936	-95.1772	2000	2014	2.87E+07	0.21274	0.48676	5.60873	22.80883
12	WDW222	29.71861	-95.0936	1983	2017	1.23E+07	0.03904	0.04742		8.78321
12	WDW223	29.7175	-95.0917	1983	2017	8.31E+06	0.02643	0.05754		9.49356
12	WDW169	29.73614	-95.0917	1981	2018	2.55E+07	0.07465	0.20892		
12	WDW249	29.7354	-95.0919	1993	2018	1.82E+07	0.07783	0.17548	0.85063	10.84782
12	WDW422	29.73424	-95.0917	2018	2021	8.73E+05	0.02428	0.17548	2.53997	11.61389
12	WDW157	29.74083	-95.0939	1980	2017	2.48E+07	0.07254	0.23954	0.52376	10.38732
12	WDW397	29.74083	-95.1897	2008	2014	2.98E+07	0.47383	0.47383		27.69735
12	WDW398	29.73667	-95.1981	2011	2014	1.86E+07	0.51699	0.5106		33.99324
13	WDW082	29.69972	-95.0386	1972	2013	5.85E+07	0.15506	0.21119	0.37616	3.84432
13	WDW083	29.70222	-95.0403	1973	2013	6.31E+07	0.17129	0.32868	0.49003	2.63476
13	WDW149	29.70139	-95.0431	1980	2013	4.14E+07	0.13539	0.31989	1.48883	4.1112
13	WDW033	29.62611	-95.0639					0.34816	0.20362	0.92497
14	WDW316	29.88868	-94.9385	1999	2019	8.01E+06	0.04243	0.12796	0.63226	7.28007
14	WDW317	29.88962	-94.9391	2013	2019	2.47E+06	0.03931	0.11699	0.2442	4.68729
14	WDW122	29.94944	-95.0225	1977	2015	2.71E+07	0.07728	0.08356	0.82303	5.14327
14	WDW230	29.95028	-95.0208	1995	2015	9.30E+06	0.04927	0.08356	0.76349	5.72611
15	WDW160	29.85389	-94.0981	1982	2021	4.39E+07	0.12206	0.26699	3.17407	9.4969

CLUSTER	PERMIT NO.	LAT	LONG	START	LAST	CUM bbl	q1(Mton/yr)	q2(Mton/yr)	q3(Mton/yr)	q4(Mton/yr)
15	WDW358	29.85438	-94.0972	2007	2015	5.76E+06	0.07124	0.24442	2.57403	4.05272
15	WDW125	29.96917	-94.0608	1977	2011	1.08E+08	0.34492			
15	WDW155	29.96861	-94.0592	1979	2011	2.45E+06	0.00825	0.16278		
15	WDW201	29.9675	-94.0592	1987	2011	9.19E+07	0.40898			
15	WDW301	29.96778	-94.0611	1992	2011	8.63E+07	0.48039			
15	WDW302	29.97056	-94.0586	1994	2011	1.43E+07	0.08841	0.35097	1.12567	1.53246
15	WDW100	30.01922	-94.0308	1972	2018	7.80E+07	0.18456	0.81614	1.09722	29.56472
15	WDW101	30.01895	-94.0286	1972	2018	9.01E+07	0.21333	0.81614	1.47738	19.55667
16	WDW054	30.05174	-93.7595	1971	1996	2.22E+07	0.10454	0.31843	0.62626	11.24764
16	WDW055	30.05093	-93.7582	1988	1998	3.24E+06	0.03275	0.14624	0.38458	1.83408
16	WDW191	30.05025	-93.7578	1984	2019	7.32E+07	0.22637	0.7298	2.69366	38.42322
16	WDW282	30.05	-93.7581	1997	2019	3.79E+07	0.18343	0.69637	3.19865	103.04657
16	WDW057							0.09887		
17	970903	30.17521	-93.3279	1977	1992	5.86E+05	0.00407	0.01252		
17	970904	30.17521	-93.3269	1971	1992	7.44E+05	0.00377	0.03482	0.07206	12.33686
17	971123	30.17333	-93.3269	1984	1992	5.94E+05	0.00734	0.00936		
17	971124	30.17417	-93.3308	1986	1992	7.40E+05	0.01177	0.62673	3.57463	16.28804
18	975071	30.21829	-91.0512	2018.5	2021	2.84E+04	0.0009	0.35619		50.64369
18	975072	30.21848	-91.0511	2018	2021	3.44E+04	0.00096	0.35619	16.6186	68.22651
19	974237	30.04277	-90.808					0.29665	0.62508	127.74823
19	974238	30.04144	-90.8243					0.24512	8.18079	65.97671
20	970803	30.00393	-90.426	1983	1988	2.02E+05	0.00374	0		
20	970802	30.00407	-90.4263	1983	1988	5.71E+04	0.00106	0.00365		
20	972060	29.98128	-90.4538	1989	2021	7.23E+05	0.00244	0.42734		30.94593

WDW080, WDW127, WDW128 all operated at some point before 1991, but the CUMVOL in the permit as well as this table reflects the amount injected since 1991. The total volume injected before then was not found.

Appendix N: Annual Volumes and Pressure

Bar charts correlate with the left axis for volume, line plot correlates with pressure.

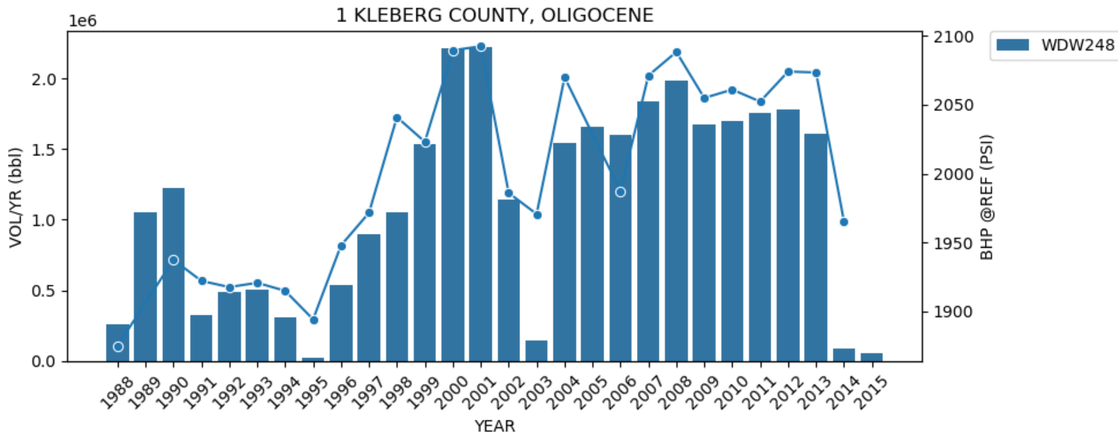

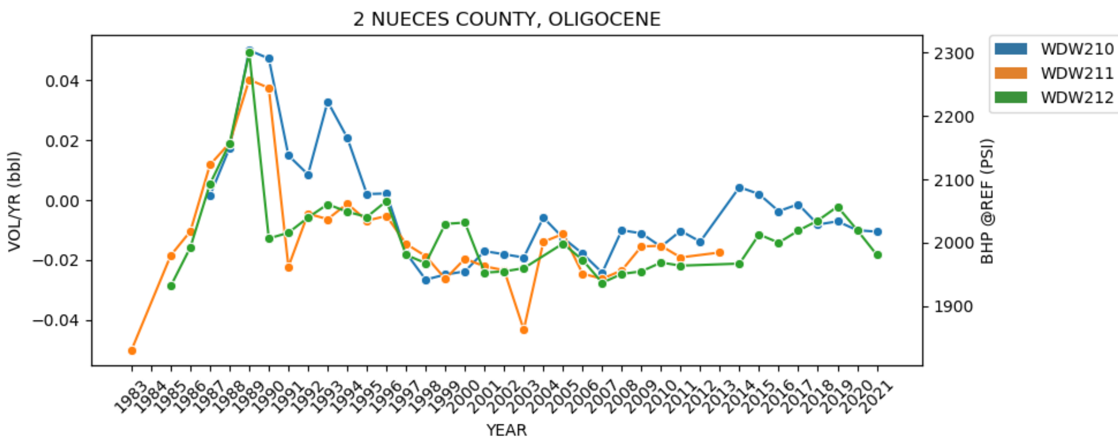

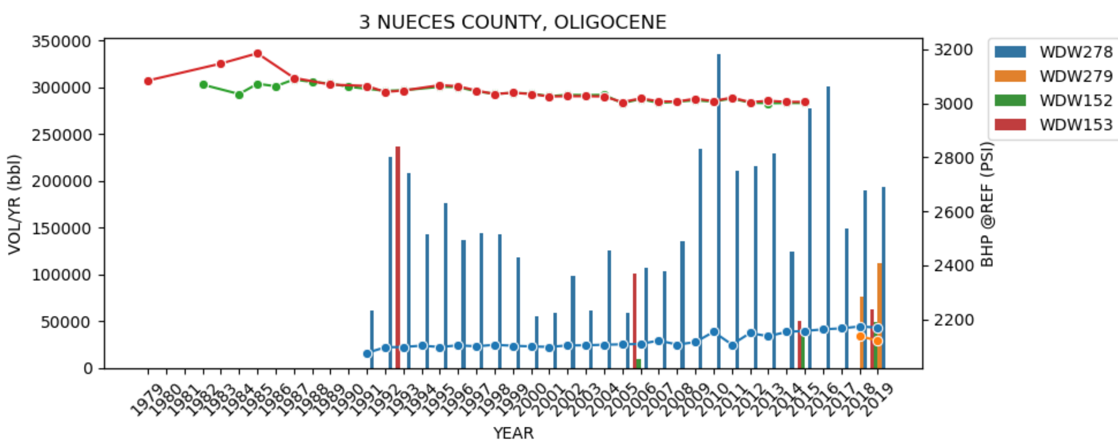

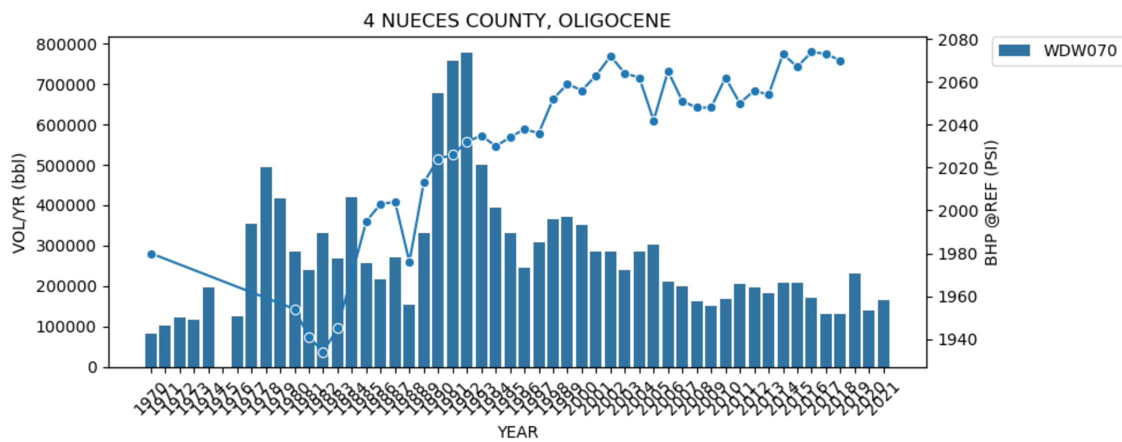
4 NUECES COUNTY, OLIGOCENE
VOL/YR (bbl)
BHP @REF (PSI)
YEAR
WDW070

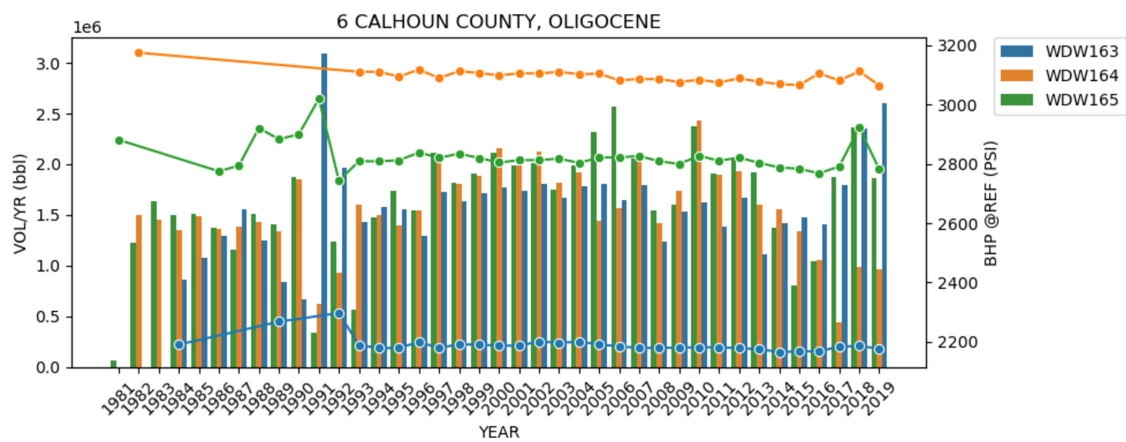
6 CALHOUN COUNTY, OLIGOCENE
1e6
VOL/YR (bbl)
BHP @REF (PSI)
YEAR
WDW163
WDW164
WDW165

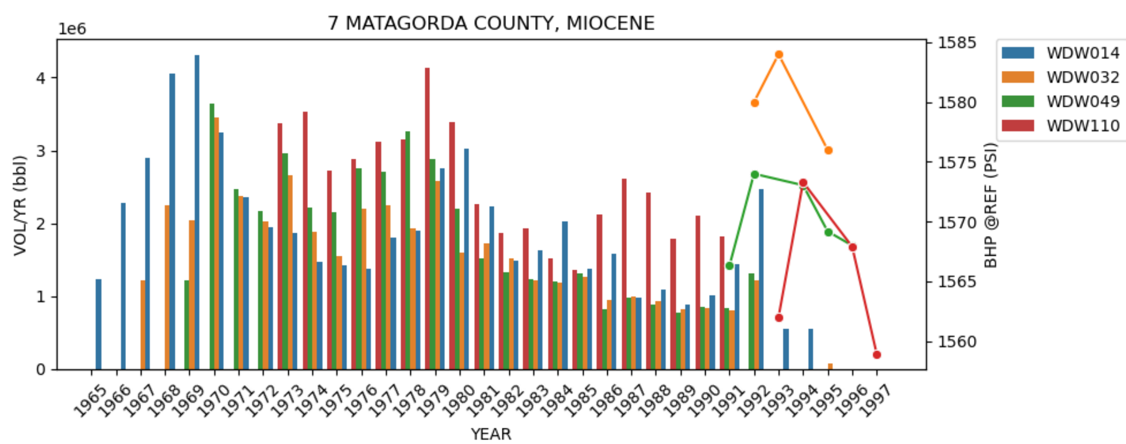
7 MATAGORDA COUNTY, MIOCENE
1e6
VOL/YR (bbl)
BHP @REF (PSI)
YEAR
WDW014
WDW032
WDW049
WDW110

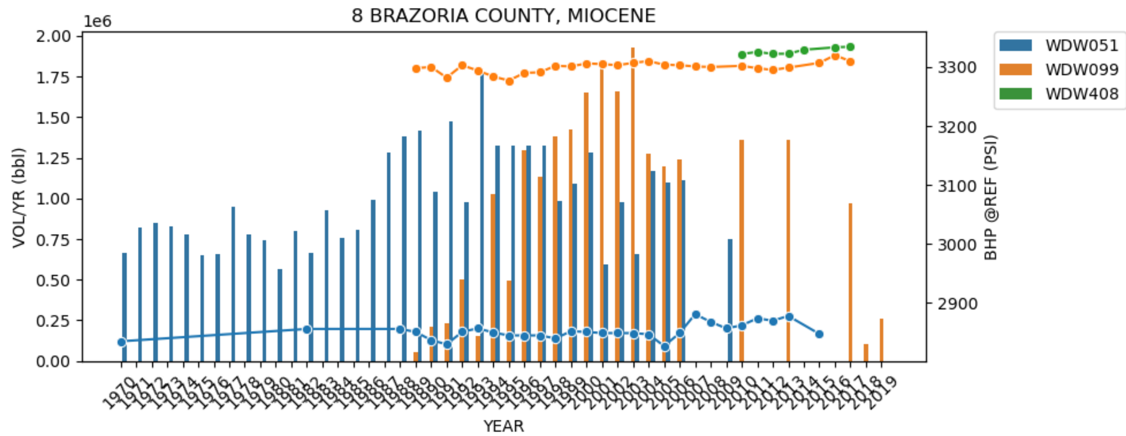
8 BRAZORIA COUNTY, MIOCENE
1e6
VOL/YR (bbl)
BHP @REF (PSI)
YEAR
WDW051
WDW099
WDW408

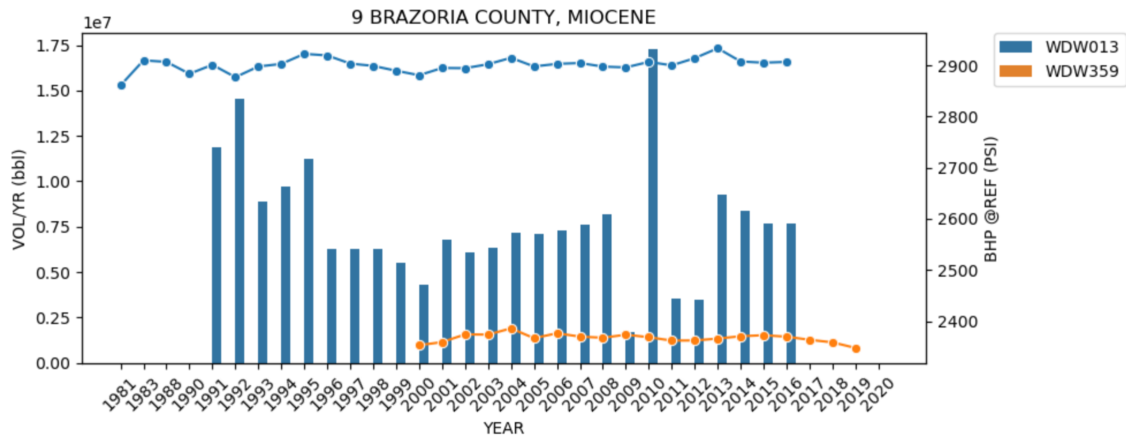
9 BRAZORIA COUNTY, MIOCENE
1e7
VOL/YR (bbl)
BHP @REF (PSI)
YEAR
WDW013
WDW359

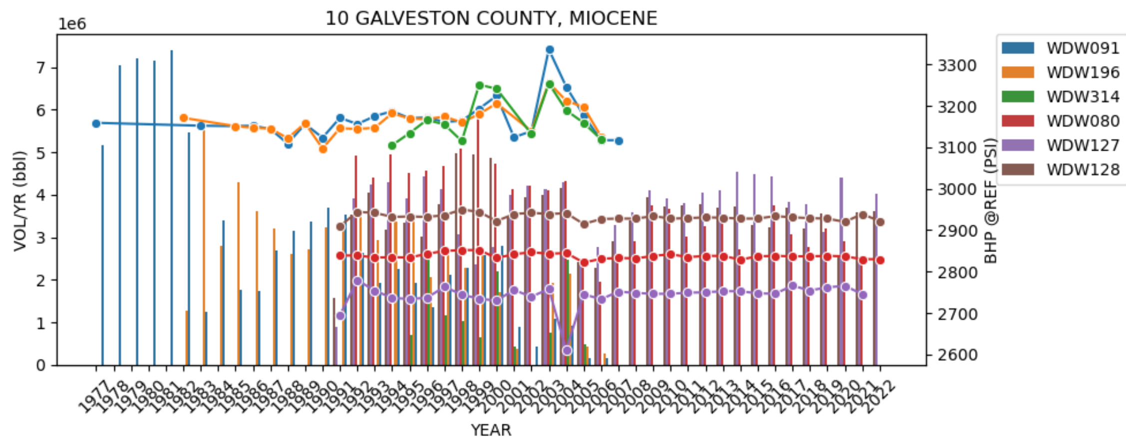
10 GALVESTON COUNTY, MIOCENE
1e6
VOL/YR (bbl)
BHP @REF (PSI)
YEAR
WDW091
WDW196
WDW314
WDW080
WDW127
WDW128

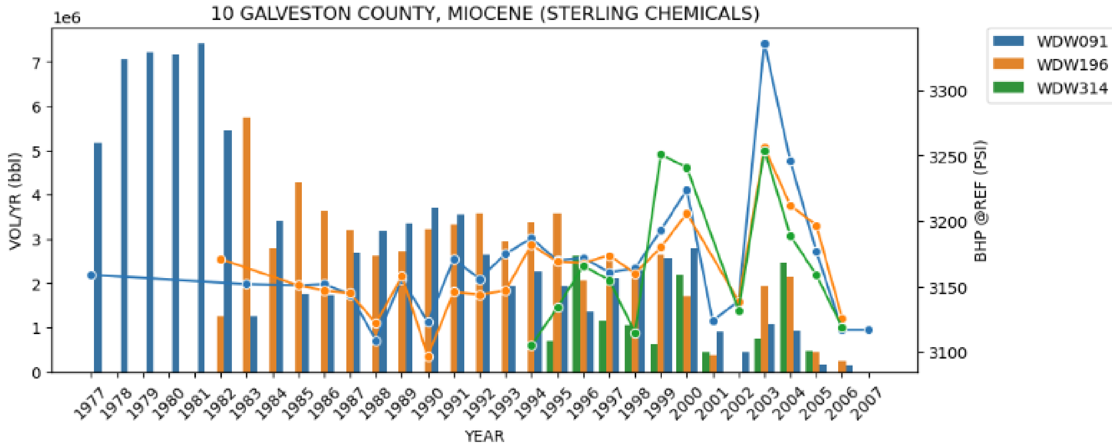

Partial plot from Cluster 10 for wells operated by single facility – Sterling Chemicals – for closer look

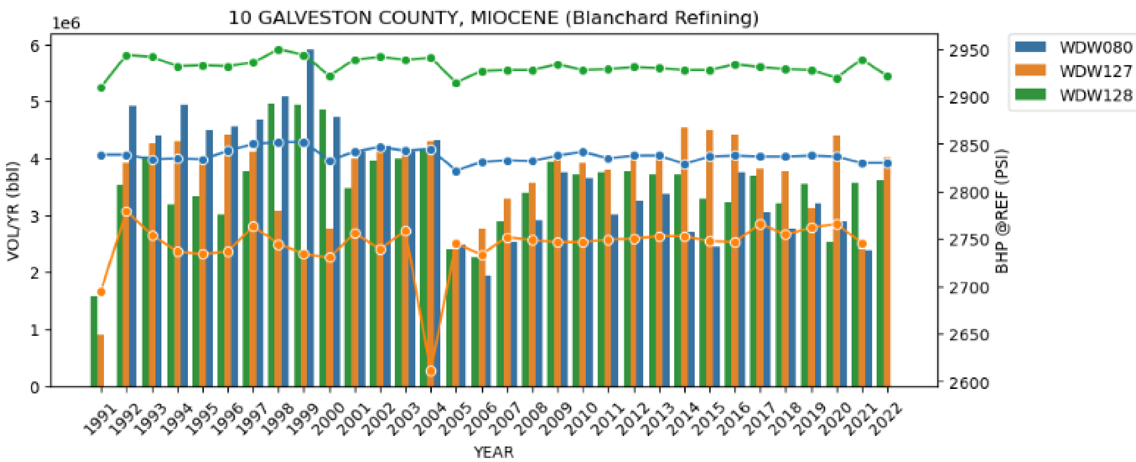

Partial plot from Cluster 10 for wells operated by single facility – Blanchard Refining – for closer look

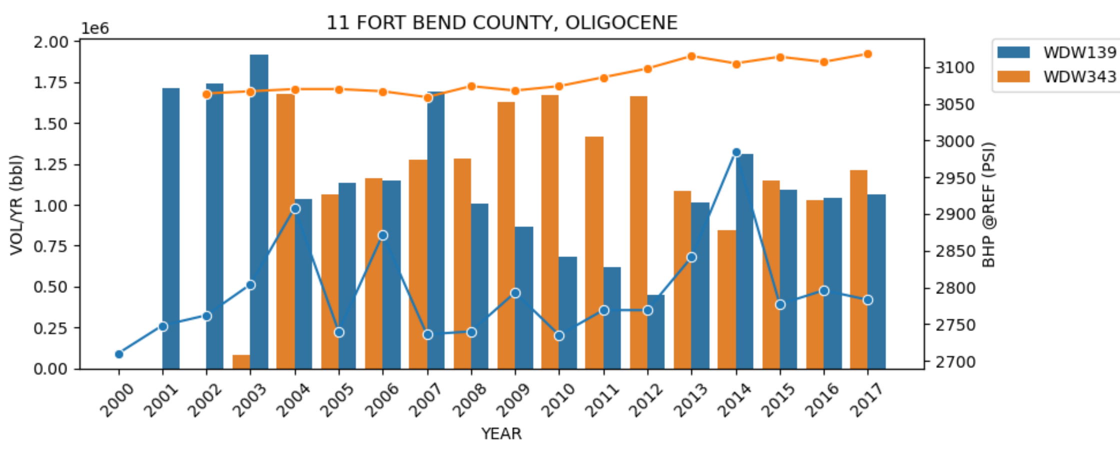

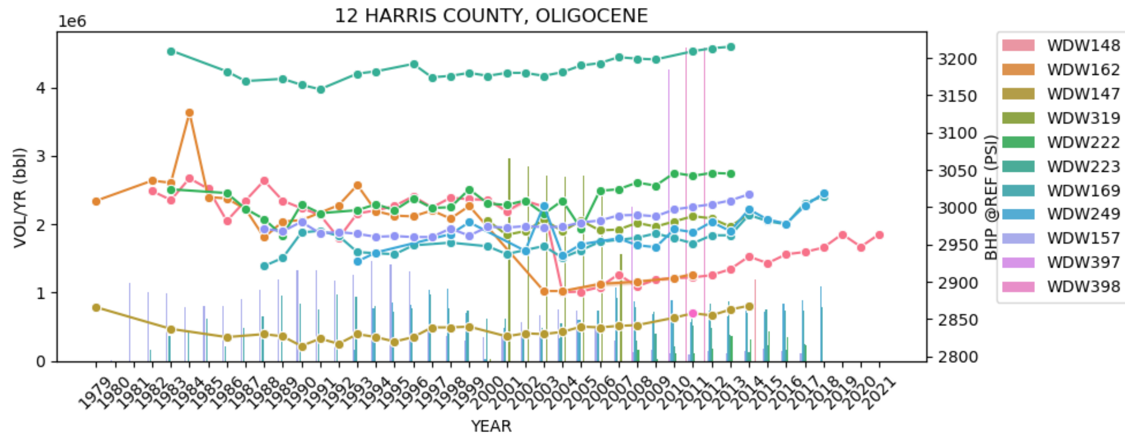

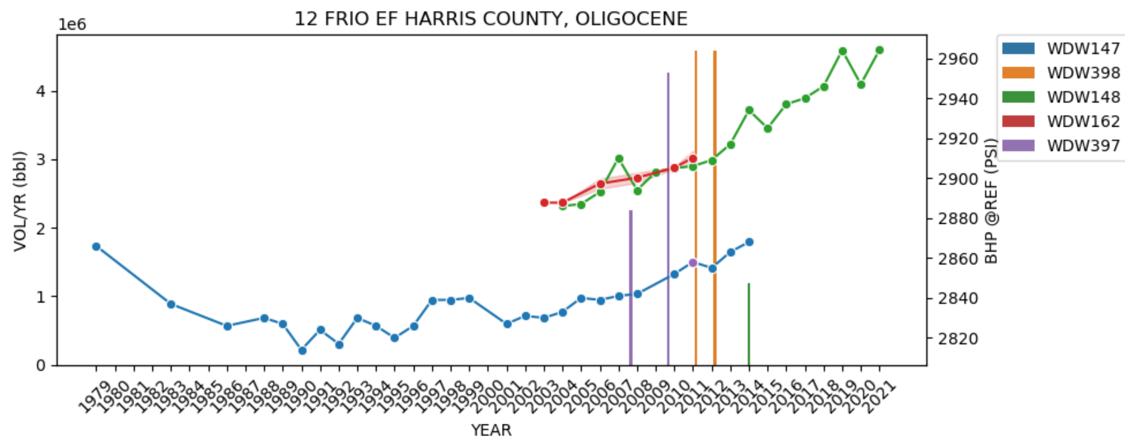

Wells from Cluster 12 injecting into same sand – Frio EF – in Houston, Texas.

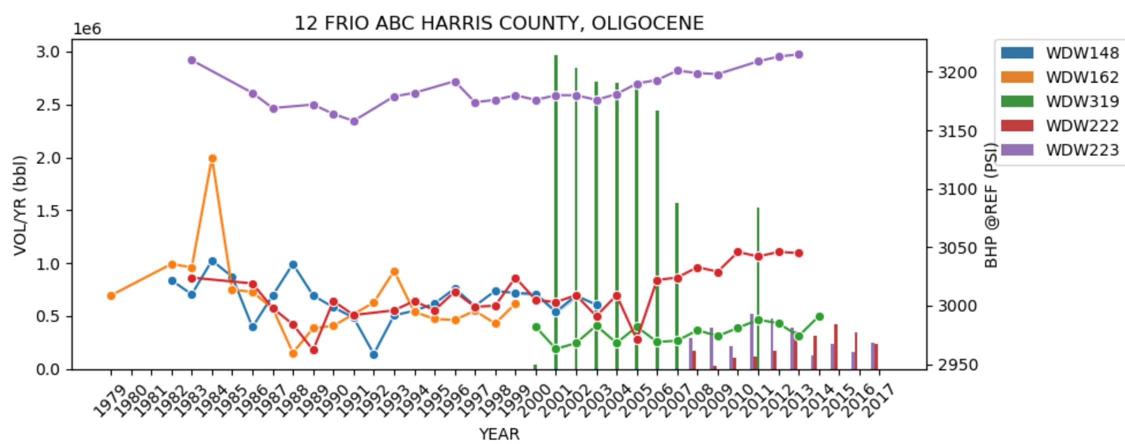

Wells from Cluster 12 injecting into same sand – commingled Frio ABC – in Houston, Texas.

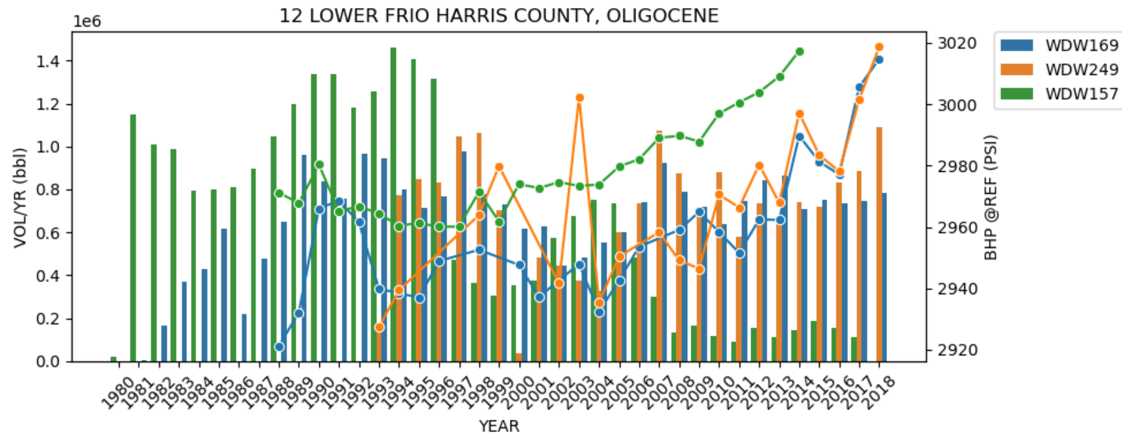

Wells from Cluster 12 injecting into same sand – Lower Frio – in Houston, Texas.

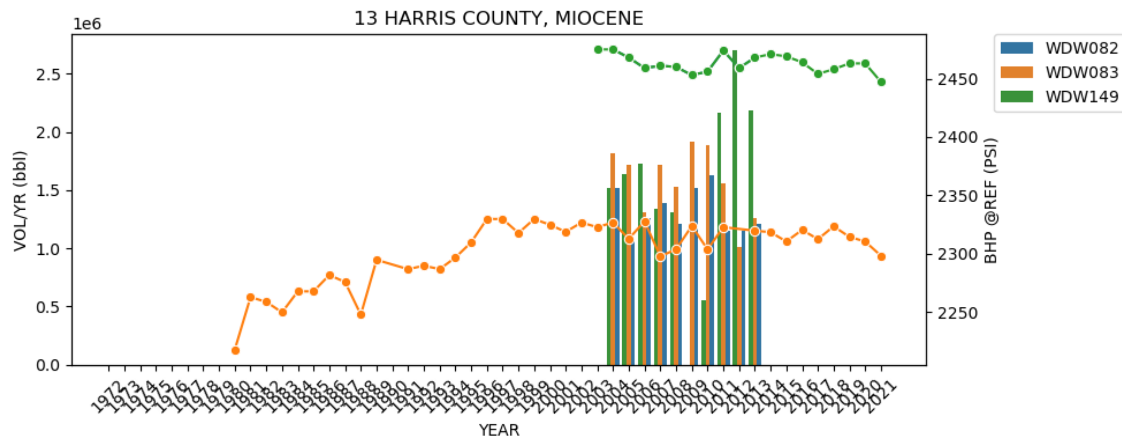

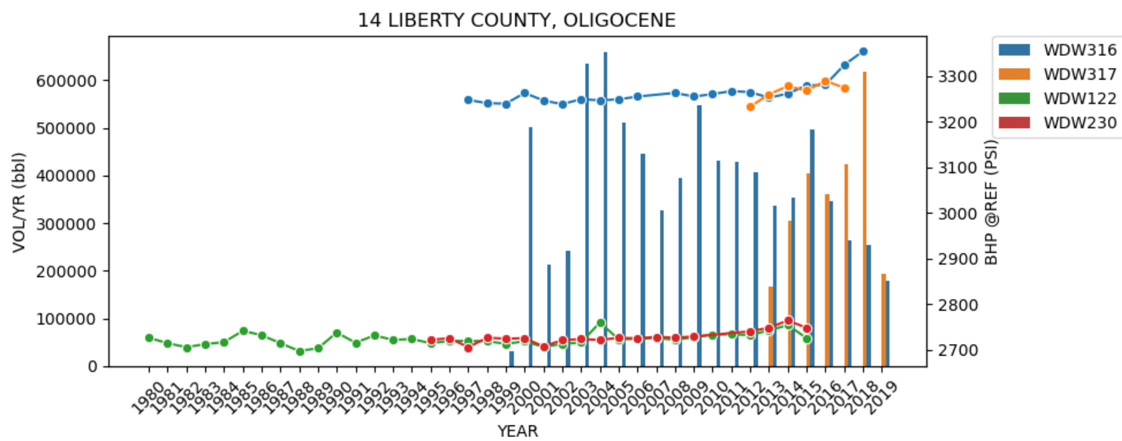

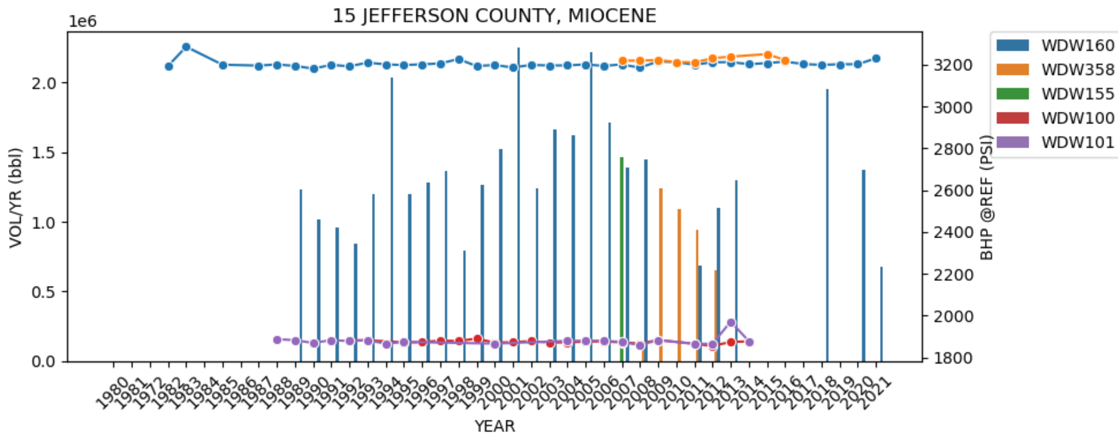
15 JEFFERSON COUNTY, MIOCENE
1e6
VOL/YR (bbl)
BHP @REF (PSI)
YEAR
WDW160
WDW358
WDW155
WDW100
WDW101

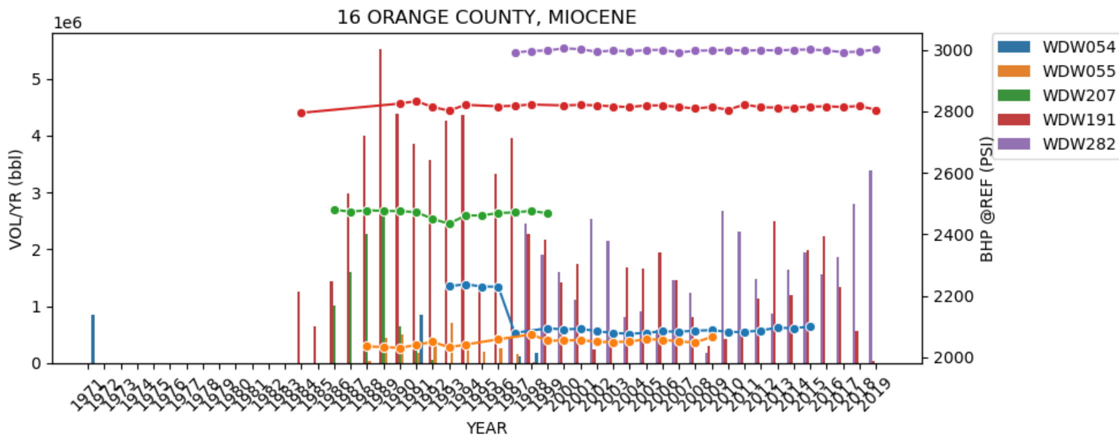
16 ORANGE COUNTY, MIOCENE
1e6
VOL/YR (bbl)
BHP @REF (PSI)
YEAR
WDW054
WDW055
WDW207
WDW191
WDW282

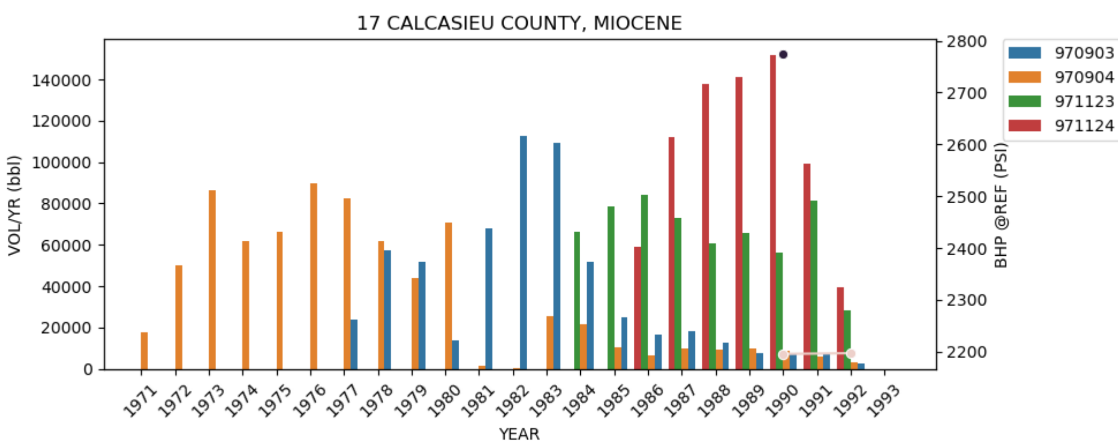
17 CALCASIEU COUNTY, MIOCENE
VOL/YR (bbl)
BHP @REF (PSI)
YEAR
970903
970904
971123
971124

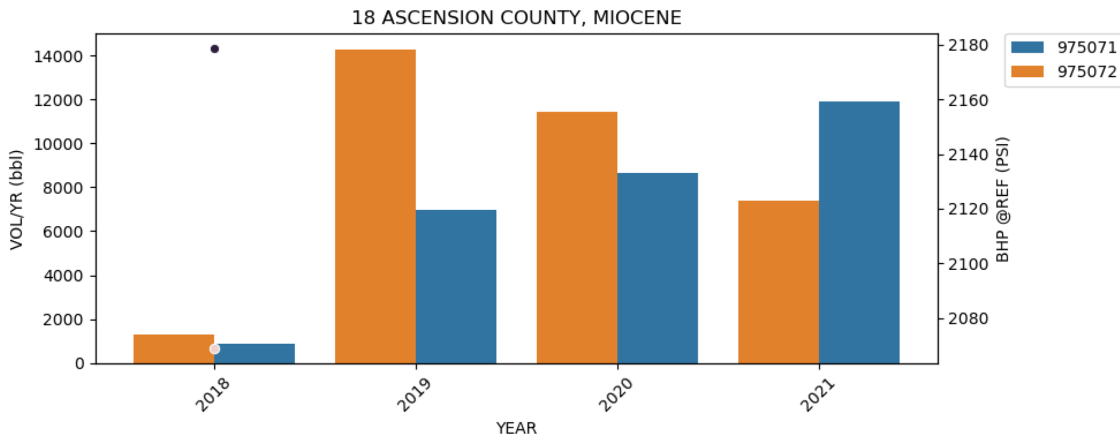
18 ASCENSION COUNTY, MIOCENE
VOL/YR (bbl)
0
2000
4000
6000
8000
10000
12000
14000
BHP @REF (PSI)
2080
2100
2120
2140
2160
2180
975071
975072
2018
2019
2020
2021
YEAR

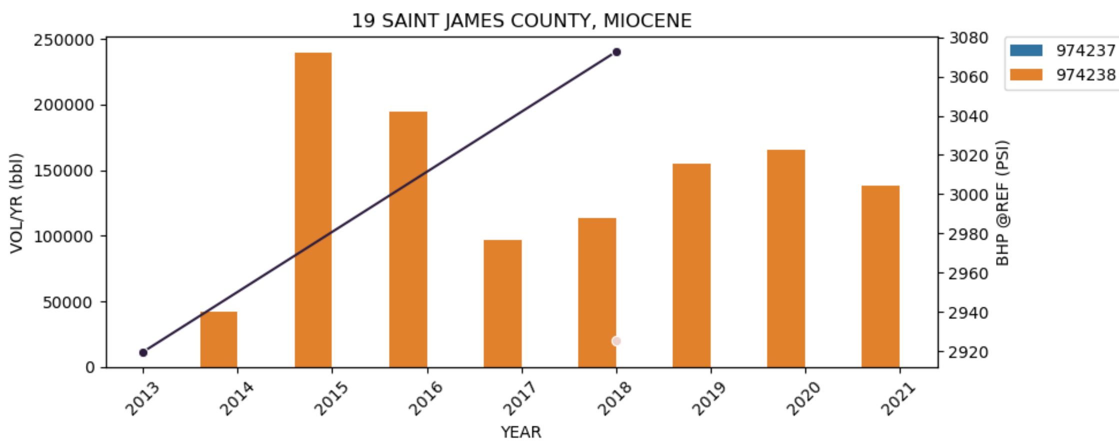
19 SAINT JAMES COUNTY, MIOCENE
VOL/YR (bbl)
0
50000
100000
150000
200000
250000
BHP @REF (PSI)
2920
2940
2960
2980
3000
3020
3040
3060
3080
974237
974238
2013
2014
2015
2016
2017
2018
2019
2020
2021
YEAR

APPENDIX O: HISTORIC STATIC PRESSURE

Static pressure measurements are taken annually to ensure the pressure buildup is less than allowed in the permit, and is more frequently reported, so there are two different 'total years' shown in this table. 'YEARS-VOL' represents the total number of years encompassing the cumulative volume injected value. 'YEARS-P' represents the total number of years encompassing the pressure measurements. In this column, if the number of years of static pressure values gathered is the same as the one representing the duration of the cumulative volume injection, the cell is filled with a dash.

'CUM V water (bbl)' is the total volume of water injected. 'CUM CO2 Mton' is the volume of water converted to million tons of CO_2 using the density of supercritical CO_2 (700 kg/m^3). 'Max Δ P (psi)' represents the difference between the minimum and maximum static bottomhole pressures ever recorded. 'Ending Δ P (psi)' represents the pressure difference from the minimum to the measurement of the most recent year available. The two columns to the right show those values as a percentage increase.

CLUSTER	PERMIT NO.	YEARS - VOL	CUM V (bbl)	CUM CO2 (Mton)	YEARS - P	Max Δ P (psi)	Ending Δ P (psi)	Max Inc %	End Inc %
1	WDW248	28	3.12E+07	3.475	-	217	90	11.57	4.8
2	WDW210	35	2.94E+07	3.275	-	361	75	18.59	3.86
2	WDW211	31	1.57E+07	1.749	-	426	153	23.27	8.36
2	WDW212	38	3.12E+07	3.472	-	367	49	19	2.54
3	WDW152	24	6.07E+06	0.675	34	88	1	2.93	0.03
3	WDW153	27	6.07E+06	0.675	37	181	1	6.03	0.03
3	WDW278	29	4.62E+06	0.514	-	98	94	4.72	4.53
3	WDW279	2	1.88E+05	0.021	-	16	0	0.75	0
4	WDW070	52	1.41E+07	1.571	-	140	136	7.24	7.03
6	WDW163	36	5.72E+07	6.364	-	131	11	6.05	0.51
6	WDW164	38	5.89E+07	6.556	-	110	0	3.59	0
6	WDW165	39	6.35E+07	7.072	-	277	39	10.1	1.42
7	WDW032	29	4.40E+07	4.899	-	8	0	0.51	0

7	WDW049	28	4.65E+07	5.170	-	7	1	0.45	0.06
7	WDW110	19	4.81E+07	0.469	25	14	0	0.9	0
8	WDW051	46	4.36E+07	4.850	-	54	20	1.91	0.71
8	WDW099	37	3.52E+07	3.919	-	43	32	1.31	0.98
9	WDW013	52	4.28E+08	47.622	-	72	46	2.52	1.61
9	WDW359	20	1.43E+07	1.590	-	38	0	1.62	0
10	WDW034	42	5.34E+07	5.944	-	79	79	4.83	4.83
10	WDW080	31	1.11E+08	12.323	32	30	8	1.06	0.28
10	WDW091	31	8.76E+07	9.748	-	227	8	7.3	0.26
10	WDW127	32	1.18E+08	13.106	-	167	134	6.39	5.13
10	WDW128	32	1.13E+08	12.594	-	40	12	1.37	0.41
10	WDW196	25	6.27E+07	6.979	-	159	29	5.13	0.94
10	WDW314	11	1.25E+07	1.387	13	149	14	4.8	0.45
11	WDW139	39	4.05E+07	4.512	-	275	73	10.15	2.69
12	WDW147	22	5.19E+07	5.773	36	54	54	1.92	1.92
12	WDW148	37	7.69E+07	8.558	44	78	78	2.7	2.7
12	WDW157	38	2.48E+07	2.756	-	57	57	1.93	1.93
12	WDW169	38	2.55E+07	2.837	-	93	93	3.18	3.18
12	WDW222	35	1.23E+07	1.366	-	84	83	2.84	2.8
12	WDW223	35	8.31E+06	0.925	-	57	57	1.8	1.8
12	WDW249	26	1.82E+07	2.024	-	91	91	3.11	3.11
12	WDW319	15	2.87E+07	3.191	-	28	28	0.94	0.94
13	WDW082	42	5.85E+07	6.512	-	22	15	0.9	0.61
13	WDW083	41	6.31E+07	7.023	49	112	80	5.05	3.61
13	WDW149	34	4.14E+07	4.603	42	27	0	1.1	0
14	WDW122	39	2.71E+07	3.014	-	62	28	2.3	1.04
14	WDW230	21	9.30E+06	1.035	-	58	42	2.14	1.55
14	WDW316	21	8.01E+06	0.891	23	115	115	3.55	3.55
14	WDW317	7	2.47E+06	0.275	8	56	41	1.73	1.27
15	WDW100	47	7.79E+07	8.674	-	35	22	1.89	1.19
15	WDW101	47	9.01E+07	10.026	-	112	19	6.02	1.02
15	WDW160	40	4.39E+07	4.882	-	104	48	3.27	1.51
15	WDW358	9	5.76E+06	0.641	10	39	11	1.21	0.34
16	WDW054	26	2.22E+07	2.718	30	161	24	7.76	1.16
16	WDW055	11	3.24E+06	0.397	-	44	36	2.17	1.77
16	WDW191	36	7.32E+07	8.149	-	38	10	1.36	0.36
16	WDW207	14	8.60E+06	1.005	-	46	34	1.89	1.4
16	WDW282	23	3.79E+07	4.219	-	14	10	0.47	0.33

References

30 TAC §331.42. Area of Review.

40 CFR §144.6. Underground Injection Control Program.

40 CFR §146 Subpart B. Criteria and Standards Applicable to Class I Wells.

40 CFR §146 Subpart H. Criteria and Standards Applicable to Class VI Wells.

40 CFR § 146.33. Operating, monitoring, and reporting requirements.

40 CFR § 146.62(c)(2)(ii). Minimum criteria for siting.

40 CFR § 146.6. Area of Review.

40 CFR § 146.83(a)(1). Minimum criteria for siting.

40 CFR § 146.90. Testing and monitoring requirements.

40 CFR § 146.91. Reporting requirements.

40 CFR § 261.20–.24. Identification and Listing of Hazardous Waste.

53 FR 28118. (1988). Underground Injection Control Program; Hazardous Waste Disposal Injection Restrictions and Requirements for Class I Wells; Final Rule. https://archives.federalregister.gov/issue_slice/1988/7/26/28110-28157.pdf

75 FR 77229. (2010). Federal Requirements Under the Underground Injection Control (UIC) Program for Carbon Dioxide (CO2) Geologic Sequestration (GS) Wells. https://www.federalregister.gov/d/2010-29954

79 FR 350. (2014) Hazardous Waste Management System: Conditional Exclusion for Carbon Dioxide (CO2).

https://www.federalregister.gov/documents/2014/01/03/2013-31246/hazardous-waste-management-system-conditional-exclusion-for-carbon-dioxide-co2

Abdelaal, M & Zeidouni, M. (2020). Pressure falloff testing to characterize CO2 plume and dry-out zone during CO2 injection in saline aquifers. International Journal of Greenhouse Gas Control. Vol. 103. https://doi.org/10.1016/j.ijggc.2020.103160

Adams, S.J. (2005). Core-to-Log Comparison—What's A Good Match? *SPE Annual Technical Conference and Exhibition.* https://doi.org/10.2118/97013-MS

Agarwal, R. G., Al-Hussainy, R., & Ramey, H.J. (1970). An Investigation of Wellbore Storage and Skin Effect in Unsteady Liquid Flow: I. Analytical Treatment." SPE J. 10: 279–290. doi: https://doi.org/10.2118/2466-PA

Aptian Technical. (2023). Ion Multiplier vs. Total Solids Concentrations. Retrieved from https://www.aptiantechnical.com/resources/interactive-crossplots/ion-multiplier-vs-total-solids-concentration

Archie, G. E. (1942). The electrical resistivity log as an aid in determining some reservoir characteristics. Retrieved from *Journal of Petroleum Geology*, pp. 54-62

Archie, G. E. (1950). Introduction to petrophysics of reservoir rocks. Retrieved from *AAPG Bulletin*, 34, pp. 943–961.

Arps, J. J. (1953). The effect of temperature on the density and electrical resistivity of sodium chloride solutions. Journal of Petroleum Technology, 5(10), 17-20.

Asquith, G. B., & Krygowski, D. (1982). Gamma Ray Logs: Chapter V. In Basic Well Log Analysis for Geologists. Retrieved from *AAPG Archives.*

Asquith, G. B., & Krygowski, D. (2004). Basic Well Log Analysis (pp.119-123). Retrieved from *AAPG Methods in Exploration Serios*, No. 16, 2004.

Baker, E. T., Jr. (1979). Stratigraphic and hydrogeologic framework of part of the coastal plain of Texas: Retrieved from *Texas Department of Water Resources* Report 236

Bateman, R.M., & C.E. Konen. (1978). The Log Analyst and The Programmable Pocket Calculator. Retrieved from *The Log Analyst* 19. SPWLA-1978-vXIXn4a2.

Bigelow, E. (1992). Introduction to Wireline Log Analysis. *Western Atlas International*, Inc. Houston, Texas.

Birkholzer, J. (2009). Basin-Scale Hydrologic Impacts of CO2 Storage: Regulatory and Capacity Implications. *Lawrence Berkeley National Laboratory*. https://escholarship.org/uc/item/3vj6h0f3

Bump, A. P., Hovorka, S. D., & Meckel, T. A. (2021). Common risk segment mapping: Streamlining exploration for carbon storage sites, with application to coastal Texas and Louisiana. *International Journal of Greenhouse Gas Control*, *111*. https://doi.org/10.1016/j.ijggc.2021.103457

Burke, Lauri. (2011). Carbon dioxide fluid-flow modeling and injectivity calculations. Retrieved from *U.S. Geological Survey Scientific Investigations*. Report 2011–5083, p.16.

Celia, M. A., Bachu, S., Nordbotten, J. M., & Bandilla, K. W. (2015), Status of CO2 storage in deep saline aquifers with emphasis on modeling approaches and practical simulations. Water Resources. Res., 51, 6846– 6892. doi:10.1002/2015WR017609.

Chalmin, A. (2021, November). The Fossil Fuel Industry has a Stake in the Majority of Known CCS and CCUS Projects. Retrieved from: https://www.geoengineeringmonitor.org/2021/11/fossil-fuel-industry-and-investments-in-ccs-ccus/#:~:text=Fossil%20fuel%20companies%20involved%20in,%2C%20Total%2C%20TUPRAS%20and%20Vattenfall

Cox, J. R. (2003). Revisiting RCRA's Oilfield Waste Exemption as to Certain Hazardous Oilfield Exploration and Production Wastes, 14 Vill. Envtl. L.J. 1

Chaudhry, A.U. (2004). Oil well testing handbook. *Gulf Professional Publishing*. https://doi.org/10.1016/B978-075067706-6/50105-3

Chowdhury, A.H. & Turco, M.J. (2006) Geology of the Gulf Coast Aquifer, Texas. In: Mace, R.E., et al., Eds., Aquifers of the Gulf Coast of Texas: Texas Water Development Board Report.

Christie, M.A. (1996, November). Upscaling for Reservoir Simulation. *Journal of Petroleum Technology*. https://doi.org/10.2118/37324-JPT

Clark, J. E., Bonura, D. K., & Van Voorhees, R. F. (2005). An Overview of Injection Well History in the United States of America. *Developments in Water Science* (Vol. 52, Issue C). https://doi.org/10.1016/S0167-5648(05)52001-X

Clean Air Task Force. (2022, August 19). Carbon Capture Provisions in the Inflation Reduction Act of 2022. Retrieved from *Clean Air Task Force* Resources. https://www.catf.us/resource/carbon-capture-provisions-in-the-inflation-reduction-act-of-2022/

Clean Air Task Force. (2023). Global Carbon Capture Activity and Project Map. https://www.catf.us/ccsmapglobal/

Congressional Research Service. (2022). Carbon Capture and Sequestration (CCS) in the United States (R44902; Oct. 5, 2022), by Angela Jones, Ashley Lawson. Retrieved from *Congressional Research Digital Collection*

Couëslan, M. L., Butsch, R., Will, R., & Lock II, R. A., (2014). Integrated reservoir monitoring at the Illinois Basin – Decatur Project. *GHGT-12*. doi: 10.1016/j.egypro.2014.11.306

Daniel B. Stephens & Associates, Inc. (2018). Application to Dispose of Waste in a Class I Injection Well. WDW316 & WDW317 Response to Technical NOD #1. Section V Geology Report. Prepared for Environmental Processing Systems, L.C.

De Figueiredo, Mark A. (2005, February). The Underground Injection Control of Carbon Dioxide a Special Report to the MIT Carbon Sequestration Initiative. *Laboratory for Energy and the Environment*. https://sequestration.mit.edu/pdf/uic.pdf

Department of Energy. (2022, December 13). Biden-Harris Administration Announces $3.7 Billion to Kick-Start America's Carbon Dioxide Removal Industry. *Department of Energy Office of Fossil Energy and Carbon Management*. https://www.energy.gov/articles/biden-harris-administration-announces-37-billion-kick-start-americas-carbon-dioxide

Desai, K.P. & Moore, E.J. (1969). Equivalent NaCl solutions from ionic concentrations: Log Analyst, v. 10, no. 3, p. 12.

Dewan, J. (1983). Essentials of Modern Open-Hole Log Interpretation. Retrieved from *Pennwell Publ.Co.*, Tulsa Oklahoma, p. 361.

Dougherty, C. (2007). Using the Class V Experimental Technology Well Classification for Pilot Geologic Sequestration Projects. Retrieved from *USEPA*. UICPG#83.

Dresser Atlas. (1975). Log Interpretation Fundamentals. *Dresser Industries, Inc*. Houston, Texas.

Du Pont Environmental Remediation Services Inc. (1993). 1992 Injection Zone Annual Report Class I Injection Wells Hoechst Celanese Chemical Group, INC. Bay City Plant. Prepared for Hoechst Celanese Chemical Group, INC.

Dunlap, H. F., & Hawthorne, R. R. (1951). The Calculation of Water Resistivities from Chemical Analyses (Vol. 192). Trans. AIME.

Eaton, B. A. (1969). Fracture gradient prediction and its application in oilfield operations: Transactions of the American Institute of Mechanical Engineers, v. 246.

ECO Solutions, Inc. (1994). Pressure Falloff/MIT Testing. Prepared for Hoechst Celanese Chemical Group, Inc. Bay City Plant.

Environmental Defense Fund v. U.S.E.P.A, 852 F.2d 1309 (D.C. Cir. 1988). https://casetext.com/case/environmental-defense-fund-v-usepa

Environmental Protection Agency. (1980). Statement of Basis and Purpose Underground Injection Control Regulations. *Office of Drinking Water*. https://www.epa.gov/sites/default/files/2020-02/documents/statement_of_basis_and_purpose_of_the_uic_program-may1980.pdf

Environmental Protection Agency. (1990, January). Investigation of the Hydraulic Effects of Deep-Well Injection of Industrial Wastes. *Office of Drinking Water*. https://nepis.epa.gov/Exe/ZyPURL.cgi?Dockey=P1013ZGO.txt

Environmental Protection Agency. (1991, October). Analysis of the Effects of EPA Restrictions on the Deep Injection of Hazardous Waste. EPA 570/9-91-031.

Environmental Protection Agency. (1998). Planning, Executing, and Reporting Pressure Transient Tests. Retrieved from USEPA Region 5 – Underground Injection Control Section Regional Guidance #6.

Environmental Protection Agency. (2001). Class I Underground Injection Control Program: Study of the Risks Associated with Class I Underground Injection Wells. *Office of Water*. EPA 816-R-01-007.

Environmental Protection Agency. (2002). UIC Pressure Falloff Testing Guideline – Third Edition. *National Service Center for Environmental Publications*. https://www.epa.gov/sites/default/files/201507/documents/Guideline.pdf

Environmental Protection Agency. (2002). Exemption of Oil and Gas Exploration and Production Wastes from Federal Hazardous Waste Regulations. https://yosemite.epa.gov/oa/eab_web_docket.nsf/Attachments%20By%20ParentF ilingId/945EF425FA4A9B4F85257E2800480C65/$FILE/28%20-%20RCRA%20E%26P%20Exemption.pdf

Environmental Protection Agency. (2005). Introduction to Treatment, Storage, and Disposal Facilities (40 CFR Parts 264/265, Subpart A-E). https://www.epa.gov/sites/default/files/2015-07/documents/tsdf05.pdf

Environmental Protection Agency. (2019). Management of Exploration, Development and Production Wastes: Factors Informing a Decision on the Need for Regulatory Action. *Office of Land and Emergency Management. Office of Resource Conservation and Recovery*. https://www.epa.gov/sites/default/files/2019-04/documents/management_of_exploration_development_and_production_wastes_4-23-19.pdf

Environmental Protection Agency. (2020, April). Underground Injection Control Program Protecting Underground Sources of Drinking Water and Public Health. *National Service Center for Environmental Publications*. EPA-816F19005.

Environmental Protection Agency. (2022, October 28). Class VI Permitting Report to Congress. Retrieved from https://www.epa.gov/uic/class-vi-wells-used-geologic-sequestration-carbon-dioxide.

Environmental Protection Agency. (2023). Class VI Wells Permitted by EPA. https://www.epa.gov/uic/class-vi-wells-permitted-epa#table

Environmental Protection Agency. (2023). Primary Enforcement Authority for the Underground Injection Control Program. https://www.epa.gov /uic/primary-enforcement-authority-underground-injection-control-program-0

Environmental Protection Agency. (2023). Class I Industrial and Municipal Waste Disposal Wells. https://www.epa.gov/uic/class-i-industrial-and-municipal-waste-disposal-wells#haz_well

Equistar Chemicals, LP. (2003). Annual Report of Ambient Monitoring to the United States Environmental Protection Agency Region 6 Pressure Falloff Test Analyses. TNRCC UIC Permit No. WDW-152 and WDW-153.

Ewing, T. E., & Galloway, W. E. (2019). Chapter 16 - Evolution of the Northern Gulf of Mexico Sedimentary Basin. https://doi.org/10.1016/B978-0-444-63895-3.00016-4

Galloway, W. E., Hobday, D. K., & Magara, K. (1982). Frio Formation of Texas Gulf Coastal Plain: Depositional Systems, Structural Framework, and Hydrocarbon Distribution. AAPG Bulletin 1982; 66 (6): 649–688. doi: https://doi.org/10.1306/03B5A2F5-16D1-11D7-8645000102C1865D

Galloway, W. E., Whiteaker, T. L., Ganey-Curry, P. (2011). History of Cenozoic North American drainage basin evolution, sediment yield, and accumulation in the Gulf of Mexico basin. Geosphere 2011; 7 (4): 938–973. doi: https://doi.org/10.1130/GES00647.1

Ganjdanesh, R. & Hosseini, S. A. (2018). Development of an Analytical Simulation Tool for Storage Capacity Estimation of Saline Aquifers." International Journal of Greenhouse Gas Control 74 (July): 142–54. https://doi.org/10.1016/j.ijggc.2018.04.017

GeoMap Company. (2009). Extended Area Reference Map 380. Gulf Coast.

Geostock Sandia, LLC. (2015). 2015 TCEQ Class I Well Application for Renewal for Waste Disposal Wells Nos. 1 (WDW147) 2 (WDW319). Prepared for Sasol Chemicals (USA), LLC Greens Bayou Plant.

Geostock Sandia, LLC. (2015). Beaumont Texas Facility TCEQ Class I Permit Renewal Application for WDW100, WDW101, WDW389, and WDW390. Prepared for Mitsubishi/Lucite International.

Geostock Sandia, LLC. (2017). 2017 Annual Injection Zone Report to TCEQ for Well Nos. 3, 4, 9, and 11. Prepared for INVISTA S.à r.l. Orange Site.

Geostock Sandia, LLC. (2018). INVISTA Orange Site 2018 HWDIR Exemption Petition Reissuance Well Nos 3, 4, 9, 11 (WDW Nos. 054, 055, 191, 282). Prepared for INVISTA S.à r.l. Orange Plant.

Geostock Sandia, LLC. (2020). 2020 TCEQ Permit Renewal Class I UIC Application for Injection Well No.7 (WDW359). Prepared for Ascend Performance Materials Chocolate Bayou Plant.

Geostock Sandia, LLC. (2021). 2021 Mechanical Integrity Test and Ambient Pressure Test Report Plant Well No. 2 (WDW212). Prepared for Ticona Polymers, Inc. Bishop Plant.

Geostock Sandia, LLC. (2021). Injection Well Testing Report. Prepared for Kuraray.

Geostock Sandia, LLC. (2021). Well Testing Report for Plant Nos. 1 (WDW148) and 2 (WDW162). Prepared for Lyondell Chemical Company.

Global CCS Institute. (2021, March). Technology Readiness and Costs of CCS. https://www.globalccsinstitute.com/resources/publications-reports-research/technology-readiness-and-costs-of-ccs/

Global CCS Institute. (2021, May). Surveying the U.S. Federal CCS Policy Landscape in 2021. https://www.globalccsinstitute.com/resources/publications-reports-research/technology-readiness-and-costs-of-ccs/

Golden StrataServices, INC. (1983). Technical Report to Accompany Class I Injection Well Permit Application for an Existing Well. Prepared for Shell Oil Company Norco Chemical Plant.

Golden StrataServices, INC. (1987). Application for Permit Amendment for WDW-33 and WDW-45. Clear Lake, Texas, Plant. Hoechst Celanese Chemical Group.

Golden StrataServices, INC. (1991). Hoechst Celanese MIT Testing (4 Wells). Prepared for Hoechst Celanese Chemical Group.

Gollakota, S. & McDonald, S. (2014). Commercial-scale CCS Project in Decatur, Illinois – Construction Status and Operational Plans for Demonstration. Energy Procedia, Volume 63, pp. 5986-5993. https://doi.org/10.1016/j.egypro.2014.11.633

Government Accountability Office. (1987). Hazardous Waste - Controls Over Injection Well Disposal Operations Protect Drinking Water. RCED-87-170.

Groundwater Protection Council. (2021, June). Injection Wells: A Guide to Their Use, Operation and Regulation. Retrieved from *GWPC Underground Injection Control*.

Guinan, Allison, Grant, Timothy, Lin, ShangMin, Shih, Chung Yan, Withum, Jeffrey A., & Vikara, Derek. (2019). UIC Class I Injection Wells – Analog Studies to Geologic Storage of CO2. *NETL*. https://doi.org/10.2172/1557140

Guo, Sun, K., & Ghalambor, A. (2008). Well productivity handbook: vertical, fractured, horizontal, multilateral, and intelligent wells / Boyun Guo, Kai Sun, Ali Ghalambor. Retrieved from Gulf Publishing Company.

Gupta, N., Mishra, S., Kelly, M., Raziperchikolae, S., Ganesh, P. R., Valluri, M., Keister, L., Burchwell, A., Mawalkar, S., & Place, M. (2020). Analysis of Transient Pressure and Rate Data in a Complex of Enhanced Oil Recovery Fields in Northern Michigan. United States. https://doi.org/10.2172/1764719

Halliburton. (2001). Halliburton Red Book Cementing Data. Talliburton Technical Data Calculations, formulae, and Slurry Tables. Section 240. https://dokumen.tips/documents/halliburton-red-book-cementing-data.html

Hasan, A. R. & Kabir, C. S. (1983). Pressure Buildup Analysis: A Simplified Approach. Society of Petroleum Engineers of A[ME. Journal of Petroleum Technology. https://blasingame.engr.tamu.edu/z_zCourse_Archive/P648_17A/P648_17A_Lectures/20170308_P648_17A_Lec_12_(Ref)_SPE_010542_(Hasan)_[PDF].pdf

Hazardous Waste Guidelines and Regulations. (1978). 43 FR 58946-59022. Federal Register, Vol. 43, No.243.

Hoechst Celanese Chemical Group, Inc. (1987). WDW-14, WDW-32, WDW-49, WDW-110. Bay City Plant.

Horner, D. R. (1951). Pressure Build-up in Wells. Proceedings of the 3rd World Petroleum Congress. https://onepetro.org/WPCONGRESS/proceedings/WPC03/All-WPC03/WPC-4135/203521

Hovorka, S. D., Doughty, C., & Holtz, M. (2004). Testing efficiency of storage in the subsurface: Frio Brine Pilot Experiment. United States.

Hovorka, S., Nicot, J., Mehdi, Z., Sun, A., Yang, C., Sava, D., Mickler, P., & Remington, R. (2014). Expert-Based Development of a Standard in CO2 Sequestration

Monitoring Technology. Gulf Coast Carbon Center Bureau of Economic Geology. Austin, Texas. https://www.beg.utexas.edu/files/publications/cr/CR2014-Hovorka-1_QAe6965.pdf

International Energy Agency Greenhouse Gas (IEAGHG). (2010). Injection strategies for CO2 storage sites. Retrieved from *IEA Greenhouse Gas R&D Programme*. Report IEA/CON/09/168

International Energy Agency. (2020). The role of CCUS in low-carbon power systems. *IEA*, Paris. License: CC BY 4.0. https://www.iea.org/reports/the-role-of-ccus-in-low-carbon-power-systems

International Energy Agency. (2020). CCUS in Clean Energy Transitions. IEA, Paris. License: CC BY 4.0. https://www.iea.org/reports/ccus-in-clean-energy-transitions

International Energy Agency. (2021). Net Zero by 2050. IEA, Paris. License: CC BY 4.0. https://www.iea.org/reports/net-zero-by-2050

International Energy Agency. (2022). CO2 Emissions in 2022. IEA, Paris. License: CC BY 4.0. https://www.iea.org/reports/co2-emissions-in-2022

International Energy Agency. (2022). Carbon Capture Utilisation and Storage. IEA, Paris. License: CC BY 4.0. https://www.iea.org/reports/carbon-capture-utilisation-and-storage-2

Inflation Reduction Act of 2022, H.R. 5376 — 117th Congress (2022). https://www.congress.gov/bill/117th-congress/house-bill/5376

Intera. (2019). Application to Dispose of Waste in a Class I Injection Well WDW316 & WDW317. Response to Technical NOD #2. Section VII Reservoir Mechanics Report. Prepared for Environmental Processing Systems, L.C.

Johnson, K., Schilling, E., & Tucker, A. (2021, November). Bipartisan Infrastructure Bill Invests Billions in CCUS. https://www.jdsupra.com/legalnews/bipartisan-infrastructure-bill-invests-9111801/

Jones, T.A. & J.S. Haimson, 1986, "Demonstration of Confinement: An Assessment of Class I Wells in the Great Lakes and Gulf Coast Regions," Journal of the Underground Injection Practices Council, Number 1, p. 279-317.

Krevor, S., de Coninck, H., & Gasda, S.E. et al. (2023). Subsurface carbon dioxide and hydrogen storage for a sustainable energy future. Nat Rev Earth Environ 4, 102–118. https://doi.org/10.1038/s43017-022-00376-8

LA Admin Code §XVII-607. Application Content.

Lake, L. (2022). What CO2-EOR Has Already Taught Us About Upscaling Permanent Carbon Sequestration. *Journal of Petroleum Technology*. https://jpt.spe.org/what-co2-eor-has-already-taught-us-about-upscaling-permanent-carbon-sequestration

Lee, J. (1982). Well Testing. SPE Textbook Series, Vol. 1.

Lococo, J. (2021, March 11). The Permitting Program Crucial for Carbon Capture's Success. Retrieved from ClearPath.org: https://clearpath.org/our-take/the-permitting-program-crucial-for-carbon-captures-success/

Lonquist & Co. LLC. (2021). 2021 Closure Report Injection Well No.4 (WDW055). Mechanical Integrity Test Program Plugging and Abandonment. Prepared for INVISTA Nylon Chemicals Americas, LLC Orange Site.

Loucks, R. G., Bebout, D. G., & Galloway, W. E. (1977). Relationship of Porosity Formation and Preservation to Sandstone Consolidation History – Gulf Coast Lower Tertiary Frio Formation. Bureau of Economic Geology.

LMNO Engineering, Research, and Software, Ltd. (2023). Hazen-Williams Friction Loss Equation. https://www.lmnoeng.com/hazenwilliams.php

Lustgarten, A. (2012). Injection Wells: The Poison Beneath Us. ProPublica. https://www.propublica.org/article/injection-wells-the-poison-beneath-us

Ma, Y. Z. (2019). Quantitative Geosciences: Data Analytics, Geostatistics, Reservoir Characterization and Modeling. https://doi.org/10.1007/978-3-030-17860-4

Miller, C.C., Dyes, A.B., & C.A. Hutchinson. (1950). The Estimation of Permeability and Reservoir Pressure from Bottom Hole Pressure Build-Up Characteristics. JPT 2:91–104. doi: https://doi.org/10.2118/950091-G

Mishra, S., Ganesh, P., Kelley, M., & Gupta, N. (2016). Analyzing the Performance of Closed Reservoirs Following CO2 Injection in CCUS Projects. Energy Procedia, pp. 3465-3475. https://doi.org/10.1016/j.egypro.2017.03.1477

Moore, E.J., Szasz, S.E., and B.F. Whitney. (1966). Determining Formation Water Resistivity from Chemical Analysis. J Pet Technol 18: 373–376. doi: https://doi.org/10.2118/1337-PA

Moradi, S., Moeini, M., al-Askari, M. K.G, & Mahvelati, E. H. (2016). IOP Conf. Ser.: Earth Environ. Sci. 44 042002. doi:10.1088/1755-1315/44/4/042002

National Energy Technology Laboratory. (2010). Geologic Storage Formation Classification: Understanding Its Importance and Impacts on CCS Opportunities in the United States. https://netl.doe.gov/sites/default/files/2019-01/BPM_GeologicStorageClassification.pdf

National Energy Technology Laboratory. (2015). Carbon Storage Atlas Fifth Edition. https://www.netl.doe.gov/sites/default/files/2018-10/ATLAS-V-2015.pdf

Ni, H., Dasari, G., Teletzke, G., & Saris, A. (2021). Evaluating Technical Feasibility of Gigaton Scale CO2 Storage using Produced Water Disposal Data in US Gulf Coast. Proceedings of the 15th Greenhouse Gas Control Technologies Conference 15-18 March 2021. https://ssrn.com/abstract=3903753

Petrotek. (2016). Response to Technical Notice of Deficiency from TCEQ Dated July 7, 2016, on Permit Application for Class I Hazardous Waste Disposal Wells WDW-452 and WDW-453. Prepared for Novus International, INC.

Petrotek. (2016). URI Permit Renewal Application & Technical Report WDW-247 & WDW-248. Prepared for URI, INC.

Pianta, S., Rinscheid, A., Weber, Elke. (2021, April). Carbon Capture and Storage in the United States: Perceptions, preferences, and lessons for policy. *Energy Policy*. https://doi.org/10.1016/j.enpol.2021.112149

Qi, D. (2004, July). Upscaling Theory, Methodology and Application Techniques for Reservoir Simulation. http://unsworks.unsw.edu.au/fapi/datastream/unsworks:43409/SOURCE02?view=true

Ramey, H. J. (1992). Advances in Practical Well-Test Analysis. https://blasingame.engr.tamu.edu/z_zCourse_Archive/P648_15A/P648_15A_Lectures_(working_lectures)/20150304_P648_15A_Lec_11_SPE_020592_[PDF].pdf

Resource Conservation and Recovery Act. (1976). 42 U.S.C. 6901. Public Law 94-580.

Rig Worker. (2023). Method Ben Eaton Method. Formulas and Calculations. https://www.rigworker.com/formulas-calculations/method-ben-eaton-method.html

Rish, W.A., T. Ijaz, & T.F. Long. (1998). A Probabilistic Risk Assessment of Class I Hazardous Waste Injection Wells. Draft. *Developments in Water Science*. Vol. 52, Issue C. https://doi.org/10.1016/S0167-5648(05)52010-0

Ritchie, H., Roser, M., & Rosado, P. (2020) - CO_2 and Greenhouse Gas Emissions. https://ourworldindata.org/co2-and-greenhouse-gas-emissions

Sabine Storage & Operations, Inc. (2018). Dow-Huntsman Huntsman EthyleneAmines LLC Stratton Ridge Well #1 (WDW-435) Class I Injection Well Drilling and Completion. Prepared for Dow Huntsman.

Safe Drinking Water Act., 42 U.S.C. § 300f et seq. (1974).

Salazar Luna, Jesús Mauricio. (2008). Simulation and Inversion of Borehole Electromagnetic Measurements for the Estimation of Petrophysical Properties in the Presence of Mud-Filtrate Invasion. [Doctoral dissertation, University of Texas at Austin]

Sandia Technologies, LLC. (2000). Injection Well Test Report. E. I. Dupont de Nemours & Co., Inc. Sabine River Works.

Sandia Technologies, LLC. (2001). 2001 Injection Well Test Report. Orange, Texas. E.I. Prepared for Du Pont de Nemours & Co., Inc.

Sandia Technologies, LLC. (2012). 2012 TCEQ UIC Class I Well Permit Renewal for Plant Well No.1 (WDW149), Plant Well No.2 (WDW162), and a New Plant Well No.3. Prepared for Lyondell Chemical Company Channelview Plant.

Sandia Technologies, LLC. (2014). TCEQ UIC Class I Injection Well Application Permit Nos. WDW082, WDW083, WDW149, WDW360. Prepared for E. I. Du Pont de Nemours & Co., Inc. LaPorte Plant.

Sandia Technologies, LLC. (2015). TCEQ UIC Class Permit Application and Technical Report for WDW004, WDW028, WDW029, WDW030, WDW105, WDW106, WDW142, WDW143, WDW144. Prepared for INVISTA S.à r.l., LLC - Victoria Site.

Sandia Technologies, LLC. (2015). TCEQ Injection Well Permit Application & Technical Report for WDW210, WDW211, WDW212, & Six Proposed Wells. Prepared for Ticona Polymers Bishop Plant.

Schlumberger. (1969). Log Interpretation Principles. Schlumberger Limited, New York.

Schlumberger. (2009). Log Interpretation Charts 2009 Edition. pp. 5-8. https://archive.org/details/2009EditionLogInterpretationCharts/page/n17/mode/2up

Schlumberger. (n.d.). Water formation volume factor. Accessed on April 2023. https://glossary.slb.com/en/Terms/w/water_formation_volume_factor.aspx

Seismic Exchange. (2012, October). Gulf of Mexico Offshore Area Map Showing Salt Domes. Retrieved from Gulf Coast Salt Dome Map. https://www.seismicexchange.com/seismic_library/geological_maps

Simpson, H. & Lester, S. (2009). Deep Well Injection an Explosive Issue. Center for Health, Environment & Justice.

Smith, R. E. (1996). EPA Mission Research in Support of Hazardous Waste Injection 1986-1994. by J.A. Apps and C.F. Tsang (eds.). *Deep Injection Disposal of Hazardous and Industrial Waste, Academic Press*, San Diego, CA. pp. 9-24.

Society of Petroleum Engineers. (2015). Upscaling of grid properties in reservoir simulation. Retrieved from *PetroWiki*.

Society of Petroleum Engineers. (2016). Productivity index (J). Retrieved from *PetroWiki*.

Solid Waste Disposal Act Amendments of 1980. (1980). Public Law 96-482. 42 U.S.C. §6921.

Speight J. G. (2020). The properties of water. Natural Water Remediation. https://doi.org/10.1016/B978-0-12-803810-9.00002-4

Strata Technologies, LLC. (2013). Annual Mechanical Integrity and Reservoir Pressure Testing of WDW-317. Prepared for Environmental Processing Systems Jesse Sinclair Plant.

Strata Technologies, LLC. (2016). Annual Mechanical Integrity and Reservoir Pressure Testing of WDW-316. Prepared for Environmental Processing Systems Jesse Sinclair Plant.

Strata Technologies, LLC. (2016). Underground Injection Control Permit WDW278 & WDW279. Prepared for US Ecology Texas, INC.

Strata Technologies, LLC. (2020). Class I UIC Permit Renewal Application WDW-163, WDW-164, WDW-165. Prepared for INEOS Nitriles USA, LLC.

Subsurface Technology, INC. (1990). Prepared for WITCO Chemical Company. Well 972060.

Subsurface Technology, INC. (2012). Permit Application Class I Hazardous Waste Injection Well Waste Disposal Well #1. Prepared for Mosaic Fertilizer, LLC.

Subsurface Technology, INC. (2012). Permit Renewal Application for WDW-125, WDW-155, WDW-201, WDW-301, WDW-302, and Proposed WDW-433 and WDW-434. Prepared for BASF Corporation.

Subsurface Technology, INC. (2012). Permit Renewal Application for WDW-80, WDW-127, WDW-128, WDW-214, and WDW-215. Prepared for BP Products North America INC.

Subsurface Technology, INC. (2014). Permit Renewal Application for Class I Hazardous Waste Injection Wells WDW-160 and WDW-358. Prepared for Veolia Es Technical Solutions, LLC.

Subsurface Technology, INC. (2015). Petition Reissuance of WDW-157. Prepared for Vopak Logistics Services, USA Inc.

Sweatman, R. E., Parker, M. E., & S. L. Crookshank. (2009, November). Industry Experience with CO2-Enhanced Oil Recovery Technology. Paper presented at the SPE International Conference on CO2 Capture, Storage, and Utilization, San Diego, California, USA. https://doi.org/10.2118/126446-MS

Terra Dynamics INC. Environmental Services. (2000). Mechanical Integrity Testing and Ambient Pressure Monitoring of WDW-316. Prepared for: Environmental processing systems. L.C. Hickory Islands Farms Facility Dayton, Texas.

Terra Dynamics, INC. (2003). Permit Application to Dispose of Waste in a Class I Injection Well - Permit Renewal Application - WDW-51 and WDW-99. Prepared for BASF Corporation.

Terra Dynamics, INC. (2006). Permit Application to Dispose of Waste in a Class I Injection Well (WDW-91 and WDW196 and WDW314 Permit Amendment Applications). Texas City, Texas. Prepared for Sterling Chemicals, INC.

Terra Dynamics, INC. (2008). Permit Application to Dispose of Waste in a Class I Injection Well Permit Renewal Applications WDW-139 and WDW-343 and Permit

Applications for Two Proposed New Wells. Prepared for Akzo Nobel Surface Chemistry LLC.

Terra Dynamics, INC. (2010). Permit Application to Dispose of Waste in a Class I Injection Well - Permit Renewal Applications WDW-34, WDW-113, WDW-114, and WDW-299 and Permit Applications for Two Proposed New Wells. Prepared for ISP Technologies INC. Texas City Facility.

Terra Dynamics, INC. (2013). Permit Renewal Application to Dispose of Waste in a Class I Injection Well WDW-397 and WDW-398. Prepared for ExxonMobil.

Terra Dynamics, INC. (2014). Permit Renewal Application to Dispose of Waste in a Class I Injection Well WDW-222 and WDW-223. Prepared for GEO Specialty Chemicals, INC.

Terra Dynamics, INC. (2016). Permit Application to Dispose of Waste in a Class I Injection Well - Permit Renewal Applications WDW-122 and WDW-230. Prepared for Arkema INC. Crosby Plant.

Terra Dynamics, INC. (2019). Permit Renewal Application to Dispose of Waste in a Class I Injection Well Permit Renewal Applications WDW-168 and WDW-425. Prepared for South Texas Mining Venture, LLP.

Texas Commission on Environmental Quality. (2021). Permit Application to Dispose of Waste in a Class I Injection Well. TCEQ. Underground Injection Control. Austin.

Texas World Operations, INC. (2003). Injection Zone Annual Report to the Texas Commission on Environmental Quality. Prepared for Equistar Chemicals, LP.

TexCom Gulf Disposal, LLC. (2006). Core Lab Analysis Results Crossroads Environmental WDW-315 TexCom's WDW-410.

The Hazardous and Solid Waste Amendments of 1984, H.R.2867 - 98th Congress. (1984). https://www.congress.gov/bill/98th-congress/house-bill/2867

Underground Injection Practices Council. (1986, April). A Class I Injection Well Survey (Phase I Report): Survey of Selected Sites. https://www.michigan.gov/-/media/Project/Websites/egle/Documents/Programs/OGMD/Catalog/15/UIPC-ClassIInjWellSurvPI-1986-Aopt.pdf?rev=38403259eae94160a6a94ae8295f62fc

Valluri, M., Mishra, S., & Ravi Ganesh, P. (2021). Injectivity index: a powerful tool for characterizing CO2 storage reservoirs—a technical note. Greenhouse Gases: Science and Technology, 11(2), 251–265. https://doi.org/10.1002/ghg.2046

Van Voorhees, R., Greenberg, S., & Whittaker, S. (2021). Observations on Class VI Permitting: Lessons Learned and Guidance Available. Illinois State Geological Survey, Prairie Research Institute, University of Illinois at Urbana-Champaign. https://www.ideals.illinois.edu/items/117640

Vikara, D. & Guinan, A. (2019). NETL's Analog Studies to Geologic Storage of CO2 – Overview. *NETL*. United States. https://doi.org/10.2172/1615146

Vikara, D., Zymroz, T., Withum, J. A., Shih, C. Y., Lin, S., Hoffman, H., Guinan, A., & Carr, T. (2019). Underground Natural Gas Storage – Analog Studies to Geologic Storage of CO2. *NETL*. https://netl.doe.gov/energyanalysis/details?id=2867

Wang, Z. & Hosseini, S. (2023). EASiTool: A Science-based Enhanced Analytical Simulation Tool for CO2 Storage Capacity Estimation.

Warner, D. L., & Orcutt, D. H. (1973). Industrial Wastewater-Injection Wells in United States--Status of use and Regulation, 1973. *AAPG Bulletin*, 57(8), 1606-1607.

Warner, T., Vikara, D., Guinan, A., Dilmore, R., Walter, R., Stribley, T., & McMillen, M. (2020, December). Overview of Potential Failure Modes and Effects Associated with CO2 Injection and Storage Operations in Saline Formations. NETL. https://www.energy.gov/sites/default/files/2021/01/f82/DOE-LPO_Carbon_Storage_Report_Final_December_2020.pdf

Westaway, C. R. & Loomis, A. W. (Ed.). (1984). Cameron Hydraulic Data. Ingersoll-Rand. https://www.pumpfundamentals.com/hazen-williams.pdf

Williams, G. S. & Hazen, A. M. (1905). Hydraulic Tables Showing the Loss of Head Due to the Friction of Water Flowing in Pipes, Aqueducts, Sewers, etc. and the Discharge Over Weirs.

Wilson, E. J. & Keith, D. W. (2002). Geologic Carbon Storage: Understanding the Rules of the Underground. Presented at 6th International Conference on Greenhouse Gas Control Technologies, Kyoto, Japan, 9/30-10/4/02.

Winsauer, W. O., Shearin, H. M., Masson, P. H., & Williams, M. (1952). Resistivity of brine-saturated sands in relation to pore geometry. *AAPGBull*.,36, pp. 253–277.

WSP USA, INC. (2017). Permit Applications to Convert Class V Stratigraphic DW Well Nos. 1 (SN 975071) and 2 (SN 975072) to Class I Hazardous Waste Injection Wells. Prepared for Innophos, Inc., Geismar Plant.

WSP USA, INC. (2017). Report of Annual Transient Pressure and Mechanical Integrity Testing - WDW160 - Project 192035M. Port Arthur, Texas. Prepared for Veolia E.S. Technical Solutions, LLC.

WSP USA, INC. (2020). Report of Annual Transient Pressure and Mechanical Integrity Testing - WDW160 - Project 192035M. Port Arthur, Texas. Prepared for Veolia E.S. Technical Solutions, LLC.

WSP USA, INC. (2020). UIC Class I Injection Well Permit Renewal Application for WDW-169, WDW-249, and WDW-422. Prepared for TM Deer Park Services LLC.

WSP USA, INC. (2021). Permit Renewal Application for WDW070. Prepared for TM Corpus Christi.

WSP USA, INC. (2022). Report of Annual Transient Pressure and Mechanical Integrity Testing - WDW160 - Project 192035M. Port Arthur, Texas. Prepared for Veolia E.S. Technical Solutions, LLC.

WSP USA, INC. (2022). UIC Class I Injection Well Permit Renewal Application for WDW-080, WDW-127, and WDW-128. Prepared for Blanchard Refining Company.